SEISMIC INVERSION AND SOURCE ROCK EVALUATION ON JURASSIC ORGANIC RICH
INTERVALS IN THE SCOTIAN BASIN, NOVA SCOTIA

by

Natasha Marie Morrison

Submitted in partial fulfilment of the requirements
for the degree of Master of Science

at

Dalhousie University
Halifax, Nova Scotia
July 2017

Table of Contents

List of Tables

List of Figures

Abstract

Source rocks are a key element of a petroleum system and have been identified as a risk in the Scotian Basin, offshore Nova Scotia, Canada. There have been 24 significant hydrocarbon discoveries, including eight commercial discoveries since 1967 in the Sable Sub-Basin of the Scotian Basin. Although there are proven hydrocarbon accumulations in both Jurassic and Cretaceous reservoirs, identification of their source is problematic. This is due to the low organic matter content of the studied sedimentary section, 'turbo' drilling practices, and extensive drilling mud contamination.

This project investigates the extent and geochemical properties of known and presumed Middle to Upper Jurassic source rocks in the Scotian Basin. The studied successions were deposited in two main depositional environments: i) Middle Jurassic distal foreslope and basinal stratigraphic equivalents of the Abenaki Bank; ii) Upper Jurassic deltaic and shelf margin carbonate sediments deposited in elongate depocenters at the shelf margin. It tests the hypothesis that source rocks, if present (in a 2120 km^2 area surrounding Sable Island), can be identified using petrophysical techniques and mapped using seismic inversion. This is the first time that these approaches to source rock presence and distribution have been publicly documented offshore Nova Scotia.

Investigation of Middle and Upper Jurassic successions and their potential as source rock was completed using a combination of petrophysical and seismic techniques. Wireline log estimation of total organic carbon (TOC) was completed using the Passey method. Seismic inversion was achieved via a 3D constrained sparse spike inversion (CSSI), based on the presence of low impedance source rocks investigated using the Løseth et al. "Source Rock from Seismic" method. The study area was selected based on well control (with 19 Jurassic penetrations) and the availability of 3D seismic data (Sable MegaMerge, courtesy of the Sable Offshore Energy Project).

The petrophysical methods did not identify intervals of source rock in the studied wells. This is consistent with the publicly available geochemical data, showing measured TOC values of generally <2%. Seismic inversion was effective in mapping low acoustic impedance intervals, especially in calcareous shales. However, without unequivocal evidence of high TOC content (>2%), low acoustic impedance cannot be interpreted as source rock, i.e. a relationship between AI and TOC was not found. A correlation was found between low impedance calcareous shales and overpressured zones with overpressure known to lower seismic velocity. It is suggested that late hydrocarbon generation and migration in the Scotian Basin are responsible for overpressure. Hence, low acoustic impedance may provide indirect evidence of source rock presence and active or late stage hydrocarbon generation from below well penetrations or from outside the study area.

List of Abbreviations Used

AC / Δt	Sonic Log
AI	Acoustic Impedance
API	American Petroleum Institute (oil gravity)
CNSOPB	Canada-Nova Scotia Offshore Petroleum Board
CSSI	Constrained Sparse Spike Inversion
DEN	Density
Fm.	Formation
Fz	Fresnel Zone
GLI	General Linear Inversion
GOC	Generative Organic Carbon
GR	Gamma Ray Log
HI	Hydrogen Index
Hz	Hertz
Km	Kilometer
L.	Lower
LOM	Level of Organic Maturity
M	Meter
Mb.	Member
MD	Measured Depth
MFS	Maximum Flooding Surface
NGOC	Non-Generative Organic Carbon
OI	Oxygen Index
PI	Production Index
QC	Quality Control
ResD / ILD	Resistivity Log
Ro%	Vitrinite Reflectance
TAI	Thermal Alteration Index
TD	Total Depth
TOC	Total Organic Carbon
TR	Transformation Ratio
TVDSS	True Vertical Depth Sub Sea
UWI	Unique Well Identifier
Wt %	Weight Percent
x^0	Initial value of a variable
x^x	Present day value of a variable
Θ	Porosity

Acknowledgements

Chapter 1:   Introduction

Source rocks are a fundamental element of any petroleum system and are a key uncertainty in the exploration of the Scotian Basin, offshore Nova Scotia, Atlantic Canada (e.g. OERA 2013). The Scotian Basin (Figure 1-1), surrounding and underlying Sable Island, has had 24 significant hydrocarbon discoveries, including two oil fields and six gas fields (Smith et al. 2014). Though there are proven hydrocarbon accumulations in both Jurassic and Cretaceous reservoirs, there has been difficulty identifying a definitive source of the hydrocarbons (Fowler et al. 2016). The accumulations are currently assumed to be predominantly sourced by pro-deltaic and basinal shales within the Upper Jurassic to Upper Cretaceous Verrill Canyon Formation (e.g. Mukhopadhyay and Wade 1990; Mukhopadhyay 2006). More precisely, Beicip-Franlab (2011) interpret Aptian and Valanginian pro-deltaic and paralic sediments, Tithonian and Callovian shales deposited during maximum flooding events, and Liassic shales as key source rocks in the Scotian Basin.
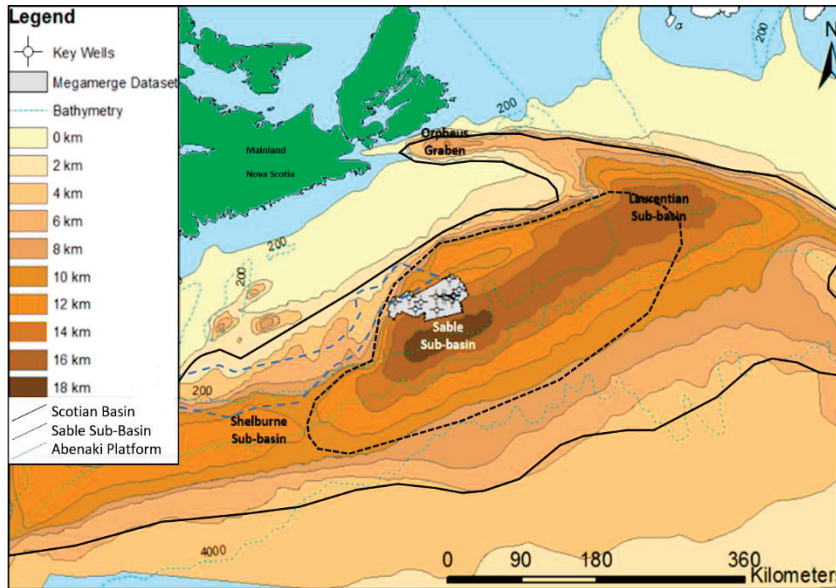
Figure 1-1: Map of the Scotian Basin with total Mesozoic and Cenozoic sediment thickness; the Sable Sub-Basin and the MegaMerge Dataset (modified from Wade 2000); outlines of the Scotian Basin and Sable Sub-Basin based on Williams et al. (1990).

The Scotian Basin stretches 1200 km from the Grand Banks in the northeast past the Shelburne Sub-basin in the southwest (Figure 1-1), covering approximately 300,000 km². Offshore Nova Scotia has had 210 wells drilled and approximately 100 penetrate the Jurassic. These include 129 exploratory, 53 development, 27 delineation, and 1 service relief well (CNSOPB 2016). Despite extensive research efforts (e.g. Mukhopadhyay and Wade 1990; Mukhopadhyay 1991, 1995) over the last 30 years, source rock intervals are still poorly characterized, due to the quality of the geochemical data collected from prospective source rock intervals, the effect of oil based muds and lignite additives (which both add external hydrocarbons into the sample) and turbo-drilling (which causes the mixing of contaminants and pulverizing of the sample) (e.g. Mukhopadhyay 1990a). As such, the Scotian Margin is recognized as having low content of organic matter, yielding low or "lean and disseminated" average total organic carbon (TOC) content (Williamson 1992). The main source rock intervals in the Scotian Basin

and Sable Sub-Basin are thought to have been deposited during the Jurassic
(Mukhopadhyay 1990a; Beicip-Franlab 2011). The Jurassic is a known time for significant
source rock deposition globally (e.g. Huc and Schneidermann 1995; Duarte et al. 2012),
commonly in restricted basins related to the break-up of the supercontinent Pangea
(e.g. Jeanne d'Arc Basin, offshore Newfoundland and Essaouira Basin, Morocco).

1.1   *What is a Source Rock?*
Source rocks are defined as rock units containing sufficient organic matter, of
suitable chemical composition, to generate and expel hydrocarbons via biogenic or
thermal processes (Miles 1994). This term is applied to all intervals that meet this
criterion, regardless of the maturity of the organic matter (Tissot and Welte 1984;
Potter et al. 1993; Belaid et al. 2010; Suárez-Ruiz et al. 2012). Deposition and
preservation of organic matter (and subsequently source rock) can occur in a variety of
depositional environments, including lacustrine, deltaic, and deep marine (e.g. Tyson
1995).

The basic criteria used in characterizing a given interval as a source rock are: i) the
quantity of organic matter; ii) the type of organic matter; and iii) and thermal maturity.
Accurately determining these parameters has been a challenge when studying source
rocks in the Scotian Basin (Mukhopadhyay 1990a; Beicip-Franlab 2011).

The type of organic matter in source rocks is commonly characterized as either
kerogen or bitumen. Kerogen is organic matter which is insoluble in organic solvents
with a high molecular weight whereas bitumen is categorized by its solubility and lower
molecular weight (Tissot and Welte 1984; Potter et al. 1993; Belaid et al. 2010; Suárez-

Ruiz et al. 2012). Based on its chemical composition, kerogen is divided into four categories, ranging from Type I, which contains the highest hydrogen/carbon and oxygen/carbon ratios, to Type IV, which consist of the lowest ratios (e.g. Van Krevelen 1993; Tissot and Welte 1984). Kerogen typing is often used to predict the kind of hydrocarbons a given source rock will produce.

A more readily used chemical characterization is the pseudo-Van Krevelen diagram (Figure 1-2). This plots the oxygen index (OI) against the hydrogen index (HI), derived from RockEval pyrolysis (Espitalié et al. 1977, 1985). This stems from the relationship observed by Van Krevelen (e.g. 1993) between hydrogen content (i.e. kerogen type) and depositional environment. Type I kerogens, which are the most enriched in hydrogen, are most commonly associated with a lacustrine setting while Type II kerogens are related to planktonic organic matter commonly deposited in an open marine (sometimes lacustrine) setting. Type III kerogens are often correlated to "woody" plant matter derived from a terrestrial source. Finally, Type IV kerogen, which has the lowest hydrogen content, is kerogen that has been previously altered, whether by carbonization or oxidization (Suárez-Ruiz et al. 2012).
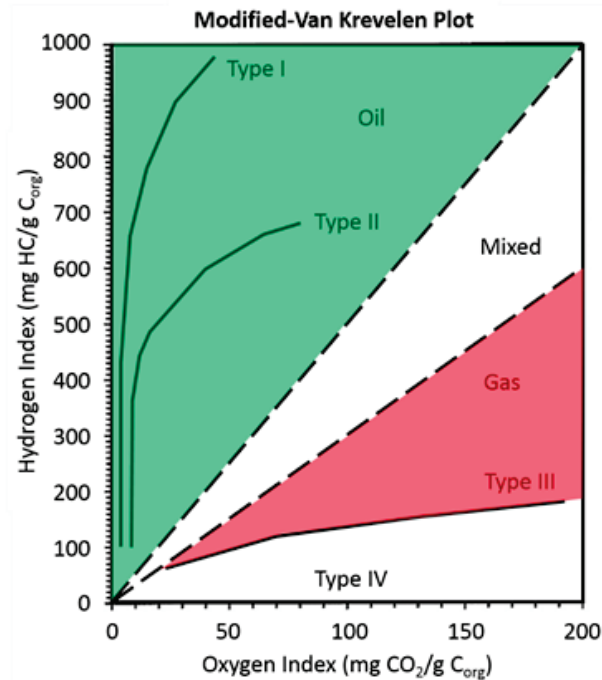
Figure 1-2: Modified Van Krevelen plot outlining the separation of kerogen and hydrocarbon type (modified from Tyson 1995).

The decrease in elemental ratios through the kerogen types allows for prediction of hydrocarbon fluid type upon maturation: i) Type I kerogens predominantly generate oil; ii) Type II kerogens can generate oil, condensate or gas; and iii) Type III kerogens produce gas. Type IV kerogens are considered to be non-productive (Suárez-Ruiz et al. 2012).

1.2   Motivation

There has been success in the use of seismic techniques to indirectly study source rocks (e.g. Løseth et al. 2011). Løseth et al. (2011) suggested that source rocks can be identified using a combination of petrophysical and seismic techniques, specifically the Passey Method and acoustic impedance seismic inversion. These authors observed that acoustic impedance (AI) decreases non-linearly with increasing TOC content. They also noted that the AI of a shale source rock (> 3% TOC) will be significantly lower than AI in a

non-organic shale. This relationship was observed through the study of significant source rocks such as the Kimmeridge Clay in southern England (e.g. Morgans-Bell et al. 2001) and the Hekkingen Formation in the Barents Sea (e.g. Langrock 2004).

The Sable Sub-Basin contains one of the most extensive 3D seismic data sets on the shelf area of the Scotian Margin (Figure 1-3). This dataset, the Sable MegaMerge, was made available to Dalhousie University by ExxonMobil and Professor Grant Wach (Principal Investigator) by ExxonMobil, operators of the Sable Offshore Energy Project. This survey consists of a post-stack merge of six 3D seismic surveys acquired in the Scotian Basin from 1996 to 1999; three using marine streamers and three using ocean bottom cables (e.g. CNSOPB 2014) (Figure 1-3). With good signal to noise ratio, stable zero phase, and reasonable bandwidth (appx. 10-60 Hz) and resolution (peak frequency ~ 15-30 Hz depending on depth and tuning at ~ 15-35 m), this merged seismic cube provides extensive coverage of part of the Sable Sub-Basin. The Sable MegaMerge provides an unprecedented view of the Middle Jurassic to Lower Cretaceous deposition in the Sable Sub-Basin, such as the Abenaki carbonate bank, the proximal siliciclastics of the MicMac Formation, and the distal finer grained siliciclastics of the Verrill Canyon Formation (e.g. Wade and MacLean 1990) (Figure 1-1 and Figure 1-3).

Understanding the extent and geochemical properties of known and presumed source rocks, as well as identifying new organic-rich intervals, is critical for future petroleum exploration offshore Nova Scotia. The possibility of using indirect methods (i.e. wireline and seismic) to improve upon the current limitations in identifying source

6

rock intervals from drill cuttings open new possibilities of research in the Sable Sub-

Basin and the Scotian Margin.
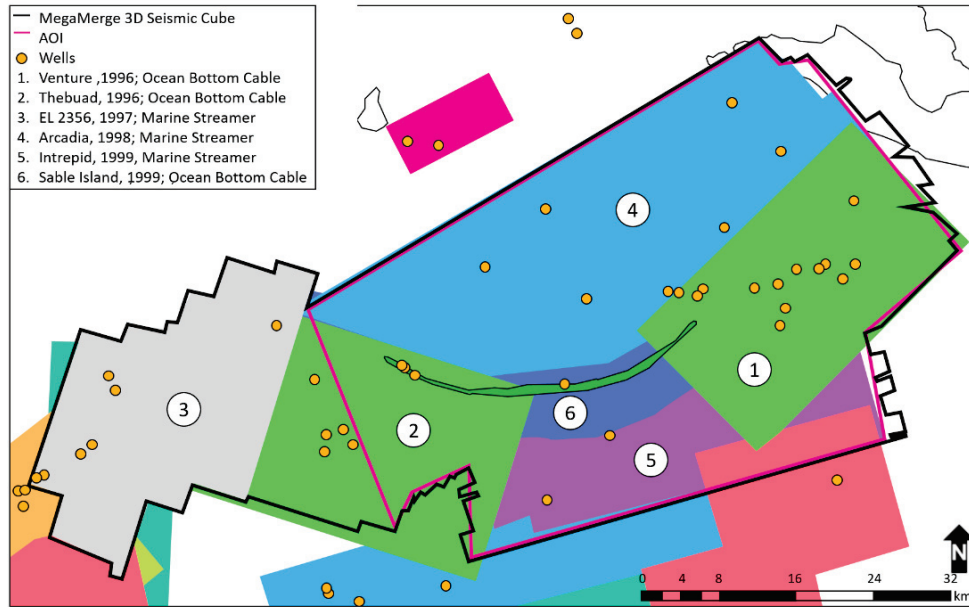
Figure 1-3: The six 3D seismic surveys included in the Sable MegaMerge survey.

1.3   Hypothesis and Objectives

In this study, I hypothesized that source rocks in the Sable Sub-Basin, if present,

can be identified using petrophysical and seismic techniques when applied to the Sable

MegaMerge dataset. To test this hypothesis: i) TOC was estimated from available

wireline data using the Passey Method (Passey et al., 1990) in selected stratigraphic

intervals and was examined for potential as source rock; ii) a seismic inversion was

completed on the available seismic data within the study area, via a 3D constrained

sparse spike inversion (CSSI, CGG Jason InverTrace[PLUS]); and iii) finally the estimated TOC

was correlated with the AI of selected intervals to identify source rock intervals (with

high TOC and low AI) (Løseth et al. 2011).

The objective was to investigate known and presumed Middle to Upper Jurassic source rocks within the Sable Sub-basin using indirect petrophysical and seismic methods. The study area excluded the proximal Abenaki carbonate bank, focusing on the area with higher potential for the occurrence of source rock in the distal, eastern portion of the dataset (Figure 1-3). This study is a component of a larger project, designed to develop new strategies to predict and define source rock characteristics and thermal maturity throughout the Scotian Basin and other conjugate basins on both sides of the Atlantic margins.

Chapter 2:   Regional Geology

2.1   *Depositional Overview*

The Scotian Basin, located in offshore Nova Scotia, contains more than 18

kilometers of Mesozoic and Cenozoic sediments in its deepest areas (Figure 1-1) (e.g.

Kidston et al. 2005; Weston et al. 2012). The Sable Sub-Basin (Williams et al. 1990) is

one of the depocenters of the Scotian Basin, adjacent to the Laurentian, Abenaki and

Shelburne sub-basins (e.g. Williams and Grant 1998). It is part of the Atlantic passive

continental margin (e.g. Weston et al. 2012).

Rifting and breakup of the supercontinent Pangea resulted in the formation of

the Scotian Basin. In the Middle Triassic, rifting of the Gondwanan and Laurentian plates

formed a series of grabens and half grabens that were filled with synrift sediments (e.g.

Wade and McLean 1990; Wade et al. 1995). The first sediments deposited comprised

continental red beds of the Eurydice Formation and thick layers of evaporites of the

Argo Formation. Deposition of the Eurydice and Argo formations ended in the Early

Jurassic with the onset of sea floor spreading and initial thermal subsidence (e.g. Wade

and McLean 1990; Wade et al. 1995; Weston et al. 2012). This triggered a transition to

marginal and then fully marine conditions in the Jurassic. In the Early Jurassic, the

margin was characterized by the deposition of marine and restricted carbonates forming

the Iroquois Formation. This formation grades laterally toward the northwest and

southeast into the fluvial, syn- and post-rift clastics of the Mohican Formation (Figure 2-

1) (e.g. McIver 1972; Wade and McLean 1990; Steel et al. 2011).
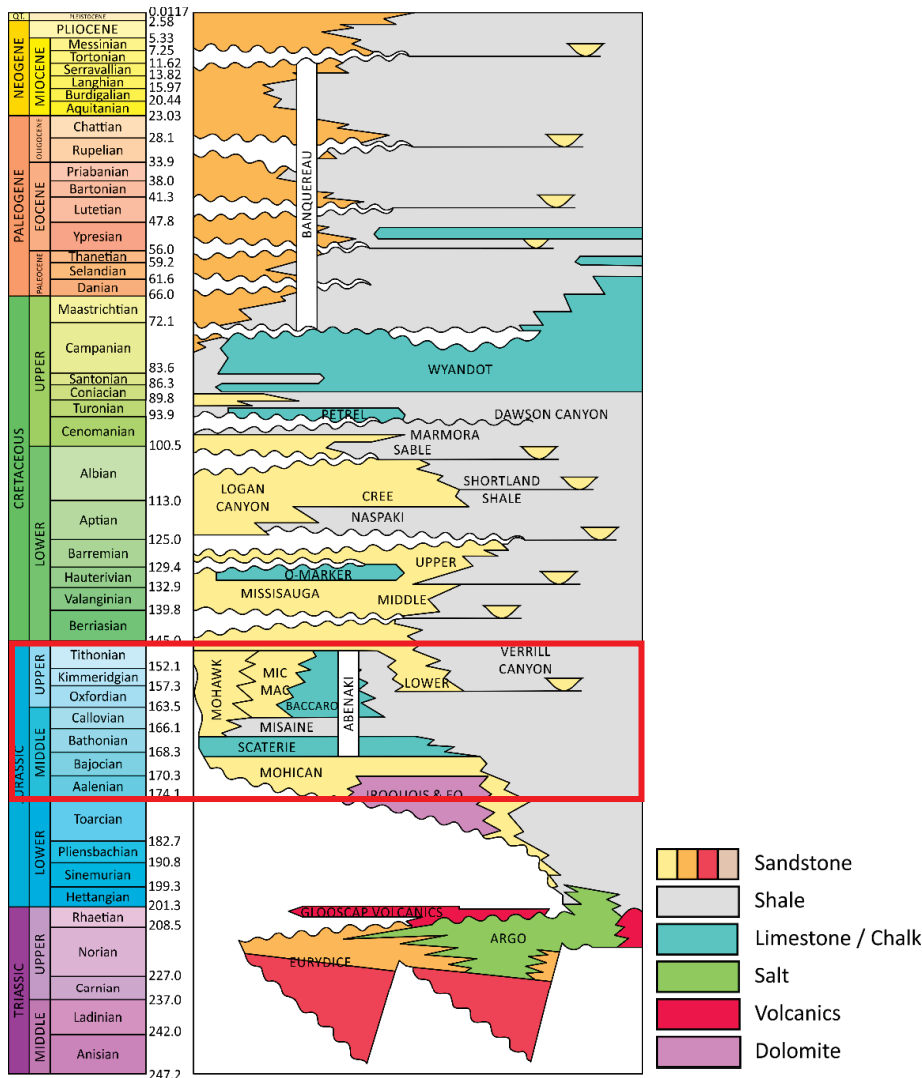
Figure 2-1: Lithostratigraphic column of the Scotian Basin. Formations of interest outlined in red (modified from Weston et al. 2012).

The Middle to Upper Jurassic Abenaki carbonate platform is part of a larger giga-platform that can be traced to the modern-day to the Caribbean (e.g. Eliuk 1978). Deposition of the Abenaki Formation, a series of stacked shallowing upward carbonate successions, began with the Scatarie Member which comprises margin and platform limestones (e.g. Eliuk 1978; Kidston et al. 2005). Margin subsidence and relative sea level rise led to a transgression, which caused the carbonate bank edge to shift to a more proximal position. This transgression was followed by the deposition of

10

progadational carbonate-rich shales of the Misaine Member. The Misaine Member was subsequently overlain by cyclic deposition of a series of shallowing-upward packages, each representing carbonate drowning, back-stepping, aggradation, and subsequent progradation (e.g. Wiesenberger et al. 2000; Kidston et al. 2005). The shelf margin was controlled by a basement hinge line with deposition of the carbonate sediments in clear, warm waters (e.g. Eliuk 1978).

The Abenaki Formation extends southwest along the western margin of the Sable Sub-Basin. Landward, it grades laterally into siliciclastics of the Mic Mac and Mohawk formations (Figure 2-1) (e.g. McIver 1972; Wade et al. 1995; Steel et al. 2011). These formations were deposited coeval with the Abenaki Formation and comprise siliciclastics derived from continental sources (Kettanah et al. 2013). The siliciclastic sediments transition into the Abenaki Formation (e.g. Wade and MacLean 1990; Eliuk 2016). Distal limestone intervals of the Abenaki Formation interfinger with basinal shales and siliciclastics of the Verrill Canyon Formation. The Verrill Canyon Formation is described as the basinal facies equivalent of the Abenaki, Mic Mac, Missisauga, and younger formations which continue into the Middle Cretaceous (e.g. Wade and MacLean 1990; PePiper and Mackay 2006).

The Mohawk, Mic Mac and Abenaki formations are immediately overlain by deltaic siliciclastics sediments (the "Sable Delta") of the Missisauga and Logan Canyon formations. In the study area, these sediments were initially deposited in elongated depocenters at the shelf margin (Lower Missisauga Member), and subsequently deposited shelf-wide (Middle and Upper Missisauga members and Logan Canyon

Formation). The depocenters formed in response to sediment loading from the Sable Delta, salt withdrawal and listric faulting (e.g. Wade and MacLean 1990; Cummings and Arnott 2005; Eliuk 2016). The elongated depocenters form the "expansion trend". They become progressively younger basinward with progradation of the shelf (e.g. Wade and MacLean 1990). Shelf margin limestones in these expansion trends have developed in successive fault slices and are not part of the Abenaki Bank (e.g. Wade and Maclean 1990; Beicip-Franlab 2011; Eliuk 2016).

The Upper Jurassic to Cretaceous Missisauga Formation was deposited in a fluvio-deltaic system (e.g. Wade and McLean 1990; Pe-Piper and MacKay, 2006). A transgression in the Hauterivian allowed for a temporary return to carbonate deposition, marked by the diachronous O-Marker. This is an easily identifiable and correlatable seismic marker, which separates the Middle and Upper Missisauga members (e.g. Jansa and Noguera Urrea 1990). The fluvio-deltaic to marginal marine sediments of the Missisauga Formation are overlain by a thick, shaley interval known as the Naskapi Shale. The Naskapi Shale is subsequently overlain by the Logan Canyon Formation, comprising a thick succession of cyclic estuarine and shallow marine sediments (Jansa and Wade 1975). This change in depositional environment was controlled by several factors, including delta lobe avulsion, eustatic sea level changes, changes in subsidence rates, and changes in sediment supply (e.g. Wach and Vincent 2005; Beicip-Franlab 2011).

The termination of the Logan Canyon Formation marks a change from shallow estuarine and paralic sediments to the deposition of deep water sediments (e.g. Beicip-

Franlab 2011). The increase in accommodation allowed for the deposition of the

Dawson Canyon Formation open marine, fine grained siliciclastics. Within the Dawson

Canyon Formation, a thin Turonian deep water chalk known as the Petrel Member was

also deposited. This was followed by a subsequent deep water chalk, the Wyandot

Formation (e.g. Wade et al. 1995; Weston et al. 2012). Finally, from the Late Eocene

onward, the Scotian Basin was dominated by clastic sedimentation (Figure 2-1) (e.g.

Jansa and Wade 1975; Weston et al. 2012).

2.2   Jurassic Stratigraphy

Deposition during the Early-Middle Jurassic in the Sable Sub-Basin began with

the Mohican Formation, composed primarily of fluvial clastic sediments. Distal, fine

grained sediments of the Verrill Canyon Formation were coevally deposited through this

entire time interval (Wade and McLean 1990). Overlying the Mohican Formation, the

deposition of the Abenaki Carbonate Bank began with the Scatarie Member. This

member comprises oolitic grain-packstone limestones of platformal origin (e.g. Eliuk

1978, 2016; Kidston et al. 2005). Landward, the Scatarie Member is interfingered with

the fluvio-deltaic sediments of the Mic Mac Formation (e.g. McIver 1972; Kidston et al.

2005). It is important to understand the geology of the carbonate bank to gain insight

on the down-dip interval of interest. A sequence stratigraphic cross-section of the

Abenaki Formation can be seen in Figure 2-2. The interval containing both the Mohican

Formation and Scatarie Member are classified as the Abenaki I interval (Weissenberger

et al. 2000).
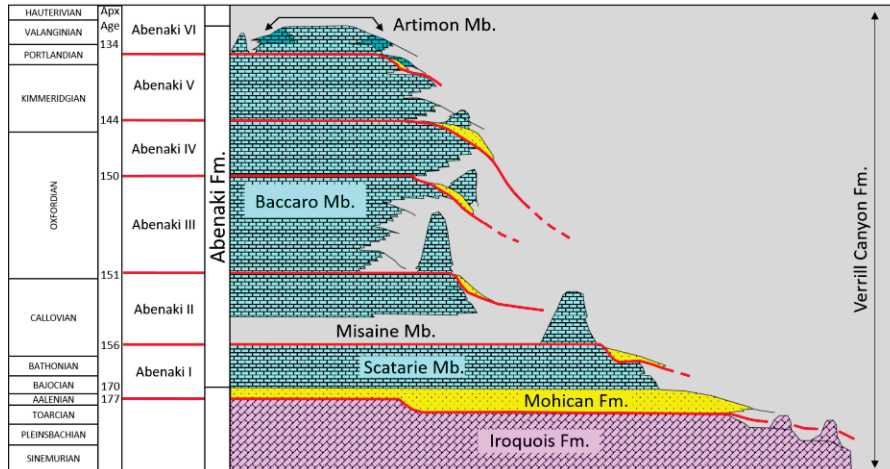
Figure 2-2: Schematic sequence stratigraphic cross-section of the Abenaki Formation and Lower Jurassic formations (modified from Weissenberger et al. 2000).

Following the Scatarie Member, the siliciclastics of the Misaine Member were deposited. This member was deposited in a neritic or shallow water environment, comprising calcareous shales with minor interbedded lime muds. This deposition followed a global transgressive event that occurred during the Callovian and provides an approximate date for the Misaine Member of middle Callovian to lower Oxfordian (e.g. Eliuk 1978, 2016; Weissenberger et al. 2000; Kidston et al. 2005). This interval is known as the Abenaki II, representing a transition from the calcareous shales of the Misaine Member to the oolitic grainstones and wackestones of the Baccaro Member (e.g. Weissenberger et al. 2000; Wierzbicki et al. 2002; Kidston et al. 2005; Eliuk 2016).

The Baccaro Member is a proven gas reservoir in the Scotian Basin and comprises multiple shallowing upward carbonate cycles (e.g. Eliuk 1978, 2016; Weissenberger et al. 2000, Kidston et al. 2005). These cycles are the Abenaki II through VI. The limestones of the Abenaki III (which correlates seismically to the Penobscot Limestone Member basinward), IV (which correlates seismically to the Citnalta

Limestone Member basinward), and V, form much of the Abenaki Carbonate Bank

(Weissenberger et al. 2000; Eliuk 2016).

Each carbonate cycle comprises a facies transition from platform interior, to reef

and reef margin, followed by the foreslope, talus, and basin (e.g. Weissenberger et al.

2000; Wierzbicki et al. 2002; Kidston et al. 2005; Eliuk 2016). Relative to each other,

these depositional cycles stack in a progradational pattern (Abenaki III to IV), an

aggradational pattern (carbonate pinnacles seen in Abenaki II and III), or a

retrogradational pattern (Abenaki I to II and Abenaki IV to V to VI). These stacking

patterns reflect relative sea level change in the Jurassic (e.g. Weissenberger et al. 2000;

Wierzbicki et al. 2002). Minor amounts of siliciclastics have been identified within these

carbonate lithofacies.

At the raised rim of the platform in the Panuke and Cohasset fields, the

deposition of the Abenaki carbonate platform ends with the Artimon Member. This is a

thin, intermittent succession, described as clay-rich cherty limestones. This member is

the only segment of the Abenaki dated as the Cretaceous (Kidston et al. 2005).

Landward of the Abenaki Platform, the shallow to marginal marine sediments of

the Mic Mac Formation were deposited (e.g. McIver 1972; Jansa and Wade 1975).

Figure 2-1 shows the Mic Mac Formation occurring landward of the Abenaki Carbonate

Platform. Previous interpretations in Wade and MacLean (1990 – Figure 5.21), interpret

sediments basinward of the Abenaki carbonate bank as Mic Mac Formation. The Mic

Mac Formation is characterised by deltaic sediments, predominantly distributary

channels and subsequent fluvial sands, which are intermittently interfingered with the

15

prodelta shales of the Verrill Canyon Formation (e.g. McIver 1972; Jansa and Wade

1975; Beicip-Franlab 2011). In the Uniacke and Arcadia wells, Jurassic aged carbonates,

such as the Penobscot and Citnalta Member limestones, can also be observed

interfingering with distal Mic Mac/ Verrill Canyon shales (e.g. Wade and Maclean 1990).

The Mohawk Formation was deposited predominantly as proximal, continental

facies, consisting of feldspathic sandstones and siltstones with interbedded shales and

limestones (e.g. McIver 1972; Beicip-Franlab 2011). This post-rift succession, including

the Mic Mac and Mohawk formations, grade laterally into the Verrill Canyon Formation

(Weston et al. 2012).

Deposition in the Jurassic concludes with the deposition of the Lower Missisauga

Member. The Missisauga Formation is divided into three sections: Upper, Middle and

Lower, with only the Lower Missisauga occurring in the Jurassic (e.g. Jansa and Noguera

Urrea 1990). The Missisauga Formation comprises regressive, fluvio-deltaic to marginal

marine interbedded shales and sandstones which also grade laterally into the distal

Verrill Canyon Formation (Wade et al. 1995).

2.2.1   Previous Work on Jurassic Source Rocks in the Study Area
Several studies regarding source rock and source rock potential within the

Scotian Basin have been published (e.g. Mukhopadhyay 1991; Mukhopadhyay 1994).

Geochemical analyses, including RockEval pyrolysis and kerogen typing, have been

completed on the Lower Missisauga Member, the Mic Mac and Verrill Canyon

formations in 11 of the wells within the study area (Mukhopadhyay 1994). In general,

TOC values range from approximately 0% to 2% with sporadic values reaching high as

18.5%. It is assumed in literature that all values above 4% are contaminated

(Mukhopadhyay 1990a). This is based on the comparison of TOC values measured in corresponding intervals on both cutting samples, which are often contaminated, and core samples, which had no measured values above 4% (Mukhopadhyay 1990a).

RockEval pyrolysis and kerogen typing of the Mic Mac Formation limestones (Citnalta and Penobscot members) and calcareous shales adjacent to Sable Island was conducted on samples from 16 wells (Mukhopadhyay 1994). TOC measurements ranged from 0.06 to 2.39 % TOC. Outlying values of >8% TOC were measured in samples from the Uniacke G-72. This was interpreted to be caused by contamination from drilling mud additives (Mukhopadhyay 1994). Additionally, Beicip-Franlab interpret the corresponding up-dip Misaine Member as a possible new source interval within the Scotian Basin. It is important to note, however, that this interpretation is based on a sample with known contamination and its proximity to Callovian maximum flooding surfaces (Beicip-Franlab 2016).

Samples from the Jurassic-Cretaceous successions, deposited within the Sable Sub-Basin, were classified based on the six organic facies described in Table 2-1 (e.g. Mukhopadhyay and Birk 1989; Mukhopadhyay and Wade 1990). Samples from South Venture O-59, a key well in this research, contain both oil prone (Type IIA-IIB) and condensate/minor oil-prone (IIB) kerogens. These intervals were found in the Oxfordian to Turonian aged Missisauga (Lower) and Mic Mac Formations (Mukhopadhyay and Birk 1989). These formations were interpreted to be deposited within a prodelta environment (e.g. Wade and MacLean 1990). Additionally, Oxfordian to Turonian aged sediments within Venture B-43 were interpreted as type IIB kerogens, representing a

deep marine, or partially oxic, prodelta environment (Mukhopadhyay and Birk 1989; Mukhopadhyay and Wade 1990). The conclusions of this study, as well as others summarized below, were reached using vitrinite reflectance, Rock-Eval pyrolysis, organic petrography, and basin modeling (e.g. Mukhopadhyay 1991; Mukhopadhyay 1994).

Outside the study area, examination of 28 samples from three wells in the Scotian Basin, Alma F-67, Glenelg J-48 and SW Banquereau F-34, concluded that the Verrill Canyon Formation had a TOC range from approximately 1 to 8%, with one anomalous measurement of 24% (Mukhopadhyay 1991). Many of the deep marine shale samples were characterized as oil prone, Type II kerogens, with some samples showing a Type III terrestrial influence. Vitrinite reflectance and maturity values from these samples have been interpreted to indicate early hydrocarbon generation and expulsion (Mukhopadhyay 1991).

A summary of the data collected by Mukhopadhyay et al. within the 11 wells used in the petrophysical methods of this project can be seen in Figure 2-3. Many of the samples used for evaluation were found to contain contaminants introduced during drilling, such as lignite, rust, and oils from the drill mud. Once again, literature states that most TOC values greater than 4% likely exhibit contamination (e.g. Mukhopadhyay and Birk 1989, 1990a). Excluding these contaminated measurements, source rock potential in the 11 wells approximates fair to good, based on Table 3-3 in Section 3.3.
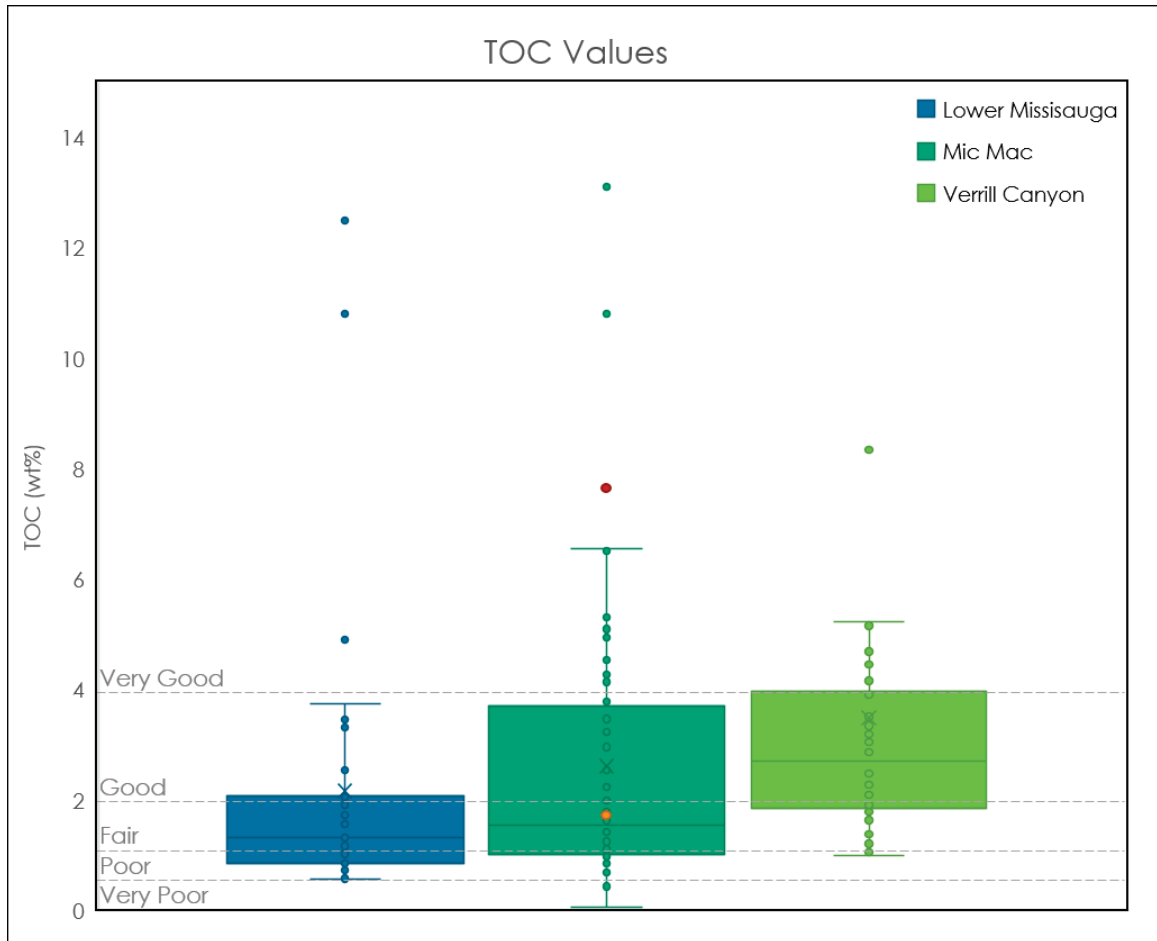
Figure 2-3: Summary of all TOC values for the 11 key wells within the study area based on studies done by Mukhopadhyay (1990a, 1990b, 1991, 1994), Mukhopadhyay and Birk (1989) and Mukhopadhyay and Wade (1990).

Table 2-1: Amorphous organic matter related to kerogen and hydrocarbon potential (Part. = particulate; wt. = weight) (Mukhopadhyay and Wade 1990)

	Amorphous Organic Matter Related to Kerogen and Hydrocarbon Potential					
	Organic Facies					
Kerogen Type	Amorphous Maceral Type (fluorescence)	Associated Major Macerals	Environment of Deposition	Range of HC Index (mg HC/g TOC)	Pyrolisis-GC Pattern	Oil/Gas Potential
I	Sapro I* (golden yellow)	Alginite	Lakes or algal mat (shallow marine or freshwater)	>800	Mainly N-alkanes between $C_{10} - C_{30}$	Oil + Condensate + Gas* (80%)
IIA	Sapro IIA* (yellow brown)	Alginite, Sapro I, Part. Liptinite A & B, Liptodetrinite	Lagoon or lakes (marine or fresh). Upwelling area (shallow or deep marine)	550-800	Dominant cyclo- and normal alkanes between $C_8 - C_{27}$	Oil + Condensate + Gas* (60 – 90%)
IIA-IIB	Sapro IIA* + Sapro IIB* (brown or orange)	Part. Liptinite A & B, Liptodetrinite, Sapro-Vitrinite	Upwelling region, prodelta. Lacustrine delta, deep marine anoxia	300-600	Mixed cyclo- and normal alkanes and aromatics between $C_6 - C_{20}$	Oil (50%) + Condensate (50%) + Gas*
IIB	Sapro IIB* (brown)	Part. Liptinite A & B, Sapro IIA, Desmocollinite	Deltaic Marsh, lagoon, back-barrier, deep marine anoxia	225-400	Mixed aromatics and cycloalkanes	Condensate (50%) + Gas (40%) + Oil (10%)
IIB-III	Sapro IIB + Humosapro	Telocollinite, Part. Liptinite B	Partially oxic prodelta or shallow marine, and lagoon	100-250	N-alkanes up to C_{22} and low molecular wt. aromatics and phenol	Gas (70%) + Condensate (30%)
III	Humosaro* (nonfluorescent to dark brown)	Part. Liptinite B, Telocollinite	Delta swamp, partially oxic. Shallow or deep marine basins	50-125	Mainy aroatics and n-alkanes up to C_{14} and phenol	Gas (>80%)
IV	Macrinite (nonfluorescent)	Fusinite, Macrinite, Recycled vitrinite	Oxic swamp, tidal flats or deep marine basins	< 50	Minor hydrocarbons	Non source

Chapter 3:   Methods

A variety of petrophysical and geophysical methods were used during this project, including but not limited to: TOC restoration, wireline TOC determinations, seismic modeling, seismic inversion and the source rock from seismic method. In this section, I will review each method. Data used in this project include the offshore Sable MegaMerge 3D seismic dataset, made available to Dalhousie University and Professor Grant Wach (Principal Investigator) by ExxonMobil, operators of the Sable Offshore Energy Project; and wireline log data, donated to Dalhousie by CanStrat and Divestco. In addition, geochemical and stratigraphic data from both the Canada Nova Scotia Offshore Petroleum Board (CNSOPB) and Natural Resources Canada (NRC) Basin Database was used.

3.1   Study Area

The study area comprises 2120 km^2 of the Sable Sub-Basin and utilized the eastern portion of the Sable MegaMerge 3D seismic dataset (Figure 3-1). The study focused on an area outboard of the Abenaki carbonate bank, where relatively deep water, fine-grained, Jurassic sediments have been deposited which have significant source rock potential (e.g. Kidston et al. 2005). The area was chosen based on this knowledge of regional geology, as well as substantial well and 3D seismic control.
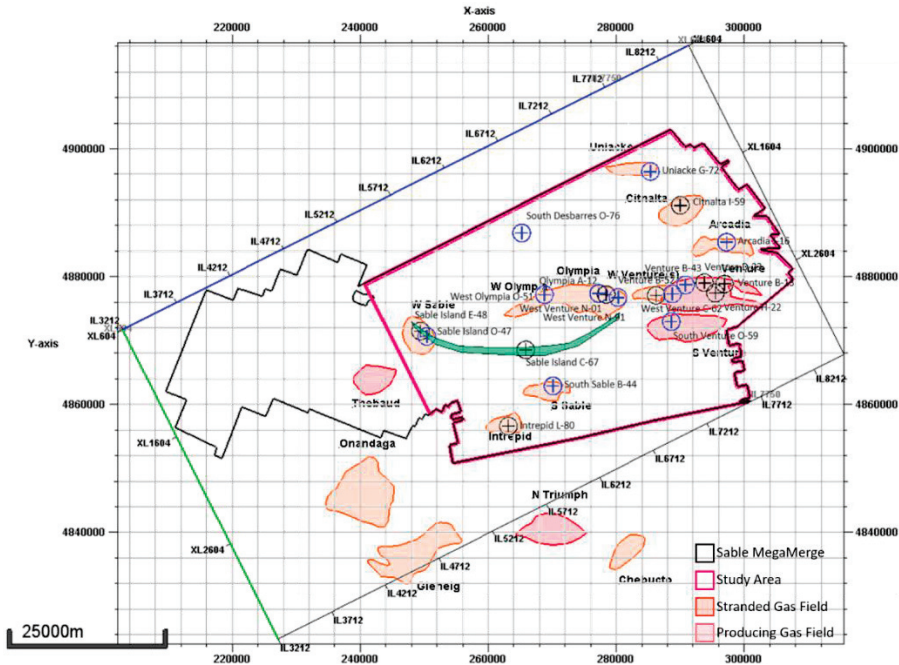
Figure 3-1: Sable MegaMerge 3D Seismic Survey framework, outlining the study area, wells used in the study, and local gas fields.

3.2   Selection of Wells

There are 37 wells within the constraints of the Sable MegaMerge study area. Of these 37 wells, all significantly deviated wells were eliminated from the dataset in areas of high well density, such as the Venture and West Sable fields, where adequate vertical wells existed. Secondly, all wells without sufficient well penetration into the Jurassic were also eliminated. The petrophysical methods were applied using a subset of these wells, filtering by presence of geochemical analysis, reducing the number of analysed wells to 11 (Table 3-1). References for this geochemical data can be found in Appendix B. The inversion process incorporated a different subset, filtering out all wells with greater than 100 m deviation, as required by the software (Table 3-2). The wireline logs used contained a full suite of logs, including gamma ray, resistivity, density/neutron, sonic.

Table 3-1: List of wells used in the petrophysical portion of this project with their corresponding Jurassic Members.

Well Name	Formations	GSC#	UWI	Spud Date	Operator	TD (m)
Arcadia J-16	L. Missisauga Mb., Mic Mac Fm.	D225	300 J16 44100 59300	27/01/1983	Mobil et al.	6005.0
Olympia A-12	L. Missisauga Mb., Mic Mac Fm.	D212	300 A12 44100 59450	20/04/1982	Mobil-Texaco-Pex	6064.0
Sable Island O-47	L. Missisauga Mb.	D213	300 O47 44000 50000	13/12/1971	Mobil-Tetco	4198.6
South Debarres O-76	L. Missisauga Mb.	D250	300 O76 44100 59450	16/04/1984	Shell Petrocan et al.	6041.0
South Sable B-44	L. Missisauga Mb., Verrill Canyon Fm.	D312	300 B44 44000 59450	27/07/1988	Mobil et al.	5207.6
South Venture O-59	L. Missisauga Mb., Mic Mac Fm.	D217	300 O59 44000 59300	29/04/1982	Mobil et al.	6176.0
Uniacke G-47	Mic Mac Fm.	D228	300 G72 44200 59300	9/5/1983	Shell Petrocan et al.	5740.0
Venture B-43	L. Missisauga Mb., Mic Mac Fm.	D202	300 B43 44100 59300	7/6/1981	Mobil-Texaco-Pex	5874.0
Venture B-52	Mic Mac Fm.	D224	300 B52 44100 59300	19/01/1983	Mobil et al.	5960.0
West Olympia O-51	L. Missisauga Mb., Mic Mac Fm.	D277	300 O51 44100 59450	23/06/1989	Mobil et al.	4816.0
West Venture N-91	L. Missisauga Mb., Mic Mac Fm.	D249	300 N91 44100 59300	19/04/1984	Mobil et al.	5548.0

Table 3-2: List of wells used in the seismic inversion portion of this project.

Well Name	GSC #	UWI	Spud Date	Operator	TD (m)
Arcadia J-16	D225	300 J16 44100 59300	27/01/1983	Mobil et al.	6005
Citnalta I-59	D123	300 I59 44100 59300	4/2/1974	Mobil et al.	4575
Intrepid L-80	D126	300 L80 43500 59450	18/05/1974	Texaco et al.	4162
Olympia A-12	D212	300 A12 44100 59450	20/04/1982	Mobil-Texaco-Pex	6064
Sable Island C-67	D213	300 O47 44000 50000	13/12/1971	Mobil-Tetco	4199
South Desbarres O-76	D250	300 O76 44100 59450	16/04/1984	Shell Petrocan et al.	6041
South Venture O-59	D217	300 O59 44000 59300	29/04/1982	Mobil et al.	6176
Uniacke G-72	D228	300 G72 44200 59300	9/5/1983	Shell Petrocan et al.	5740
Venture B-13	D195	300 B13 44100 59300	17/08/1980	Mobil et al.	5368
Venture B-43	D202	300 B43 44100 59300	7/6/1981	Mobil-Texaco-Pex	5874
Venture B-52	D224	300 B52 44100 59300	19/01/1983	Mobil et al.	5960
Venture D-23	D178	300 D23 44100 59300	28/11/1978	Mobil et al.	4945
Venture H-22	D232	300 H22 44100 59300	15/04/1984	Mobil et al.	5944
West Olympia O-51	D277	300 O51 44100 59450	23/06/1989	Mobil et al.	4816
WestVentureN-91	D249	300 N91 44100 59300	19/04/1984	Mobil et al.	5548

3.3   Total Organic Carbon (TOC) and Kerogen Typing

Total organic carbon is generally determined using a LECO elemental analyzer (e.g.

Tissot and Welte 1984; Tyson 1995). Because hydrocarbons are composed of, on average,

82 to 88 mol wt% carbon, TOC can be used to determine a rock's potential to generate

hydrocarbons (e.g. Jarvie 2012). Table 3-3 summarises the general potential of a source

rock based the content of the TOC (Peters et al. 2005). It is important to note, however,

that TOC will decrease with increasing maturation. That is, the more "cooked" the source

rock becomes, the more degradation of the TOC (kerogen).

Espitalié et al. (1977) introduced the analytical technique of RockEval pyrolysis

for source rock characterization through the development of a method used to rapidly

characterize organic matter. This method involves first flushing the pyrolysis oven with

an inert helium atmosphere then heating it to 300°C (Espitalié et al. 1977). The oven is

kept at this temperature for five minutes to allow for the volitization of free

hydrocarbons. The free hydrocarbons volatilised are measured as the S1 peak, which is

detected by a Flame Ionization Detector. The temperature of the oven is then steadily

increased by 25 °C/min until it reaches 550 °C. The S2 peak is the measurement of the

hydrocarbons released during this heating. The maturity and type of kerogen controls

the T_{MAX} (°C), which is the temperature at which the S2 peaks (Espitalié et al. 1977).

Finally, between 300 and 390 °C, the cracking of the kerogens releases CO2 which is

detected by a Thermal Conductivity Detector and measured as the S3 peak. Hydrogen

Index (HI = S2/TOC*100), Oxygen Index (OI = S3/TOC*100) and Production Index (PI =

S1/(S1 + S2)) can also be derived (e.g. Espitalié et al. 1977, 1985; Peters 1986). Tables 3-3

to 3-5 outline the several criteria used to characterize source rock in this study.

Table 3-3: Characterization of the general potential of source rock with corresponding range of RockEval measurements (Peters et al. 2005).

Potential	TOC (wt %)	Rock-Eval (mg/g rock)		Bitumen (ppm)	Hydrocarbons (ppm)
		S1	S2		
Poor	<0.5	<0.5	<2.5	<500	<300
Fair	0.5-1	0.5-1	2.5-5	500-1000	300-600
Good	1-2	1-2	5-10	1000-2000	600-1200
Very Good	2-4	2-4	10-20	2000-4000	1200-2400
Excellent	>4	>4	>20	>4000	>2400

Table 3-4: Kerogen types with corresponding range of RockEval measurements (Peters et al. 2005).

Kerogen Type	Hydrocarbon Index (mg HC/g TOC)	S2/S3	Atomic H/C	Main product at peak maturity
I	>600	>15	>1.5	Oil
II	300-600	10-15	1.2-1.5	Oil
II/III	200-300	5-10	1.0-1.2	Oil/Gas
III	50-200	1-5	0.7-1.0	Gas
IV	<50	<1	<0.7	None

Table 3-5: Maturation with corresponding range of RockEval and maturity measurements (Peters et al. 2005).

Maturity	Maturation			Generation		
	Ro (%)	Tmax (°C)	TAI	Bitumen/TOC	Bitumen (mg/g rock)	Production Index (S1/(S1+S2))
Immature	0.20-0.60	<435	1.5-2.6	<0.05	<50	<0.10
Mature						
Early	0.60-0.65	435-445	2.6-2.7	0.05-0.10	50-100	0.10-0.15
Peak	0.65-0.90	445-450	2.6-2.7	0.15-0.25	150-250	0.25-0.40
Late	0.90-1.35	450-470	2.9-3.3	-	-	>0.40
Postmature	>1.35	>470	>3.3	-	-	-

3.3.1 Total Organic Carbon (TOC) Restoration

Jarvie (2012) discussed that present-day TOC values (TOC^x) of a source rock may not be the most accurate way to define a source rock. TOC^x values are dependant on both the type and quality (i.e. core vs cuttings, presence of contamination) of a sample, as well as the thermal maturity of a sample. Furthermore, kerogen types estimated from Rock-Eval pyrolysis of core or cutting samples reflect present day thermal maturity and thus only provide estimates of the potential for future hydrocarbon expulsion (S2) (Jarvie et al. 2005). Accounting for this issue requires the calculation of the original quantity of TOC (TOC^0) to understand the original potential of the shale as a source rock (e.g. Jarvie et al. 2005). Knowing TOC^0 then allows for a more accurate classification of a rocks source potential as it restores hydrogen and carbon content that may have been lost during hydrocarbon generation, as well as removes the effects of contamination or sampling errors (Jarvie et al. 2005; Jarvie 2012). This project tested three different methods, one empirical and two mass balance, to evaluate TOC^0, as well as the methods themselves as they are used on the shales of the Sable Sub-basin.

3.3.1.1 Jarvie et al. (2005) TOC Restoration Method

While studying the Barnett Shale, Jarvie et al. (2005) observed that TOC values in the dry gas zone decreased by approximately 36%, relative to immature samples, due to hydrocarbon generation. This was found to be in good correlation with artificially matured samples, also from the Barnett Shale. Though the TOC was only found to decrease by 36%, it was concluded that the HI and remaining source potential were reduced by values greater than 90%. This decrease is indicative of high conversion of the

organic matter to hydrocarbon during generation (Jarvie et al. 2005). These findings

allowed for the calculation of TOC^0, which is expressed as follows:

$$TOC^0 = \frac{TOC^x}{0.64} \tag{1}$$

where TOC^0 is original TOC, TOC^x is present day, measured TOC (both measured in wt%),

and 0.64 is the conversion factor used to account for the 36% decrease in TOC (Jarvie et

al. 2005). An equation for the restoration of S2 was also derived as follows:

$$S2^0 = \left(\frac{TOC^0 - TOC^x}{0.083}\right) + S2^x \tag{2}$$

where $S2^0$ (mg HC/g rock) is the restored S2 value and $S2^x$ (mg HC/g rock) is the present

day, measured value of S2. The value of 0.083 is the average percentage of carbon in

hydrocarbons, used as a conversion factor to convert TOC from wt% to mg of

hydrocarbon/g rock (ppt) (Jarvie et al. 2005). By deriving the loss of TOC, and adding the

present-day value, $S2^0$ is calculated. Since HI is the product of the S2 divided by TOC,

initial HI can then be calculated by:

$$HI^0 = \left(\frac{S2^0}{TOC^0}\right) * 100 \tag{3}$$

where HI^0 is the restored, original HI value. Finally, the calculation of HI^0 allows for the

calculation of the transformation ratio (TR), that is, the amount of kerogen transformed

into hydrocarbons:

$$TR = \left(\frac{HI^0 - HI^x}{HI^0}\right) * 100 \tag{4}$$

3.3.1.2   Jarvie (2012) TOC Restoration Method

Jarvie improved upon on the original equations set out in 2005 by considering

additional variables and produced mass balance equations to calculate TOC^0. The author

explains that TOC measurements completed by LECO TOC analysis may include

additional organic matter from oil or bitumen that may not have been removed prior to

analysis (Jarvie 2012). Ideally, bitumen and oil-free TOC is composed of generative (or

reactive) organic carbon (GOC), which has enough hydrogen to generate hydrocarbons,

and non-generative (or inert) organic carbon (NGOC), which does not produce

significant amounts of hydrocarbon. The decomposition, with increasing thermal

maturity, of GOC produces hydrocarbon. Therefore, rocks with high thermal maturity

are dominated by NGOC and have little to no GOC remaining (Jarvie 2012).

The derivation of TOC^0 often requires the knowledge or estimation of HI^0. If

immature samples, which have not lost hydrogen due to hydrocarbon generation, are

unavailable, HI^0 must be estimated. This project utilized the values in Table 3-4,

according to kerogen type, as estimates of HI^0 when immature samples were not

available. The minimum and maximum HI^0 were used, with the resulting TOC^0 results

averaged to obtain the final value. Once this value was attained, the percent of GOC

could then be calculated. This equation assumes that hydrocarbons comprise 85%

carbon. The reciprocal of this value can then be used to calculate %GOC as follows:

$$\% \ GOC_{in \ TOC} = \left(\frac{HI^0}{1177} \right) * 100 \qquad\qquad (5)$$

where 1177 mg HC/g TOC is the reciprocal value (1/0.085), indicating the maximum

potential of HI^0 (Jarvie 2012). The calculated value represents the percent of TOC that

has the potential to generate hydrocarbons.

With LECO TOC analysis, measured values of S1 and S2 can be used to derive the

bitumen, oil and kerogen free TOC value. This is calculated though the subtraction of the

carbon held in S1 and S2 from the measured TOC, expressed as:

$$TOC_{bkfree}^{x} = TOC^{x} - (0.085 * (S1^{x} - S2^{x})) \tag{6}$$

where TOC^{x}_{bkfree} (wt%) is the present-day bitumen and kerogen free TOC value, TOC^{x},

$S1^{x}$, and $S2^{x}$ are measured, present day values and 0.085 is the percent of carbon

making up the hydrocarbons (Jarvie 2012). The author further modified this equation,

considering the formation of carbonaceous char (solid residue) from bitumen or oil

cracking in carbonaceous material, resulting in the updated equation:

$$TOC_{bkfree}^{x} = TOC_{bkfree}^{x} - (HI^{0} * 0.0008) \tag{7}$$

where 0.0008 is the derived value to account for increase char formation (Jarvie 2012).

With this corrected present-day value, TOC^0 (wt%) is then calculated though the

following equation:

$$TOC^{0} = \frac{TOC_{bkfree}^{x}}{(1 - \frac{\% \, GOC}{100})} \tag{8}$$

This equation divides the corrected bitumen and kerogen free, measured TOC value by

the percent of NGOC to obtain TOC^0.

With the derivation of TOC^0, the author then rearranged the equations to

calculate for restored GOC (GOC^0):

$$GOC^0 = \left(TOC^0 * \left(\% \frac{GOC}{100} \right) \right) \qquad (9)$$

where GOC^0 (wt%) is calculated from the multiplication of restored TOC by the percent

of GOC, as well as restored NGOC (NGOC^0):

$$NGOC^0 = TOC^0 - GOC^0 \qquad (10)$$

This equation is a simple mass balance equation as TOC is comprised of GOC and NGOC.

Finally, a calculation for initial generation potential (S2^0) was derived:

$$S2^0 = \frac{GOC^0}{0.085} \qquad (11)$$

where the S2^0 (mg HC/g rock) is the quotient of the original generative organic carbon

and the 85% carbon ratio in hydrocarbons (Jarvie 2012). These updated, mass balance

equations are more specific and provide a more accurate result than the empirical

calculation in Jarvie et al. 2005.

3.3.1.3   Peters et al. (2005) TOC Restoration Method

Peters et al. (2005) used an alternative approach to determine TOC^0. The first

step in the restoration is to calculate the fractional conversion of organic matter to

petroleum. Once again, the HI^0 was assumed, based on kerogen type, from Table 3-4,

following the method outlined above. The equation was derived as follows:

$$F(\text{Factor Conversion}) = 1 - \left(\frac{HI^x * \dfrac{1200 - HI^0}{1 - PI^0}}{HI^0 * \left(1200 - \left(\dfrac{HI^x}{1 - PI^x}\right)\right)} \right) \tag{12}$$

where HI^x and HI^0 are, once again, the present day and initial HI values and PI^x and PI^0 are the measured, present day and initial PI values. The value of 1200 was derived from the assumption that hydrocarbons comprise 83.33% carbon (Peters et al. 2005). In this publication, and for this project, PI^0 is assumed to be 0.02, the value of a thermally immature source rock. With the conversion factor established, a mass balance equation was used to calculate TOC^0 (wt%) by:

$$TOC^0 = \frac{83.33 * HI^x * TOC^x}{\left(HI^0 * (1 - F) * \left((83.33 - TOC^x)\right) + (HI^x * TOC^x)\right)} \tag{13}$$

Once again, the value of 83.33 is the assumed percentage of carbon within generated hydrocarbons. With the knowledge of TOC^0, the authors were then able to calculate the free hydrocarbons expelled from the source rock ($S1_{expelled}$) (mg HC/g rock), as follows:

$$S1_{expelled} = \frac{1000 * (TOC^0 - TOC^x)}{83.33 - TOC^x} \tag{14}$$

where the difference in TOC is divided by the generation potential to identify prior generation, as well as the expulsion efficiency (Peters et al. 2005). The expulsion efficiency, measured in %, combined the fractional conversion with the production index, that is, the estimation of maturity from measured RockEval data, to measure how efficient the source is at generating hydrocarbons. The equation is expressed as:

$$\text{Expulsion Efficiency} = \left(1 - \frac{(1-F)*\left(\frac{\text{PI}^\text{X}}{1-\text{PI}^\text{X}}\right)}{F+\left(\frac{\text{PI}^0}{1-\text{PI}^0}\right)}\right) * 100 \qquad (15)$$

where F is the conversion factor, and PI$^\text{X}$ and PI^0 are the present day and initial

production index values respectively (Peters et al. 2005).

3.3.2 Wireline TOC Determinations

A comparison of different wireline logs can be used to estimate TOC content

within any stratigraphic interval. Wireline logs are continuous measurements of rock

properties within a borehole (e.g. Rider and Kennedy 2011; Schlumberger 2015). These

properties include the density, resistivity, or gamma radiation emitted from a rock. The

four key log types used throughout this project are the gamma ray, density, resistivity,

and sonic logs (e.g. Passey et al. 1990; Issler et al. 2002). Together these logs allow for

the completion of the methods reviewed below.

3.3.2.1 Gamma Ray Logs

Gamma logging tools measure the naturally occurring radioactivity of a rock. This

radioactivity is measured in American Petroleum Institute(API) units which displays the

measurements in terms of gamma ray intensity. The common scale for the gamma ray is

0 to 150; 0 representing the low intensities and 150 representing the high. The radiation

measured is emitted from the naturally occurring uranium, thorium and potassium (e.g.

Rider and Kennedy 2011). Gamma ray logs are used in lithology identification. Fine

grained sediments often generate high natural gamma radiation due to the increased

presence of potassium in the clays and thus measure higher API intensities. Clean

sandstones or limestones, that is, high quartz or carbonate content, typically measure

low API intensities. Recognition of this range allow for lithological identification (e.g.

Rider and Kennedy 2011).

3.3.2.2   Resistivity Logs

The resistivity logging tool measures a rock's ability to conduct (or resist)

electricity and is measured in ohm-m. The more difficult it is to pass a current through

the rock, the higher the resistance (its resistivity). Much of the fluids and minerals that

the subsurface rocks are composed of are highly resistive, however, salt water, the most

common formation fluid, is not. Because of this, it is often the fluid in the pore space

that controls the resistivity log; most importantly, water (e.g. Rider and Kennedy 2011).

When the rock has a high porosity, and is full of highly conductive saline formation

water, there will be an overall low resistivity reading in the log. Hydrocarbons, however,

are highly resistive and will cause a higher resistivity measurement if hydrocarbon is

infilling the pores, in both reservoirs or mature source rocks. High resistivity can also

indicate low-porosity rocks such as tight sandstones, limestones, and salt/evaporites

(e.g. Rider and Kennedy 2011).

3.3.2.3   Sonic (Acoustic) Logs

Sonic logging tools measure the acoustic properties if a rock. The tool sends a

seismic wave from a transmitter at the top of the tool through the subsurface and

measures the travel time to a receiver at the base of the tool. The time it takes for

these waves to reach the receiver is measured in microseconds per meter (or foot). The

inverse of this value is the rock's velocity, allowing the sonic log, in conjunction with a

vertical seismic (checkshot) survey, to be used in tying wells to seismic data via a

synthetic seismogram (reviewed in Section 4.2.2) (e.g. Rider and Kennedy 2011).

3.3.2.4 Density Logs

Density logging tools measure the bulk density of a rock through the bombardment of the formation with gamma rays. Most of these gamma rays are absorbed by the matrix and fluids of the formation. The gamma rays that are not absorbed or scattered are detected at the base of the tool. The gamma rays detected are inversely proportional to the electron density of the rock, therefore electron density is then proportional to the actual density of the rock itself. This log is most commonly measured in gm/cc or Kg/m^3. Each rock type has a typical range of densities, dependant on variables such as compaction, pore fluid and porosity, which allow for the general identification of lithologies (e.g. Rider and Kennedy 2011).

3.3.2.5 Passey TOC Method

One of the most common wireline TOC estimation methods is known as the "Passey Method" (Passey et al. 1990). This method analyzes source rock both qualitatively, by identifying source intervals, and quantitatively, by calculating a TOC value. It is utilized by overlaying and scaling the sonic and resistivity logs, so that the relative scale of the sonic log is -328 µs/m per two logarithmic resistivity cycles. The curves are then normalized, or baselined, where the logs overlay
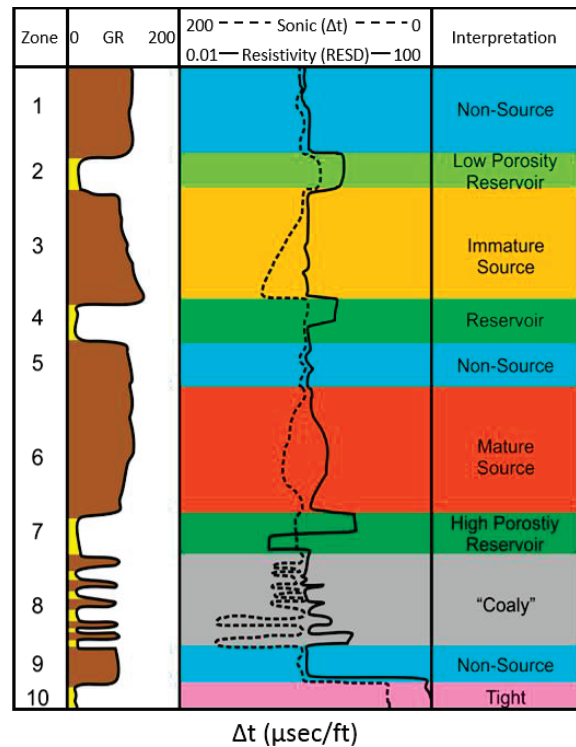
Figure 3-2: Schematic for interpretation of the Passey Method with corresponding equations (modified from Passey et al. 1990).

34

each other in fine-grained, non-source intervals (Figure 3-2 - blue intervals), with a

baseline value obtained for the resistivity and sonic logs to be used in the following

equations (Passey et al. 1990). In practice, this baseline was estimated visually for each

non-source shale interval in a formation or member and averaged to obtain a single

value for that interval. An example of this visualization can be seen in Figure 3-3, where

the red box outlines an overlying interval in a fine grained, non-source interval.
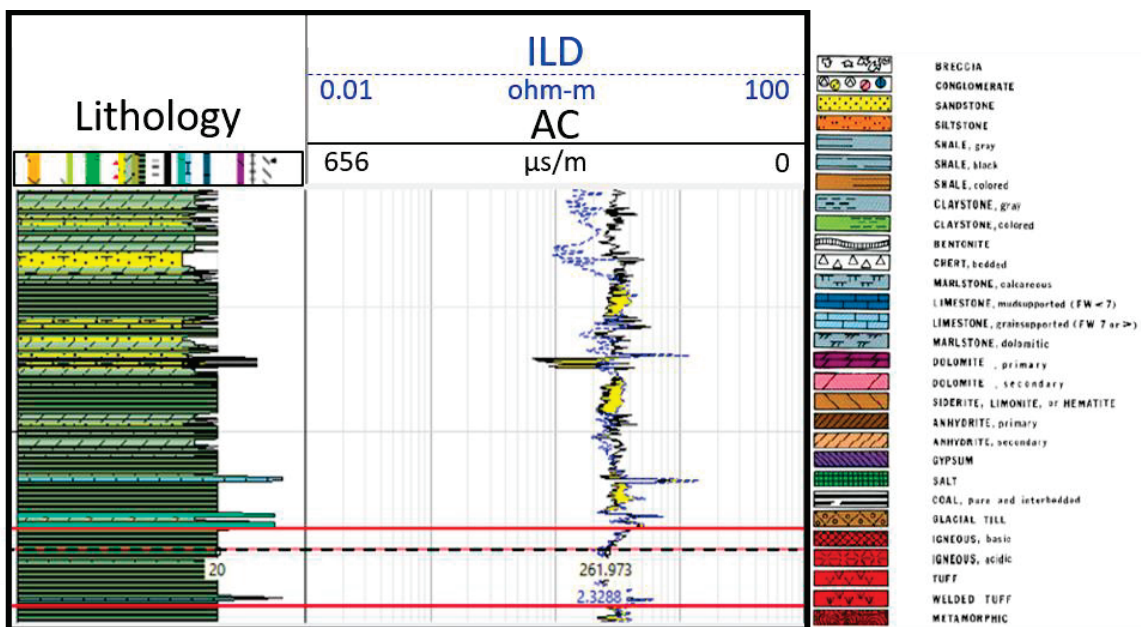
*Figure 3-3: Visual estimation of a sonic and resistivity baselined interval in the South
Venture O-59 well with the corresponding sonic and resistivity values.*

This method assumes that non-source rocks comprise two components; the

matrix and the fluid filling pore space (commonly saline water). An organic-rich source

rock will then contain matrix, pore fluid, and organic matter. As a source rock matures,

hydrocarbon will begin to fill in the pore space and displace the water (Passey et al.

1990). A schematic of this can be seen in Figure 3-4.
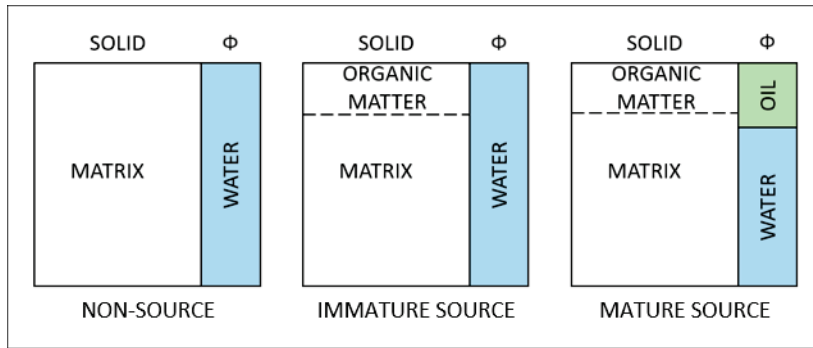
Figure 3-4: Schematic depicting fluid and solid components in both source and non-source rocks (modified from Passey et al. 1990).

Once a baseline is established, organic-rich source rocks can be identified by observing the separation of the log curves. This separation, termed ΔLogR, is linearly related to the TOC content and is dependent on a rocks thermal maturity (Passey et al. 1990). The empirical equation used to calculate ΔLogR is expressed as:

$$\Delta\text{LogR} = \log\left(RESD/_{\text{RESDbase}}\right) + 0.02 * \frac{(\Delta t - \Delta\text{tbase})}{3.281} \tag{16}$$

where RESD and RESD$_{base}$ are the resistivity value and resistivity baseline (measured in ohm*m) and Δt and Δt_{base} are the sonic travel time and sonic baseline (measured in μs/m). The units of these factors cancel each other out, leaving ΔLogR unit-less. The value of 0.02 is a scaling factor based on the -164 μs/m per one logarithmic cycle of resistivity ratio applied to the logs and 3.281 is the conversion factor from μs/ft to μs/m (Passey at al. 1990).

As ΔLogR is linearly related to TOC, an additional empirical equation was derived by the authors to calculate TOC in clay-rich rocks. However, this can only be completed if the maturity of the rock is known or estimated. This method measures maturity in level of organic metamorphism (LOM) units. Once determined, TOC (wt%) is calculated, dependant on ΔLogR, for a known LOM (Passey et al. 1990):

$$TOC = \Delta\text{LogR} * 10^{(2.297-(0.1688*LOM))} \tag{17}$$

36

As per Passey et al. (1990), the calculated TOC values must be compared to measured TOC values for calibration to ensure accurate quantitative results. In this project, estimated TOC values were scaled in attempt to achieve a more accurate fit with the measured TOC values. This was done by modifying Equation 17 as follows:

$$TOC = (SF * (\Delta\text{LogR} * 10^{(2.297-(0.1688*LOM))})$$ (18)

where SF is the scaling factor or multiplier applied to the estimation.

3.3.2.5.1 Estimation of LOM

The level of organic metamorphism (LOM) is a continuous, numerical scale which is used to describe the progression of thermal metamorphism of organic matter during burial. This scale is used measure the entire thermal history of a rock, scaled 1-20, including the generation and destruction of hydrocarbons (Hood et al. 1975). This classification was created based on the traditional coal rank, allowing for the correlation with other scales of organic metamorphism (Figure 3-5). With the goal of estimating a source rock's LOM from observed burial history, Hood et al. (1975) derived a relationship between temperature and time of hydrocarbon generation, in sedimentary rocks, specifically within the 9-16 LOM range.

Figure 3-5: Comparison of LOM to a traditional coal rank (Hood et al. 1975).

This relationship requires accurate formation temperatures (T_{max}) to ensure accurate estimates (Hood et al. 1975).

This relationship allowed for the estimation of LOM using vitrinite reflectance (Ro%), thermal alteration index (TAI), or T_{max} values. Passey et al. (1990) stated that, if the maturity (LOM) is incorrectly estimated, the vertical variability in TOC will still be correctly represented. LeCompte et al. (2010) derived the following equation to estimate Ro% from LOM based on Hood's (1975) data set (Figure 3-6Figure 3-6):

$$\% R_o = -0.0039(LOM)^3 + 0.1494(LOM)^2 - 1.5688(LOM) + 5.5173 \quad (19)$$

where %Ro is the vitrinite reflectance and LOM is the level of organic metamorphism. The inverse of this equation:

$$LOM = 0.897(\%Ro^3) - 4.7202(\%Ro^2) + 10.914(\%Ro) + 3.4139 \quad (20)$$

was used in this project to estimate LOM from Ro% data. The %Ro data used in this equation was derived from the relationship between the measured %Ro data and depth. This relationship, calculated for each well, allowed for a %Ro value to be calculated at any point within the studied interval. The sources of the %Ro values for each well can be found in Appendix B.
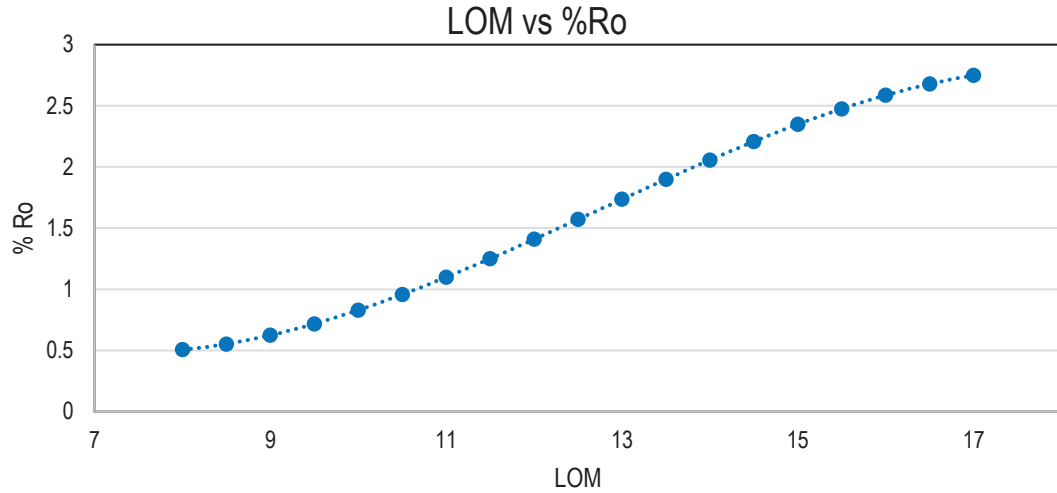
Figure 3-6: Relationship used to derive the equation to convert LOM to % Ro (LeCompte et al. 2010, modified from Hood 1975).

3.3.2.6 Issler TOC Method

The Issler cross-plot method was applied as a second method of wireline TOC estimation (Issler et al. 2002). This method uses the relationship between the bulk density and resistivity logs, as well as the sonic and resistivity logs, similarly to the Passey Method. However, Issler's model includes rock characteristics (mineral matrix, organic carbon, pore fluid) and physical parameters, derived from wireline and geochemical data (Figure 3-7). Each of the models in Figure 3-7 assume that the measured wireline data are function of TOC content, lithology and an unknown parameter, θ, representing porosity. These cross-plots allow for the estimate of TOC directly from log data, without the need for subjective user input such as the level of organic maturity (LOM) or log normalization (Issler et al. 2002). TOC estimation from the sonic and resistivity logs is as follows:

$$TOC = 0.0714 * (\Delta t + 195 * \log(R_{fm})) - 31.86 \tag{21}$$

where Δt is sonic travel time (μs/m) and R_{fm} is formation resistivity (ohm-m). Similarly, the equation using bulk density is:

$$TOC = -0.1429 * \left(\frac{\rho_b - 1014}{\log(R_{fm}) + 4.122} \right) + 45.14 \qquad (22)$$

where ρ_b is the rocks bulk density (kg/m^3) (Issler et al. 2002).
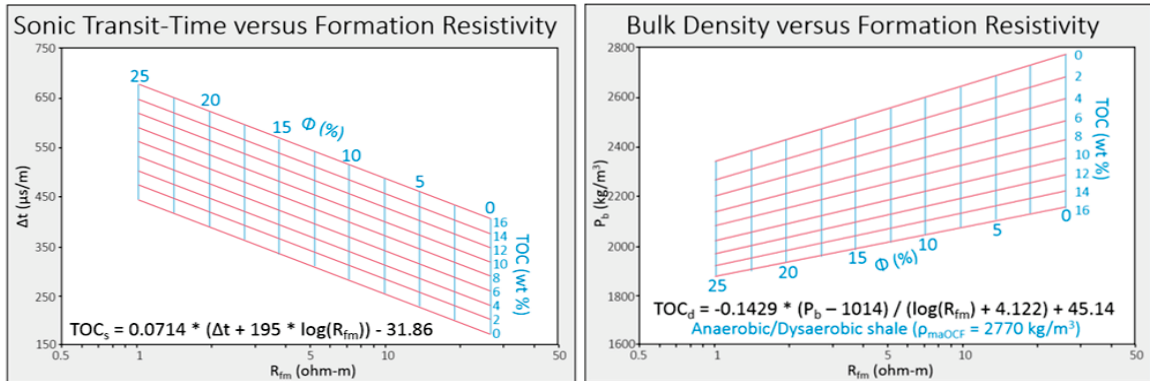
Figure 3-7: Formation resistivity vs sonic and resistivity vs bulk density cross-plots (modified from Issler et al. 2002).

3.3.2.7 Limitations & Quality Control

There are numerous limitations to these methods and special consideration and analysis was completed to ensure accurate estimates. Many of these limitations have been outlined by Passey et al. (1990). First and foremost, without core derived TOC values (TOC wt. %) or vitrinite reflectance data (%Ro), the LOM cannot be calculated or calibrated, thus TOC% will be skewed. In addition, small organic rich intervals, less than 0.5 m thick, cannot be accurately estimated (Passey et al. 1990).

Reservoir intervals can cause anomalous ΔLogR separation due to the presence of hydrocarbons in the interval, which increases the resistivity. Anomalous separation can also be observed in zones of low porosity, less than 3%, due to an increase in resistivity due to lack of conductive fluid, as well as intervals of both intrusive and

extrusive igneous rocks (Passey et al. 1990). Additionally, uncompacted sediments often have much longer sonic travel times, which creates poor correspondence between the resistivity and sonic curves. Finally, evaporates commonly have very high resistivity which cause anomalous ΔLogR separation, therefore you cannot distinguish between organic rich shale intervals and carbonates without the use of a gamma ray or lithology log (Passey et al. 1990). It is also important to note that the Issler Method is calibrated specifically to the Cretaceous shales of the Northwest and Central Plains of the Western Canadian Sedimentary Basin (Issler et al. 2002).

Further quality control was completed identifying possible sources of error within the method. Well log data, RockEval pyrolysis, and drilling practices all have an associated error that can affect the results of the method. There is added uncertainty associated with the RockEval measurements. In the Sable Sub-Basin, these measurements are commonly derived from cuttings, instead of the more ideal (due to pureness of sample) cores and sidewall cores. On a broad scale, the comparison between TOC measurements from cuttings and Passey calculated TOC can vary greatly due to factors such as drilling rate, quality control of the cuttings and borehole quality (Passey et al 1990). Drilling mud types and mud additives, such as oil based muds or lignite, can drastically skew the RockEval data (e.g. Mukhopadhyay and Birk 1989). The addition of lignite would not only change the weight of the sample, but add additional organic carbon that is not native to the rock being tested, therefore skewing the data. For example, the South Venture O-59 well has been noted to have extensive lignite contamination. A cutting sample from 6115m contain 40-50 % vitrinite and 10-20%

exinite from the lignite contamination alone. Lignite contamination was concluded to

have distorted the geochemical data (Mukhopadhyay and Wade 1990). The same could

be said about the use of oil-based muds. Furthermore, many intervals in the well are

turbo-drilled. This produces smaller particles which allow for additional contaminants

from other intervals, the drill, pipes, etc. to be included, which in turn can then skew the

weight percent calculations of the RockEval method. According to Passey et al. (1990), if

the cutting collecting interval is three meters or less, and the well bore is in good

condition, an adequate agreement, often within the same order of magnitude, can be

achieved (Passey et al. 1990). Examination of the well reports for the wells used in this

project show that these ideal wellbore conditions and sampling rates are not the norm.

This meant that the relationship between these two variables was not ideal in this

project. The uncertainties associated with each well are outlined Section 4.1.2.12.

3.3.2.8   Sonic/Resistivity Cross-plotting

As outlined above, both sonic and resistivity logs react in specific ways to specific

lithologies. When the values from these logs are cross-plotted, regardless of lithology,

they typically display high sonic transit times and low resistivities, due to un-compacted

or under-compacted sediments, at shallow depths. As depth increases, sonic transit

time will decrease and the resistivity will increase as the rocks become more competent

(e.g. Meyer et al. 1984; Ryder and Kennedy 2011). Mature source rocks, as discussed by

Meyer et al. (1984) based on source rocks world wide, have increased resistivity, do to

the resistive hydrocarbons within the rock. Additionally, source rocks have increased

sonic travel time due to the presence of organic matter. These phenomena allow for the

identification of source as it creates a deviation from the general "wet compacted

sediment trend", that is, source rocks plot on the right-hand side of the trend (e.g.

Meyer et al. 1984; Ryder and Kennedy 2011). An example of this deviation, as derived

by Meyer et al. (1984), is seen in Figure 3-8. This method was used in this project by

simply visually estimating the sediment compaction trend in an attempt to visually

identify possible source intervals within the studied section.
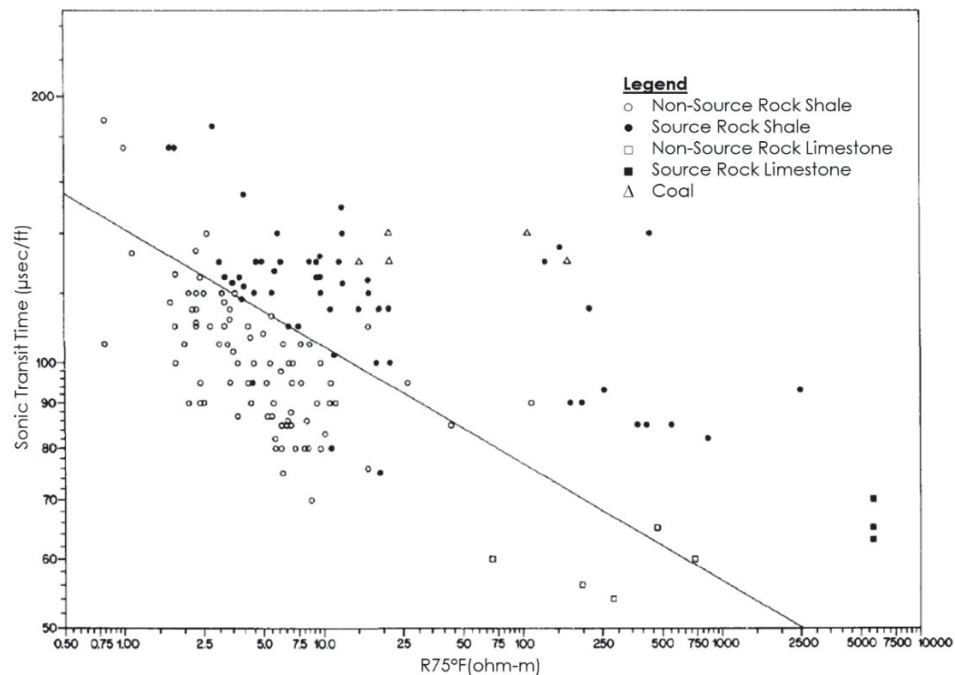
Figure 3-8: Cross-plot of sonic transit time versus resistivity at 75° F (23.9° C) consisting of samples from prolific source rocks from 15 wells located in 9 different countries (Meyer et al. 1984).

3.4   Seismic Methods
3.4.1   Principles

Seismology is the study of elastic (seismic) waves and how they interact with the

rocks within the Earth's subsurface. Seismic waves are transmitted as compressional (P)

waves, which move laterally or longitudinally, and shear (S) waves, which move

transversely. Frequencies of these waves can range from 1 to approximately 100 Hz,

however typical marine seismic encompasses approximately 5- to 65 Hz (e.g.

Schlumberger 2015). This range is known as the seismic bandwidth.

Seismic waves travel though the earth at specific velocities which are controlled

by factors such as lithology, pore fluid and compaction (e.g. Burger et al. 2006).

Reflection seismology is a common way of studying seismic waves. As a seismic wave

interacts with an interface between rocks of differing acoustic impedances, that is, rocks

with different velocities and densities, a fraction of the wave will be reflected while the

rest is transmitted through the rock. The reflected waves are recorded and processed to

produce a seismic reflection image. The contrast between acoustic impedances is

directly correlatable to the strength of the seismic reflection; the higher the acoustic

impedance contrast, the stronger the reflection (e.g. Burger et al. 2006). This contrast is

known as a reflection coefficient and can be calculated as follows:

$$R = \frac{\rho2v2 - \rho1v1}{\rho2v2 + \rho1v1} \tag{23}$$

In this equation R is the reflection coefficient, $\rho1$ and $\rho2$ are the densities and v1 and v2

are the velocity of the first and second layers respectively (e.g. Burger et al. 2006).

3.4.1.1 Acoustic Impedance

Acoustic impedance (AI) is the product of a rock's density and the velocity of a

seismic wave through that rock (Becquey et al. 1979). The AI varies among different rock

layers due to the changing densities and velocities of the different layers of strata (Table

3-6). There are many factors that can affect the AI of a rock, including lithology,

compaction, porosity, and cementation (e.g. Barber 2001). In shallow rocks, sands

typically have a lower AI than that of shales. However, with increasing depth and

compaction, there is a distinct polarity reversal and shales then has a lower AI than

sands (e.g. Brown 2004). This general trend can be seen in Figure 3-9.

Table 3-6: Average range of density, velocities and acoustic impedance (e.g. Glover n.d.; EduMine 2016).

Rock Type	Density (g/cm^3)	Velocity (m/s)	Calculated AI (kPa s/m)
Compact Sandstone	2.2 - 2.8	5490 - 5950	12078 - 16660
Limestone	2.3 - 2.7	6400 - 7010	14720 - 18927
Dolomite	2.8 - 2.9	7010 - 7920	19628 - 22968
Anhydrite	2.9	6096	17678.4
Halite	2.5 - 2.6	4572	11430
Shale	2.4 - 2.8	1790 - 5805	4296 - 16254
Bitumous Coal	1.1 - 1.4	2180 - 3050	2398 - 4270
Lignite	1.3	1690 - 2180	2197 - 2834
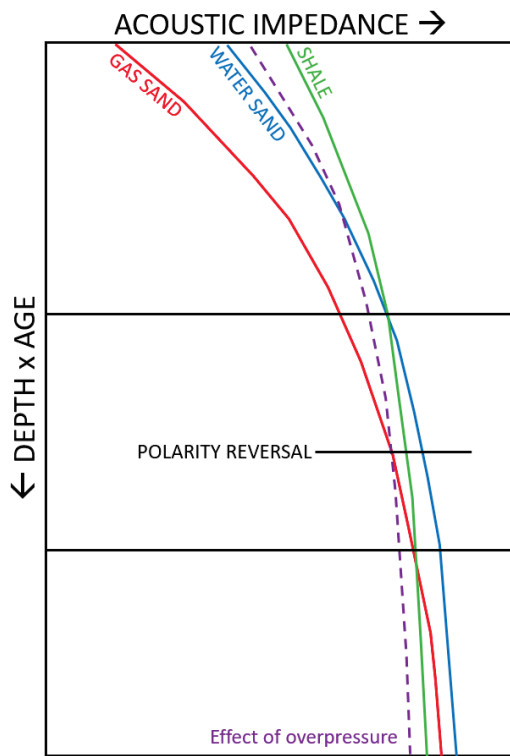
Figure 3-9: Changes in acoustic impedance of shale, wet sand and reservoir with depth and overpressure (modified from Brown 2004).

3.4.1.2   Seismic Resolution

Seismic resolution describes the ability to distinguish separate features within

seismic data. That is, minimum distance between two bodies that both features can still

be identified before they appear as one (e.g. Meckel and Nath 1977; Sherriff 1997).

Resolution of seismic data is measured in both vertical and horizontal directions. In the vertical sense, based on the wedge model shown in Meckel and Nath (1977 - Figure 3), an approximately 20 Hz wavelet will have an approximate tuning thickness of 20 ms. Above tuning, interfaces are fully resolved, i.e. the isochron between the top and base reflections are directly proportional to the isochore. Below tuning, bed thickness is proportional to the amplitude and the bed is said to be detectable but not resolved, that is, the same interval could be modeled by a single interface (Meckel and Nath 1977). This quantification of vertical resolution is often known as the Rayleigh limit of resolution (e.g. Sheriff 2002). Given that the average seismic velocity ranges from 2000 to 5000 m/s, and the average acquisition frequency 20-50 Hz, the average vertical seismic resolution in offshore data ranges from 10 to 62 m. Ideal seismic resolution is obtained from higher frequencies or shorter wavelengths (Sheriff 1997).

Horizontal resolution of seismic data is controlled by what is known as the Fresnel zone (Fz). Simply put, this is a zone in which seismic waves constructively interfere with each other and occurs when their paths differ by less than half a wavelength. When this happens, arrival times of the waves are detected as a single unit. This zone most often occurs as circle with a set radius (e.g. Sheriff 1996). This radius, and the horizontal resolution of the seismic data, can be quantified through the following equation:

$$Fz = v(\frac{t}{f})^{0.5} \tag{24}$$

where v is velocity, t is time and f the frequency of the seismic data.

3.4.2   Seismic Interpretation

Seismic interpretation was completed on the eastern portion of the Sable

MegaMerge, outlined in Figure 1-3, within the Schlumberger Petrel™ software. The

project described here started with preloaded wells, check shots, GSC formation tops,

auxiliary well data and seismic data, as well as some horizons and faults which came

from a continually updated collective project in the Basin and Reservoir Lab at Dalhousie

University. The well data included CanStrat and Divestco logs. The CanStrat logs contain

information about lithology, color, fossil content, porosity, and hydrocarbons

occurrences, while the Divestco wireline logs are acquired during the drilling operations.

Horizons and faults have been previously interpreted across parts of the Sable

MegaMerge data cube (notably project work by Bill Richards (personal communication

(2017)) and Carla Skinner (2016) among others) and these were used as a reference

base for interpretation for this project, however all faults and the majority of the

horizons (excluding the Venture carbonates) were reinterpreted to ensure a complete

understanding of how the geology changed throughout the study area. Although these

faults and horizons are new, changes from the reference data were minor.

A 3D model of the structure and stratigraphy (known in Petrel as the

"framework") was developed in the study area. Horizons and faults were picked and

modeled over the entire MegaMerge Survey. The interpreted horizons marked the

locations of the upper boundaries of the formations (formation tops), defined according

to the standard lithostratigraphic scheme for the Scotian Basin (e.g. Wade and MacLean,

1990; Weston et al. 2012; NRCan 2016). These lithostratigraphic surfaces often

correspond to major lithological variations producing a sharp change in seismic characteristics, enabling them to be imaged as discrete surfaces (horizons) and traced through the study area. This interpretation was completed using a combination of both manual, 2D and 3D autotracking, which follows a picked surface within a defined distance. Though only the Middle and Upper Jurassic interval was of interest, important formations through the entire seismic survey were interpreted.

Once horizon and fault interpretations were completed, the faults were imported to a 'fault model' section of a newly created Petrel model. The faults were then pillar gridded, where an *a priori* geocelluar grid was created such that grid boundaries lay on pillar gridded faults (in a non-Cartesian 'IJK' grid). All faults were extended to the O-marker and to -5000 ms to ensure the grid captured the interval of interest. Fault pillars were checked and edited to remove areas that touched or crossed over one another or became heavily distorted during test pillar gridding. A few antithetic faults were also removed as they distorted the grid too extensively.

The interpreted horizons were imported into the geocellular model; further modifying the IJK grid. The horizons control the grid boundaries. The horizons and faults form a structural and stratigraphic framework that was then used as input to the inversion. The modeled faults and horizons were also used to create three cross-sections of the study area, chosen to model the geology through key wells in the basin. The inlines chosen model the NNW-SSE trending expansion trend of the basin.

3.4.3   Seismic Inversion

Seismic inversion is a mathematical procedure that uses a 3D seismic survey and wireline log data as input data to create a meaningful geologic boundary model of the subsurface as an output (Veeken et al. 2004). There are different types of seismic inversion which investigate different parameters. This project completed an AI seismic inversion through a progression of set steps known as the InverTrace^PLUS workflow available within CGG Jason software (donated to Dalhousie University and Professor Grant Wach Principal Investigator). The Jason software utilized a constrained sparse spike (CSSI), deterministic inversion approach. As described by Campbell et. all (2015), CSSI is a form of General Linear Inversion (GLI). General linear inversion is a widely used method applied to both pre- and post-stack seismic data. It is a deterministic approach to inversion, which requires a single wavelet estimation to produce a single inversion output (Cooke and Cant 2010). According to Cooke and Cant (2010), a deterministic approach is preferred for a post-stacked inversion when it will be used for stratigraphic interpretation and testing for hydrocarbon presence. This approach outputs only the best-fit model for the data provided (Cooke and Cant 2010). This approach was chosen based on the type of seismic data (post-stack), as well as its availability of the software. The inversion process is iterative, therefore if the model failed validation of quality control, the inversion method was repeated until a best fit model was generated.

The first step in the InverTrace^PLUS workflow is creating a new project and integrating the required data in the Project Setup step. The wireline logs were quality controlled in Project Feasibility step to insure there was a notable difference in the

49

characteristics of lithology types (sand versus shale) for the inversion to be completed,

as per software requirements (Fugro-Jason 2013). The overall workflow of this method

is detailed in Figure 3-10.
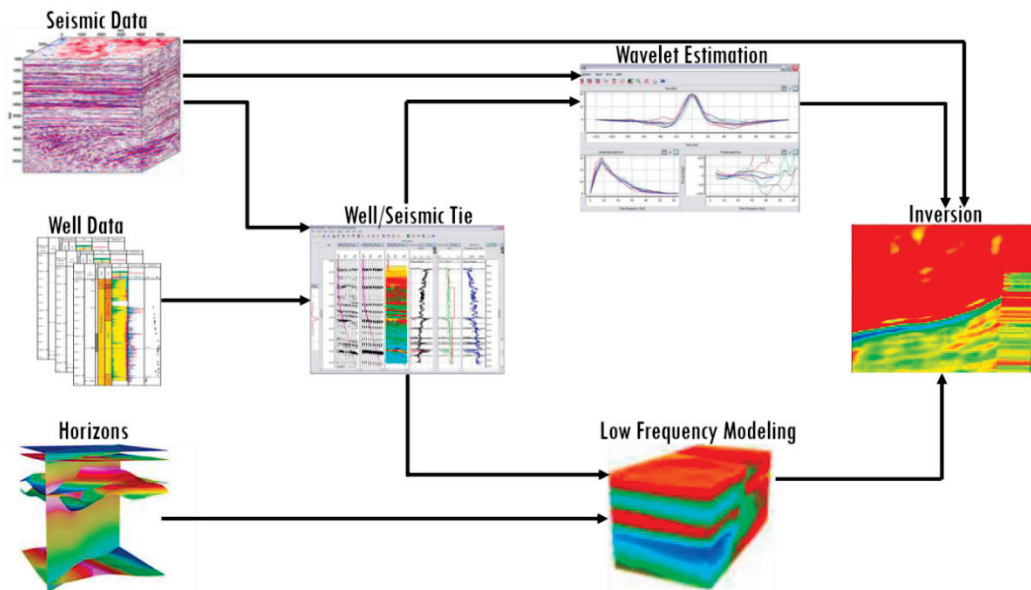
Figure 3-10: A schematic of the InverTrace^PLUS seismic inversion process (modified from Fugro-Jason 2013).

3.4.3.1   Well/Seismic Tie

Once the project was created, a time-to-depth relationship was calculated,

linking the travel time of the seismic to a specific depth. This was completed using the

Backus Averaged method. Simply, this method matched a seismic horizon in time with

corresponding well top in depth by using a harmonic averaging formula to upscale sonic-

log velocity data to create a synthetic seismogram (e.g. Backus 1962). The O-Marker, a

basin-wide carbonate (e.g. Wade and Maclean 1990), was used as the datum or tying

point. Per software limitations set by Fugro-Jason (2013), wells that were too strongly

deviated could not be used, as they can create inaccurate synthetics. Of the 37 wells

within in the study area, 22 exceeded the 100 m deviation limit and were omitted.

Once the relationship was established, synthetic seismograms were created using a simple, zero-phased 25 Hz Ricker Wavelet (common industry default). A wavelet is a one-dimensional pulse of acoustic energy, which is created in response to a reflection change within seismic data (Schlumberger 2015). Minor adjustments were then made by shifting, stretching or squeezing the logs in time. This was completed by aligning the major peaks and troughs to obtain the best fit with the original seismic and well log data. Editing of the logs in this way ensure the velocity used to create the time-depth relationship matches that measured by the sonic log (Fugro-Jason 2013). These alterations were tracked using a TD QC well log, which trends around 1. When this log deviated too far away from the trend, the alteration created unrealistic velocities and was considered over-edited (Fugro-Jason 2013).

3.4.3.2 Wavelet Estimation

Once the wells were converted to time, a wavelet was estimated for each well. Wavelet length, start time, and maximum frequency were input to extract a wavelet corresponding to the well. These variables changed the bandwidth of the estimated wavelet. Four wavelets of varying bandwidths (0–50, 0-55, 0-60, and 0-70 Hz) were tested and quality controlled to identify the best fit for the seismic data by observing the cross-correlations (calculated synthetic vs original seismic) for each well. Fugro-Jason (2013) recommends cross correlations of 50% (0.5) within the studied interval to ensure accurate inversion results.

The individual wavelets extracted at each well were then merged to create the multi-well wavelet for the tested bandwidth. This was used as the single wavelet input

in the inversion process. The program completed this by overlaying and averaging the

wavelets to calculate the multi-well wavelet (Fugro-Jason 2013). Of the 15 usable wells,

a subset of seven undeviated wells were used to test the different bandwidth wavelets.

This process was repeated using all 15 wells to derive the final inversion wavelet.

3.4.3.3   Low Frequency Model

The next step in the InverTrace^{PLUS} workflow was to create a low frequency, and

thus an *a priori*, model. High frequency seismic data allows for the qualitative

identification of geologic boundaries and general lithologies. Low frequencies, however,

allow for a quantitative interpretation, as they translate to rock properties such as

porosity, density and velocity (Kumar et al. 2012). During seismic acquisition, dependant

on the medium, certain low frequencies are not detected and produce a frequency gap.

For marine seismic data, and the Sable MegaMerge dataset, the average bandwidth is

approximately 10-60 Hz, meaning there is a 0-10 Hz frequency gap (e.g. Schlumberger

2015). Creating a low frequency model interpolated the low frequency data from the

well logs and allowed for the closure of this frequency gap. That is, the extracted low

frequency data from the well logs were used to increase the bandwidth to

approximately 0-60 Hz to ensure the best fit to the well log data (Fugro-Jason 2013).

Merging the low frequency model with the geocellular model created in Petrel resulted

in an *a priori* model containing the appropriate bandwidth and data necessary to

complete the inversion.

3.4.3.4   InverTrace Plus Inversion

The InverTrace^{PLUS} Inversion is a CSSI process which was completed in three

steps. To begin, the P-Impedance contrasts were estimated to create the synthetic

seismograms outlined above. Following this, traces of these P-Impedances were created

through the integration of the P-Impedance contrasts. Finally, optimization of the P-

impedance values was completed by merging the low frequency trends from the well

logs (Fugro-Jason 2013). Simply, the inversion isolated the AI by the deconvolution of

the seismic data by the estimated wavelet to produce a 3D model of AI. A schematic of

this is seen in Figure 3-11 (Fugro-Jason 2013).
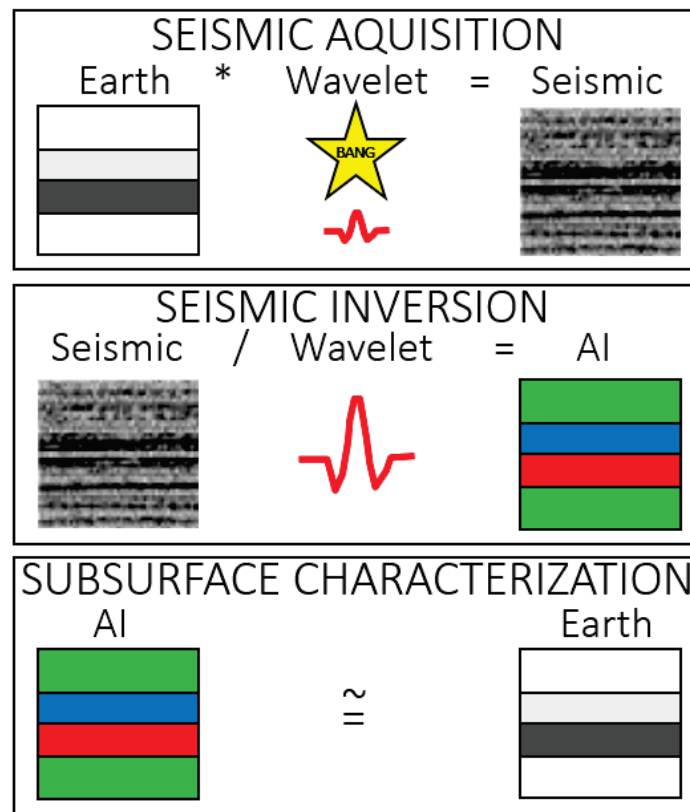
*Figure 3-11 : The process of seismic inversion where * represents convolution and / represents deconvolution (modified from Fugro-Jason 2013).*

To obtain optimal P-Impedance values, the objective function (F_{Ip}) was used to

estimate the P-Impedance contrasts (Step 1):

$$F(Ip) = \text{Fcontrast} + \text{Fseismic} + \text{Ftrend} + \text{Fspatial} \quad (25)$$

where each variable is a function of a misfit which directly control the impedance values and act in equilibrium within the weighted equation (Fugro-Jason 2013). The $F_{contrast}$ function controls the sparseness of the values, that is, keeps the solution as simple as possible to eliminate seismic noise. The $F_{seismic}$ function controls the correlation of the created impedance value to the input seismic data. Finally, the F_{trend} and $F_{spatial}$ functions ensure the solution is constrained within the geology modeled by the seismic (Fugro-Jason 2013).

As discussed in Fugro-Jason (2013), the misfit functions (F) were calculated though a normalized average known as an "L_P Norm". The L_P Norm (L_Px) is derived though:

$$Lp(x) = \frac{1}{\sqrt{\sigma_x}}\left(\frac{1}{n}\sum_{k=1}^{n}(|x_k|)^P\right)^{\left(\frac{1}{P}\right)} \tag{26}$$

where n is the number of samples in the trace and σ is the standard deviation of the samples. Each term was normalized by the sample standard deviation to allow for the use in a single objective function (Fugro-Jason 2013). As per Fugro- Jason (2013), P was a value of 1 or 2. An L1-norm equated to the normalized average of the summation:

$$L_1(x) = \frac{1}{\sqrt{\sigma_x}}\left(\frac{1}{n}\sum_{k=1}^{n}|x_k|\right) \tag{27}$$

where n is the number of samples in the trace and σ is their corresponding standard deviation, and the L-norm to the normalized root mean square (RMS):

$$L_2(x) = \frac{1}{\sqrt{\sigma_x}} \sqrt{\left(\frac{1}{n} \sum_{k=1}^{n} x_k{}^2\right)} \tag{28}$$

The objective function, and the corresponding functions therein, are directly controlled by the inversion parameters. These parameters are known as contrast misfit, seismic misfit S/N, seismic misfit power, wavelet scale and merge cut-off frequency where the $F_{contrast}$ function is controlled by the contrast misfit, the $F_{seismic}$ function is controlled by the seismic misfit S/N ratio, seismic misfit power and the wavelet scale factor and F_{trend} and $F_{spatial}$ functions are controlled by the merge cut-off frequency (Fugro-Jason 2013).

Beginning with the contrast misfit, this parameter added the reflection coefficients of the seismic while subtracting, or normalizing to, the low frequency trend. This was completed though the following equation:

$$F_{contrast} = \frac{1}{u_{I_P}} * L_1(\Delta I_P) \tag{29}$$

where u is the uncertainty associated with the contrast misfit, L_1 is the normalized average and ΔIp is the vertical (time) elastic parameter variance (Fugro-Jason 2013). The seismic misfit, the seismic misfit power and the wavelet scale factor parameters are used together to control the $F_{seismic}$ misfit:

$$F_{seismic} = {}^S\!/_N * L_2(seismic - synthetic) \tag{30}$$

where S/N is the signal to noise ratio (Db) and L^2 is the RMS value. The product of the synthetic seismogram subtracted from the seismic data is known as the residual. The seismic misfit assumes:

$$S = R * W \tag{31}$$

where S is the synthetic seismogram, R is the reflectivity (calculated from the inverted impedance), and W is the wavelet (Furgo-Jason 2013).

The F_{trend} misfit relied on the merge cut-off frequency parameter to stabilize the low frequencies though the following equation:

$$F_{trend} = \frac{1}{u_{T\ Elastic}} * L_2(\Delta P_{lowpass}) \tag{32}$$

where $u_{T\ Elastic}$ is the soft trend misfit uncertainty of the P-impedance and $\Delta P_{lowpass}$ is the low pass filtered P-Impedance trace subtracting the low pass filtered trend. The user defined merge cut-off frequency is simply the frequency of the low pass filter (Fugro-Jason 2013).

Finally, the soft spatial or $F_{spatial}$ misfit was used to control the smoothness of the resulting inversion. This was completed using:

$$F_{spatial} = \sum_{direction} \frac{correlation\ length}{ssu_{P-impedance}} * L_1(\Delta P_1 - \Delta P_{I+1}) \tag{33}$$

where ΔP_1 is the directional impedance change relative to the low pass trend and *ssu* is the corresponding soft spatial uncertainty. In this equation, a small uncertainty over a large correlation length equated to a smoother result (Fugro-Jason 2013).

Once again, these "misfit parameters" act at an equilibrium within a weighted equation; i.e. changing one will affect the others. To ensure these parameters were optimized to the dataset, a quality control (QC) was completed. Each parameter was subjected to five different tests, where each must equal or trend toward a specific value. The parameter value that best matched the ideal QC value in all five tests was used. This test allowed for the observation of the effect of each individual parameter on the inversion (Fugro-Jason 2013). The QC tests observed the signal to noise ratio, well log correlation, well log normalized standard deviation, sparseness, and a combined misfit.

The inverted signal to noise ratio curve, derived from the synthetic and residual data, was compared to that of the input seismic data. A good correlation was found when values were consistent with the input data, having a high signal to noise ratio (Fugro-Jason 2013). The well log correlation parameter represents the cross correlation between the extracted pseudo log and the original well log data. This indicated the accuracy of the inversion at that point, with a value of 1 being a perfect match (Fugro-Jason 2013). The normalized standard deviation of the well logs was also tested. This value represents the standard deviation of the pseudo log divided by the standard deviation of the original well log. This value measured the deviation from the trend and should be as close to 1 as possible (Fugro-Jason 2013).

The sparseness parameter measured the sum of the P-impedance contrasts. Low contrasts indicated an accurate inversion. For the most accurate inversion, the contrasts

should be as low as possible. Finally, the combined misfit parameter measured the

overall performance of all criteria and was kept near zero (Fugro-Jason 2013). A single

value for the tested misfit parameter was extracted where these five tests were as close

to optimal values as possible and used to run the inversion.

3.4.3.5   *Limitations of Constrained Sparse Spike Inversion*

There are limitations surrounding the CSSI seismic inversion process used that

should be noted. Deterministic inversions, such as CCSI, output only a single impedance

property model. The biggest assumption the deterministic inversions make is that the

impedance of the subsurface can be described using a blocky model. The blocky

impedance model approach can allow for the input of possible high frequencies that are

not found within the input seismic data, possibly altering the uniqueness of the

inversion result (Cooke and Cant 2010). Furthermore, if a layer, or layers, are thinner

than the tuning thickness of the seismic, they can appear as one single high amplitude

event (e.g. Meckel and Nath 1977). This means, for any interval thinner then the tuning

thickness, there can be infinite combinations of impedance and thicknesses that can

produce the same seismic amplitude (e.g. Cooke and Cant 2010). Therefore, because

only a single result is derived, it may not be completely unique and may alter key

intervals within the seismic.

Additional uncertainty is added though the addition of the low frequency model.

Once again, the frequency gap of marine seismic data is often 0 to 10 or 12 Hz (e.g.

Mougenot 2005). Within the extrapolation of the low frequencies and absolute

impedance values from the well log data and subsequent interpolation into the model,

it is possible that important low frequency anomalies could be missed if they are not

adequately imaged by the well control (Cooke and Cant 2010). Furthermore, even if the

low frequency models contain this important information, it is possible that the

synthetics they create will look almost identical. Once again, this a non-uniqueness

limitation of a deterministic inversion. However, per Cooke and Cant (2010), this non-

uniqueness is not a problem if the inversion is simply being used to interpret

stratigraphic boundaries.

3.5   Interpretation of Acoustic Impedance Cube
3.5.1   Source Rock from Seismic Method

Løseth et al. (2011) suggested that AI decreases non-linearly with increasing TOC

content; the AI of an organic rich source rock (> 3% TOC) will be significantly lower than

that of its non-organic counterparts. This relationship was extracted though the study of

significant source rocks such as the Kimmeridge Clay in southern England (e.g. Morgans-

Bell et al. 2001) and the Hekkingen Formation in the Barents Sea (e.g. Langrock 2004).

An example of the non-linear relationships derived from the TOC and AI in the

Kimmeridge Clay and Hekkingen Formation shale is seen in Figure 3-12. In this

relationship, the top of a source rock interval is marked by a substantial reduction in AI,

while the bottom is marked by an increase in AI (Løseth et al. 2011).
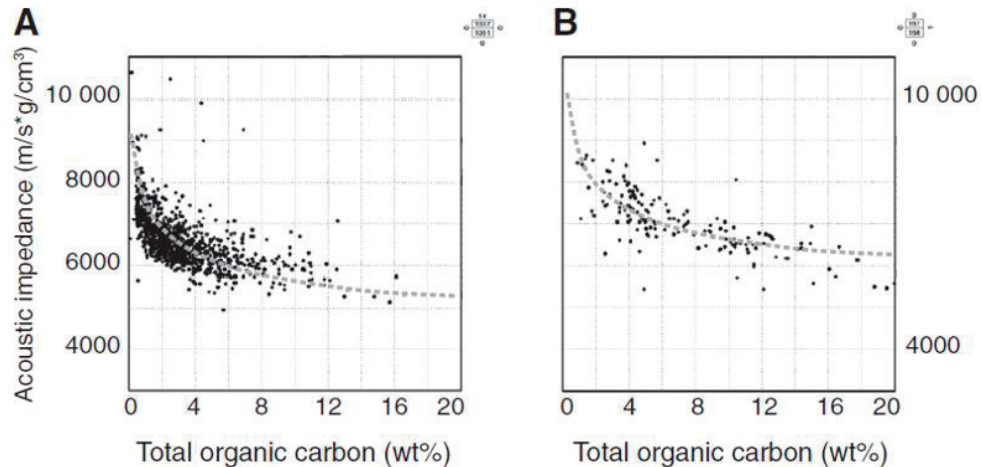
Figure 3-12: Cross-plots of Acoustic Impedance vs TOC depicting a clear non-linear relationship in A) the Kimmeridge Clay, southern England, and B) the Hekkingen Formation in the Barents Sea.

Løseth et al. (2011) suggest that using the derived TOC/AI relationship for a specific source interval, a TOC profile can be generated. These profiles outline the changes in TOC throughout the interval by correlating, and subsequently smoothing, the calculated TOC values with changes in AI to create the TOC profile. Basically, the relationship allowed for the conversion of the AI cube to TOC (Løseth et al. 2011). The AI model can detect changes in AI of approximately 10 m in height, with the resolution supplemented by wireline TOC determinations, such as the Passey Method (Løseth et al. 2011).

In this study, the method was attempted through the whole inverted interval, using all wells with estimated TOC to examine a possible broad scale relationship, followed by individual well correlation throughout the entire inverted interval. Finally, the method was attempted within individual shale intervals in the South Venture O-59 well.

3.5.2 Lithology Extraction

The seismic inversion allowed for a more in-depth identification of lithology within the seismic cube. Based on visual calibration of well ties to the inversion, a simple empirical calibration of AI to lithology was applied (Table 3-7). Lithologies were split into three simple groups; fine grained clastics, coarse grained clastics, and carbonates.

Table 3-7: Acoustic impedance cut-offs for bulk lithology determinations (based on Table 3-6).

Lithology	Acoustic Impedance Range (kPa.s/m)
Fine Grained Clastics	< 10,000,000
Coarse Grained Clastics	10,000,000 – 12,000,000
Carbonates	>12,000,000

Chapter 4:   Results

4.1   *Geochemical and Wireline Methods*

4.1.1   *TOC Restoration*

The three TOC restoration techniques discussed above were completed on the 11 wells listed in Table 3-1. Figure 4-1 summarizes the results for the Jarvie et al. (2005), Jarvie (2012), and Peters et al. (2005) TOC restoration methods tested. They are separated by formation (column) and method (row). The blue line shows the restored TOC with depth, with error bars outlining the maximum and minimum values. These values were derived from the maximum and minimum HI^0 range for the given kerogen type. The empirical Jarvie et al. (2005) method was the most optimistic, as it simply increased each measured TOC value by 36%. The majority of the results from the mass balance methods, Jarvie (2012) and Peters et al. (2005), fall within the error bars, indicating no measurable change in TOC over time.
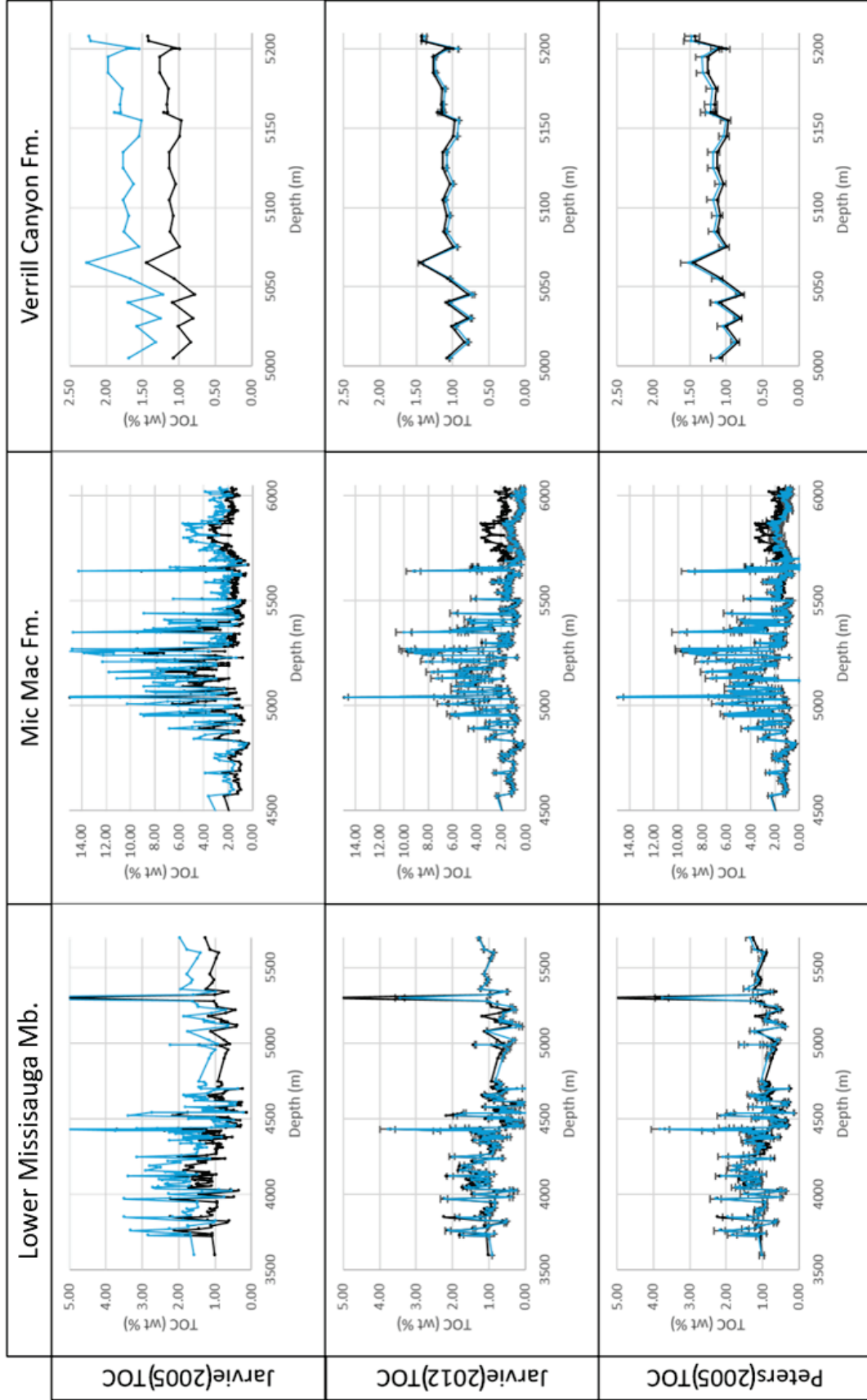
Figure 4-1: TOC Restoration separated by method and formation. The Black line represents the measured TOC and the Blue line the restored values.

63

4.1.1.1   Source Rock Potential

Referring to Table 3-3, source rock potential can be estimated through TOC contents, with potential ranging from poor (<0.5 % TOC) to excellent (>4 % TOC) (Peters et al. 2005). Both the measured and restored TOC values were evaluated using these guidelines. The Jarvie et al. (2005) method (Figure 4-2) represents the most optimistic values, and provided an estimation of source rock potential. Note that most of the measured TOC values above 4% are likely contaminated (Mukhopadhyay 1990a), and restored TOC values for those measurements are skewed.
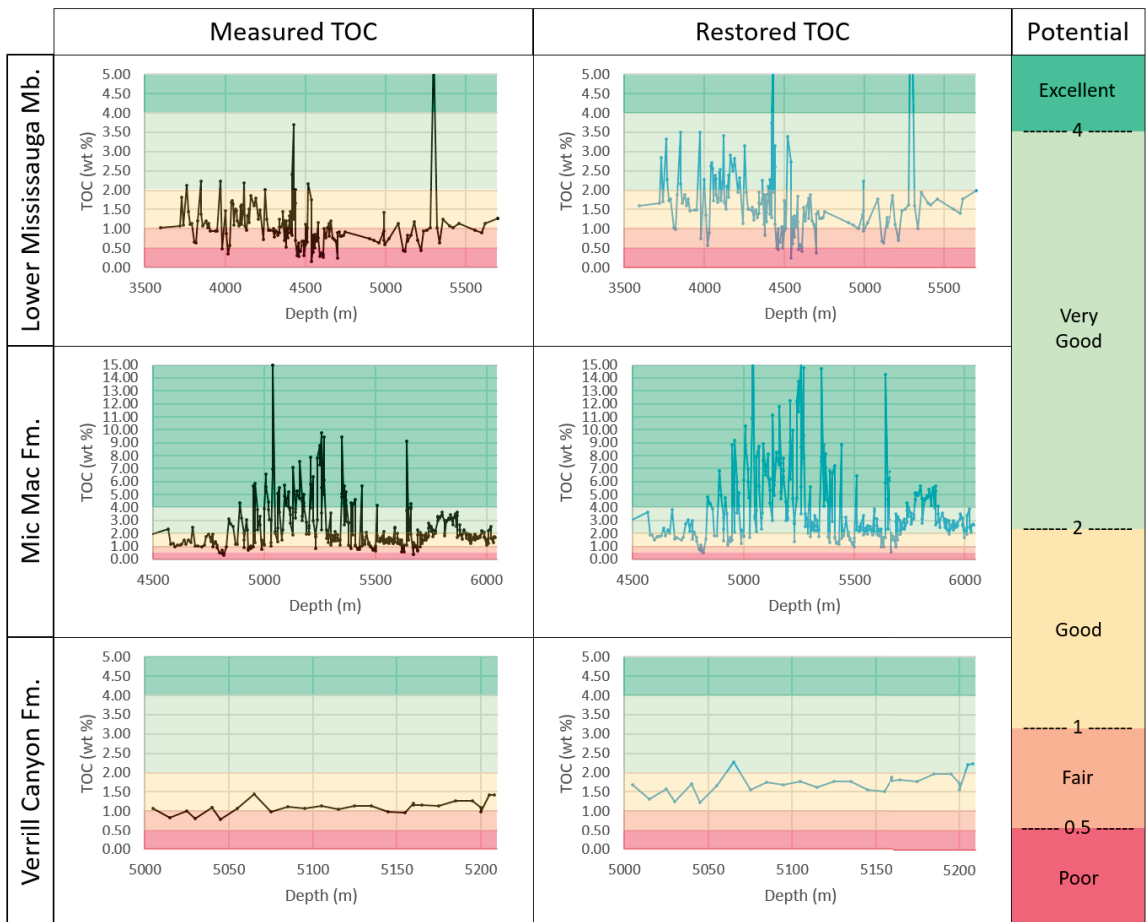
Figure 4-2: Source rock potential of the 11 key wells separated by formation and TOC Type (based on designations by Peters et al. 2005).

4.1.2 Wireline TOC Determinations

The Passey method was applied to the wells in Table 3.1. The data includes the derived equation for Ro% (used to calculate LOM), the scaling and baseline parameters for each well, and the resulting TOC estimations (filtered by lithology to display only shale values) within the studied interval. The relationships used to derive the %Ro equation and their corresponding R^2 and correlation values can be found in Appendix F. Results were variable when compared to measured TOC results, showing both inconclusive results, with no discernible correlation to the measured TOC values, to promising results, with an adequate correlation to measured TOC. Initial tests of the Issler method yielded poor results and were inconclusive (Appendix G). Estimations from this method are excluded from the results and are not discussed further.

4.1.2.1 Arcadia J-16

The equation derived to estimate %Ro is as follows:

$$Ro\% = (1.748081e^{-8} * (D^2)) - (5.738214e^{-5} * D) + 0.5367801 \qquad (34)$$

where %Ro is the vitrinite reflectance and D is depth in meters.

Table 4-1: Arcadia J-16 Passey Method sonic corrections and baselines.

	Corrections	Baselines	
	Scale Factor	**Sonic** AC (µs/m)	**Resistivity** ILD (ohm-m)
Lower Missisauga			
3393 - 4730 m	0.5	240	3.2
Mic Mac			
4730 - 6005 m	2	280	1.8
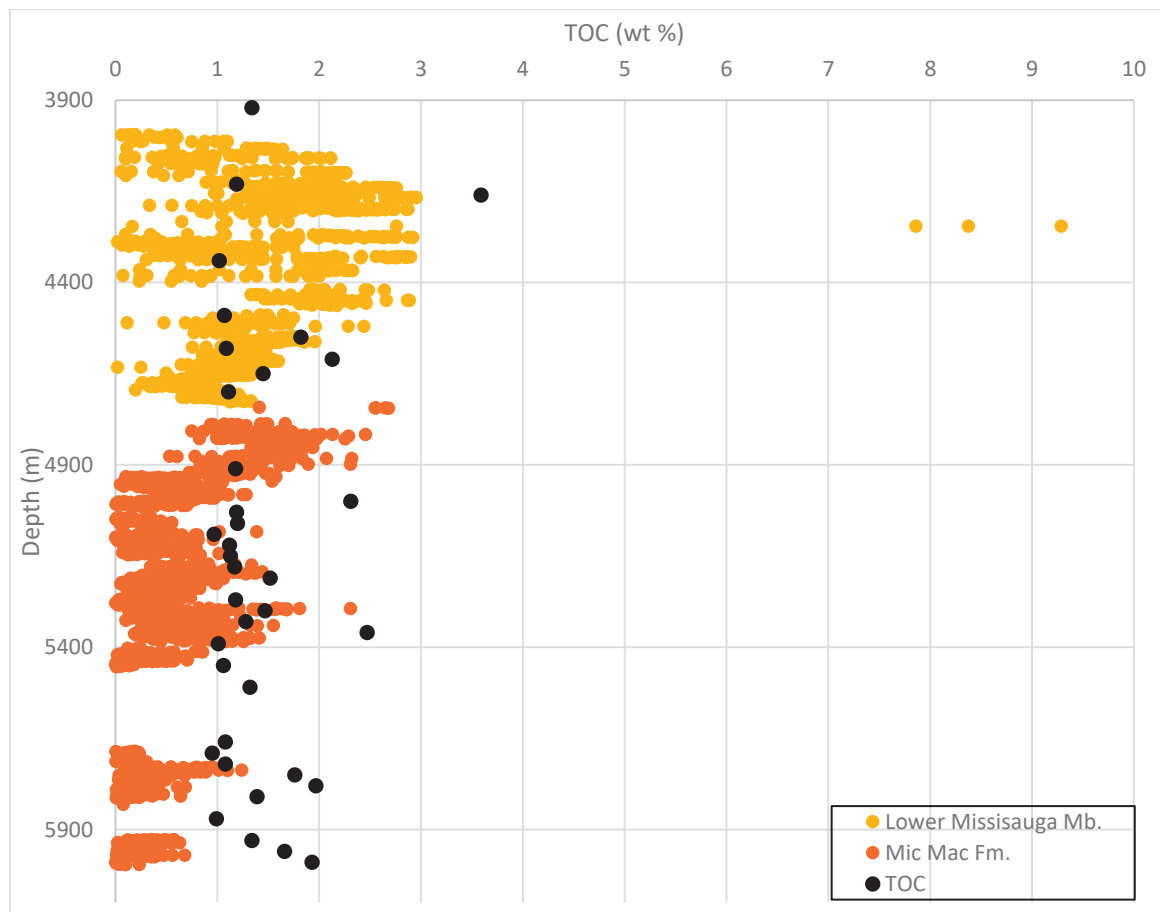
Figure 4-3: Calculated TOC estimates in the shales of Arcadia J-16.

4.1.2.2   Olympia A-12

The equation derived to estimate %Ro is as follows:

$$Ro\% = (9.869768e^{-8} * (D^2)) - (3.514078e^{-4} * D) + 0.6703756 \qquad (35)$$

where %Ro is the vitrinite reflectance and D is depth in meters.

Table 4-2: Olympia A-12 Passey Method corrections and baselines.

	Corrections	Baselines	
	Scale Factor	**Sonic** AC (µs/m)	**Resistivity** ILD (ohm-m)
Lower Missisauga			
3395 - 4752 m	1	225	3.5
Mic Mac			
4752 – 5300 m	4	270	2.1
5300 – 6071 m	10	270	2.1
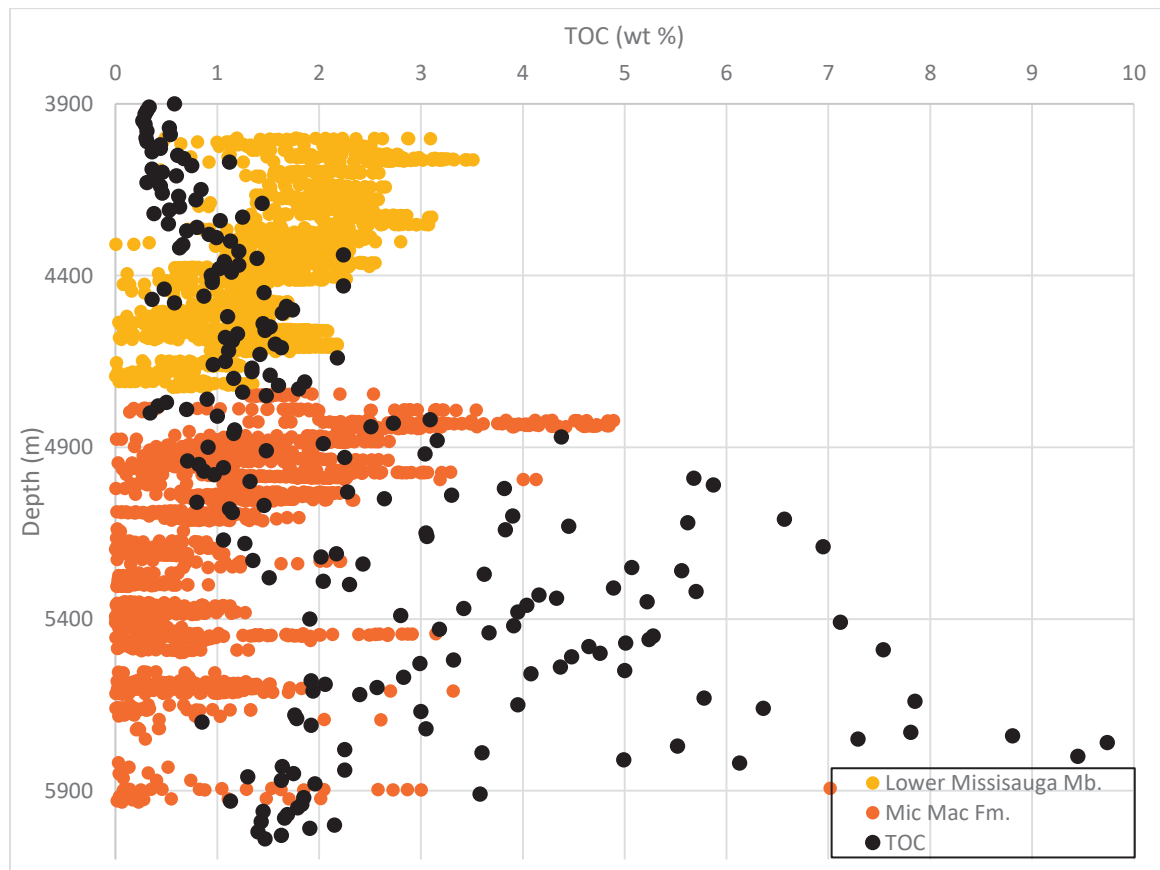
Figure 4-4: Calculated TOC estimates in the shales of Olympia A-12.

4.1.2.3 Sable Island O-47

The equation derived to estimate %Ro is as follows:

$$Ro\% = (9.883437e^{-8} * (D^2)) - (3.412911e^{-4} * D) + 0.6352011 \qquad (36)$$

where %Ro is the vitrinite reflectance and D is depth in meters.

Table 4-3: Sable Island O-47 Passey Method corrections and baselines.

	Corrections	Baselines	
	Scale Factor	**Sonic** AC (µs/m)	**Resistivity** ILD (ohm-m)
Lower Missisauga			
3191 - 3888 m	0.25	250	2.5
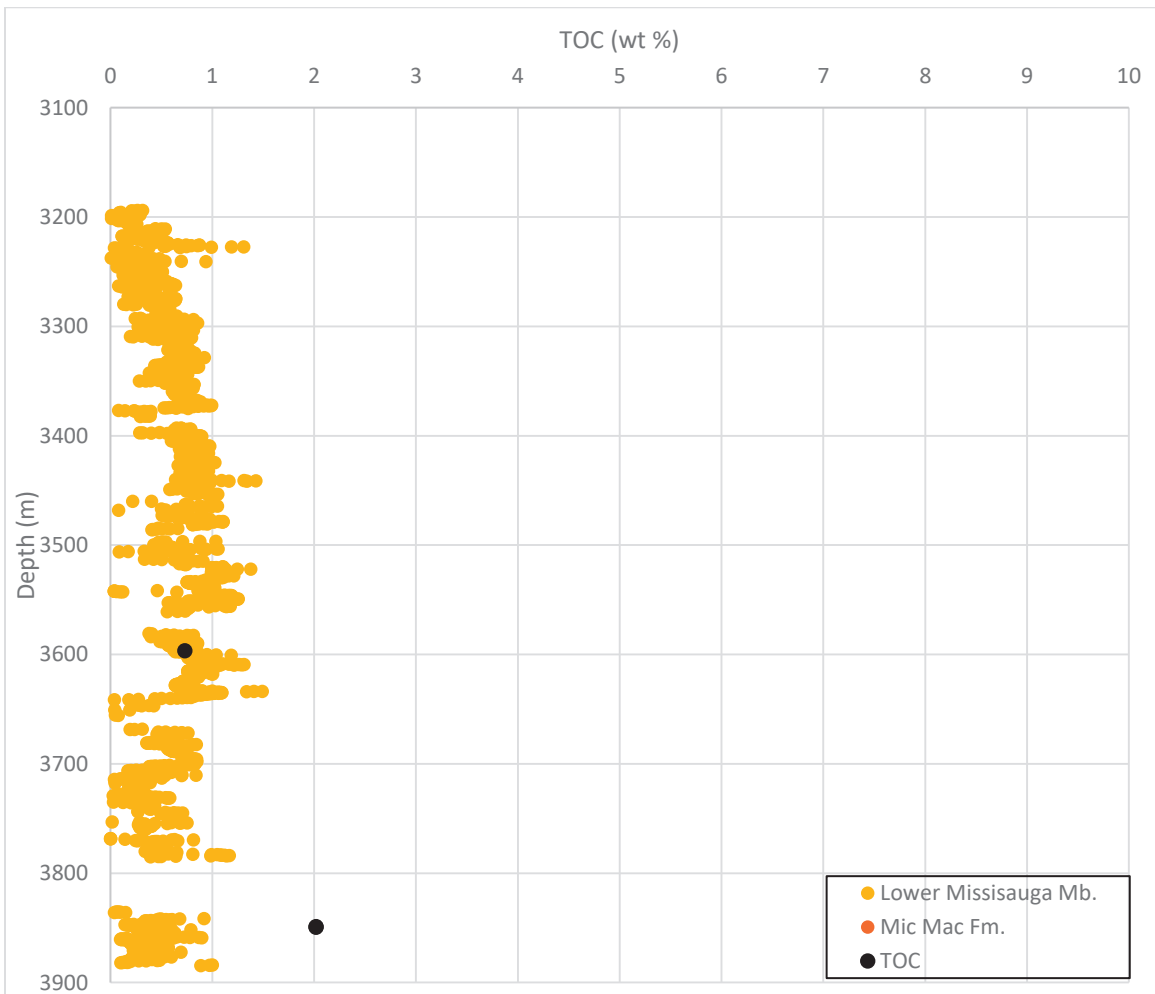
Figure 4-5: Calculated TOC estimates in the shales of Sable Island O-47.

4.1.2.4   South Desbarres O-76

The equation derived to estimate %Ro is as follows:

$$Ro\% = (8.649106e^{-8} * (D^2)) - (2.819618e^{-4} * D) + 0.5235 \qquad (37)$$

where %Ro is the vitrinite reflectance and D is depth in meters.

Table 4-4: South DesBarres O-76 Passey Method corrections and baselines.

	Corrections	Baselines	
	Scale Factor	**Sonic** AC (µs/m)	**Resistivity** ILD (ohm-m)
Lower Missisauga			
3572 - 3860 m	1	230	3.2
Mic Mac			
3860 - 4700 m	1	270	3.1
4700 - 6039 m	25	280	2
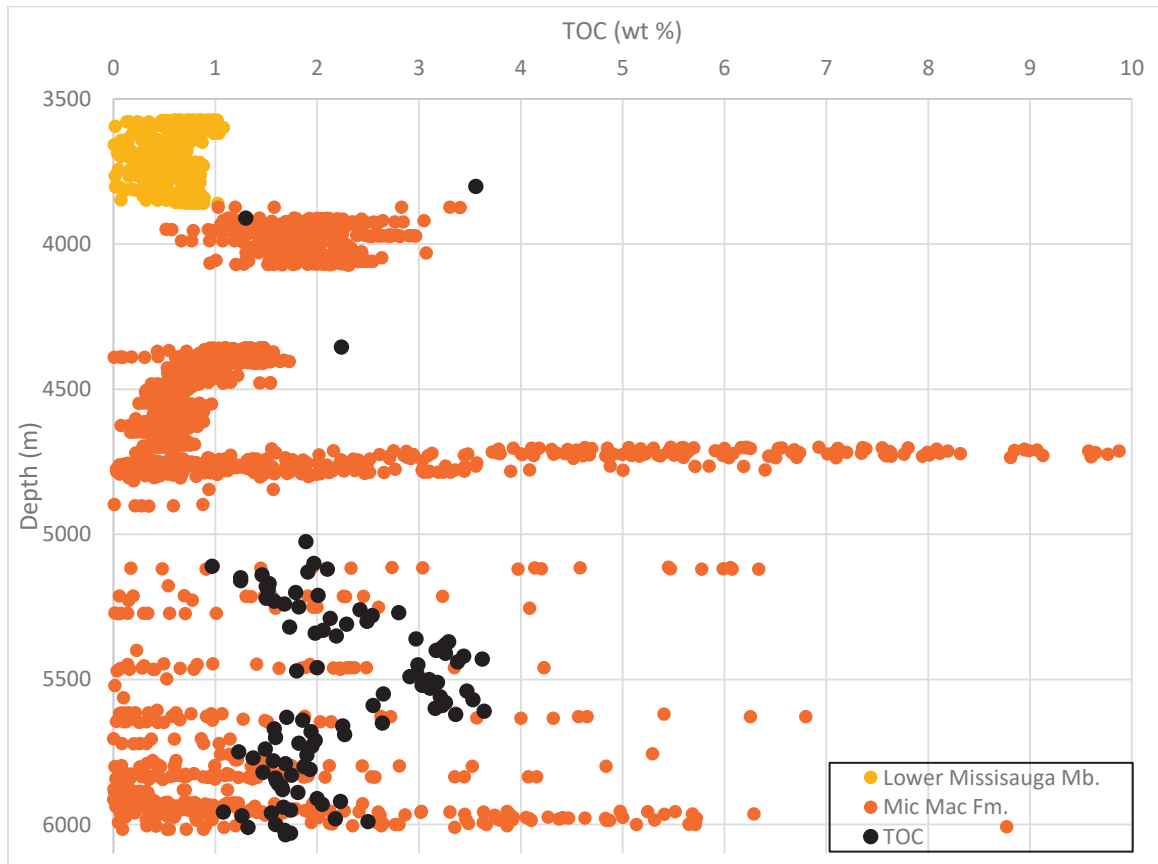
Figure 4-6: Calculated TOC estimates in the shales of South DesBarres O-76.

The equation derived to estimate %Ro is as follows:

$$Ro\% = (6.092124e^{-8} * (D^2)) - (3.138085e^{-4} * D) + 0.9252505 \qquad (38)$$

where %Ro is the vitrinite reflectance and D is depth in meters.

Table 4-5: South Sable B-44 Passey Method corrections and baselines.

	Corrections	Baselines	
	Scale Factor	**Sonic** AC (µs/m)	**Resistivity** ILD (ohm-m)
Lower Missisauga			
4606 - 4980 m	0.25	230	3.4
Mic Mac			
4980 - 5100 m	0.75	260	2.6
5100 - 5213 m	1	260	2.6
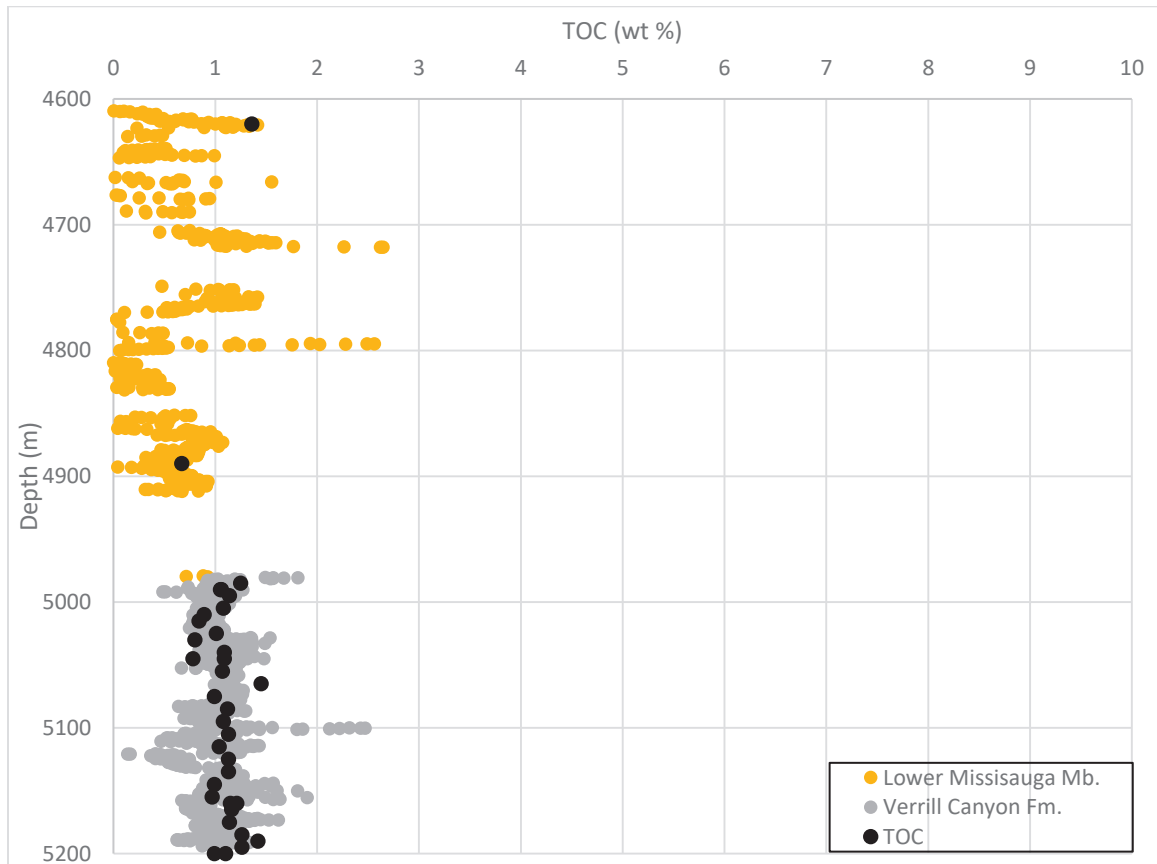
Figure 4-7: Calculated TOC estimates in the shales of South Sable B-44.

4.1.2.6 South Venture O-59

The equation derived to estimate %Ro is as follows:

$$Ro\% = (1.094737e^{-7} * (D^2)) - (4.275807e^{-4} * D) + 0.6665302 \qquad (39)$$

where %Ro is the vitrinite reflectance and D is depth in meters.

Table 4-6: South Venture O-59 Passey Method corrections and baselines.

	Corrections	Baselines	
	Scale Factor	Sonic AC (μs/m)	Resistivity ILD (ohm-m)
Lower Missisauga			
4335 – 4750 m	0.375	260	2.5
4750 – 5100 m	0.5	260	2.5
5100 – 5300 m	1	260	2.5
5300 – 5776 m	3	260	2.5
Mic Mac			
5776 - 6176 m	10	250	1.9
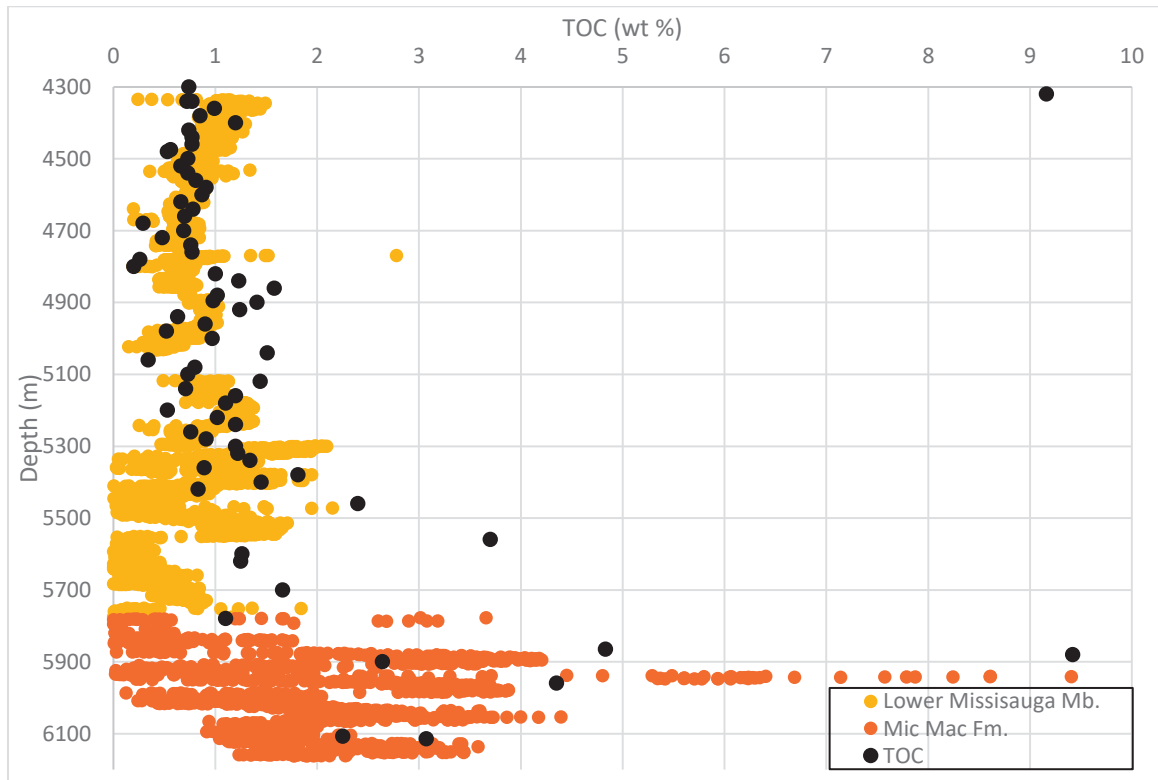
Figure 4-8: Calculated TOC estimates in the shales of South Venture O-59.

4.1.2.7   Uniacke G-72

The equation derived to estimate %Ro is as follows:

$$Ro\% = (7.329561e^{-8} * (D^2)) - (2.664736e^{-4} * D) + 0.6184732 \qquad (40)$$

where %Ro is the vitrinite reflectance and D is depth in meters.

Table 4-7: Uniacke G-72 Passey Method corrections and baselines.

	Corrections	Baselines	
	Scale Factor	**Sonic** AC (µs/m)	**Resistivity** ILD (ohm-m)
Lower Missisauga			
3716 - 4011 m	1	260	2.2
Mic Mac			
4011 - 5735 m	0.75	260	2.6
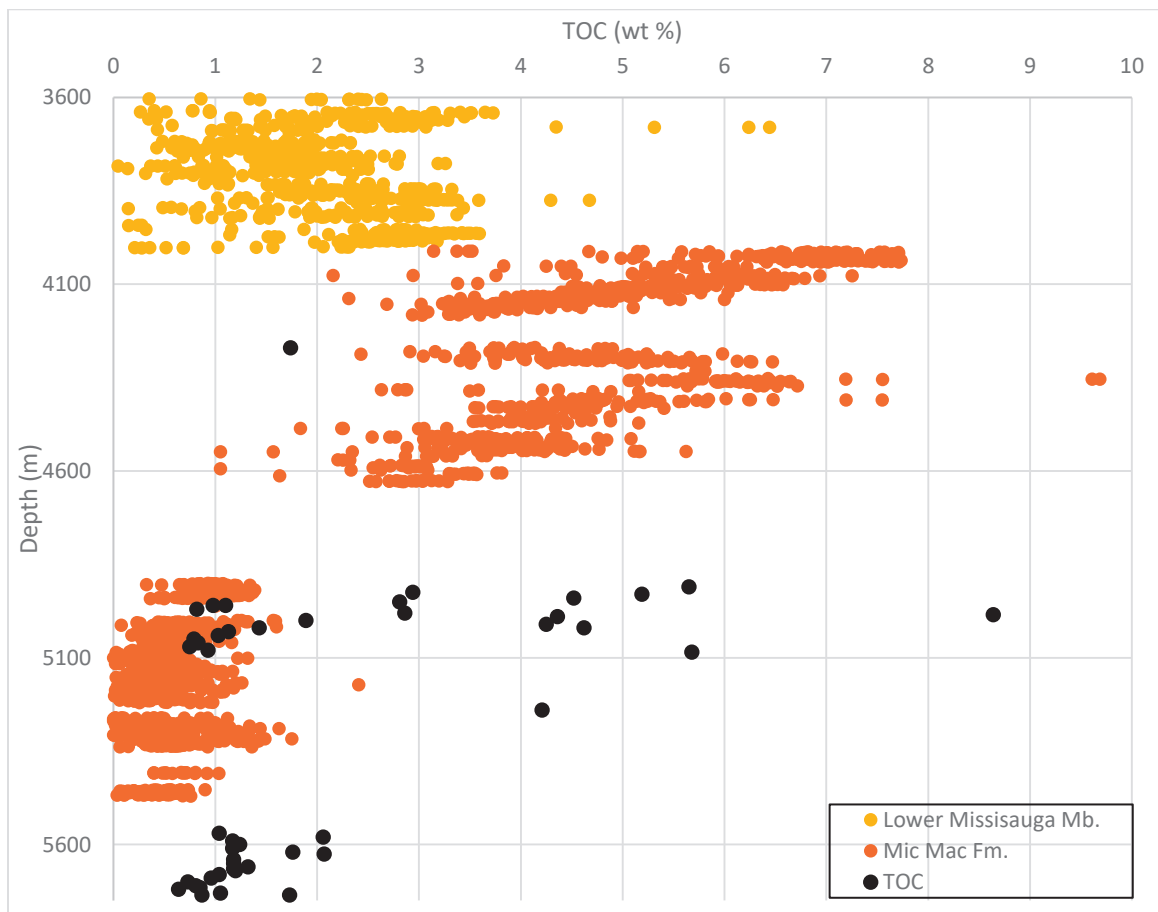
Figure 4-9: Calculated TOC estimates in the shales of Uniacke G-72.

4.1.2.8 Venture B-43

The equation derived to estimate %Ro is as follows:

$$Ro\% = (8.916213e^{-8} * (D^2)) - (3.139547e^{-4} * D) + 0.5627593 \qquad (41)$$

where %Ro is the vitrinite reflectance and D is depth in meters.

Table 4-8: Venture B-43 Passey Method corrections and baselines.

	Corrections	Baselines	
	Scale Factor	Sonic AC (µs/m)	Resistivity ILD (ohm-m)
Lower Missisauga			
4112 - 5135 m	1	240	3.2
Mic Mac			
5135 - 5560 m	1	240	3.5
5560 - 5872 m	1	280	1.6
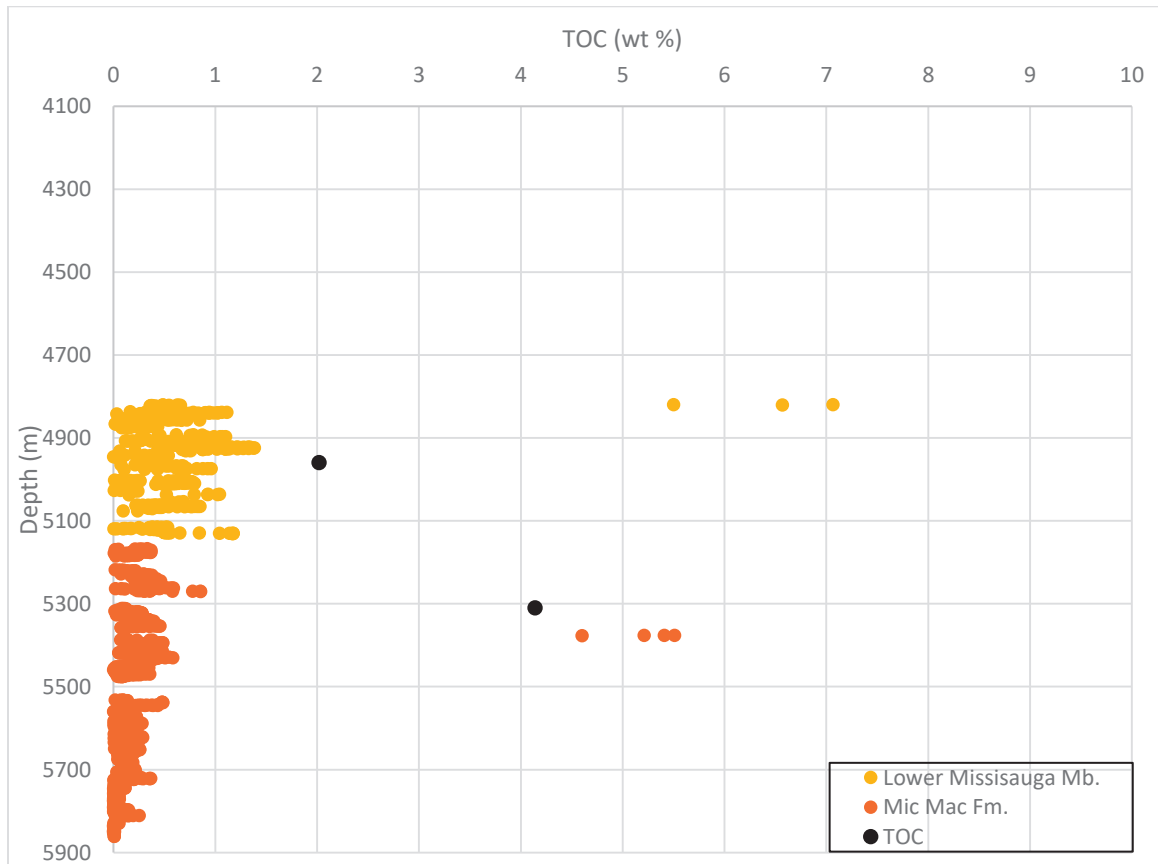
Figure 4-10: Calculated TOC estimates in the shales of Venture B-43.

Venture B-52

The equation derived to estimate %Ro is as follows:

$$Ro\% = (3.401056e^{-8} * (D^2)) - (1.790354e^{-4} * D) + 0.8563295 \qquad (42)$$

where %Ro is the vitrinite reflectance and D is depth in meters.

Table 4-9: Venture B-52 Passey Method corrections and baselines.

	Corrections	Baselines	
	Scale Factor	**Sonic** AC (µs/m)	**Resistivity** ILD (ohm-m)
Lower Missisauga			
4185 – 4700 m	0.5	240	3.2
4700 – 5138 m	2	240	3.2
Mic Mac			
5135 – 5560 m	2	245	3.2
5560 – 5960 m	10	245	3.2
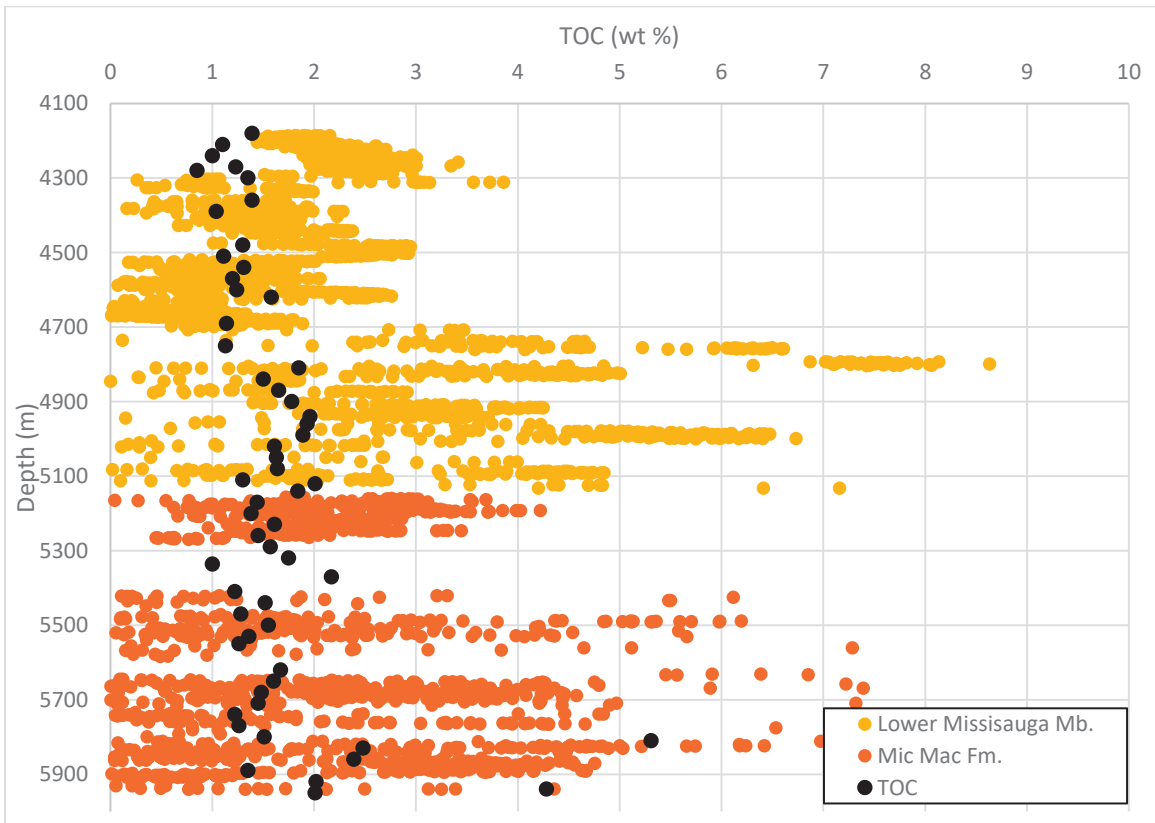
Figure 4-11: Calculated TOC estimates in the shales of Venture B-52.

4.1.2.10 West Olympia O-51

The equation derived to estimate %Ro is as follows:

$$Ro\% = (1.275328e^{-9} * (D^2)) + (1.735124e^{-4} * D) + 0.1376904 \qquad (43)$$

where %Ro is the vitrinite reflectance and D is depth in meters.

Table 4-10: West Olympia O-51 Passey Method corrections and baselines.

	Corrections	Baselines	
	Scale Factor	**Sonic** AC (µs/m)	**Resistivity** ILD (ohm-m)
Lower Missisauga			
4140 - 4565 m	1	225	3.5
Mic Mac			
4565 - 4700 m	1	240	3.3
4700 - 4817 m	2	240	3.3
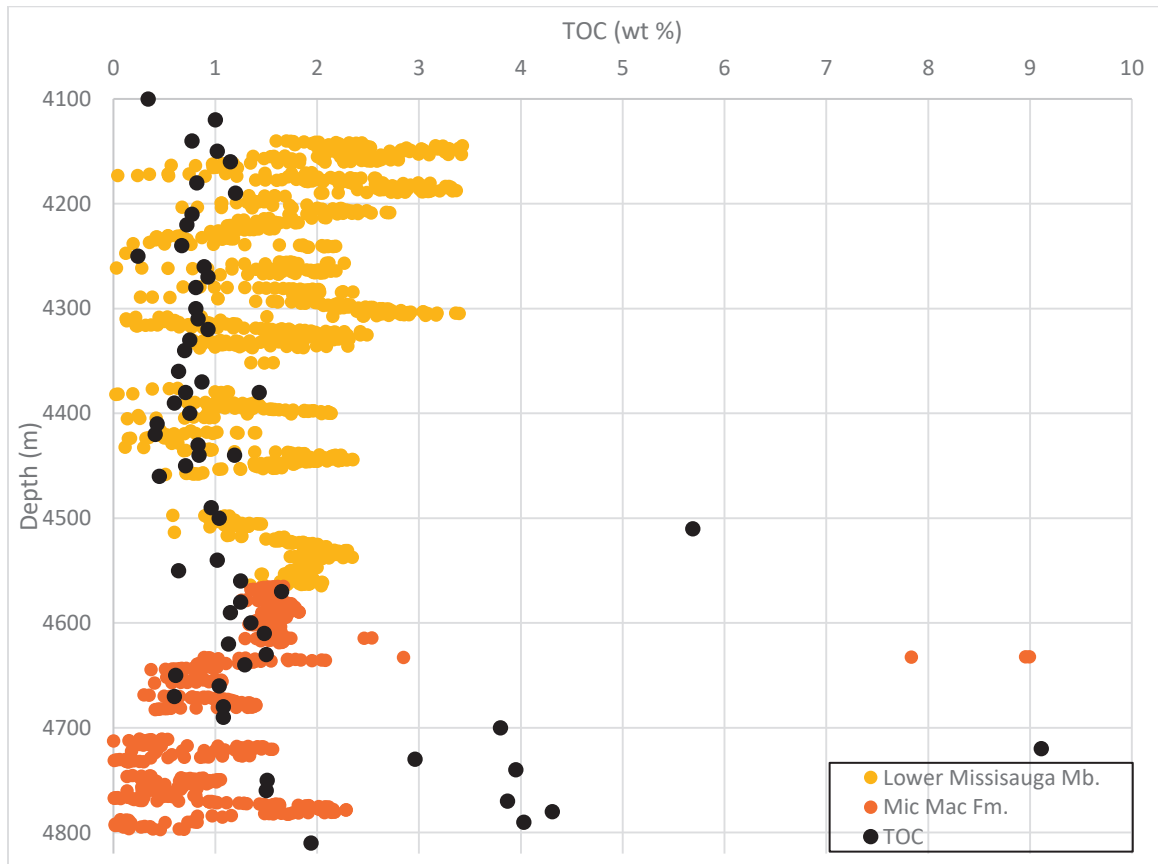
Figure 4-12: Calculated TOC estimates in the shales of West Olympia O-51.

The equation derived to estimate %Ro is as follows:

$$Ro\% = (3.808208e^{-8} * (D^2)) - (2.340418e^{-6} * D) + 0.3824566 \qquad (44)$$

where %Ro is the vitrinite reflectance and D is depth in meters.

Table 4-11: West Venture N-91 Passey Method corrections and baselines.

	Corrections	Baselines	
	Scale Factor	**Sonic** AC (µs/m)	**Resistivity** ILD (ohm-m)
Lower Missisauga			
4136 - 4600 m	0.75	225	3.5
4600 - 5150 m	2.5	225	3.5
Mic Mac			
5150 - 5548 m	4	250	2.6
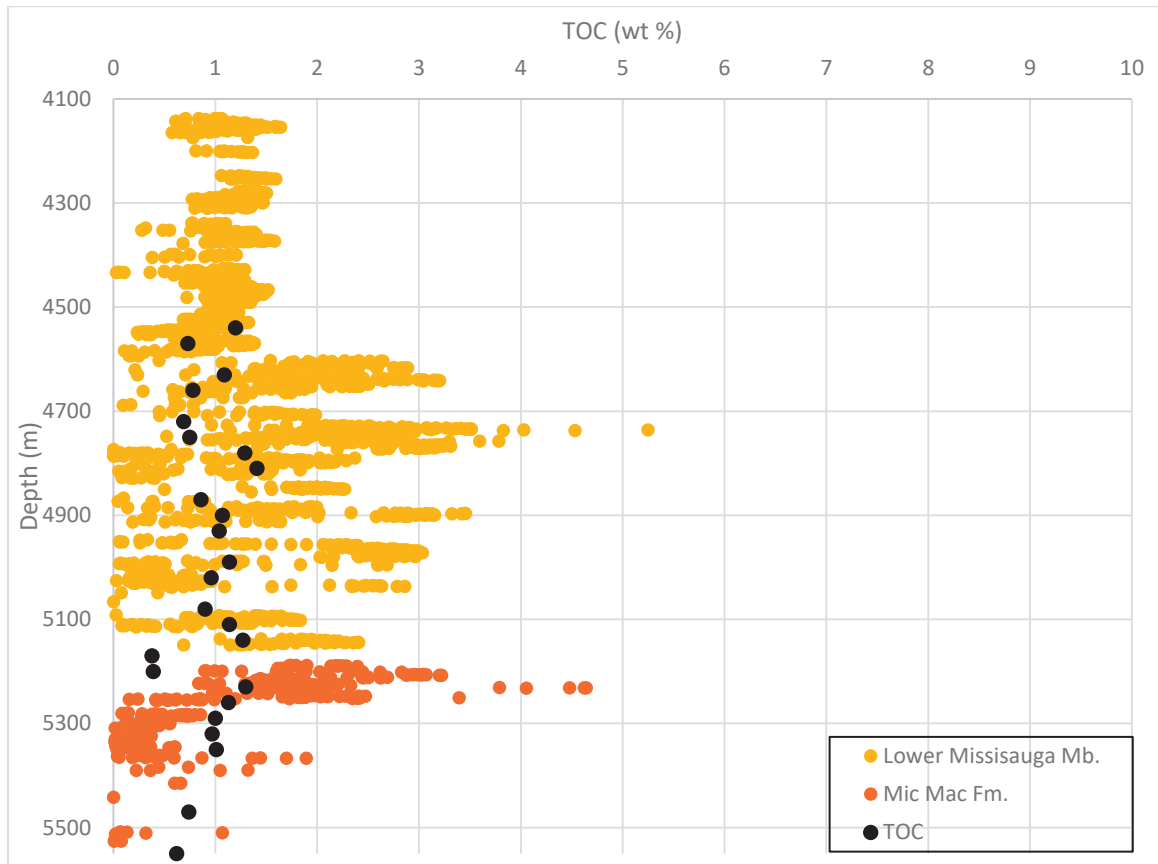
Figure 4-13: Calculated TOC estimates in the shales of West Venture N-91.

4.1.2.12 Uncertainties

Uncertainty with this method could have altered the results. These include effects on wireline log quality, such as oil based, or lignite drilling fluid and mud additives, casing size changes, and open hole conditions. Error surrounding contamination of the measured TOC samples, the use of cutting samples (which are inherently skewed) and turbo-drilling (which can allow for the addition of contaminants), also introduce uncertainty to the correlation of the results to the measured TOC samples. These uncertainties are listed below for each well. Difficulties in establishing a baseline are discussed in Section 5.2.1.

4.1.2.12.1 Arcadia J-16

The baseline in the Lower Missisauga Member was unable to be determined, thus it was taken from the nearest well with a clear baseline, Venture B-43. The geochemical data was derived from cutting samples, including the interval between 4898-5904 m MD, which was turbo-drilled and likely introduced contaminants to the samples (Geochem Laboratories 1983a; Creybohm et al. 1983). Contaminants were identified in the cuttings in both the Lower Missisauga Member and the Mic Mac Formation. In the Lower Missisauga Member, metal shavings, rust spots, fluorescent grease balls and sand sized artificial pellets were identified within the washed samples. The unwashed samples contained floating grease balls from drilling operations and a slight petroleum order (GeoChem Labs 1983a). Within the Mic Mac Formation, the washed samples contained metal shavings, rust, sand sized artificial pellets of glass or clear plastic, oil stain coatings and well bore cavings. The unwashed samples had an abundance of floating grease balls in the oily drilling fluid (GeoChem Labs 1983a).

Uncertainty from the drilling fluid was also identified. From 3023 m to TD, there was a freshwater polymer with a chrome lignite mud used. Furthermore, there is also open hole from 5864 m MD as well as casing size changes at 4694 m MD which could have altered wireline log quality (Creybohm et al. 1983). The combination of open hole setting, fine cuttings and lignitic mud could lead to contamination and high TOC values from 5900 m to TD.

4.1.2.12.2 Olympia A-12
The baseline in the Lower Missisauga Member was unable to be determined, thus it was taken from the nearest well with a clear baseline, West Venture N-91. Geochemical data used in this analysis have been derived from cutting samples, including from the intervals between 5091-5289, 5412-5889, and 5914-6064 m measured depth (MD), which was turbo-drilled and likely introduced contaminants to the samples (Geochem Laboratories 1983b; Sidwell et al. 1983). Contaminants found in both the Lower Missisauga Member and the Mic Mac Formation included iron fillings (seen only in Lower Missisauga Member), mica flakes, metal shavings, pipe dope, filling material, grease, abundant pellets of glass or plastic, wood chips, cavings, and welding drops. Many of the contaminants found in the Mic Mac Formation were found in the turbo drilled areas (Geochem Laboratories 1983b).

Additional uncertainty from the drilling fluid additives were also identified. From 3028 m to TD, there was freshwater polymer with a chrome lignitic mud (with a pipelax additive at 4707 m) used. There were also open hole conditions from 5892 m MD, as well as casing size changes at 4743 and 3006 m MD which could have altered wireline

log quality (Sidwell et al. 1983). The combination of open hole setting, fine cuttings and lignite mud could lead to contamination and skewed TOC values throughout the well.

4.1.2.12.3 Sable Island O-47

There was limited geochemical data for this well, with the two points derived from cutting samples. This sample came from an interval with dispersed lignosulphonate drilling mud with lignite, walnut and pipelax additives used. Furthermore, open hole conditions from 3931.9 m MD and a casing size change at 3770.12 m MD which could have altered wireline log quality (Dawson et al. 1972).

4.1.2.12.4 South DesBarres O-76

The geochemical data in this well was derived from cutting samples, including the intervals of turbo-drilling between 5343–6006 m MD (Sine et al. 1984a). The use of oil based drilling mud for this well made it difficult for analytical geochemical techniques to be completed on these samples. Finally, casing size changes at 2736 and 5076 m MD could have altered wireline log quality (Sine et al. 1984a).

4.1.2.12.5 South Sable B-44

A baseline could not be determined for both the Lower Missisauga Member and the Verrill Canyon Formation, thus were taken from the Thebaud C-74 well. The geochemical data has been derived from the cutting samples (GeoChem Labs 1989). Open hole conditions from 4108 m MD to TD, and a casing size change at 2837.9 m MD could have altered the TOC data and wireline log quality (McLelan et al. 1988).

4.1.2.12.6 South Venture O-59

The geochemical data in this well were derived from cutting samples, including from six turbo-drilled intervals between 3696–5753 m MD. Contaminants such as iron

filings were found in both the Lower Missisauga Member and the Mic Mac Formation

(GeoChem Labs 1983c; Love et al. 1983). Additional uncertainty, from the freshwater

polymer drilling fluid from 3085 m MD to TD and casing size changes at 3080, 4763, and

5750 m MD, could have altered wireline log quality (Love et al. 1983).

4.1.2.12.7 Uniacke G-72

The limited geochemical samples in this well were derived from cutting samples,

including from intervals of turbo-drilling from 4832-5142 m MD (Sine et al. 1984b).

Additional uncertainty was introduced though the use of numerous drilling fluid

additives including chrome lignite, with cromex, lignosol, thannathin, weikseal, nutplug,

oilphase and pipelax. Furthermore, there were two casing size changes, at 4790 and

5142 m MD which could have altered wireline log quality (Sine et al. 1984b).

4.1.2.12.8 Venture B-43

The Venture B-43 well contained only one geochemical sample, derived from

cuttings, for each of the formations (GeoChem Labs 1982). GeoChem Labs (1982) list no

contaminants in the Lower Missisauga Member, however note coal and iron fillings

found within the Mic Mac Formation. Furthermore, casing size changes at 3672, 4815

and 5372 m MD, coupled with an open hole setting in the basal 100 m of the well and

the use of chrome lignite drilling fluid with cromex, tannanthin, nutplut, kwikseal,

celloseal, pipelax, and oilphase additives could have skewed the wireline logs (Cuthill et

al. 1982). Finally, there was a large interval of the sonic log missing which limited the

results.

4.1.2.12.9 Venture B-52

The baseline for the Lower Missisauga Member was unable to be determined,

thus the baseline was taken from the neighbouring Venture B-43 well. The geochemical

data was derived from the cutting samples, noted to contain contaminants. Within the

Lower Missisauga Member, these included metal shavings, rust spots, fluorescent

grease balls, oil stained spots, yellow paint chips and artificial pellets of glass or plastic

(GeoChem Labs 1983d). The Mic Mac Formation contained fluorescent grease balls

(unwashed sample), artificial pellets of glass or plastic, metal shavings, rust spots and

grease spots (GeoChem Labs 1983d). Three intervals of turbo-drilling, between 4578 -

5902 m MD, could have also influenced the geochemical data. Sources of uncertainty in

the wireline logs included the freshwater polymer, chrome lignite drilling mud as well as

a casing size change at 4788 m (Burrel et al. 1983).

4.1.2.12.10   West Olympia O-51

The baseline within the Lower Missisauga Member was unable to be

determined, thus it was taken from the West Venture N-91 well. The geochemical data

in this well was derived from cutting samples. GeoChem Labs (1985) indicate the

presence of contaminants however do not indicate their nature. Other sources of

uncertainty were the open hole setting from 4632 m MD, a casing size change at 4351 m

MD and the seawater gel polymer drilling fluid which could have altered the wireline log

data (Tweed and Nachtigall 1986).

4.1.2.12.11   West Venture N-91

West Venture N-91 had a wealth of geochemical data derived from cutting

samples. A turbo-drilled interval from 3414-3477 m MD could have allowed for the

introduction of contaminants in samples from this interval. Contaminants found in the

Lower Missisauga Member included green fluid contents, fluorescent specks, slight

diesel odor and small grease balls and flakes in the unwashed samples with grease, pipe

dope, metal shavings, fluorescent specks and paint chips. The Mic Mac Formation

contained fluorescent grease balls and flakes, as well as a diesel odor in the unwashed

samples. The washed samples contained metal shavings, grease spots fluorescent black

specks and flakes, pain chips and rust spots (GeoChem Labs 1984; Siefert et al. 1985).

Additional uncertainty surrounding altered wireline log data included the use of

freshwater polymer lignosulphonate or polymer lignite drilling muds, as well as an open

hole setting from 4727 m MD to TD (Siefert et al. 1985).

4.1.2.13 Sonic/Resistivity Cross-plotting

Sonic/Resistivity cross-plotting was used a proxy for identifying areas of potential

organic richness. Cross-plotting was completed on all wells but was not able to identify

deviations from the wet compacted sediment trend, i.e. did not identify organic rich

shales. Data were color-coded by gamma-ray, allowing for the identification of higher

API shales. Two examples of the cross-plots from the Acadia J-16 and South Venture O-

59 wells are shown in Figure 4-14. The solid black line depicts the estimated wet

compacted sediment trend (modified from Meyer et al. 1984), and the dashed black line

indicates where you may see high TOC source rock. The cross-plots were plotted over

the entire studied interval and showed no significant deviations away from the wet,

compacted sediment line.
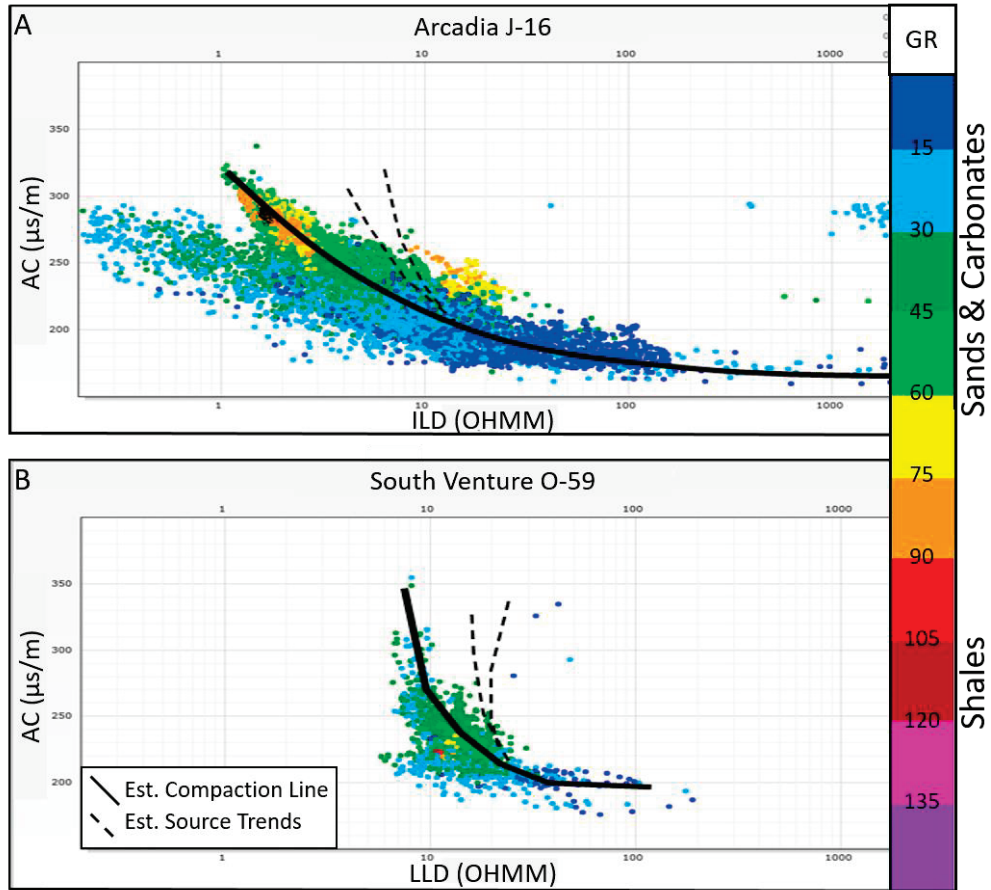
Figure 4-14 Sonic-resistivity cross plots, colored per gamma ray API values for the (A) Arcadia J-16 and (B) South Venture O-59 wells. The solid black like represents the regression or wet, compacted sediment line while the dashed lines indicate possible trends any high TOC point would likely follow.

4.2 Seismic Methods

4.2.1 Seismic Interpretation

The result of the seismic interpretation of the eastern Sable MegaMerge was a

Petrel framework incorporating all faults (Figure 4-15 and Figure 4-16) and eight seismic

horizons (Table 4-12) calibrated via synthetic seismograms at each of the wells.

Schematic transects of this framework are shown in Figure 4-17, Figure 4-18, and Figure

4-19. The frameworks illustrate the relationship between the Venture stratigraphy in

the expansion trends with the older Jurassic sediments to the northwest.
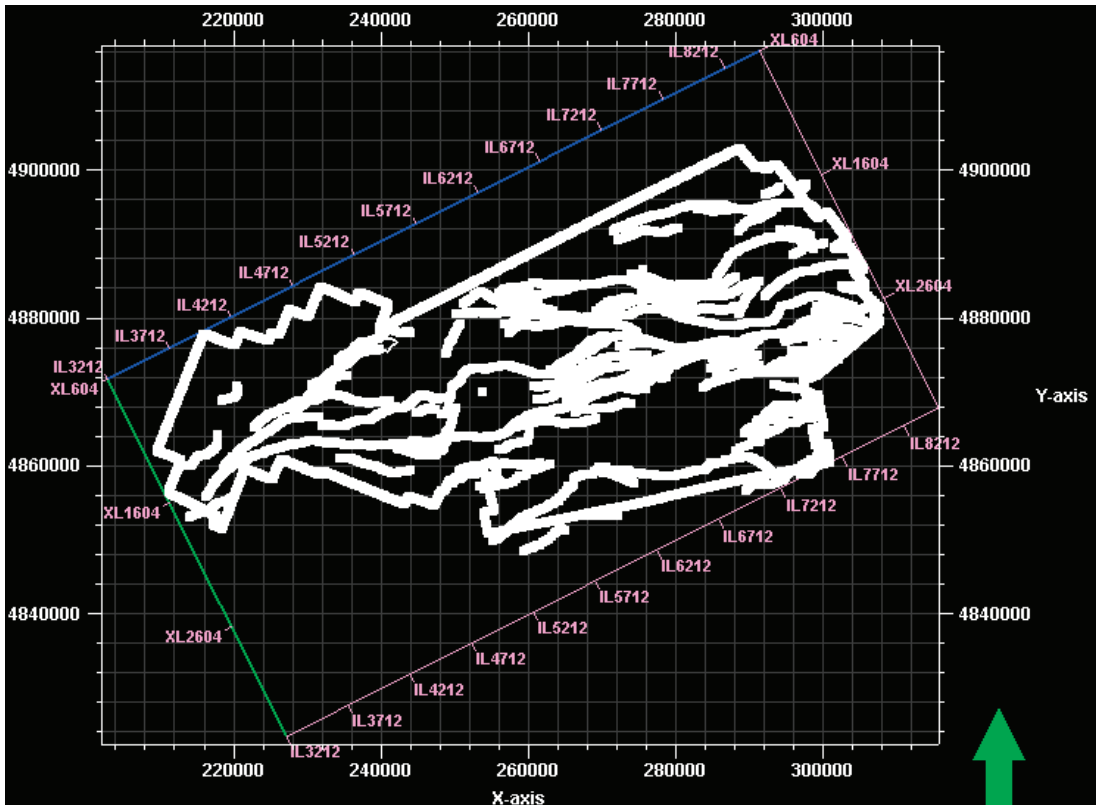
Figure 4-15: 2D view of fault framework built in Petrel.
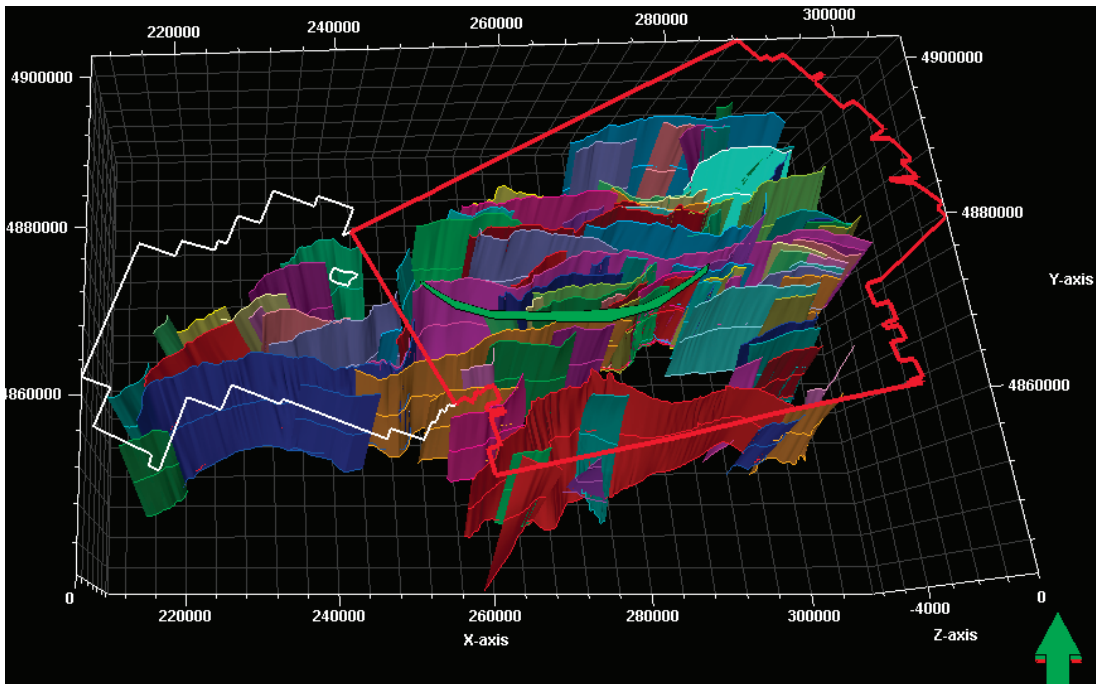
Figure 4-16: 3D view of fault model with the Sable MegaMerge outlined in white, the study area outlined in red and Sable Island shown in green.

Table 4-12: Interpreted horizons with corresponding geologic age.

Horizon	Age
Water Bottom	Present
Wyandot	Upper Cretaceous
Petrel	Upper Cretaceous
O-Marker	Lower Cretaceous
J150	Tithonian Flooding Surface
Lower Missisauga	Upper Jurassic
Citnalta	Upper Jurassic
Penobscot	Upper Jurassic
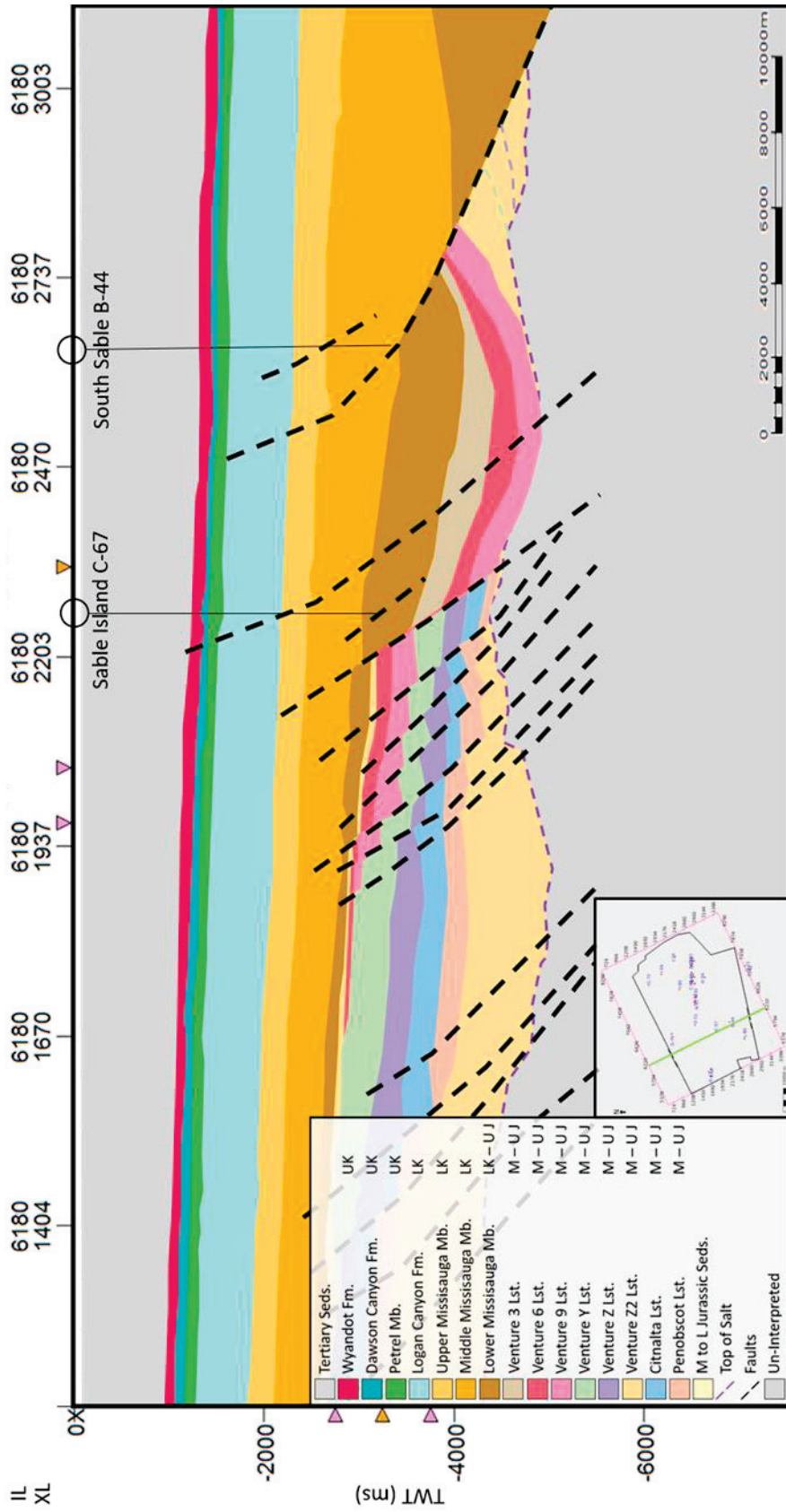
Figure 4-17: Cross-section of Inline 6180 intersecting wells Sable Island C-67 and South Sable B-44. Solid lines are interpreted seismic horizons and dashed are inferred.
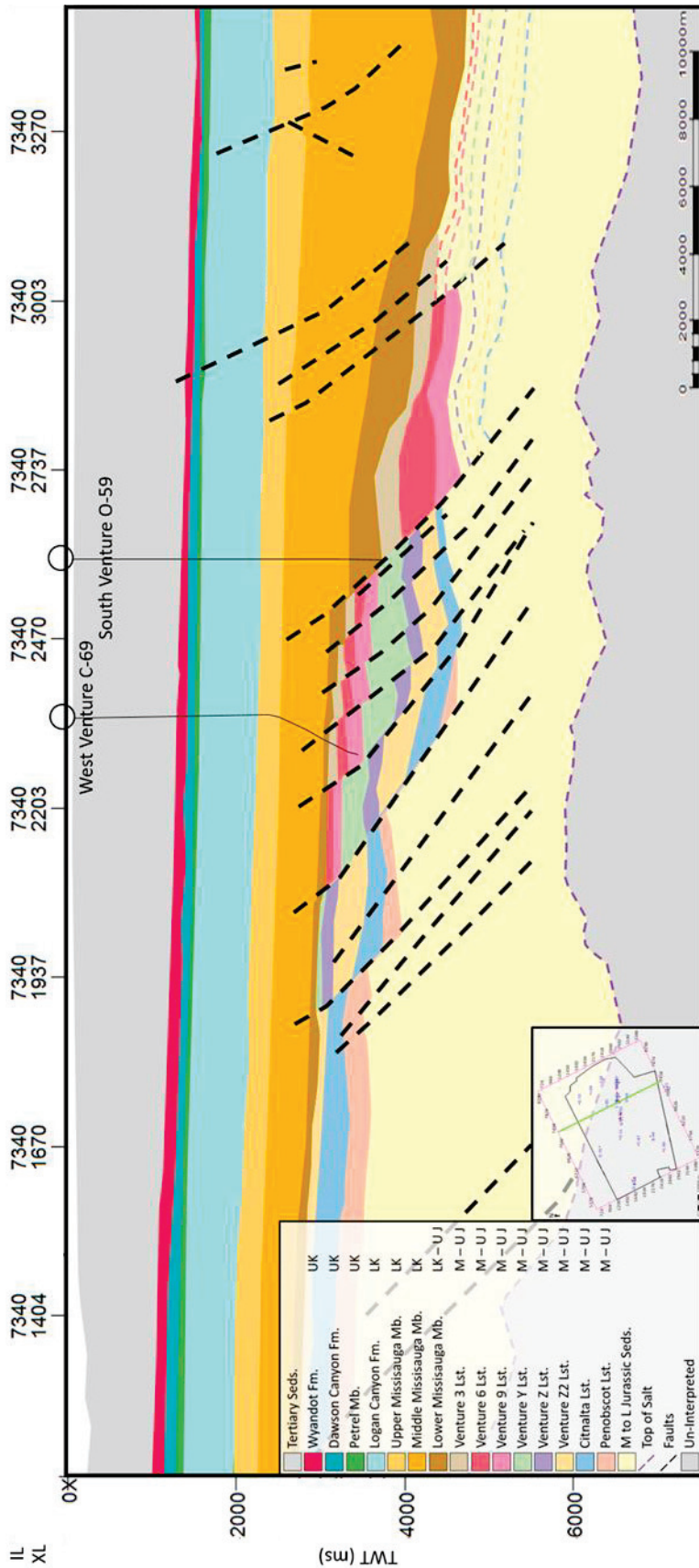
Figure 4-18: Cross-section of Inline 7340 intersecting wells West Venture C-69 and South Venture O-59. Solid lines are interpreted seismic horizons and dashed are inferred.

87
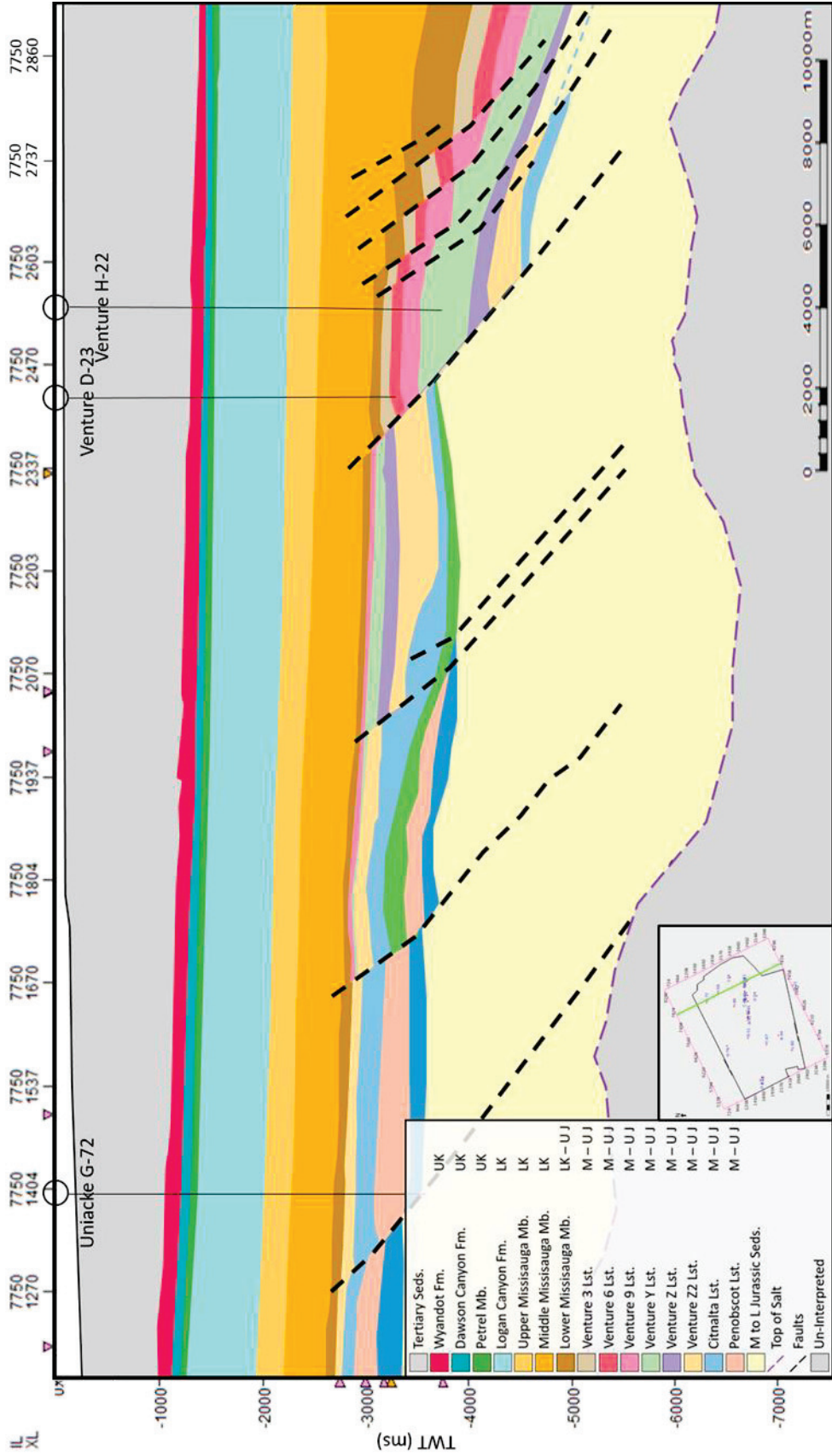
Figure 4-19: Cross-section of Inline 7750 intersecting wells Uniacke G-72, Venture D-23 and H-22. Solid lines are interpreted seismic horizons and dashed are inferred.

4.2.2   Seismic Inversion

The result of seismic inversion was four acoustic impedance cubes, each run with one of four tested wavelets. Explanation and results of these tests can be found in Appendix H. Based on the results of the wavelet tests, a wavelet with a 0 to 55 Hz bandwidth (Figure 4-20) and a 1.5 second two-way time (TWT) interval was chosen to run the final inversion. This was based an extensive quality control of the accuracy of the results, including cross correlations with well logs and the residuals between the input seismic and derived synthetic seismogram. An example of the final inversion is seen in Figure 4-21, with its corresponding residuals and cross correlation illustrated in Figure 4-22 and Figure 4-23. Finally, the parameters used in the final inversion are detailed in Table 4-13. This was the basis for subsequent interpretation between the 2.5 to 4 second TWT interval of interest.
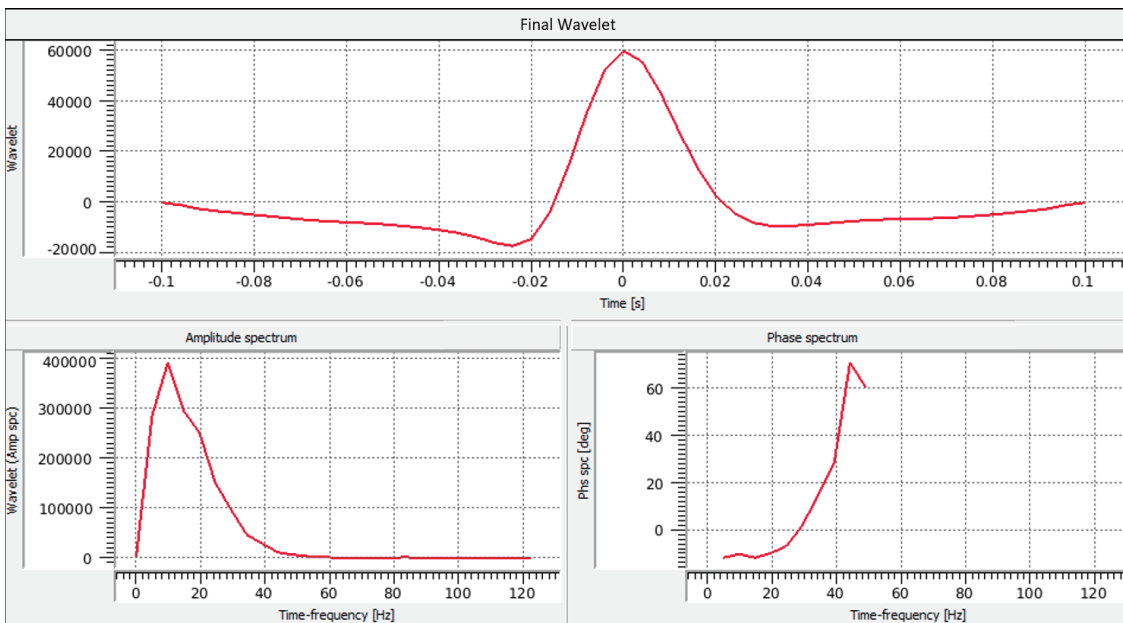
Figure 4-20: Derived wavelet used in the final inversion with its corresponding amplitude and phase spectra.

89
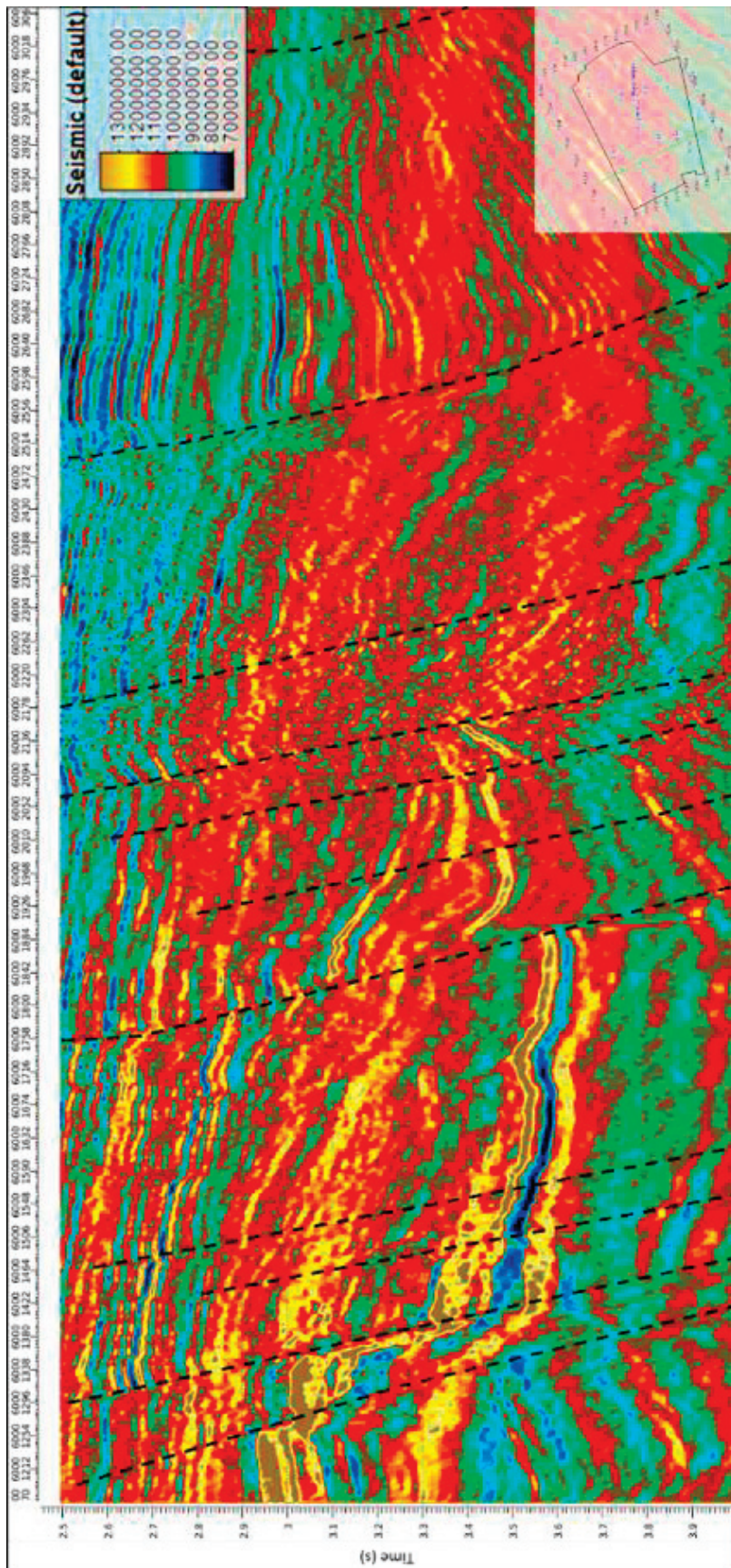
Figure 4-21: Final inversion merged with the low frequency model at inline 6000.
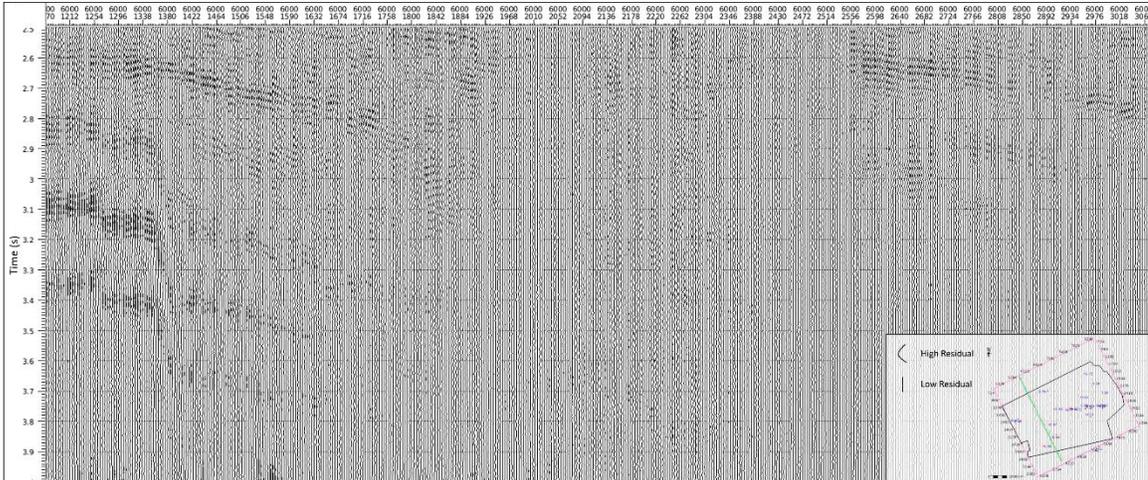
Figure 4-22: Residuals of the final inversion at the inline 6000.
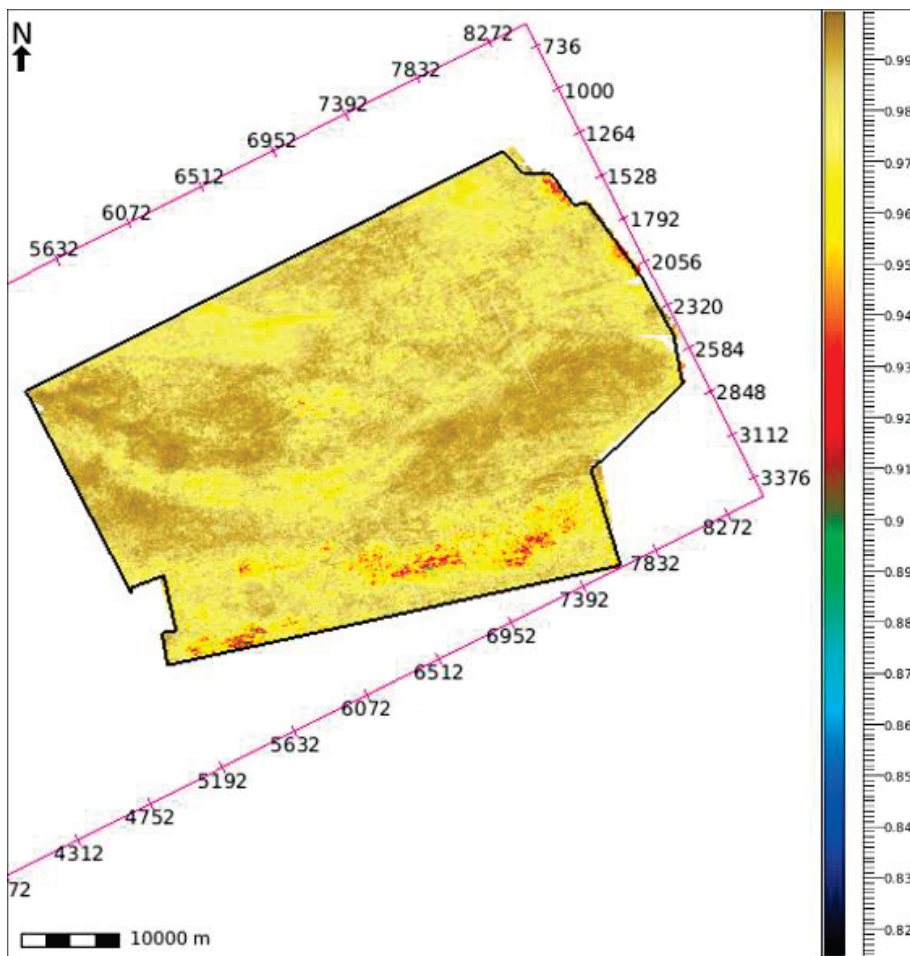
Figure 4-23: Cross-correlation of the synthetic seismogram used to create the inverted seismic versus the original seismic at the 3s interval, all areas are correlated above 0.9 (90%).

Table 4-13: Final inversion parameters for the 2.5 to 4 second interval.

		Parameters	
Solid Model	Wells & Correlation	Arcadia J-16	0.672684
		Citnalta I-59	0.777791
		Intrepid L-80	0.491473
		Olympia A-12	0.63425
		Sable Island C-67	0.343224
		South DesBarres O-76	0.730569
		South Venture O-59	0.400555
		Uniacke G-72	0.642016
		Venture B-13	0.610699
		Venture B-43	0.584100
		Venture B-52	0.445953
		Venture D-23	0.476588
		Venture H-22	0.772630
		West Olympia O-51	0.463221
		West Venture N-91	0.724041
	Trace Gate	Survey 1	
		5170 - 8490	
		1170 - 3490	
	Time Gate	2.5 - 4 s	
	Interpolation Method	Natural Neighbor	
		Plane Fit	
		50000	
	Areal Weight Interpolation	Natural Neighbor	
		(Internally set to Inverse Distance Weighted)	
	Log Parameters	0.004 s (default)	
	Control Weights	1 for all wells	
Model Generator	Seismic	Seismic Property\Survey 3\ZGY8bit37by37 [Realized] 2.mod	
	Wavelet	20 Hz Multi Well	
		Start Time: -0.1	
		Wavelet Length: 0.2	
	Trace Gate	Survey 1	
		line 5170 to line 8490, incr 2	
		CMP 1170 to CMP 3490, incr 2	
	Control Point	X: 277999	
		Y: 4873270	
		Below All: 3.99999	
InverTrace-Plus	Seismic Data	Seismic Property\Survey 3\ZGY8bit37by37 [Realized] 2.mod	
	Wavelets	20 Hz Multi Well	
	Trend	SM_Full_DIR_FINALALL\Tinterface.hor, all horizons	
		SM_Full_DIR_FINALALL\Timpedance.mod trend, no constraints	
	Time Gate	2 - 4.5 s	
	Trace Gate	Survey 1	
		line 5170 to line 8490, incr 2	
		CMP 1170 to CMP 3490, incr 2	
		3D, 1928421 traces	
	QC Time Gate	3 - 3.2 s	
	QC Using Wells	ArcadiaJ-16_ed	
		CitnaltaI-59_ed_2	
		IntrepidL-80_ed_2	
		OlympiaA-12	
		SableIslandC-67_ed_2	
		SouthDesBarresO-76	
		SouthVentureO-59	
		UniackeG-72_take2_ed	
		VentureB-13	
		VentureB-43	
		VentureB-52	
		VentureD-23_ed	
		VentureH-22	
		WestOlympiaO-51_ed_2	
		WestVentureN-91	
	Constraints	Disable hard trend constraints only	
	Merge Frequency	4.25 [Hz]	
QC Parms	Contrast Misfit	0.0138798	
	Seismic Misfit	15.6667	
	Seismic Power	1.65972	
	Wavelet Scale	0.87447	
	Merge Cut-Off Freq	4.5	

4.3 Interpretation of Acoustic Impedance Cube

4.3.1 AI/TOC Relationship

An attempt to derive a relationship between AI and TOC was completed on the shales within the studied interval, using the derived AI from the inversion and the estimated TOC from the Passey Method. No meaningful relationship could be established in these shales when applied at a broad scale to the shales in all of the wells over the entire interval, visualized in Figure 4-24. A relationship at an individual well level could also not be calculated, yielding R^2 values ranging from 0.0012 to 0.4564. Although some wells seemed to show a general non-linear relationship, there were still clusters of values in the low AI/ low TOC area. Two examples of this can be seen in Figure 4-25.

The South Venture O-59 well (Figure 4-25 A) yielded a low R^2 value when applied to the whole interval, but it visually showed the best non-linear relationship and the method was attempted on an interval between 5850 – 6000 m MD (Figure 4-26 and Figure 4-27). The relationship between AI and TOC in this interval was derived as follows:

$$AI = -(59.453 * TOC^2) + (11.861 * TOC) + 10726 \qquad (45)$$

where AI is acoustic impedance and TOC is total organic carbon. The corresponding R^2 value was relatively low, at 0.4786. This was applied to the 5x5 km interval surrounding the well to produce the estimated TOC profile in Figure 4-28.
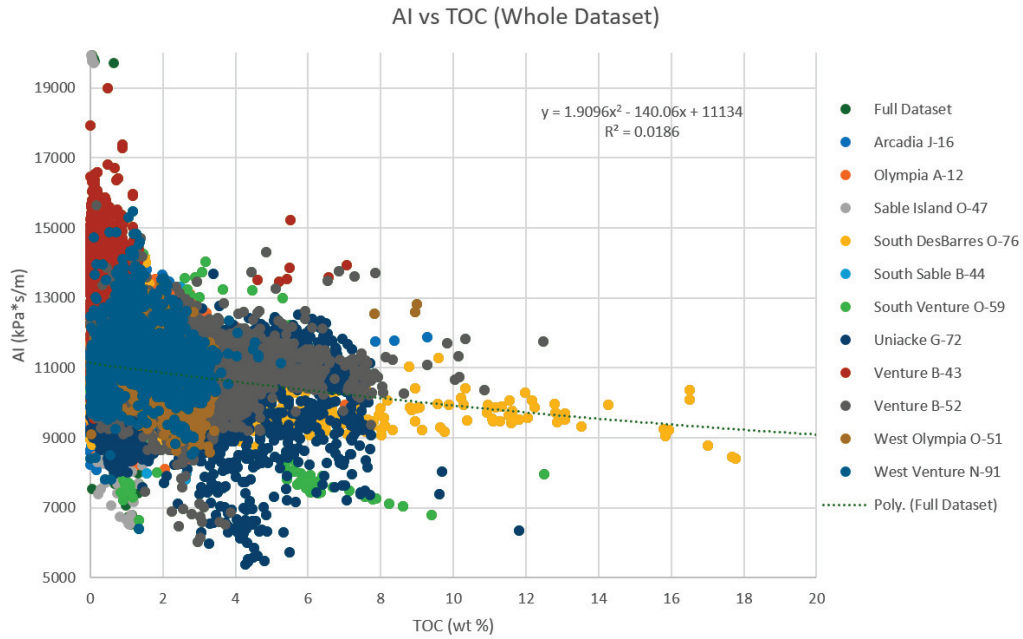
Figure 4-24: Acoustic impedance versus estimated TOC cross-plot for the shales over the entire inverted interval using all wells with TOC calculations completed.
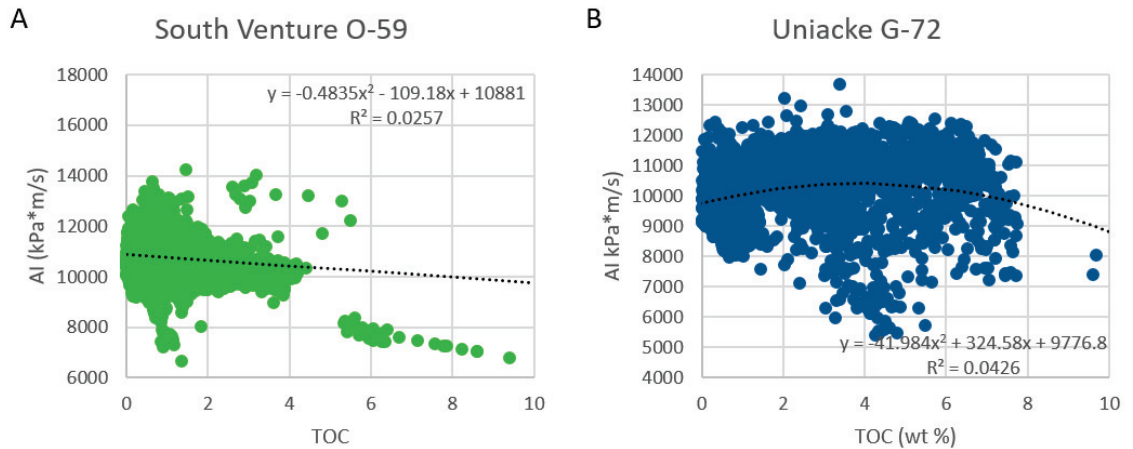
Figure 4-25: Acoustic impedance versus TOC cross-plots for the shales in A) South Venture O-59 and B) Uniacke G-72 for the inverted interval.
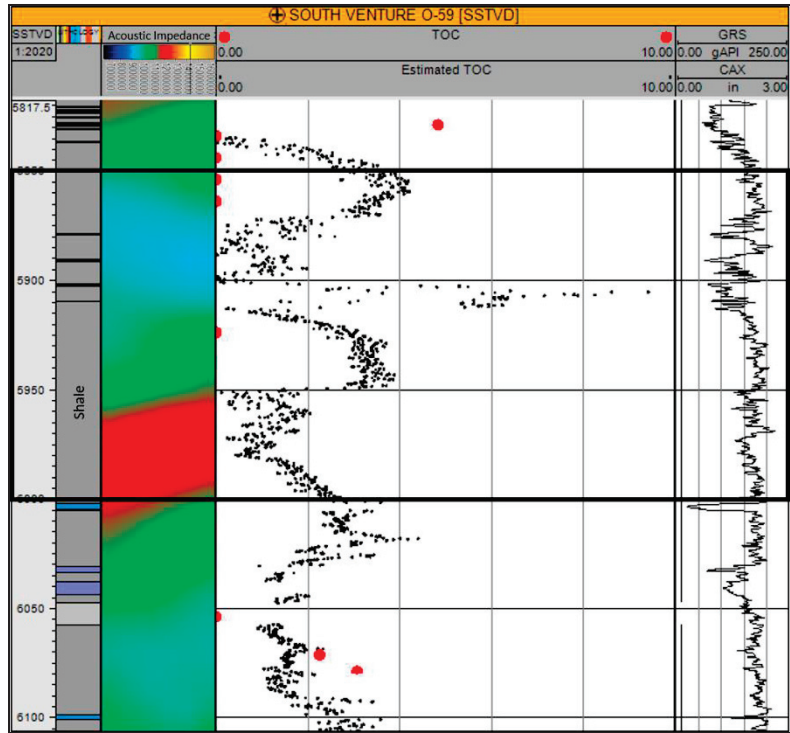
Figure 4-26: Well section of the South Venture O-59 well, outlining the correlated area in black, where increases in TOC correspond to lower AI values and higher estimated TOC values.

South Venture O-59 (5850-6000 m)

$y = -59.453x^2 + 11.861x + 10726$

$R^2 = 0.4786$
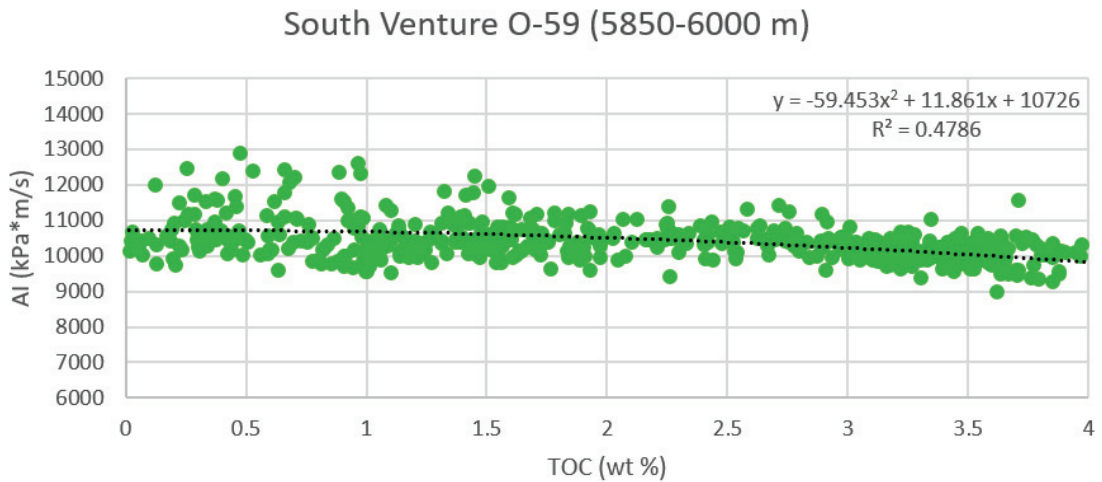
Figure 4-27:Acoustic impedance versus TOC cross-plot from the shales in South Venture O-59 between 5850-6000 m TVDSS.

95
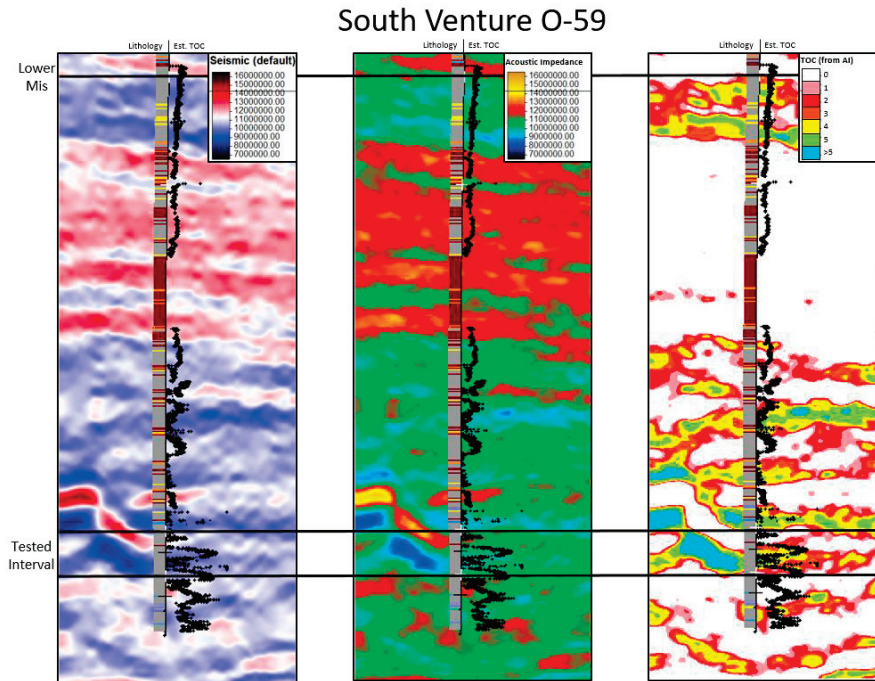
Figure 4-28: Seismic Inline surrounding the South Venture O-59 well, highlighting A) the original seismic data, B) the inverted seismic, and C) the TOC profile.

4.3.2   Inversion Derived Lithologies

The derived lithologies were extracted from the inverted cube and compared to CanStrat lithology logs, as well as calculated lithology logs. Figure 4-29, Figure 4-30, and Figure 4-31 compare the inverted cube to the lithological derivation at the three key cross-sections; IL 6180, IL 7340 and IL 7750. The correlation with the lithology logs are varied, achieving the highest correlation in IL 7750. Overlapping AI values, discussed in Section 5.3.2, are the main cause of error in this method. Furthermore, it is important to note that these derivations are not depth dependant. The calculation of a depth dependant relationship is a key point of future work to increase the accuracy of this result.
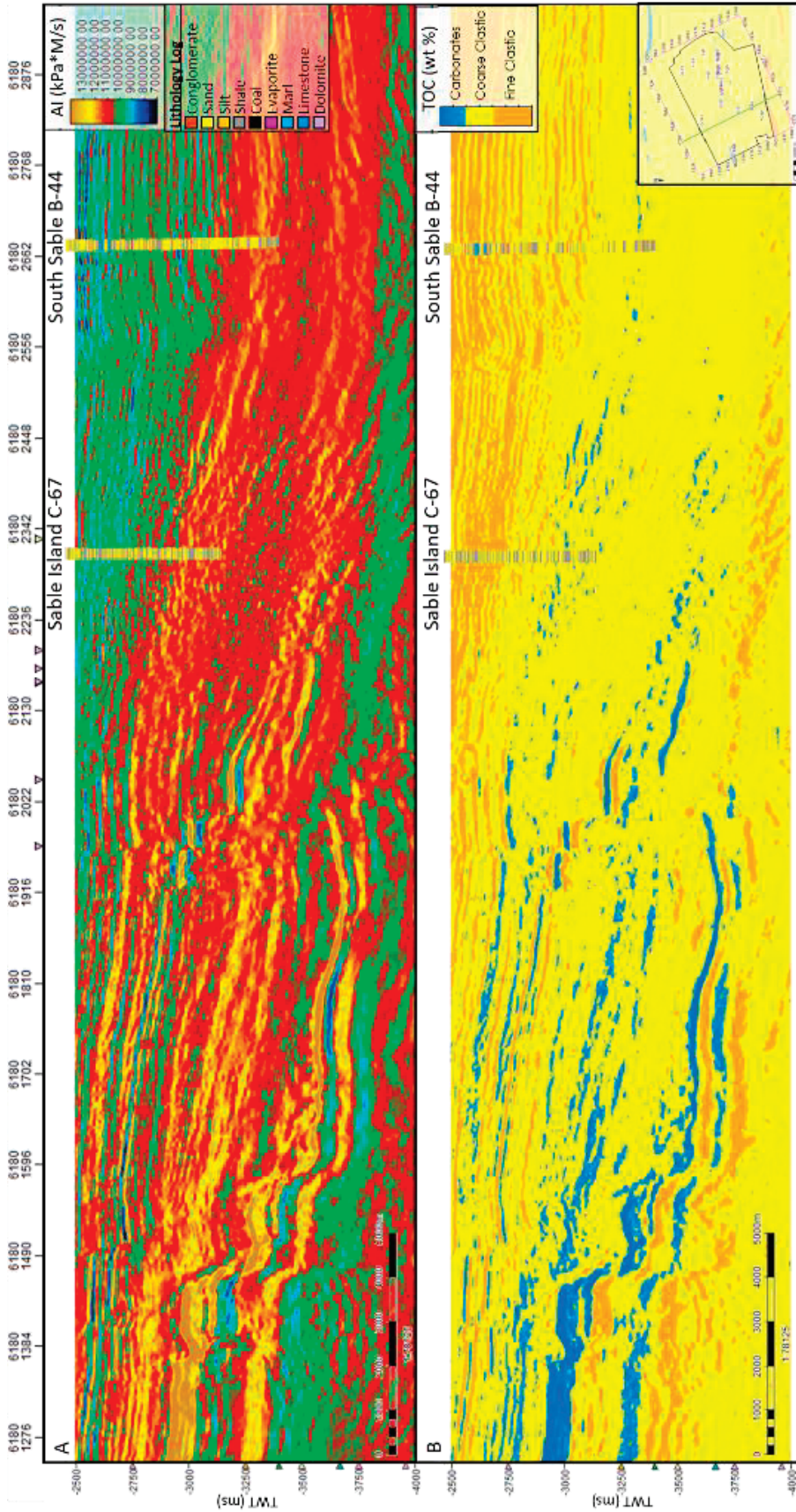
Figure 4-29: IL 6180; inverted seismic cube on top with derived lithology cube on the bottom, highlighting carbonates (blue), fine (orange), and coarse grained clastics (yellow). Wells displaying CanStrat lithology logs for broad comparison to derived lithologies.
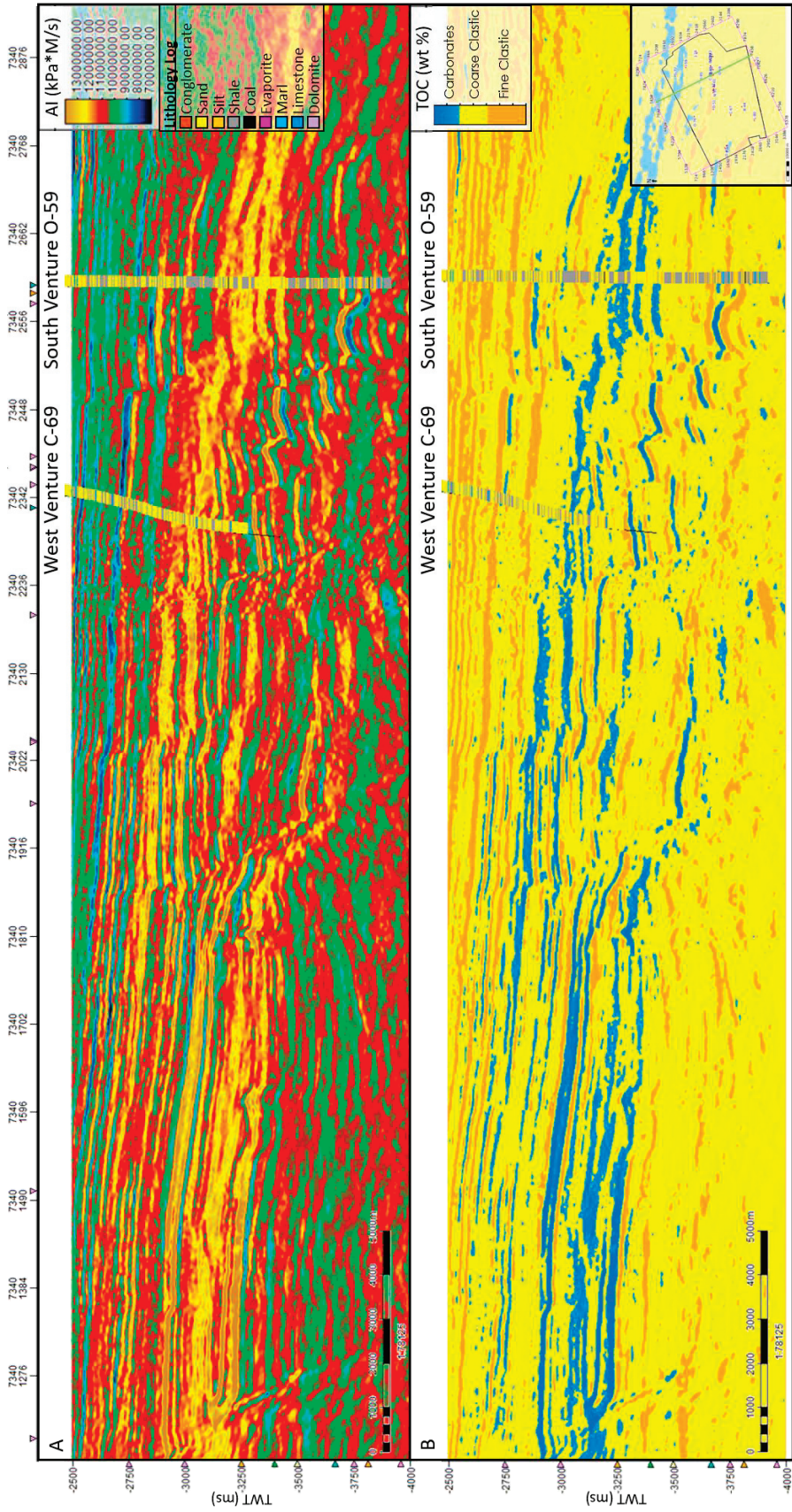
Figure 4-30: IL 7340; inverted seismic cube on top with derived lithology cube on the bottom, highlighting carbonates (blue), fine (orange), and coarse grained clastics (yellow). Wells displaying CanStrat lithology logs for broad comparison to derived lithologies.

98
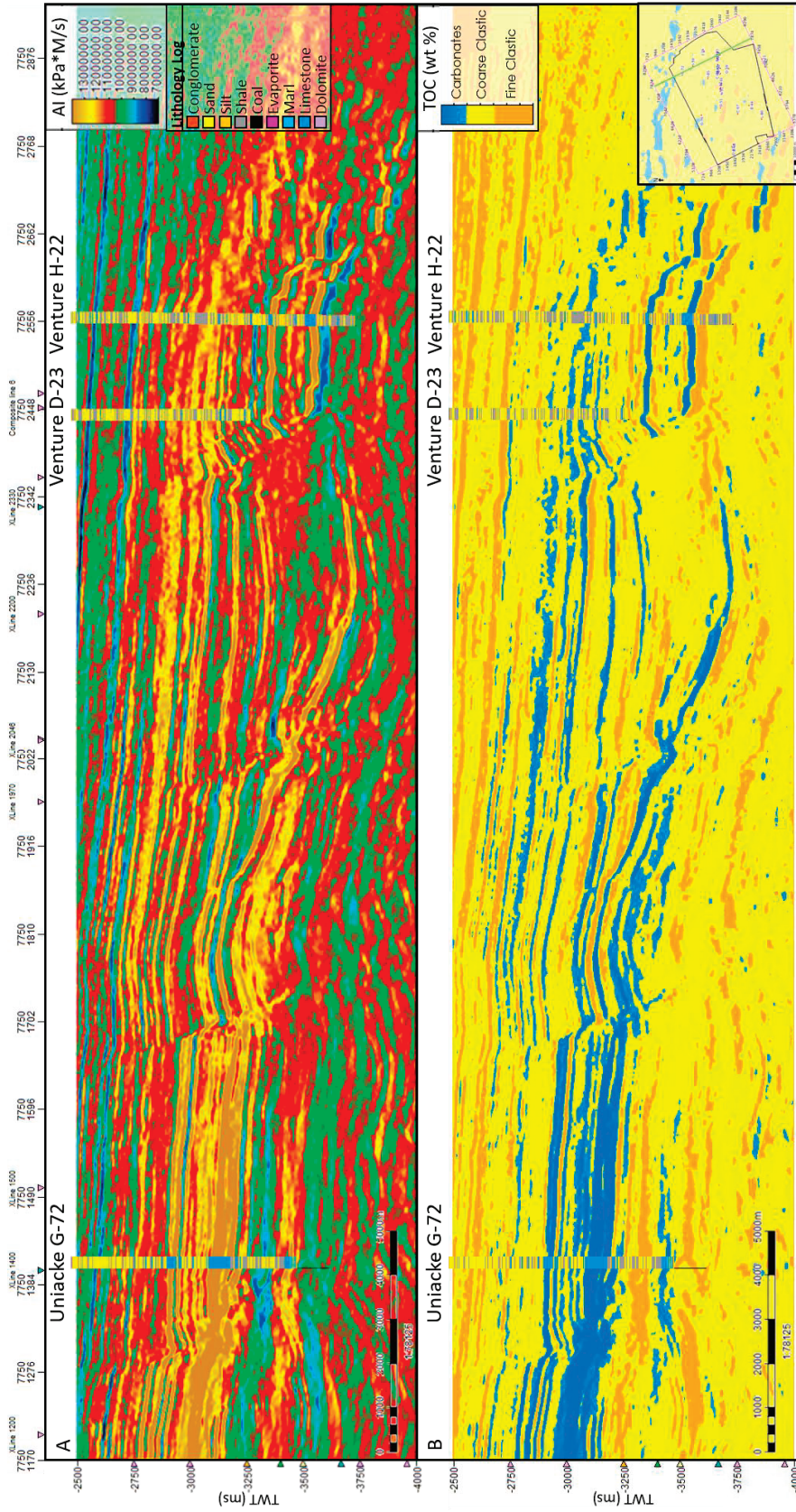
Figure 4-31: IL 7750; inverted seismic cube on top with derived lithology cube on the bottom, highlighting carbonates (blue), fine (orange), and coarse grained clastics (yellow). Wells displaying CanStrat lithology logs for broad comparison to derived lithologies.

Chapter 5:   Discussion

The main objective of this project was to investigate known and presumed Middle

to Upper Jurassic within the Sable Sub-basin using indirect petrophysical and seismic

methods. This was completed with focus on the Lower Mississauga Member, and the

MicMac and Verrill Canyon formations. In this section, each of the methods are

discussed in detail, including advantages, disadvantages, and why they yielded their

results. Furthermore, their applicability to the Scotian Basin was also reviewed.

5.1   TOC Restoration

TOC restoration was an important building block of this project. The method was

used to calculate the original TOC at the time of deposition. When compared to present

day TOC amounts, TOC^0 values allowed for a sense of how much hydrocarbons were

generated, if any, through time. Three separate methods were applied to the data, one

empirical and two mass balance respectively, to restore TOC values to their original

concentrations at the time of deposition: 1) Jarvie et al. (2005); 2) Jarvie (2012); and 3)

Peters et al. (2005).

It was evident that the calculated values (Figure 4-1) of the empirical equation

were much higher than those of the mass balance equations. The empirical equation of

method 1 (Jarvie et al. 2005) simply increased the measured TOC by 36%, based on the

assumption that the TOC of a source rock will decrease by approximately 36% from time

of deposition to generation in the dry gas zone (based on a dry gas zone of the Barnett

Shale) (Jarvie et al. 2005). This was the most optimistic of the three methods, showing a

consistent increase in source rock potential of the three formations analysed (Figure

5.2). It is important to note that if the high (> 4%) TOC values (assumed to represent contamination) were omitted, the source rock potential of the studied intervals does not reach "very good" (2-4% TOC). This suggests the studied intervals in the Sable Sub-Basin will not be prolific source rocks compared to intervals like the Egret Member (Jeanne d'Arc Basin) (e.g. Magoon et al. 2005; von der Dick 1989) or the Kimmeridge Clay (South West England) (e.g. Morgans-Bell et al. 2001, Hesselbo et al. 2009).

The biggest limitation of the mass balance equations (methods 2 and 3) was the assumption of initial hydrogen index (HI^0). In the absence of an immature sample or interval to obtain a value, HI^0 was based on the generic range values, based on kerogen type (Table 3-4) (Peters et al. 2005). For this project, the maximum and minimum values of HI were both used in the calculations, with the results averaged to obtain a final result. This allowed for a range of error estimation (error bars in Figure 4-1).

Method 2 (Jarvie 2012) results were more realistic than that of Jarvie et al. (2005). Though the restored values increased from the measured values, almost all fell within range of the error bars. The same observation was drawn from Method 3 (Peters et al. 2005). Figure 4-1 shows that some of the restored value calculations were lower than that of the measured TOC. This is likely due to underestimation of HI^0. However, these values still fall within the error bars. Overall, this indicated that there has been no measurable change between the initial and measured TOC values.

No measurable change in TOC from methods 2 and 3, in conjunction with the low source rock potential in the most optimistic method 1, leads to the conclusion that

there has been no significant change in the TOC content, thus little to no hydrocarbon generation in the studied intervals. It is important to note that these results are limited to the study area and does not indicate that there has been no generation from these intervals outside of the Sable Mega-Merge area. It is also important to note that the Sable fields have produced hydrocarbons for 20 years, and have an effective petroleum system with a viable source rock (e.g. Smith et al. 2014).

5.2   Wireline Methods
5.2.1   Passey Method
 The Passey Method (Passey et al. 1990) is an empirical method that calculates TOC and can aid in the identification of TOC-rich source rocks. The first point of discussion surrounding this method is the identification of a baseline. Passey et al. (1990) state that, in general, the sonic baseline used in this method stays the same throughout the entire well, while only the resistivity values are varied. Logs in the study area showed shales decreasing velocity with depth, therefore both baselines were re-evaluated within each formation or member of interest.

Within the data constraints of this project, the method was completed on the shales in the whole Middle–Upper Jurassic interval. These sections contained thick carbonate beds, as well as overpressured zones and reservoir intervals. These features have been known to cause anomalous log separations when using this method (Passey

et al. 1990). For instance, carbonate formations commonly have high resistivity due to low porosity and higher crystalline content, due to diagenesis (e.g. Rider and Kennedy 2011). The high resistivity increases ΔLogR response, seen in the Uniacke G-72 (Figure 5-1). Upon entering the carbonate interval, the resistivity increased close to an order of magnitude higher than the surrounding clastics. Though the sonic log decreased, due to the increase in seismic velocity, the increase in resistivity increased the ΔLogR response (Passey et al. 1990).
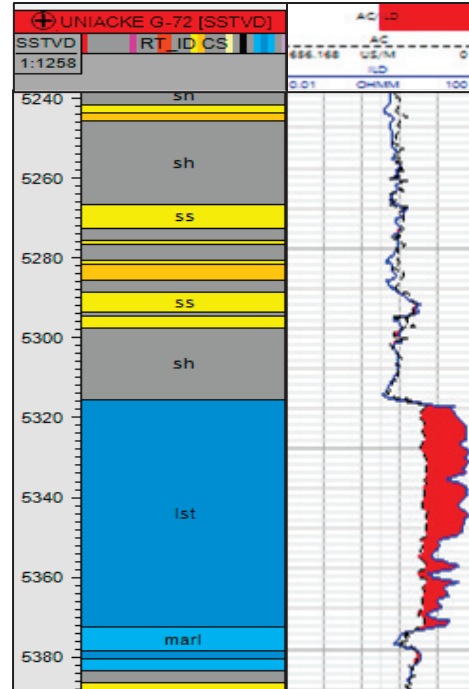
Figure 5-1: Limestone interval with Mic Mac Formation of the Uniacke G-72 well illustrating anomalous ΔLogR values in carbonate intervals due to increased resistivity.

Overpressured zones are also prevalent within the Sable Sub-Basin (e.g. Wielens 2003; Skinner 2016). Overpressured zones that are hydrocarbon bearing, or organic rich, often show higher porosity than expected for a given depth (Hancock 1992). The porosity in these shales appear higher due to the pressure pushing the tightly compacted grains apart (e.g. Hunt 1990). This phenomenon has been noted to cause additional anomalous separation of the sonic and resistivity curves (Passey et al. 1990). Finally, reservoir intervals gave anomalous ΔLogR separations due to the high resistivity of the hydrocarbons present (Passey et al. 1990; Rider and Kennedy 2011). The anomalous ΔLogR responses created difficulty when attempting to establish a baseline

in some wells, as these anomalous separations could often interfere with the separation in non-source intervals.

A second point of discussion was the comparison and scaling of the calculated TOC% data to measured TOC. This comparison was recommended by Passey et al. (1990) to ensure the most accurate results. Overall, the results of this method were inconsistent in some areas, when compared to the measured TOC values. Figure 5-2 shows two example wells, Olympia A-12 (A) and South Venture O-59 (B). Both the unscaled and scaled data are shown, both providing examples of an adequate and inadequate fit, when compared to the measured TOC values. The Olympia A-12 well estimated very accurate results within the Lower Missisauga Member, with no scaling required to adjust for measured TOC values. Within the MicMac Formation, even with a large scaling factor to adjust to measured TOC, estimates could not accurately be represented. Within the South Venture O-59 well, the unscaled data showed a trend in TOC estimates, from higher in the Lower Missisauga Member to very low in the Mic Mac Formation, which did not match the measured data. However, scaling was able to create an adequate correlation to measured TOC. Section 5.2.3 provides a discussion of the possible limitations of this method when used in the Scotian Basin.
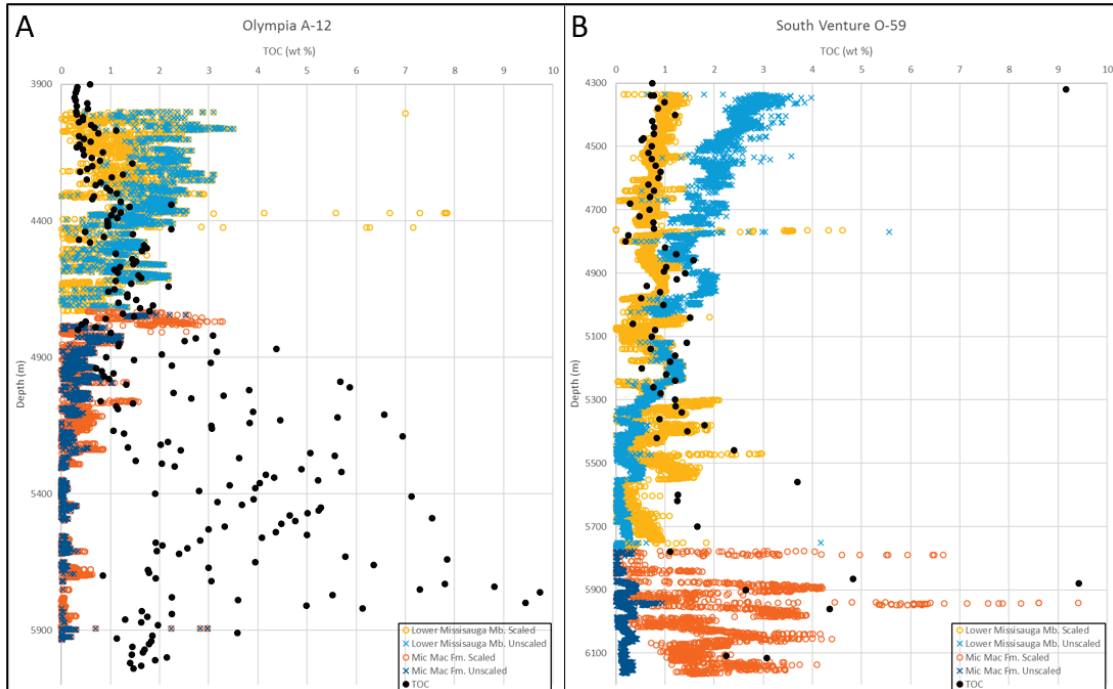
Figure 5-2: Unscaled vs scaled TOC estimation results for the (A) Olympia A-12 and (B) South Venture O-59 wells providing an example of both adequate and inadequate correlation to measured TOC data.

Note that many of the measured TOC data points measuring over 4%, like the anomalous values seen throughout the Mic Mac Formation, are likely contaminated and not true representations of the TOC throughout this interval (e.g. Mukhopadhyay 1990a). Section 3.3.2.7 outlines the contaminants and other factors, such as turbo-drilling and mud type, that could create these anomalous TOC values.

5.2.2 Sonic-Resistivity Cross Plotting

The Sonic-Resistivity cross plotting made use of the same basic principles as the Passey Method; however, it was used here only as a visual aid in identifying possible TOC rich intervals. The plots showed the expected general trends, with low velocity/resistivity, uncompacted sediments plotting in the top left and high velocity/resistivity compacted sediments trending toward the bottom right. However,

no outliers identifying high TOC content, i.e. no values presented excess resistivity when compared to the general trends of non-organic lithologies. Two examples of these cross-plots were shown in Figure 4-14. The cross-plots from Acadia J-16 and South Venture O-59, color coded by gamma ray intensity, were plotted over the entire studied interval and showed no values occur on these high TOC "branches". This was additional evidence that the TOC values in the studied intervals are too low to produce a log response.

5.2.3   Applications to the Scotian Basin

Wireline TOC determination methods, such as the Passey Method, are proven to work best in thick organic-rich shale intervals (e.g. Passey et al. 1990). Within the Sable Sub-Basin, extensive and high TOC shales are not a common, which meant there were some issues in applying the method. For instance, difficulty in establishing a baseline was a problem encountered for a portion of the wells, including Venture B-52. This was likely due to extensive overpressure, and possible carbonate intervals, creating anomalous separation in the ΔLogR response in the non-organic shale intervals. When a baseline was unable to be established, the baseline from the closest well, in this came the neighboring Venture B-43 well (appx. 2500 m away) was used. This extrapolated baseline, from a neighbouring well, adds uncertainty when estimating the TOC values. Furthermore, the stratigraphic and structural variability made calibration between wells difficult.

Secondly, the limited thickness of the shales in the study area altered the effectiveness of this method. Typically, the Passey Method is completed on wide-

spread, thick shales. Within the Sable Sub-Basin, there are many thin interbedded shales less than a few meters thick. Petrophysically, intervals with thicknesses less than the combined resolution of the resistivity and sonic logs, approximately 1 m, cannot be reliably quantified (Passey et al. 1990). A strong shale signal from a thin bed may be masked by surrounding geology, giving an incorrect TOC estimate. Though it is possible source rocks as thin as 0.33 m can be identified using this method, results are not accurate (Passey et al. 1990). Many of the shales within the study area are only approximately 0.5 m thick and could fall below log resolution. Though shales this thick would not be considered viable source rocks, this could mask high TOC intervals.

Finally, this method was calibrated using TOC measurements. As discussed above, it is accepted that drilling practices have introduced contaminants to many of the samples tested in the basin and many of the high TOC values measured are likely a result of contamination (e.g. Mukhopadhyay 1990a; Fowler et al. 2016). Overall, the Passey method's accuracy and success in the Sable Sub-Basin was variable. The method did not identify new intervals of high TOC values. Nevertheless, it did help identify possible contaminated intervals within the geochemical data. Within a single well interval, adequate estimations were achieved, especially when tested on thicker shale intervals outside the studied area (i.e. the Lower Cretaceous Shortland Shale in the Louisbourg J-47 well). However, both baselines and scale factors change from well to well, even with RockEval calibration. This level of uncertainty, as well as needing the comparison of the measured data, has deemed the method inapplicable on a basin wide scale in the study area.

5.3 Seismic Methods
5.3.1 Seismic Interpretation

The seismic modeling was completed on the eastern portion of the Sable MegaMerge (Figure 1-3). The salt deposited in the Late Triassic to Early Jurassic created a mobile substrate. Relatively rapid sediment loading from the Sable Delta initiated salt movement created significant listric faulting throughout the basin (e.g. Cummings and Arnott 2005; Adam et al. 2010). This expansion trend allowed for the storage of additional siliciclastic sediment and carbonate sedimentation not observed higher on the shelf (Eliuk 2016). This depositional trend can be seen in the lithostratigraphic cross-sections in Figures 4-17, 18 and 19. These formations disappear higher on the shelf due to insufficient accommodation space or sediment bypassing (G.D. Wach (personal communication, 2017)). These elongate depocenters may have had the required conditions for the accumulation and preservation of organic matter; therefore, these regions were highlighted as areas of interest to re-evaluate once the inversion was completed.

5.3.2 InverTrace Plus Inversion

Throughout the course of this project, approximately 30 inversions were run on the eastern Sable MegaMerge study area. Due to the post-stack nature and unknown parameters surrounding the seismic data (e.g. acquisition and processing methodology), the identification of an appropriate wavelet was crucial in completing the most accurate inversion possible (Cooke and Cant 2010). Therefore, testing of four wavelets, with varying bandwidths, was completed to identify a suitable wavelet, with the final

inversion completed over an interval between 2500 to 4000 milli-seconds using a 0 to 55

Hz bandwidth wavelet and all wells with deviations of less than 100 m.

The resulting inversion cube allowed for the lithologies and stratigraphy of the basin

to be qualitatively discriminated. However, many lithologies have similar acoustic

impedance values, as seen in the overlapping values in Table 3.6. Understanding the

geology of the basin and the depth at which the inversion has been run, coupled with

the attempt at lithology extraction, allowed for a more accurate discrimination (eg.

Løseth et al. 2011). For instance, the outlined area in Figure 5-3 shows high impedances

values of approximately 14000000 kPa*m/s (darkest yellow color). Referring to Table

3.6, this value could fall into the range of a limestone, shale or sandstone. Lithofacies

and stratigraphic analysis of the CanStrat lithology logs indicate that these high AI values

correspond to carbonates at this depth in the basin.
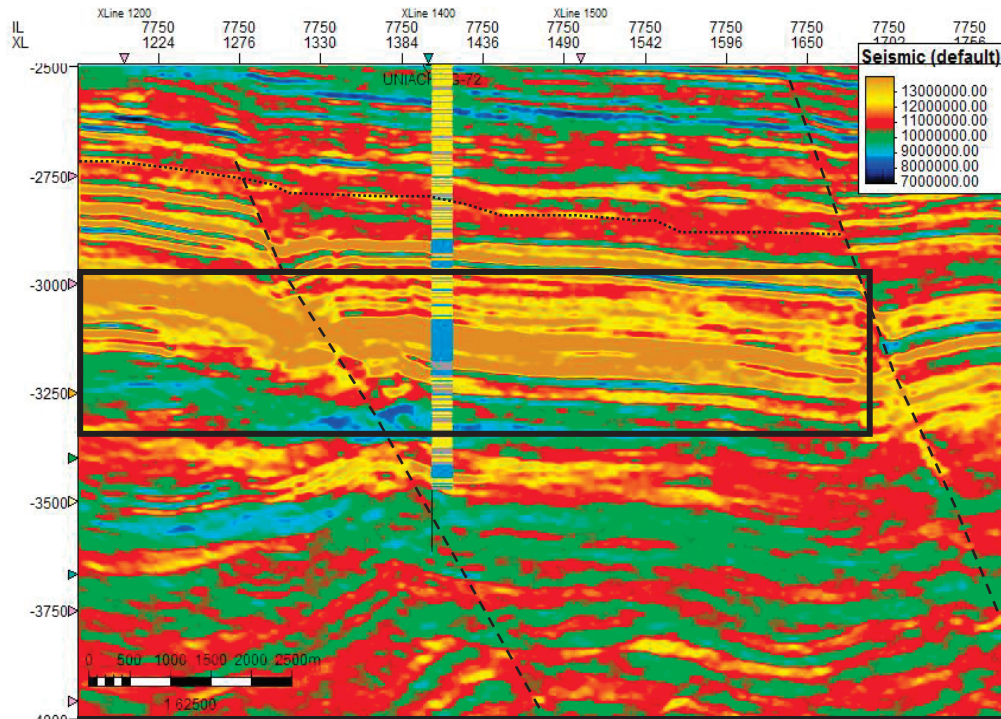
Figure 5-3: Acoustic Impedance inversion cross-section of Inline 7750 highlighting the high impedances of the Penobscot Limestones and their agreement with the limestones highlighted by the CanStrat lithology logs.

The assumption that the highest impedances equate to carbonates stays consistent within the Mic Mac Formation (black dotted line), as seen in Figure 5-4. Within the overlying Lower Missisauga Formation, deposited in a siliciclastic regime, the high impedances often correspond to tight sand intervals, which have similar high impedances to limestones (yellow and orange on CanStrat log).

Shales however, at this depth and in both formations, consistently have lower impedance. With increasing depth and compaction, porosity decreases which increases density and lowers sonic travel time, thus lowering acoustic impedance. The decrease in acoustic impedance follows the trend in Figure 3-9 (Brown 2004). This point highlighted the need for additional work, taking depth dependence into account to derive a more accurate lithology extraction.

110

The AI inversion highlighted major changes in lithology, aided in the interpretation of major facies changes, especially where carbonates begin to "shale out" (transition from carbonate) and become shale. An example of this can be seen in Figure 5-4, along IL 7750. Following the Penobscot Limestone horizon in black from left (NW) to right (SE), a change in acoustic impedance is observed, from close to 14000000 kPa*s/m decreasing to 9000000 kPa*s/m within the next fault block, illustrated by the color change from yellow/red to green/blue. These lower impedances are interpreted as shales or marls at the tip of the carbonate bank. Identification of areas like this was important, as these shales are often highly organic rich (e.g. Harris et al. 2008).
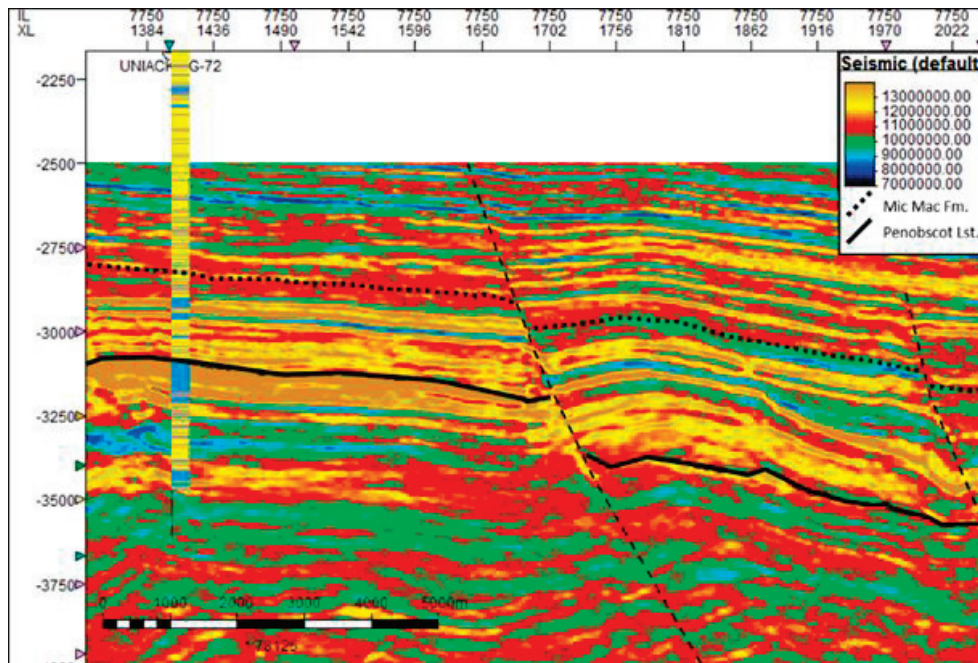
Figure 5-4: AI inversion cross-section of Inline 7750 highlighting the top of the Mic Mac Formation (black dotted line) and the top of the Penobscot Limestone (solid black line).

5.3.2.1 Low Impedance Identification

The overall goal of the inversion process was to locate low impedance (possibly organic-rich) shales. Low impedance intervals were observed in all three of the key seismic cross-sections (Figure 5-5, Figure 5-6, and Figure 5-7). The first intervals that stood out were the low impedances under the Citnalta and Penobscot limestones in the northwest. The distal shales at the toes of these carbonates also displayed promising low impedance values. These facies represent the distal foreslope and basinal equivalents of the Abenaki Bank (e.g. Weissenberger et al. 2000). Moving toward the southeast, a second set of low impedance intervals was found deeper in the expansion trend, pinching out toward the northwest; these intervals stratigraphically fell below the Venture carbonates. These sediments are deltaic in nature, interbedded with shelf margin carbonates (Wade and Maclean 1990). Possible reasons for these low impedance zones included the possibility that these intervals are organic-rich shales, explained by the non- linear relationship between AI and TOC (e.g. Løseth et al. 2011), as well as the Venture sands, which are charged with hydrocarbons, created a lower impedance response in some areas. Identification of the reservoir intervals, however, indicated a higher impedance than the surrounding shales.
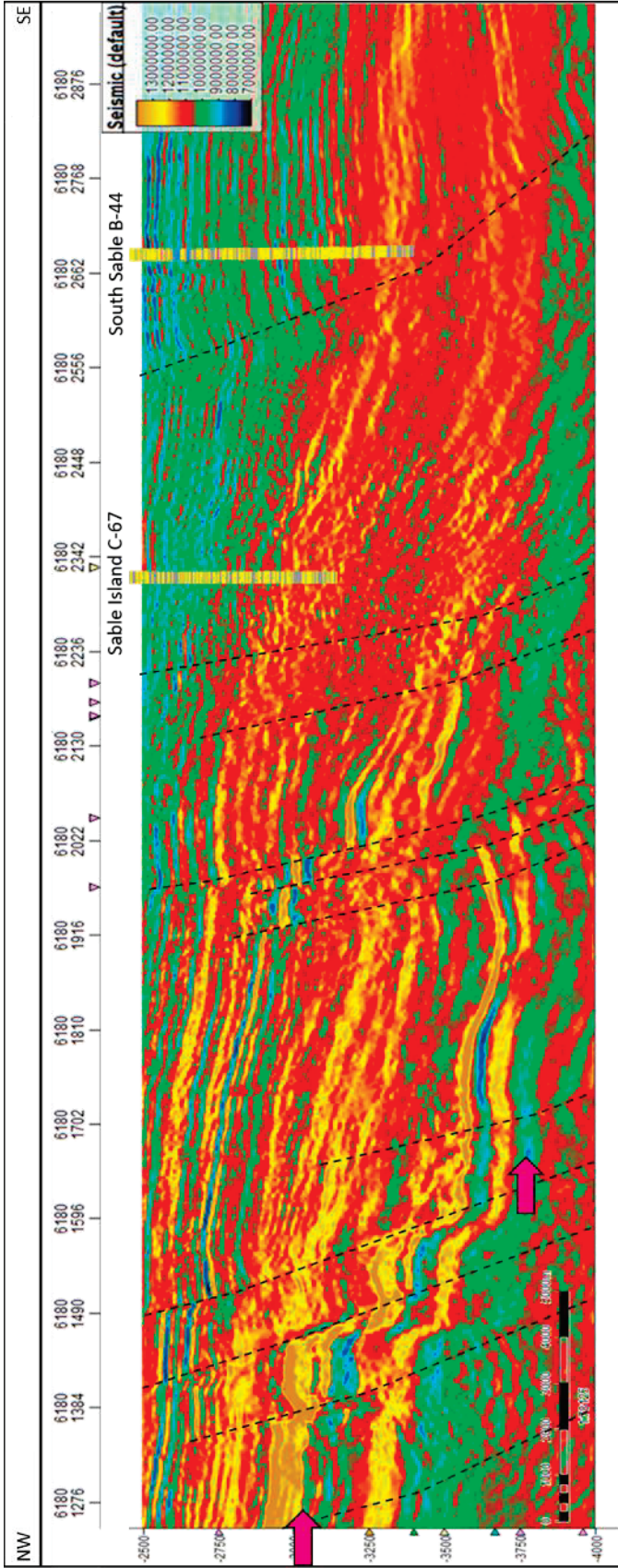
Figure 5-5: Acoustic impedance cross-section of Inline 6180 with the sub-carbonate, low impedance intervals identified by the pink arrows.
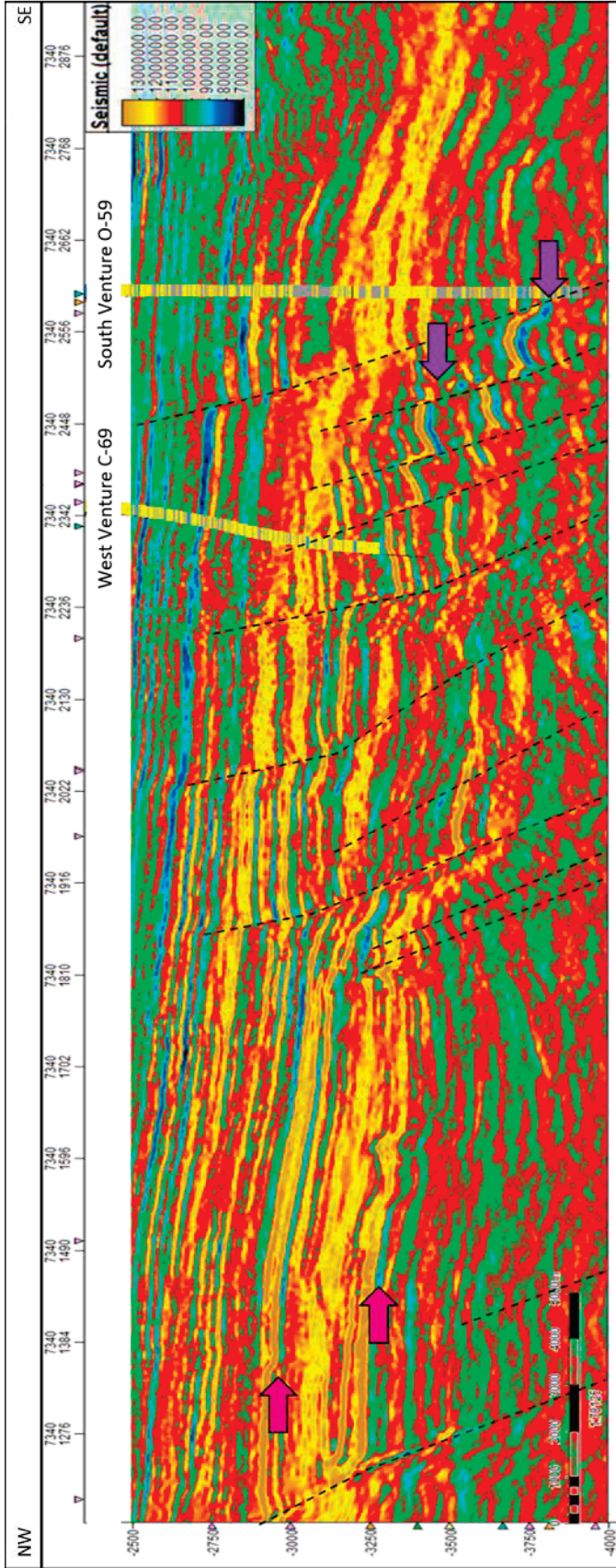
Figure 5-6: Acoustic impedance cross-section of Inline 7340, with the sub-carbonate low impedance intervals identified by the pink arrows and the expansion trend, low-impedance intervals by the purple arrows.
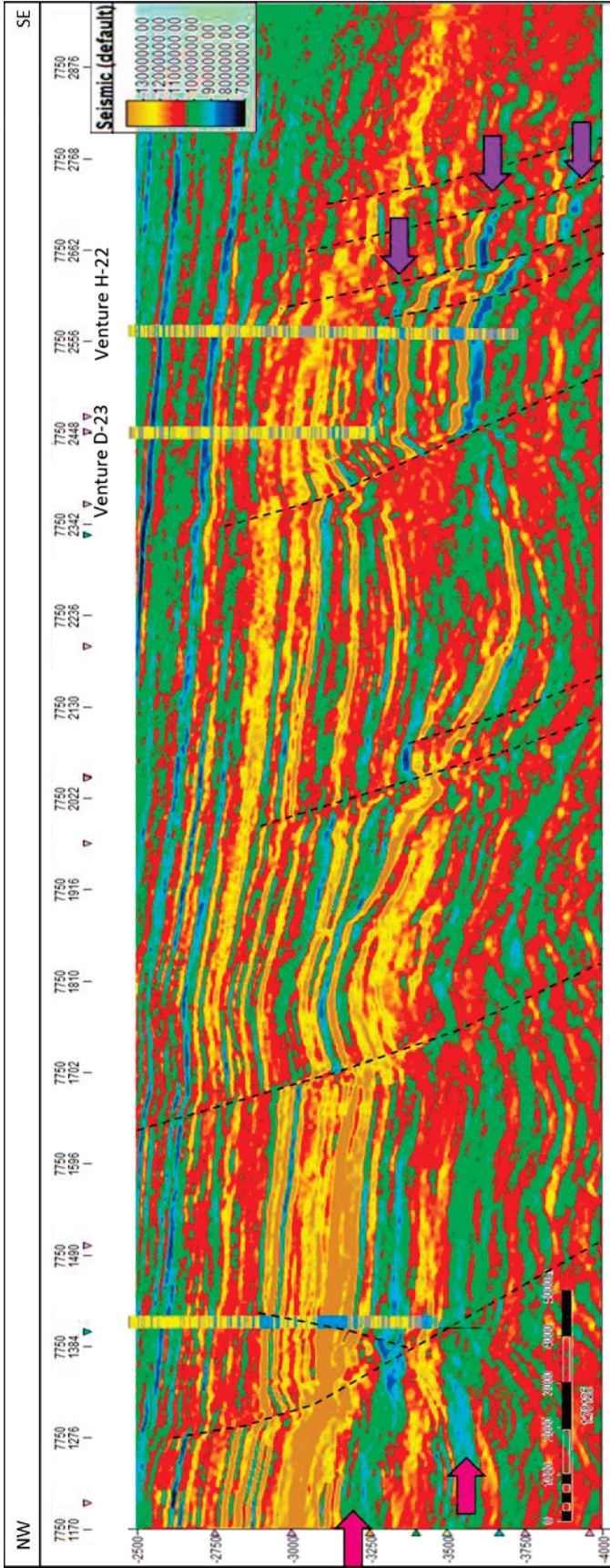
Figure 5-7: Acoustic impedance cross section of Inline 7750, with the sub-carbonate low impedance intervals identified by the pink arrows and the expansion trend, low-impedance intervals by the purple arrows.

It is interesting to note that the expansion trend seen in inline 6180 appears to contain no low impedance intervals (Figure 5-5). This is contrary to the prediction that these basins would be ideal for the deposition and preservation of organic matter, if anoxic. That being said, well control was limited in this area; therefore, the low frequency model was extrapolated from other areas, which potentially skewed the inversion. An overprint of high impedance values from higher-up on the shelf due to this extrapolation was seen quite extensively in the IL 6180 cross-section. This is not the case for all the sediments in the expansion trends. Both cross-sections of IL 7340 and 7750 clearly displayed higher impedance values in shales.

5.3.3 Software Uncertainties

There were limitations in the inversion process surrounding constraints of the software. There was uncertainty surrounding how large of an interval an estimated wavelet can adequately model. Schakel (n.d.) states that conventional inversions, such as the Jason CSSI, use wavelet estimations for intervals less than 200 ms (Schakel n.d.). This project completed inversions on much larger intervals, ranging from 1000 to 4000 ms. This had the potential to inadequately model the AI, by extrapolating values using a wavelet not specific enough to fully resolve an interval of that size. Testing of both smaller and larger intervals were completed and an interval of 1500 ms was selected to have satisfactory resolution and was used in the final inversion. That is, no major change in resolution and inversion quality was observed when compared to a much smaller, 500 ms time range at this depth.

An important limitation of the software is that a seismic-to-well tie is unreliable if the well is deviated beyond 100 m (Fugro-Jason, 2013). Within the study area, this reduced the number of usable wells to 15. Limiting the well control had the possibility of decreasing the accuracy of the inversion in these areas. However, a blind test was completed which compared the log derived AI values of the eliminated wells to the derived AI values from the inversion at the well location and the values were found to trend well with one other.

Finally, the low frequency model is only accurate and reliable to the depth of the wells. Below the well data depth, the software no longer has the data or input it to fit, interpolate and extract the data from (Fugro-Jason, 2013). Therefore, the software estimated or extrapolated AI values from neighbouring wells, which may not have equivalent geologies at that depth. Simply, that meant the depths not penetrated by a well could exhibit a decrease in accuracy of the inversion. This factor was considered, in combination with the interval of interest and the chosen wavelet interval, when deciding the interval at which to run the inversion. It was concluded the 2500 to 4000 ms interval would produce the most accurate and reliable results. To increase the depth of the inverted interval, future work could include the creation of pseudo-logs for each well, which would allow for deeper extension of shallower wells and more accurate extrapolation.

5.3.4   Seismic Uncertainties

The post-stack nature of the Sable MegaMerge seismic cube introduced additional limitations, most obvious being that inversions that incorporate AVO are not possible.

However, in consolidated Jurassic rocks, with thin hydrocarbon reservoirs and good

zero-offset synthetic ties, this is a minor shortcoming in lithology estimation via AVO.

Similar to the drawbacks of the Penobscot inversion completed by Campbell et al.

(2015), this project assumed zero- offset or normal incidence, which omitted the

oblique ray path interaction between S- and P-waves. These ray paths are important

when distinguishing fluid effects from normal lithology changes, which added

uncertainty in reservoir rich areas such as the Venture Field (Campbell et al. 2015).

Furthermore, the Sable MegaMerge is a merged volume. There were minor

degradations in data quality found where the surveys were merged, as well as seismic

acquisition overprints around Sable Island (Figure 1-3).

Anderson (2009) states that a pre-stack inversion produces a more valuable result

when compared to a post-stack. In younger, less compacted sediments, this is often the

case. Preforming a post-stack inversion requires the P- and S- impedance models to be

inverted as separate entities (Anderson 2009). This means that the signal to noise ratios

of each are not correlated, and thus act independently within their respective models. In

addition, post-stack data does not allow for angle-dependant (AVO) study, which could

affect the accuracy of reflectivity estimations, and has also been known to include high

frequency artefacts (Anderson 2009). It was important to keep these considerations in

mind when interpreting the inversion data.

5.4   *Source Rock from Seismic Method*
Shales at the depth of interest accurately appeared as low impedance values, starkly

contrasted by the high impedance carbonate and sandstones around them. This is

consistent with the principles outlined in Løseth et al.'s "Source Rock from Seismic method". However, the non-linear relationship between AI and TOC described by Løseth et al. (2011) was not found. This was determined to be caused by the overall low TOC contents of the studied shales and the inconsistent results of the Passey method. Additionally, this project attempted to apply this method at a much larger scale than Løseth et al. (2011). Løseth focuses on an approximate 50 ms seismic intervals of interest, over single shale units. In this study, the seismic intervals studied were up to 300 ms and often consisted of more than one shale interval.

The ideal parameters of this method, as laid out by Løseth et al. (2011), state shales must be greater than 20 m (above tuning thickness), and have TOC values higher than 3 or 4 %, to produce a substantial reduction and increase (top and base reflection) in AI. TOC values in the Scotian Basin are generally not this high. Furthermore, the Scotian Basin does not have thick, TOC rich shales, compared to the Kimmeridge Clay or Draupne shales tested in Løseth et al. (2011).

An additional limitation is the depth of the potential source intervals in the Scotian Basin. It has been observed, as presented in Løseth et al. (2011), that the AI contrast between organic and non-organic rich claystones remains stable down to a depth of 4500 m (an oil mature source rock). Although not explained in their study, it is assumed that below this depth the AI contrast is reduced, due to loss of TOC content during hydrocarbon generation (Løseth et al. 2011). Observing the wells and seismic data used in this study of the Scotian Basin, the identification of some areas of interest below this depth meant that the probability of identifying the exact intervals of organic richness

was reduced, as the non-organics will have a similar AI signature to the organic rich

rocks. Finally, Dutta et al. (2002a) noted acoustic impedance in overpressured zones can

appear lower than surrounding normally pressured zones. Because overpressure is

known to occur in the Scotian Basin (e.g. Wielens 2003; Skinner 2016), low impedance

intervals had the possibility of being incorrectly identified as TOC rich shales.

5.4.1   Scotian Margin Results

The results of the source rocks from seismic method were inconclusive and

varied from the examples presented in Løseth et al. (2011) (see also Ouadfuel and

Auadfeul 2016). Attempting to plot acoustic impedance values versus TOC of the shales

within the entire studied interval yielded no discernible relationship (Figure 4-24).

Attempting this correlation at an individual well level yielded similar results in the

majority of the wells. Some wells, such as South Venture O-59, visually illustrated a

more meaningful correlation (Figure 4-25 A), however clusters of low impedance/ low

TOC values were present which created a low R^2 value of the trendline.

The method was then attempted at a 150 m interval on the South Venture O-59

well. Though it yielded a trendline with a relatively low R^2 value of 0.4786, a profile was

still created to test the method. The profile created from the AI relationship seemed to

overestimate the TOC values in shales outside the tested 150 m. There is an additional

uncertainty in this section, where a coal is identified by the CanStrat logs, that could be

the overlying cause of the low impedance values.

With no discernible correlation between AI and TOC, coupled with the

uncertainties surrounding the geochemical analysis and the Passey Method, it was

concluded that the TOC profiling would not work on a basin wide or seismic cube (~2100 km^2) scale.

5.5 Overpressure

An alternative explanation for the anomalous low acoustic impedance in some shale intervals is overpressure. Pennebaker (1968) described the change in bulk elastic properties of a rock due to the relationship between the expansion of the rock from overpressured fluids and the reduction in bulk density and velocity. Dutta et al. (2002a) highlights the observation that seismic velocity, thus acoustic impedance, in overpressured zones appears to be lower than in normally pressured intervals at equal depths.

In this study, low impedance calcareous shales, highlighted in the seismic inversion can be correlated, via well calibration, to overpressured zones (Figure 5-8). This means it is possible, as outlined by Dutta et al. (2002b), to image overpressured zones using the obtained seismic inversion. It was suggested that late stage hydrocarbon generation and migration in the Scotian Basin (see Skinner 2016 and Wong et al. 2015) is the cause of the overpressured intervals in certain areas of the Sable Sub-Basin. I suggest that the low acoustic impedance shales highlighted in this study result from overpressure. If this assumption is true and overpressure results from hydrocarbon generation processes, then it provides indirect evidence of source rock presence outside the study area. Since overpressure is a key risk factor in the Scotian Basin (e.g. Skinner 2016), this would be an excellent topic for future work.
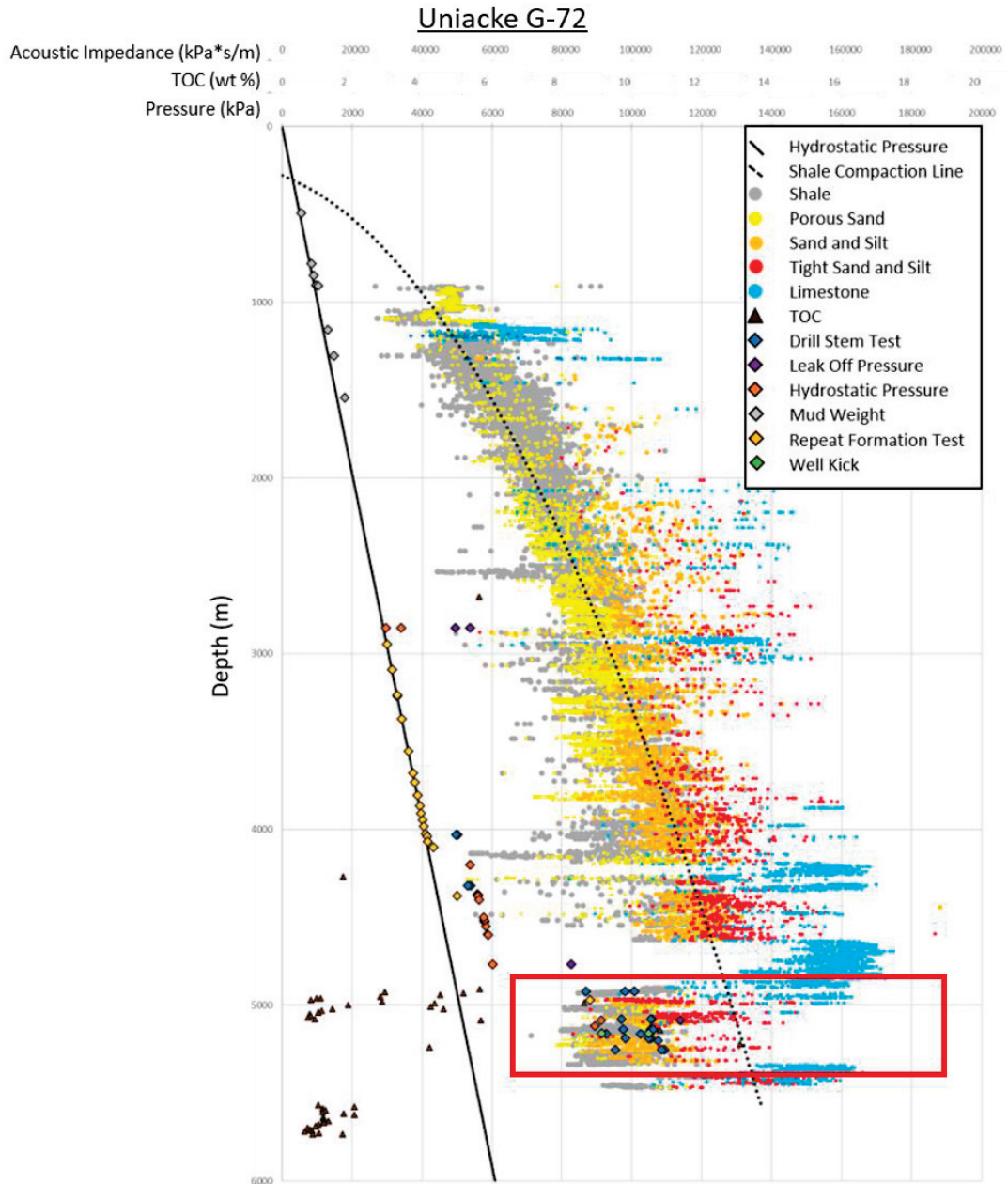
Figure 5-8: Cross-plot of AI, TOC and pressure measurements versus depth. The red box shows the interval of low AI that corresponds with excess pressure values.

Chapter 6:   Conclusions and Future Work

6.1   Conclusions

Though there are proven hydrocarbon accumulations in both Jurassic and Cretaceous reservoirs, as well as numerous studies and analysis done on shales in the Sable Sub-Basin, there have been difficulties identifying a definitive source of the hydrocarbons in what is an effective petroleum system (Fowler et al. 2016). The published TOC and RockEval pyrolysis data are often unreliable due to extensive use of oil based muds, lignite additives and turbo-drilling practices (e.g. Mukhopadhyay 1990a). The Scotian Margin is considered to have lean or low organic matter content, yielding low average TOC values, with a basinal average of approximately 0 to 2% (e.g. Mukhopadhyay 1989, 1990a, 1990b, 1991). Well penetrations of Jurassic sediments, a known time of prolific source generation along the Atlantic Margin, are very limited in this area.

The objective of this project was to investigate known and presumed Middle to Upper Jurassic source rocks within the Sable Sub-basin using indirect methods. It was hypothesized that source rocks intervals could be identified by petrophysical and seismic techniques, making use of the Sable MegaMerge seismic survey and calibrated well logs.

Results of this hypothesis were negative; though lean organic matter is present throughout the study area (e.g. Mukhopadhyay 1989, 1990a, 1991), prevalent source rocks could not be imaged using seismic inversion. The petrophysical methods did not identify specific intervals of source rock in the eleven wells studied, even when the TOC

123

values calculated were compared to the measured TOC values from studies published on these wells (e.g. Mukhopadhyay et al. 1990a, 1995). TOC and RockEval data in these studies, and data from the BASIN Database, show similar low TOC values and identify contaminants that can skew results to over 4% TOC (Mukhopadhyay 1990a; NRCan 2016).

The seismic inversion was effective in mapping low acoustic impedance intervals, especially calcareous shales; however, a strong relationship between AI and TOC was not found. This was the result of the low TOC contents of the thin shales that were investigated. The studied shale intervals have insufficient thickness and organic richness to be considered viable source rocks.

The conclusion of this research is that the petrophysical and seismic techniques used in this project do not identify presumed or potential source rocks within the study area of the Sable Sub-Basin. This is the first time that these approaches to source rock presence and distribution have been publicly documented in offshore Nova Scotia. Though the results were not promising for source rock identification in the study area and stratigraphic interval, the method should not be ruled out for use on other parts of the Margin, and did identify a link between low AI sections mapped via seismic inversion and overpressure.

6.2   Future Work

This project identified future work surrounding the wireline TOC determinations. Firstly, a more in-depth screening of poor borehole conditions, which skew the log and thus create anomalous ΔLogR separation, will need to be completed to ensure invalid

TOC estimations are not included within the results. In addition, modifications to numerous factors within the Passey Method were recognized to increase the accuracy of the TOC estimation. The first of these factors recognised was the identification of the baseline. Using a compaction trend, derived from both the sonic and resistivity logs using an algorithm such as the Hamouz-Mueller Method, will increase the accuracy of the estimation. This is preferable to using a single value estimated over a studied interval would take depth and compaction into consideration and could be adjusted for factors such as overpressure, which is common in many of the wells within this study and is present in other basins around the world.

Additional work could also be completed on the TOC estimation equation. For instance, attempting to use a natural log, instead of the base ten, to calculate the TOC. When tested on an interval in the South Venture O-59 well, suitable results were obtained. Possible adaptations, such as this, to the original equation could produce a more accurate result. Furthermore, modifications such as eliminating the need for maturity LOM input, much like that of the Issler Method, could increase the accuracy of the result and the usability of the method in wells without geochemical data.

Additional work on the lithology extraction should also be completed; adjusting the broad scale method to make it depth dependent. This would take compaction and velocity changes into account and could eliminate some of the error and uncertainty discussed in Section 5.3.2.

Finally, the link between overpressure and low impedance intervals could be explored in greater detail. This could lead to overpressure identification and risk mitigation in undrilled areas of the Scotian Basin. To do this, however, would require additional seismic data. Dutta (2002) indicated pressure analysis work should be completed on migrated and dip move-out processed datasets. The Sable MegaMerge was not processed for velocity analysis. Therefore, velocity inversions of this dataset could produce ambiguous velocities and alter overpressure findings.

References

Adam, J., Cody, M., Campbell, C., Cribb, J., Kreszek, C., Nedimovic, M., and Grujic, D. 2010. Basin-Scale Salt Tectonic Processes and Sediment Progradation in the Slope and Deepwater Basin of the North-Central Scotian Margin. *In* Proceedings of the International conference on Salt Tectonics, Sediments, and Prospectivity.

Anderson, P. 2009. Comparing post-stack AVO inversion to prestack inversion for estimating rock properties. *In* Proceedings of the Frontiers and Innovation CSPG CSEG CWLS Convention, Calgary, Ab. pp. 669-672.

Backus, G. E. 1962. Long-Wave Elastic Anisotropy Produced by Horizontal Layering. Journal of Geophysical Research, **67**(11): 4427-4440.

Barber, S. 2001. Investigations to Seismic Inversion – Preface. Presented at the Huston Geologic Society, Huston, TX.

Becquey, M., Lavergne, M., and Willm, C. 1979. Acoustic impedance logs computed from seismic traces. Geophysics, **44**(9): 1485-1501.

Belaid, A., Krooss, B.M., and Littke, R. 2010. Thermal history and source rock characterization of a Paleozoic section in the Awbari Trough, Murzuq Basin, SW Libya. Marine and Petroleum Geology, **27**: 612-632.

Beicip-Franlab. 2011. Play Fairway Analysis (PFA) offshore Nova Scotia Canada [online]. Available from http://www.oera.ca/offshore-energy-research/geoscience/play-fairway-analysis/ [cited September 30 2014].

Beicip-Franlab. 2016. Central Scotian Slope Atlas [online]. Available from http://www.oera.ca/offshore-energy-research/geoscience/central-scotian-slope-atlas-2016/ [cited March 1 2017].

Brown, A.R. 2004. Chapter 5 - Reservoir Identification. *In* Memoir 42 and SEG Investigations in Geophysics, No. 9: Interpretation of Three-Dimensional Seismic Data (Sixth Edition). American Association of Petroleum Geologists, Tulsa, Ok., pp. 153-197.

Burger, H., Sheehan, A., and Jones, C. 2006. Introduction to Applied Geophysics: Exploring the Shallow Subsurface. W. W. Norton & Company, New York, N.Y.

Burrel, S., Earley, K., Ellison, K., and Seifert, M. 1983. Well History Report. Mobil et al. Venture B-52.

Campbell, T.J., Richards, F.W., Silva, R.L., Wach, G., and Eliuk, L. 2015. Interpretation of the Penobscot 3D Seismic Volume Using Constrained Sparse Spike Inversion, Sable Sub-Basin, Offshore Nova Scotia. Marine and Petroleum Geology, **68**: 73-93.

CNSOPB, C.-N.S.O.P.B. 2014. Information on Well Data, Geological Data, and Geophysical Data [online]. Available from http://www.cnsopb.ns.ca/sites/default/files/pdfs/information_on _well_data_geological_data_and_geophysical_data_april_2014.pdf [cited 23 March 2017].

CNSOPB, C.-N.S.O.P.B. 2016. CNSOPB Directory of Wells: Nova Scotia Offshore Area [online]. Available from http://www.cnsopb.ns.ca/sites/default/files/pdfs/directory_of_offshore _wells.pdf [cited 20 November 2016].

Cooke, D., and Cant, J. 2010. Model-based Seismic Inversion: Comparing deterministic and probabilistic approaches. CSEG Recorder, **35**(4): 28-39.

Creybohm, J.R., Earley, K.M., Gunn, D., and Lackie, C. 1983. Well History Report. Mobil et al Arcadia J-16.

Cummings, D.I. and Arnott, W.C. 2005. Growth-faulted shelf-margin deltas: a new (but old) play type, offshore, Nova Scotia. Bulletin of Canadian Petroleum Geology, **53**(3): 211-236.

Cuthill, G.T., Conrad, P.R., and Fife, R.J. 1982. Well History Report. Mobil Texaco Pex Venture B-43.

Dawson, W.E., Morrow, D.L. and Harris, R.L. 1972. Well History Report. Mobil Tetco Sable Island O-47.

Duarte, L.V., Silva, R.L., Mendonça Filho, J.G., Poças Ribeiro, N., and Chagas, R.B.A. 2012. High-resolution stratigraphy, Palynofacies and source rock potential of the Água de Madeiros Formation (Upper Sinemurian) of the Lusitanian Basin, Portugal. Journal of Petroleum Geology, **35**(2): 105–126.

Dutta, N., Mukerji, T., Prasad, M., and Dvorkin, J. 2002a. Seismic Detection and Estimation of Overpressures Part I: the Rock Physics Basis. CSEG Recorder, **27**(7): 34-57.

Dutta, N., Mukerji, T., Prasad, M., and Dvorkin, J. 2002b. Seismic Detection and Estimation of Overpressures Part II: Field Applications. CSEG Recorder, **27**(7): 58-73.

Dutta, N. C. 2012. Geopressure prediction using seismic data: Current status and the road ahead. Geophysics, **67**(6): 2012-2041.

EduMine. 2016. Average Specific Gravity of Various Rock Types [online]. Available from http://www.edumine.com/xtoolkit/tables/sgtables.htm [cited 16 January 2017].

Eliuk, L.S. 1978. The Abenaki Formation, Nova Scotia Shelf, Canada - Depositional and diagenetic model for a Mesozoic carbonate platform. Bulletin of Canadian Petroleum Geology, **26**(4): 424-514.

Eliuk, L.S. 2016. Abenaki Carbonate Platform in Relation to the Jurassic-Cretaceous Sable Island Delta, Offshore Nova Scotia, Canada. PhD Thesis, Department of Earth Sciences, Dalhousie University, Halifax, N. S.

Espitalié, J., Laporte, J.L., Madec, M., Marquis, F., Leplat, P., Paylet, J., and Boutefeu, A. 1977. Rapid Method for Characterisation of Source Rocks and for Determination of Petroleum Potential and Degree of Evolution. Oil and Gas Science and Technology – IFP Review, **32**: 23-42.

Espitalié, J., Deroo, G., and Marquis, F. 1985. La pyrolyse Rock-Eval et ses applications: première partie. Revue de l'Institut Français du Pétrole, **40**: 563–579.

Fugro-Jason. 2013. Introduction to Acoustic Impedance Inversion. Trainer Course Book, Fugro Jason, Netherlands, BV.

Fowler, M., Webb, J., Obermajer, M., Monnier, F., Mort, A., Kuheshi, M., and MacDonald, A. 2016. Petroleum Systems of the Scotian Basin. *In* Proceedings of the AAPG 2016 Annual Convention and Exhibition, Calgary, Ab. AAPG Search and Discovery, Article #10871.

GeoChem Laboratories (Canada) Ltd. 1982. Hydrocarbon Source Facies Analysis: Mobil Texaco Pex Venture B-43 Well, Scotian Shelf, Canada. Prepared for Mobil Oil Canada Ltd. and Partners.

GeoChem Laboratories (Canada) Ltd. 1983a. Hydrocarbon Source Facies Analysis: Mobil et al Arcadia J-16 Well. Prepared for Mobil Oil Canada Ltd.

GeoChem Laboratories (Canada) Ltd. 1983b. Hydrocarbon Source Facies Analysis: Mobil et al Pex Olympia A-12 Well, Scotian Shelf, Canada. Prepared for Mobil Oil Company and Partners.

GeoChem Laboratories (Canada) Ltd. 1983c. Hydrocarbon Source Facies Analysis: Mobil et al Venture B-52 Well, Scotian Shelf, Canada. Prepared for Mobil Oil Company.

GeoChem Laboratories (Canada) Ltd. 1983d. Hydrocarbon Source Facies Analysis: Mobil et al South Venture O-59 Well, Scotian Shelf, Canada. Prepared for Mobil Oil Company and Partners.

GeoChem Laboratories (Canada) Ltd. 1984. Hydrocarbon Source Potential and Maturity: Mobil et al West Venture N-91, Scotian Shelf, Canada. Prepared for Mobil Oil Canada Ltd.

GeoChem Laboratories (Canada) Ltd. 1985. Hydrocarbon Source Facies Analysis on: Mobil et al. West Olympia O-51. Prepared for Mobil Oil Canada Ltd.

GeoChem Laboratories (Canada) Ltd. 1989. Hydrocarbon Source Facies Analysis: Mobil et al South Sable B-44, Sable Island. Prepared for Mobil Oil Canada Ltd.

Glover, P. W. J. n.d. Petrophysics Course Notes [online]. Available from https://www.scribd.com /doc/110298097/Petrophysics-P-glover-1 [cited 17 January 2017].

Hancock, N. J. 1992. Quick-Look Lithologies from Logs. *In* Methods in Exploration 10: Development Geology Reference Manual. AAPG Special Volume, Tulsa, Ok. pp. 174-179.

Harris, P. M. and Katz, B. J. 2008. Carbonate Mud and Carbonate Source Rocks. *In* Proceedings of the AAPG Annual Convention, Calgary, Ab. AAPG Search and Discovery, Article #40305.

Hesselbo, S.P. Deconinck, J.F., Muggett, J.M., and Morgans-Bell, H.S. 2009. Late Jurassic paleoclimatic change from clay mineralogy and gamma-ray spectrometry of the Kimmeridge Clay, Dorset, UK. Journal of the Geological Society, London, **166**: 1123-1133.

Hood, A., Gutjahr, C.C.M., and Heacock, R.L. 1975. Organic metamorphism and the generation of petroleum. American Association of Petroleum Geology Bulletin, **59**: 986-996.

Huc, A.-Y., and Schneidermann, N. 1995. Paleogeography, Paleoclimate, and Source Rocks. *Edited by* A.-Y. Huc. AAPG Studies in Geology, 40, Tulsa, O.K.

Hunt, J.M. 1990. Generation and migration of petroleum from abnormally pressured fluid compartments. AAPG Bulletin, **74**: 1-12.

Issler, D. R., Hu, K., Black, J. D., and Katsube, T. J. 2002. Organic carbon Content Determined from Well Logs: Examples from Cretaceous Sediments of Western Canada. Geologic Survey of Canada, Open File #4362.

Jansa, L.F. and Wade, J.A. 1975. Geology of the continental margin off Nova Scotia and Newfoundland. *In* Offshore Geology of Eastern Canada, Vol. 2, Regional Geology. *Edited by* W.J.M Vander Linden and J.A. Wade. Geological Survey of Canada, **74**(30): 51-106.

Jansa, L.F., and Noguera Urrea, V.H. 1990. Geology and Diagenetic History of Overpressured Sandstone Reservoirs, Venture Gas Field, Offshore Nova Scotia, Canada. The American Association of Petroleum Geologist Bulletin, **74**(10): 1640-1658.

Jarvie, D.M., Hill, R.J., and Pollastro, R.M. 2005. Assessment of the Gas Potential and Yields from Shales: the Barnett Shale Model. Unconventional energy resources in the southern Midcontinent, 2004 symposium: Oklahoma Geological Survey Circular, **110**: 37-50.

Jarvie, D.M. 2012. Shale Resource Systems for Oil and Gas: Part 1 – Shale-gas Resource Systems. *In* Memoir 97: Shale Reservoirs – Giant resources for the 21st century. American Association of Petroleum Geologists, Tulsa, Ok. pp. 69-87.

Kettanah, Y.A., Kettanah, M.Y., and Wach, G.D. 2013. Provenance, diagenesis and reservoir quality of the Upper Triassic Wolfville Formation, Bay of Fundy, Nova Scotia, Canada. *In* Sediment Provenance Studies in Hydrocarbon Exploration and Production. *Edited by* R.A. Scott, H.R. Smyth, A.C. Morton, and N. Richardson. 2014. Geological Society London, Special Publications, **386**: 75-110.

Kidston, A.G., Brown, D.E., Smith B.M. and Altheim, B. 2005. The Upper Jurassic Abenaki Formation Offshore Nova Scotia: A Seismic and Geologic Perspective. Canada-Nova Scotia Offshore Petroleum Board, Halifax, N.S.

Kumar, N., and Negi, S.S. 2012. Low frequency modeling and its impact on seismic inversion data. *In* 9th Biennial International Conference & Exposition on Petroleum Geophysics, Hyderabad, India.

Langrock, U., 2004, Late Jurassic to Early Cretaceous black shale formation and paleoenvironment in high northern latitudes. Ber Polarforsch Meeresforsch, **472**: 27-40.

Lecompte, B., and G. Hursan. 2010. Quantifying Source Rock Maturity from Logs: How to Get More Than TOC from Delta Log R. *In* Proceedings of the SPE Annual Technical Conference and Exhibition, Florence, Italy, Paper 133128.

Løseth, H., Wensaas, L., Gading, M., Duffaut, K., and Springer, M. 2011. Can hydrocarbon source rocks be identified on seismic data?. Geology, **39**: 1167–1170.

Love, H.G., and Ellison, K.J. 1983. Well History Report. Mobil Texaco Pex South Venture O-59.

Magoon, L.B., Hudson, T.L. and Peters, K.E. 2005. Egret-Hibernia(!), a significant petroleum system, northern Grand Banks area, offshore eastern Canada. American Association of Petroleum Geology Bulletin, **89**(9): 1203-1237.

McIver, N.L., 1972. Mesozoic and Cenozoic stratigraphy of the Nova Scotia Shelf. Canadian Journal of Earth Sciences, **9**: 54-70.

McLelan, H.C., and Boissonneault, J.M. 1988. Well History Report. Mobil et al South Sable B-44.

Meckel, L.D. and Nath, A.K. 1977. Geologic Considerations for Stratigraphic Modeling and Interpretation. *In* Memoir 26: Seismic stratigraphy – applications to exploration. *Edited by* C.E. Payton. American Association of Petroleum Geologists, Tulsa, Ok. pp. 417-438.

Miles, A.J. 1994. Glossary of Terms Applicable to the Petroleum System. *In* Memoir 60: The Petroleum System - from source to trap. *Edited by* L.B. Magoon, and W.G. Dow. American Association of Petroleum Geologists, Tulsa, Ok. pp. 643-644.

Morgans-Bell, H S., Coe, A.L., Hesselbo, S.P., Jenkyns, H.C., Weedon, G.P., Marshall, J.E.A., Tyson, R.V., and Williams, C.J. 2001. Integrated stratigraphy of the Kimmeridge Clay Formation (Upper Jurassic) based on exposures and boreholes in south Dorset, UK. Geologic Magazine, **138**(5): 511-539.

Mougenot, D. 2005. Pushing toward the low frequencies. World Oil, **9**:25-28.

Meyer, B.L., and Nederlof, M.H. 1984. Identification of source rocks on wireline logs by density/resistivity and sonic transit time/resistivity crossplots. American Association of Petroleum Geology Bulletin, **68**: 121-129.

Mukhopadhyay, P.K., and Birk, D. 1989. Organic Facies in the Sable Sub-Basin, Scotian Shelf. Geologic Survey of Canada, Open File #2027.

Mukhopadhyay, P.K. 1990a. Characterization and maturation of selected Cretaceous and Jurassic source rocks and crude oil, Scotian Shelf. Geologic Survey of Canada, Open File #2621.

Mukhopadhyay, P.K. 1990b. Characterization and Maturation of Selected Oil and Condensate Samples and Correlation with Source Beds, Scotian Shelf. Geologic Survey of Canada, Open File #2620.

Mukhopadhyay, P.K. 1991. Evaluation of organic facies of the Verrill Canyon Formation, Sable Sub-Basin, Scotian Shelf. Geologic Survey of Canada, Open File #2435.

Mukhopadhyay, P.K. 1994. Organic Petrography and Kenetics of Limestone and Shale Source Rocks in Wells Adjacent to Sable Island, Nova Scotia and the Interpretation on Oil-Oil or Oil-Source Rock Correlation and Basin Modeling. Geologic Survey of Canada, Open File #3167.

Mukhopadhyay, P.K. 1995. Organic Organic Petrography and Kinetics of Jurassic/Cretaceous Shales and Geocemistry of Selected Liquid Hydrocarbons, Scotian Basin. Geologic Survey of Canada, Open File #3284.

Mukhopadhyay, P.K. 2006. Evaluation of the petroleum systems by 1D and 2D numerical modeling and geochemical analysis in the area of most recent exploration wells on

the deepwater Scotian slope, offshore Nova Scotia. Nova Scotia Department of Energy, unpublished report.

Mukhopadhyay, P.K., and Wade, J.A. 1990. Organic facies and maturation of sediments from three Scotian Shelf wells. Bulletin of Canadian Petroleum Geology, **38**(4): 407-425.

NRCan. 2016. BASIN Database. Natural Resources Canada.

Offshore Energy Research Association of Nova Scotia (OERA). 2013. OERA Recommended Research Programs; 2013 to 2016 [online]. Available from http://www.oera.ca/wp-content/uploads/2013/07/OERA-Geoscience-Programs-11-April-2013.pdf [cited 8 December 2014].

Ouadfuel, S.I., and Auadfeul, L. 2016. Total organic carbon estimation in shale-gas reservoirs using seismic genetic inversion with an example from the Barnett Shale. The Leading Edge, **35**(9): 790-794.

Passey, Q.R., Creaney, S., Kulla, J.B., Moretti, F.J., and Stroud, J.D. 1990. A practical model for organic richness from porosity and resistivity logs. American Association of Petroleum Geology Bulletin, **74**: 1777-1794.

Pennebaker, E.S. 1968. Seismic data indicate depth, magnitude of abnormal pressure. World Oil, **166**: 73-78.

Pe-Piper, G., and Mackay, M. 2006. Provenance of Lower Cretaceous sandstones onshore and offshore Nova Scotia from electron microscope geochronology and chemical variation of detrital monazite. Bulletin of Canadian Petroleum Geology, **54**: 366-379.

Peters, K.E. 1986. Guidelines for Evaluating Petroleum Source Rock Using Programmed Pyrolysis. American Association of Petroleum Geology Bulletin, **70**: 318-329.

Peters, K.E., Walters, C.C., and Moldowan, J.M. 2005. Chapter 4-Geochemical Screening. *In* The Biomarker Guide. Cambridge University Press, Cambridge, U.K. pp 72-118.

Potter, J., Richards, B.C., and Goodarzi, F. 1993. The organic petrology and thermal maturity of lower Carboniferous and Upper Devonian source rocks in the Liard basin, at Jackfish Gap-Yohin Ridge and North Beaver River, northern Canada: implications for hydrocarbon exploration. Energy Sources, **15**: 289-314.

Rider, M. H. and Kennedy, M. 2011. The Geologic Interpretation of Well Logs. Rider-French Consulting Ltd., U.K.

Schakel, M. n.d. Broadband Wavelet Estimation. *For* Hampson-Russel Software [online]. Available from http://www.cgg.com/technicalDocuments/cggv_0000022643.pdf [cited 22 March 2017].

Schlumberger Limited. 2015. Oil Field Glossary [online]. Available from http://www.glossary.oil field.slb.com [cited 2 February 2015].

Seifert, M.M., Ward, D.G., Madell, G., and Sidwell, H.C. 1985. Well History Report. Mobil et al. West Venture N-91.

Sheriff, R. E. 1996. Geophysical Corner: Understanding the Fresnel Zone. AAPG Explorer, 10.

Sheriff, R. E. 1997. Geophysical Corner: Seismic Resolution a Key Element. AAPG Explorer, 12.

Sheriff, R.E. 2002. Encyclopedic Dictionary of Exploration Geophysics. Society of Exploration Geophysicists, Tulsa, Ok.

Sidwell, H.C., Bergsland, H., and Ellison, K.J. 1983. Well History Report. Mobil Texaco Pex Olympia A-12.

Sine, G., Ellsworth, W., and Donnely, D. 1984a. Well History Report. Shell Petrocan et al South DesBarres O-76.

Sine, G., MacInnis, S., and Donnelly, D. 1984b. Well History Report. Shell Petrocan et al. Uniacke G-72.

Skinner, C.H. 2016. Excess Pressure and Reservoir Compartmentalization in the Sable SubBasin, Offshore Nova Scotia. M.Sc. Thesis, Department of Earth Sciences, Dalhousie University, Halifax, N. S.

Smith, B.M., Makrides, C., Altheim, B., and Kendell, K. 2014. Resource Assessment of Undeveloped Significant Discoveries on the Scotian Shelf. Canada-Nova Scotia Offshore Petroleum Board.

Steele, D.R., Mulders, J., and Crisp M. 2011. Sable Sub-Basin Near-Field Exploration Prospectively. *In* Proceedings of the Offshore Technology Conference, Houston, Texas.

Suárez-Ruiz, I., Flores, D., Mendonça Filho, J.G., and Hackley, P. C. 2012. Review and update of the applications of organic petrology: Part 1, geological applications. International Journal of Coal Geology, **99**: 54-112.

Tissot, B.P., and Welte, D.H. 1984. Petroleum Formation and Occurrence. Springer-Verlag Berlin Heidelberg, New York, USA.

Tweed, D.M., and Nachtigall, K. G. 1986. Well History Report. Mobil et al. West Olympia O-51.

Tyson, R.V. 1995. Sedimentary Organic Matter. Organic Facies and Palynofacies. Chapman & Hall, London, U.K.

Van Krevelen, D.W. 1993. Coal: typology–physics–chemistry–constitution, 3rd edition. Elsevier Science Publishers, Amsterdam, NL.

Veeken, P.C.H., and Da Silva, M. 2004. Seismic Inversion Methods and some of their constraints. First Break, **40**(6): 47-70.

von der Dick, H. 1989. Environment of petroleum source rock deposition in the Jeanne d'Arc Basin off Newfoundland. *In* Memoir 46: Extensional tectonics and stratigraphy of the North Atlantic margins. *Edited by* A.J. Tankard and H.R. Balkwill. American Association of Petroleum Geologists, Tulsa, Ok. pp. 295– 303.

Wach, G.D., and Hasley L. Vincent. 2005. Reservoir Heterogeneity and Characterization in Deltaic Depositional Systems; Outcrop Analogs for Nova Scotia's Offshore Developments. *In* Proceedings of the AAPG Annual Meeting, Calgary, Ab. AAPG Search and Discovery, Article #90039.

Wade, J.A. and MacLean, B.C. 1990. Chapter 5 - The geology of the southeastern margin of Canada, Part 2: Aspects of the geology of the Scotian Basin from recent seismic and well data. *In* Geology of Canada No.2 - Geology of the continental margin of eastern Canada. *Edited by* M.J. Keen and G.L. Williams. Geological Survey of Canada, Ottawa, 190-238.

Wade, J.A., MacLean, B.C., and Williams, G.L. 1995. Mesozoic and Cenozoic stratigraphy, eastern Scotian Shelf: new interpretations. Canadian Journal of Earth Science, **32**: 1462-1473.

Wade, J.A. 2000. Depth to pre-Mesozoic and Pre-Carboniferous basements. Geological Survey of Canada, Open File #3842.

Wielens, J.B.W. 2003. Overpressures on the Scotian Shelf. Geological Survey of Canada, Open File #1557.

Weissenberger, J. A. W., Harland, N. J., Hogg, R., and Syhlonyk, G. 2000. Sequence stratigraphy of Mesozoic carbonates, Scotian Shelf, Canada. *In* Proceedings of GeoCanada 2000 – the Millenium Geoscience Summit, Joint Convention of the CSPG, CSEG, GAC, MAC, CGU & CWLS, Conference, Calgary, Ab. CD-ROM Disk, 1262.

Weston, J.F., MacRae, R.A., Ascoli, P., Cooper, M.K., Fensome, R.A., Shaw, D., and Williams, G.L. 2012. A revised biostratigraphic and well-log sequence-stratigraphic

framework from the Scotian Margin, offshore Eastern Canada. Canadian Journal of Earth Sciences, **49**: 1417–1462.

Wierzbicki, R., Harland, N. and Eliuk, L. 2002. Deep Panuke and Demascota core from the Jurassic Abenaki Formation, Nova Scotia – Facies model, Deep Panuke, Abenaki Formation. *In* Proceedings of the Canadian Society of Petroleum Geologists 75th Diamond Jubilee Convention and Core Conference, Abstracts and Extended Abstracts, Calgary, Ab. p.p. 71-101.

Williams, G.L., Ascoli, P., Barss, M.S., Bujak, J.P. Favies, E.H., Fensome, R.A., and Williamson, M.A. 1990. Chapter 3 – Biostratigraphy and Related Studies. *In* Geology of Canada No.2 - Geology of the continental margin of eastern Canada. *Edited by* M.J. Keen and G.L. Williams. Geological Survey of Canada, Ottawa, Can. pp. 89-137.

Williams, H., and Grant, A.C. 1998. Tectonic assemblages, Atlantic Region, Canada. 1:3 000 000 map. Geological Survey of Canada, Open File 3657.

Williamson, M.A., and Desroches, K. 1992. Source Rock Maturity Modeling: Sable and Jeanne D'Arc Basins Offshore Eastern Canada. *In* Proceedings of the AAPG Annual Meeting, Calgary, Ab. AAPG Search and Discovery, Article #91012.

Wong, J.C., Skinner, C.H., Richards, F.W., Silva, R.L., Morrison, N., and Wach, G. 2016. 1D thermal model of South Venture O-59, Sable Subbasin (Scotian Basin, Nova Scotia). *In* The Atlantic Geoscience Society 42nd Colloquium and Annual Meeting. *Edited by* T. Fedak, B. Grantham and R. Raeside and C. White. Atlantic Geoscience Society, Truro NS. p. 68.

Appendix A: Well Summary Table

Table A-1: Well Summary Table (NRCan 2016).

Well	UWI	Spud Year	Operator	Status	Surface X	Surface Y	UTM Zone	Water Depth (ft/m)	Well Datum - RT (ft/m)	TD (m)
ARCADIA J-16	300 J16 44100 59300	1983	MOBIL ET AL	P&A	297235	4885377	21	184 / 56.0	125 / 38.0	6005
CITNALTA I-59	300 I59 44100 59300	1974	MOBIL-TETCO-TEXACO	P&A	290001	4891132	21	310 / 94.5	98 / 29.9	4575
INTREPID L-80	300 L80 43500 59450	1974	TEXACO-SHELL	P&A	263148	4856617	21	143 / 43.6	103 / 31.4	4162
MARINER I-85	300 I85 44100 59300	2003	CANADIAN SUPERIOR EL PASO	P&A	283634	4883560	21	182 / 55.5	154 / 47.0	5408
OLYMPIA A-12	300 A12 44100 59450	1982	MOBIL-TEXACO-PEX	P&A	277259	4877363	21	134 / 41.0	125 / 38.0	6064
SABLE ISLAND 2H-58	302 H58 44000 60000	1972	MOBIL-TETCO	P&A	730501	4870955	20	6.5 / 2.0	35 / 10.8	2758
SABLE ISLAND 3H-58	303 H58 44000 60000	1973	MOBIL-TETCO	P&A	730501	4870955	20	6.5 / 2.0	35 / 10.8	3740
SABLE ISLAND 4H-58	304 H58 44000 60000	1973	MOBIL-TETCO	P&A	730501	4870955	20	6.5 / 2.0	35 / 10.8	4519
SABLE ISLAND 5H-58	305 H58 44000 60000	1973	MOBIL-TETCO	P&A	730501	4870955	20	6.5 / 2.0	35 / 10.8	2478
SABLE ISLAND 6H-58	306 H58 44000 60000	1973	MOBIL-TETCO	P&A	730501	4870955	20	6.5 / 2.0	35 / 10.8	2355
SABLE ISLAND C-67	300 C67 44000 59450	1967	MOBIL	P&A	265861	4868541	21	13 / 4.0	27 / 8.2	4604
SABLE ISLAND E-48	300 E48 44000 60000	1971	MOBIL-TETCO	P&A	730818	4870760	20	6 / 1.8	21 / 6.4	3603
SABLE ISLAND H-58	300 H58 44000 60000	1972	MOBIL-TETCO	P&A	730501	4870955	20	6.5 / 2.0	35 / 10.8	3039
SABLE ISLAND O-47	300 O47 44000 60000	1971	MOBIL-TETCO	P&A	731865	4870007	20	6 / 1.8	24 / 7.3	4198
SOUTH DESBARRES O-76	300 O76 44100 59450	1984	SHELL PETROCAN ET AL	P&A	265225	4886825	21	226 / 69.0	78 / 23.7	6039
SOUTH SABLE B-44	300 B44 44000 59450	1988	MOBIL ET AL	P&A	270114	4862882	21	115 / 35.0	138 / 42.0	5208
SOUTH VENTURE 1	300 P60 44000 59300	2002	EXXON MOBIL ET AL	PROD	289271	4874718	21	75 / 23.0	159 / 48.7	4439
SOUTH VENTURE 2	302 P60 44000 59300	2004	EXXON MOBIL ET AL	PROD	289268	4874718	21	75 / 22.9	156 / 47.6	5315
SOUTH VENTURE 3	303 P60 44000 59300	2005	EXXON MOBIL ET AL	PROD	289268	4874718	21	75 / 22.9	183 / 55.8	4666
SOUTH VENTURE O-59	300 O59 44000 59300	1982	MOBIL ET AL	P&A	288611	4872962	21	79 / 24.0	115 / 35.0	6176
UNIACKE G-72	300 G72 44200 59300	1983	SHELL PETROCAN ET AL	P&A	285334	4896428	21	501 / 152.9	77 / 23.4	5735
VENTURE 1	300 O32 44100 59300	1998	SABLE OFFSHORE ENERGY	P&S	293053	4878583	21	72 / 22.0	131 / 40.0	5314
VENTURE 2	302 O32 44100 59300	1998	SABLE OFFSHORE ENERGY	PROD	293057	4878589	21	72 / 22.0	183 / 55.9	5586
VENTURE 3	303 O32 44100 59300	1998	SABLE OFFSHORE ENERGY	PROD	293053	4878585	21	72 / 22.0	131 / 40.0	5110
VENTURE 4	304 O32 44100 59300	1998	SABLE OFFSHORE ENERGY	PROD	293057	4878587	21	72 / 22.0	131 / 40.0	5469
VENTURE 5	305 O32 44100 59300	1998	SABLE OFFSHORE ENERGY	P&S	293050	4878585	21	72 / 22.0	167 / 51.0	6029
VENTURE 6	306 O32 44100 59300	2002	EXXON MOBIL ET AL	PROD	293050	4878588	21	72 / 22.0	187 / 57.2	6025
VENTURE 7	307 O32 44100 59300	2005	EXXON MOBIL ET AL	PROD	293053	4878588	21	72 / 22.0	197 / 60.2	6483
VENTURE B-13	300 B13 44100 59300	1980	MOBIL-TEXACO-PEX	P&A	296931	4878840	21	81 / 24.7	111 / 33.8	5368
VENTURE B-43	300 B43 44100 59300	1981	MOBIL-TEXACO-PEX	P&A	290824	4878694	21	67 / 20.4	111 / 33.8	5872
VENTURE B-52	300 B52 44100 59300	1983	MOBIL ET AL	P&A	288765	4877282	21	64 / 19.5	118 / 36.0	5960
VENTURE D-23	300 D23 44100 59300	1978	MOBIL-TEXACO-PEX	P&A	293791	4879038	21	66 / 20.1	104 / 31.7	4945
VENTURE H-22	300 H22 44100 59300	1983	MOBIL ET AL	P&A	295492	4877418	21	72 / 22.0	125 / 38.1	5944
WEST OLYMPIA O-51	300 O51 44100 59450	1985	MOBIL ET AL	P&A	268793	4877177	21	125 / 38.0	128 / 39.0	4816
WEST VENTURE C-62	300 C62 44100 59300	1984	MOBIL ET AL	P&A	286236	4877052	21	52 / 16.0	112 / 34.0	5522
WEST VENTURE N-01	300 N01 44100 59450	1985	MOBIL ET AL	P&A	278421	4877186	21	231 / 79.5	126 / 38.4	3632
WEST VENTURE N-91	300 N91 44100 59300	1984	MOBIL ET AL	P&A	280286	4876723	21	125 / 38.1	129 / 39.3	5547

Appendix B: Geochemistry Sources

Table B-1: Sources of RockEval data used in this project, as referenced by the BASIN Database (NRCan 2016).

Well	RockEval Source			
	Author	Year	Ref. #	Journal
Arcadia J-16	Geochem Laboratories	1983	10276	Mobil Oil Can Ltd Well History Rep.
Olympia A-12	GSC Calgary	1986	10311	GSC Open File Report #1403
	Mukhopadhyay, P. K.	1991	10258	GSC Open File Report #2621
Sable Island O-47	Mukhopadhyay, P. K.	1989	10255	GSC Open File Reoprt #2282
	Mukhopadhyay, P. K.	1990	10257	GSC Open File Report #10257
	Mukhopadhyay, P. K.	1991	10258	GSC Open File Report #2621
South DesBarres O-76	GSC Calgary	1991		GSC Calgary
	Mukhopadhyay, P. K.	1991	10258	GSC Open File Report #2621
	Mukhopadhyay, P. K.	1994	10260	GSC Open File Report #3167
South Sable B-44	Geochem Laboratories	1988	10276	Mobil Oil Can Ltd Well History Rep.
	GSC Calgary	1991		GSC Calgary
	Mukhopadhyay, P. K.	1991	10258	GSC Open File report #2621
South Venture O-59	GSC Calgary	1984		GSC Calgary
	GSC Calgary	1988		GSC Calgary
	Mukhopadhyay, P. K.	1989	10254	GSC Open File Report #2027
	Mukhopadhyay, P. K.	1990	10257	GSC Open File Report #2620
	Mukhopadhyay, P. K.	1995	10261	GSC Open File Report #3284
Uniacke G-72	GSC Calgary	1993		GSC Calgary
	Mukhopadhyay, P. K.	1991	10258	GSC Open File report #2621
	Mukhopadhyay, P. K.	1994	10260	GSC Open File report #3167
Venture B-43	Mukhopadhyay, P. K.	1989	10254	GSC Open File Report #2027
	Mukhopadhyay, P. K.	1994	10260	GSC Open File Report #3167
Venture B-52	Geochem Laboratories	1983	10276	Mobil Oil Can Ltd Well History Rep.
	Mukhopadhyay, P. K.	1991	10258	GSC Open File Report #2621
	Mukhopadhyay, P. K.	1994	10260	GSC Open File Report #3167
West Olympia O-51	Geochem Laboratories	1985	10276	Mobil Oil Can Ltd Well History Rep.
	GSC Calgary	1995		GSC Calgary
West Venture N-91	Geochem Laboratories	1984	10276	Mobil Oil Can Ltd Well History Rep.

Table B-2: Sources of Vitrinite Refection data used in this project, as referenced by the BASIN Database (NRCan 2016). Multiple sources were used to increase sample size if data was limited.

Well	Vitrinite Reflectance Source			
	Author	Year	Ref. #	Journal
Arcadia J-16	Geochem Laboratories	1983	10276	Hydrocarbon Source Facies Analysis
Olympia A-12	Avery, M.P.	1984	153	GSC Open File Report #1172
Sable Island O-47	Mukhopadhyay, P.K.	1991	10258	GSC Open File Report #2621
	Mukhopadhyay, P.K.	1989	10255	GSC Open File Report #2282
	Issler, D.R.	1984	10017	Can. J. Earth Sci. 21, P. 477
South DesBarres O-76	Avery, M.P.	1994	216	GSC Open File Report #3115
	Avery, M.P.	1993	212	GSC Open File Report #2706
	Avery, M.P.	1991	208	GSC Open File Report #2455
	Mukhopadhyay, P.K.	1991	10258	GSC Open File Report #2621
	Mukhopadhyay, P.K.	1990	10257	GSC Open File Report #2620
South Sable B-44	Mukhopadhyay, P.K.	1991	10258	GSC Open File Report #2621
	Geochem Laboratories	1988	10276	Hydrocarbon Analysis
South Venture O-59	Avery, M.P.	1984	137	Epgs-Dom-02-84mpa
Uniacke G-72	Avery, M.P.	1994	214	GSC Open File Report #2902
	Mukhopadhyay, P.K.	1991	10258	GSC Open File Report #2621
	Avery, M.P.	1989	193	GSC Open File Report #2052
Venture B-43	Avery, M.P.	1983	136	Epgs-Dom-09-83mpa
Venture B-52	Geochem Laboratories	1983	10276	Hydrocarbon Source Facies Analysis
West Olympia O-51	Geochem Laboratories	1985	10276	Hydrocarbon Source Facies Analysis
West Venture N-91	Avery, M.P.	1991	208	GSC Open File Report #2455
	Mukhopadhyay, P.K.	1990	10257	GSC Open File Report #2620
	Geochem Laboratories	1984	10276	Hydrocarbon Source Potential & Maturity Report

Appendix C: Restored TOC Values

Table C-1: Minimum, maximum and average restored TOC values from the Jarvie et al. 2005, Jarvie 2012, and Peters et al. 2005 methods and the corresponding decrease from initial present day TOC for Arcadia J-16.

Well	Depth	TOC^x	TOC J2005 Min	TOC J2005 Max	TOC J2005 AVG	% Dec	TOC J2012 Min	TOC J2012 Max	TOC J2012 AVG	% Dec	TOC Peters Min	TOC Peters Max	TOC Peters AVG	% Dec
	4340	1.02	1.59	1.59	1.59	36	0.92	0.92	0.92	-10.9	0.95	1.09	1.02	0
	4490	1.07	1.67	1.67	1.67	36	1	1.01	1.01	-6.47	1.03	1.18	1.11	3.27
	4550	1.82	2.84	2.84	2.84	36	1.69	1.81	1.75	-4	1.71	1.96	1.84	0.82
	4580	1.09	1.7	1.7	1.7	36	0.86	0.85	0.86	-27.5	0.89	1.02	0.96	-12.4
	4610	2.13	3.33	3.33	3.33	36	2.04	2.2	2.12	-0.47	2.04	2.34	2.19	2.82
	4650	1.45	2.27	2.27	2.27	36	1.37	1.43	1.4	-3.57	1.38	1.58	1.48	2.07
	4700	1.11	1.73	1.73	1.73	36	1.04	1.06	1.05	-5.71	1.06	1.22	1.14	2.7
	4910	1.18	1.84	1.84	1.84	36	1.14	1.17	1.16	-2.16	1.16	1.33	1.25	5.51
	5000	2.31	3.61	3.61	3.61	36	2.24	2.44	2.34	1.28	2.24	2.57	2.41	4.11
	5030	1.19	1.86	1.86	1.86	36	1.12	1.15	1.14	-4.85	1.14	1.31	1.23	2.94
	5060	1.2	1.88	1.88	1.88	36	1.14	1.17	1.16	-3.9	1.16	1.33	1.25	3.75
	5090	0.97	1.52	1.52	1.52	36	0.91	0.91	0.91	-6.59	0.94	1.08	1.01	4.12
	5120	1.12	1.75	1.75	1.75	36	1.06	1.08	1.07	-4.67	1.08	1.24	1.16	3.57
	5150	1.13	1.77	1.77	1.77	36	1.04	1.05	1.05	-8.13	1.06	1.22	1.14	0.88
Arcadia J-16	5180	1.17	1.83	1.83	1.83	36	1.11	1.14	1.13	-4	1.13	1.3	1.22	3.85
	5210	1.52	2.38	2.38	2.38	36	1.47	1.56	1.52	-0.33	1.49	1.7	1.6	4.93
	5270	1.18	1.84	1.84	1.84	36	1.14	1.17	1.16	-2.16	1.16	1.33	1.25	5.51
	5300	1.47	2.3	2.3	2.3	36	1.39	1.46	1.43	-3.16	1.41	1.61	1.51	2.72
	5330	1.28	2	2	2	36	1.22	1.26	1.24	-3.23	1.23	1.42	1.33	3.52
	5360	2.47	3.86	3.86	3.86	36	2.42	2.65	2.54	2.56	2.42	2.77	2.6	5.06
	5390	1.01	1.58	1.58	1.58	36	0.95	0.96	0.96	-5.76	0.98	1.12	1.05	3.96
	5450	1.06	1.66	1.66	1.66	36	1.03	1.04	1.04	-2.42	1.05	1.2	1.13	6.13
	5510	1.32	2.06	2.06	2.06	36	1.25	1.3	1.28	-3.53	1.27	1.46	1.37	3.41
	5660	1.08	1.69	1.69	1.69	36	1.05	1.06	1.06	-2.37	1.06	1.22	1.14	5.56
	5690	0.95	1.48	1.48	1.48	36	0.9	0.9	0.9	-5.56	0.93	1.06	1	4.74
	5720	1.08	1.69	1.69	1.69	36	1.05	1.07	1.06	-1.89	1.07	1.23	1.15	6.48
	5750	1.76	2.75	2.75	2.75	36	1.75	1.87	1.81	2.76	1.75	2.01	1.88	6.82
	5780	1.97	3.08	3.08	3.08	36	1.95	2.1	2.03	2.72	1.95	2.24	2.1	6.35
	5810	1.39	2.17	2.17	2.17	36	1.36	1.43	1.4	0.36	1.38	1.58	1.48	6.47
	5870	0.99	1.55	1.55	1.55	36	0.95	0.95	0.95	-4.21	0.97	1.11	1.04	5.05
	5930	1.34	2.09	2.09	2.09	36	1.25	1.3	1.28	-5.1	1.27	1.45	1.36	1.49
	5960	1.66	2.59	2.59	2.59	36	1.62	1.73	1.68	0.9	1.63	1.87	1.75	5.42
	5990	1.93	3.02	3.02	3.02	36	1.91	2.06	1.99	2.77	1.92	2.2	2.06	6.74

Table C-2: Minimum, maximum and average restored TOC values from the Jarvie et al. 2005, Jarvie 2012, and Peters et al. 2005 methods and the corresponding decrease from initial present day TOC for Olympia A-12.

Well	Depth	TOC^x	TOC J2005 Min	TOC J2005 Max	TOC J2005 AVG	% Dec	TOC J2012 Min	TOC J2012 Max	TOC J2012 AVG	% Dec	TOC Peters Min	TOC Peters Max	TOC Peters AVG	% Dec
Olympia A-12	4300	1.13	1.77	1.77	1.77	36	1.01	1.02	1.01	-11.7	1.03	1.19	1.11	-1.88
	4310	0.66	1.03	1.03	1.03	36	0.58	0.52	0.55	-19.9	0.61	0.7	0.65	-0.92
	4320	0.63	0.98	0.98	0.98	36	0.55	0.49	0.52	-21.3	0.58	0.67	0.62	-0.87
	4330	1.21	1.89	1.89	1.89	36	1.08	1.1	1.09	-10.8	1.11	1.27	1.19	-1.88
	4340	2.24	3.5	3.5	3.5	36	1.81	1.94	1.87	-19.7	1.83	2.1	1.96	-12.4
	4350	1.39	2.17	2.17	2.17	36	1.22	1.26	1.24	-11.9	1.24	1.43	1.33	-4.01
	4360	1.07	1.67	1.67	1.67	36	0.97	0.97	0.97	-10.5	0.99	1.14	1.06	-0.5
	4370	1.21	1.89	1.89	1.89	36	1.07	1.09	1.08	-12.2	1.09	1.25	1.17	-2.97
	4380	1.02	1.59	1.59	1.59	36	0.92	0.92	0.92	-11.2	0.94	1.08	1.01	-0.58
	4390	1.14	1.78	1.78	1.78	36	1.05	1.07	1.06	-7.59	1.07	1.23	1.15	1.14
	4400	0.94	1.47	1.47	1.47	36	0.85	0.84	0.84	-11.4	0.88	1.01	0.94	0.22
	4410	0.95	1.48	1.48	1.48	36	0.84	0.83	0.83	-13.9	0.87	1	0.93	-1.87
	4420	0.95	1.48	1.48	1.48	36	0.86	0.85	0.85	-11.6	0.88	1.01	0.95	-0.08
	4430	2.24	3.5	3.5	3.5	36	2.14	2.33	2.23	-0.29	2.14	2.46	2.3	2.66
	4440	0.48	0.75	0.75	0.75	36	0.43	0.35	0.39	-24	0.46	0.53	0.49	2.92
	4450	1.46	2.28	2.28	2.28	36	1.39	1.45	1.42	-2.86	1.4	1.61	1.5	3.06
	4460	0.87	1.36	1.36	1.36	36	0.79	0.77	0.78	-11.2	0.82	0.94	0.88	1.29
	4470	0.36	0.56	0.56	0.56	36	0.3	0.21	0.26	-40.6	0.34	0.39	0.37	1.71
	4480	0.58	0.91	0.91	0.91	36	0.42	0.34	0.38	-51.1	0.46	0.53	0.5	-14.6
	4490	1.68	2.63	2.63	2.63	36	1.5	1.58	1.54	-8.98	1.52	1.74	1.63	-3.1
	4500	1.74	2.72	2.72	2.72	36	1.61	1.72	1.66	-4.54	1.63	1.87	1.75	0.35
	4510	1.64	2.56	2.56	2.56	36	1.5	1.59	1.55	-6.06	1.52	1.74	1.63	-0.58
	4520	1.1	1.72	1.72	1.72	36	1	1.01	1.01	-9.45	1.03	1.18	1.1	0.13
	4540	1.45	2.27	2.27	2.27	36	1.29	1.34	1.31	-10.5	1.31	1.5	1.4	-3.16
	4550	1.52	2.38	2.38	2.38	36	1.31	1.37	1.34	-13.6	1.33	1.53	1.43	-6.05
	4560	1.47	2.3	2.3	2.3	36	1.32	1.37	1.35	-9.25	1.34	1.53	1.44	-2.36
	4570	1.2	1.88	1.88	1.88	36	1.08	1.1	1.09	-9.92	1.1	1.27	1.19	-1.18
	4580	1.08	1.69	1.69	1.69	36	0.97	0.97	0.97	-11.2	0.99	1.14	1.07	-1.22
	4590	1.15	1.8	1.8	1.8	36	1.04	1.05	1.05	-10.1	1.06	1.22	1.14	-0.87
	4600	1.57	2.45	2.45	2.45	36	1.43	1.5	1.46	-7.19	1.45	1.66	1.55	-1.18
	4610	1.63	2.55	2.55	2.55	36	1.45	1.53	1.49	-9.53	1.47	1.68	1.58	-3.28
	4620	1.11	1.73	1.73	1.73	36	1.01	1.02	1.01	-9.53	1.03	1.18	1.11	-0.14
	4630	1.42	2.22	2.22	2.22	36	1.3	1.35	1.33	-7.04	1.32	1.51	1.42	-0.21
	4640	2.18	3.41	3.41	3.41	36	1.99	2.15	2.07	-5.1	2	2.3	2.15	-1.39
	4650	1.08	1.69	1.69	1.69	36	1	1.01	1	-7.82	1.02	1.17	1.1	1.51
	4660	0.96	1.5	1.5	1.5	36	0.88	0.87	0.87	-10.2	0.9	1.04	0.97	0.93
	4670	1.34	2.09	2.09	2.09	36	1.24	1.29	1.27	-5.82	1.26	1.45	1.36	1.21
	4680	1.34	2.09	2.09	2.09	36	1.25	1.3	1.27	-5.18	1.27	1.46	1.36	1.65
	4690	1.52	2.38	2.38	2.38	36	1.4	1.47	1.44	-5.83	1.42	1.63	1.52	0.19
	4700	1.16	1.81	1.81	1.81	36	1.06	1.08	1.07	-8.55	1.08	1.24	1.16	0.16

Well	Depth	TOC^x	TOC J2005 Min	TOC J2005 Max	TOC J2005 AVG	% Dec	TOC J2012 Min	TOC J2012 Max	TOC J2012 AVG	% Dec	TOC Peters Min	TOC Peters Max	TOC Peters AVG	% Dec
Olympia A-12	4710	1.86	2.91	2.91	2.91	36	1.72	1.84	1.78	-4.31	1.73	1.99	1.86	0.09
	4720	1.6	2.5	2.5	2.5	36	1.46	1.54	1.5	-6.37	1.48	1.7	1.59	-0.56
	4730	1.8	2.81	2.81	2.81	36	1.69	1.8	1.74	-3.3	1.7	1.95	1.82	1.29
	4740	1.25	1.95	1.95	1.95	36	1.15	1.18	1.17	-7.02	1.17	1.35	1.26	0.75
	4750	1.48	2.31	2.31	2.31	36	1.36	1.43	1.4	-6.02	1.38	1.59	1.48	0.3
	4760	0.9	1.41	1.41	1.41	36	0.83	0.81	0.82	-9.34	0.86	0.98	0.92	2.3
	4770	0.5	0.78	0.78	0.78	36	0.44	0.37	0.4	-23.8	0.48	0.55	0.51	2.42
	4780	0.42	0.66	0.66	0.66	36	0.36	0.28	0.32	-31	0.4	0.46	0.43	2.17
	4790	0.7	1.09	1.09	1.09	36	0.64	0.59	0.61	-13.9	0.67	0.77	0.72	2.39
	4800	0.34	0.53	0.53	0.53	36	0.29	0.19	0.24	-43.2	0.32	0.37	0.35	2.2
	4810	1	1.56	1.56	1.56	36	0.95	0.95	0.95	-4.85	0.97	1.12	1.05	4.7
	4820	3.09	4.83	4.83	4.83	36	2.97	3.29	3.13	1.25	2.97	3.39	3.18	2.87
	4830	2.73	4.27	4.27	4.27	36	2.61	2.86	2.74	0.24	2.61	2.98	2.79	2.35
	4840	2.51	3.92	3.92	3.92	36	2.41	2.64	2.52	0.58	2.41	2.76	2.58	2.91
	4850	1.17	1.83	1.83	1.83	36	1.11	1.13	1.12	-4.37	1.13	1.3	1.21	3.7
	4860	1.16	1.81	1.81	1.81	36	1.08	1.11	1.09	-5.99	1.11	1.27	1.19	2.46
	4870	4.38	6.84	6.84	6.84	36	4.23	4.74	4.49	2.36	4.21	4.8	4.5	2.8
	4880	3.16	4.94	4.94	4.94	36	3.04	3.36	3.2	1.2	3.03	3.46	3.25	2.7
	4890	2.04	3.19	3.19	3.19	36	1.96	2.12	2.04	0.01	1.97	2.25	2.11	3.44
	4900	0.91	1.42	1.42	1.42	36	0.87	0.85	0.86	-5.91	0.89	1.02	0.96	5.16
	4910	1.48	2.31	2.31	2.31	36	1.43	1.5	1.47	-0.97	1.44	1.66	1.55	4.72
	4920	3.04	4.75	4.75	4.75	36	2.95	3.26	3.11	2.2	2.94	3.37	3.15	3.77
	4930	2.25	3.52	3.52	3.52	36	2.17	2.36	2.26	0.53	2.17	2.49	2.33	3.49
	4940	0.71	1.11	1.11	1.11	36	0.65	0.6	0.63	-13.3	0.68	0.78	0.73	2.61
	4950	0.82	1.28	1.28	1.28	36	0.76	0.73	0.75	-9.98	0.79	0.9	0.85	3.23
	4960	1.06	1.66	1.66	1.66	36	0.98	0.98	0.98	-7.94	1	1.15	1.08	1.61
	4970	0.87	1.36	1.36	1.36	36	0.8	0.78	0.79	-10.6	0.82	0.95	0.89	1.79
	4980	0.97	1.52	1.52	1.52	36	0.91	0.91	0.91	-6.88	0.93	1.07	1	3.39
	4990	5.68	8.88	8.88	8.88	36	5.51	6.21	5.86	3.09	5.46	6.22	5.84	2.87
	5000	1.32	2.06	2.06	2.06	36	1.26	1.31	1.28	-2.88	1.28	1.46	1.37	3.8
	5010	5.87	9.17	9.17	9.17	36	5.74	6.47	6.1	3.84	5.68	6.47	6.08	3.51
	5020	3.82	5.97	5.97	5.97	36	3.72	4.14	3.93	2.77	3.69	4.22	3.96	3.55
	5030	2.28	3.56	3.56	3.56	36	2.2	2.4	2.3	0.85	2.2	2.52	2.36	3.65
	5040	3.3	5.16	5.16	5.16	36	3.21	3.56	3.39	2.52	3.2	3.66	3.43	3.83
	5050	2.64	4.13	4.13	4.13	36	2.53	2.77	2.65	0.37	2.52	2.89	2.71	2.5
	5060	0.8	1.25	1.25	1.25	36	0.75	0.72	0.74	-8.2	0.78	0.9	0.84	4.83
	5070	1.46	2.28	2.28	2.28	36	1.41	1.48	1.44	-1.22	1.42	1.63	1.52	4.43
	5080	1.12	1.75	1.75	1.75	36	1.07	1.09	1.08	-4.06	1.09	1.25	1.17	4.4
	5090	1.15	1.8	1.8	1.8	36	1.09	1.12	1.1	-4.14	1.11	1.28	1.19	3.88
	5100	3.9	6.09	6.09	6.09	36	3.77	4.21	3.99	2.22	3.74	4.28	4.01	2.85
	5110	6.57	10.27	10.27	10.27	36	6.44	7.28	6.86	4.2	6.37	7.25	6.81	3.64
	5120	5.62	8.78	8.78	8.78	36	5.59	6.3	5.94	5.43	5.52	6.29	5.9	5.06
	5130	4.45	6.95	6.95	6.95	36	4.41	4.94	4.68	4.83	4.37	4.99	4.68	5.15
	5140	3.83	5.98	5.98	5.98	36	3.8	4.24	4.02	4.76	3.77	4.31	4.04	5.53

Well	Depth	TOC^x	TOC J2005 Min	TOC J2005 Max	TOC J2005 AVG	% Dec	TOC J2012 Min	TOC J2012 Max	TOC J2012 AVG	% Dec	TOC Peters Min	TOC Peters Max	TOC Peters AVG	% Dec
Olympia A-12	5150	3.05	4.77	4.77	4.77	36	3.05	3.38	3.21	5.08	3.03	3.47	3.25	6.54
	5160	3.06	4.78	4.78	4.78	36	3.05	3.37	3.21	4.73	3.03	3.47	3.25	6.18
	5170	1.06	1.66	1.66	1.66	36	0.97	0.97	0.97	-9	0.99	1.14	1.07	0.75
	5180	1.27	1.98	1.98	1.98	36	1.22	1.26	1.24	-2.72	1.23	1.42	1.32	4.26
	5190	6.95	10.86	10.86	10.86	36	6.66	7.54	7.1	2.08	6.6	7.5	7.05	1.48
	5200	15	23.36	23.36	23.36	36	14.63	16.73	15.68	4.66	14.49	16.24	15.36	2.78
	5210	2.17	3.39	3.39	3.39	36	2.11	2.29	2.2	1.31	2.11	2.42	2.26	4.3
	5220	2.02	3.16	3.16	3.16	36	1.99	2.16	2.07	2.65	2	2.29	2.14	6.06
	5230	1.35	2.11	2.11	2.11	36	1.3	1.36	1.33	-1.35	1.32	1.51	1.42	4.96
	5240	2.43	3.8	3.8	3.8	36	2.38	2.6	2.49	2.53	2.38	2.73	2.55	5.1
	5250	5.07	7.92	7.92	7.92	36	5.01	5.64	5.33	4.82	4.96	5.66	5.31	4.76
	5260	5.56	8.69	8.69	8.69	36	5.48	6.18	5.83	4.67	5.43	6.18	5.81	4.42
	5270	3.62	5.66	5.66	5.66	36	3.55	3.95	3.75	3.47	3.53	4.03	3.78	4.37
	5280	1.51	2.36	2.36	2.36	36	1.46	1.54	1.5	-0.89	1.47	1.69	1.58	4.64
	5290	2.04	3.19	3.19	3.19	36	1.95	2.11	2.03	-0.56	1.96	2.24	2.1	2.97
	5300	2.3	3.59	3.59	3.59	36	2.21	2.41	2.31	0.5	2.22	2.54	2.38	3.35
	5310	4.89	7.64	7.64	7.64	36	4.7	5.28	4.99	2.06	4.67	5.32	5	2.18
	5320	5.7	8.91	8.91	8.91	36	5.48	6.18	5.83	2.18	5.43	6.19	5.81	1.96
	5330	4.16	6.5	6.5	6.5	36	4.08	4.56	4.32	3.68	4.05	4.62	4.33	4.13
	5340	4.33	6.77	6.77	6.77	36	4.12	4.61	4.36	0.76	4.09	4.67	4.38	1.26
	5350	5.22	8.16	8.16	8.16	36	5.06	5.69	5.37	2.85	5.02	5.72	5.37	2.87
	5360	4.04	6.31	6.31	6.31	36	3.88	4.34	4.11	1.69	3.86	4.41	4.13	2.3
	5370	3.42	5.34	5.34	5.34	36	3.32	3.69	3.5	2.37	3.3	3.77	3.54	3.46
	5380	3.95	6.17	6.17	6.17	36	4.08	4.56	4.32	8.58				
	5390	2.8	4.38	4.38	4.38	36	2.72	3	2.86	2.08	2.72	3.11	2.91	4.01
	5400	1.91	2.98	2.98	2.98	36	1.8	1.93	1.86	-2.56	1.81	2.07	1.94	1.67
	5410	7.12	11.13	11.13	11.13	36	6.88	7.79	7.33	2.89	6.82	7.75	7.28	2.31
	5420	3.91	6.11	6.11	6.11	36	3.83	4.27	4.05	3.46	3.8	4.34	4.07	4.11
	5430	3.18	4.97	4.97	4.97	36	3.04	3.37	3.21	0.79	3.04	3.47	3.26	2.37
	5440	3.67	5.73	5.73	5.73	36	3.6	4.01	3.8	3.46	3.57	4.08	3.83	4.31
	5450	5.28	8.25	8.25	8.25	36	5.14	5.78	5.46	3.33	5.09	5.81	5.45	3.23
	5460	5.24	8.19	8.19	8.19	36	5	5.62	5.31	1.37	4.97	5.67	5.32	1.55
	5470	5.01	7.83	7.83	7.83	36	4.87	5.47	5.17	3.04	4.82	5.5	5.16	2.98
	5480	4.65	7.27	7.27	7.27	36	4.47	5.01	4.74	1.92	4.44	5.06	4.75	2.11
	5490	7.54	11.78	11.78	11.78	36	7.23	8.2	7.72	2.28	7.17	8.14	7.65	1.51
	5500	4.76	7.44	7.44	7.44	36	4.57	5.13	4.85	1.92	4.55	5.19	4.87	2.25
	5510	4.48	7	7	7	36	4.39	4.92	4.65	3.76	4.35	4.96	4.66	3.96
	5520	3.32	5.19	5.19	5.19	36	3.22	3.57	3.39	2.19	3.21	3.67	3.44	3.53
	5530	2.99	4.67	4.67	4.67	36	2.82	3.11	2.97	-0.84	2.82	3.22	3.02	0.96
	5540	4.37	6.83	6.83	6.83	36	4.21	4.71	4.46	2.09	4.19	4.78	4.49	2.69
	5550	5	7.81	7.81	7.81	36	4.83	5.43	5.13	2.48	4.79	5.46	5.12	2.45
	5560	4.08	6.38	6.38	6.38	36	4.01	4.48	4.24	3.83	3.98	4.54	4.26	4.38
	5570	2.83	4.42	4.42	4.42	36	2.71	2.98	2.84	0.47	2.71	3.1	2.9	2.49
	5580	1.92	3	3	3	36	1.78	1.91	1.85	-3.91	1.8	2.06	1.93	0.42

Well	Depth	TOC^x	TOC J2005 Min	TOC J2005 Max	TOC J2005 AVG	% Dec	TOC J2012 Min	TOC J2012 Max	TOC J2012 AVG	% Dec	TOC Peters Min	TOC Peters Max	TOC Peters AVG	% Dec
Olympia A-12	5590	2.06	3.22	3.22	3.22	36	1.9	2.04	1.97	-4.58	1.91	2.19	2.05	-0.38
	5600	2.57	4.02	4.02	4.02	36	2.41	2.64	2.53	-1.73	2.41	2.76	2.59	0.73
	5610	1.94	3.03	3.03	3.03	36	1.77	1.9	1.83	-5.78	1.79	2.05	1.92	-1.2
	5620	2.4	3.75	3.75	3.75	36	1.99	2.15	2.07	-15.8	2.02	2.31	2.16	-9.9
	5630	5.78	9.03	9.03	9.03	36	5.33	6	5.67	-2.02	5.31	6.04	5.67	-1.83
	5640	7.85	12.27	12.27	12.27	36	7.65	8.68	8.16	3.81	7.57	8.59	8.08	2.92
	5650	3.95	6.17	6.17	6.17	36	3.81	4.25	4.03	1.87	3.79	4.33	4.06	2.68
	5660	6.36	9.94	9.94	9.94	36	6.02	6.8	6.41	0.85	5.98	6.81	6.39	0.53
	5670	3	4.69	4.69	4.69	36	2.92	3.23	3.08	2.46	2.91	3.33	3.12	3.96
	5680	1.76	2.75	2.75	2.75	36	1.57	1.67	1.62	-8.7	1.59	1.82	1.71	-3.1
	5690	1.78	2.78	2.78	2.78	36	1.64	1.75	1.69	-5.18	1.65	1.89	1.77	-0.5
	5700	0.85	1.33	1.33	1.33	36	0.75	0.72	0.73	-15.9	0.78	0.89	0.84	-1.74
	5710	1.92	3	3	3	36	1.75	1.87	1.81	-5.93	1.77	2.03	1.9	-1.19
	5720	3.05	4.77	4.77	4.77	36	2.71	2.98	2.85	-7.2	2.72	3.11	2.91	-4.54
	5730	7.81	12.2	12.2	12.2	36	7.51	8.52	8.02	2.56	7.45	8.45	7.95	1.78
	5740	8.81	13.77	13.77	13.77	36	8.51	9.68	9.09	3.13	8.44	9.56	9	2.11
	5750	7.29	11.39	11.39	11.39	36	6.87	7.78	7.32	0.46	6.83	7.76	7.29	0.06
	5760	9.74	15.22	15.22	15.22	36	8.99	10.23	9.61	-1.32	8.97	10.15	9.56	-1.83
	5770	5.52	8.63	8.63	8.63	36	5.31	5.98	5.65	2.23	5.27	6	5.64	2.11
	5780	2.25	3.52	3.52	3.52	36	2.08	2.25	2.17	-3.86	2.09	2.39	2.24	-0.54
	5790	3.6	5.63	5.63	5.63	36	3.46	3.85	3.65	1.5	3.44	3.94	3.69	2.49
	5800	9.45	14.77	14.77	14.77	36	9.14	10.4	9.77	3.28	9.05	10.25	9.65	2.12
	5810	4.99	7.8	7.8	7.8	36	4.85	5.45	5.15	3.07	4.81	5.49	5.15	3.2
	5820	6.13	9.58	9.58	9.58	36	5.91	6.67	6.29	2.49	5.86	6.67	6.27	2.22
	5830	1.64	2.56	2.56	2.56	36	1.45	1.53	1.49	-10.1	1.47	1.69	1.58	-3.75
	5840	2.25	3.52	3.52	3.52	36	2.12	2.3	2.21	-1.66	2.13	2.44	2.28	1.38
	5850	1.75	2.73	2.73	2.73	36	1.61	1.71	1.66	-5.39	1.62	1.86	1.74	-0.35
	5860	1.3	2.03	2.03	2.03	36	1.2	1.24	1.22	-6.44	1.22	1.4	1.31	0.75
	5870	1.63	2.55	2.55	2.55	36	1.52	1.6	1.56	-4.49	1.53	1.76	1.65	0.97
	5880	1.96	3.06	3.06	3.06	36	1.92	2.07	1.99	1.57	1.92	2.2	2.06	5.21
	5910	3.58	5.59	5.59	5.59	36	3.25	3.6	3.43	-4.5	3.25	3.71	3.48	-2.79
	5920	1.85	2.89	2.89	2.89	36	1.77	1.9	1.83	-0.97	1.78	2.04	1.91	3.2
	5930	1.13	1.77	1.77	1.77	36	1.07	1.08	1.08	-5.11	1.09	1.25	1.17	3.43
	5940	1.83	2.86	2.86	2.86	36	1.74	1.87	1.8	-1.39	1.76	2.01	1.89	3.04
	5950	1.79	2.8	2.8	2.8	36	1.71	1.83	1.77	-1.27	1.72	1.97	1.84	3.05
	5960	1.45	2.27	2.27	2.27	36	1.37	1.44	1.4	-3.25	1.39	1.59	1.49	2.78
	5970	1.69	2.64	2.64	2.64	36	1.58	1.68	1.63	-3.6	1.6	1.84	1.72	1.64
	5980	1.66	2.59	2.59	2.59	36	1.55	1.64	1.59	-4.29	1.56	1.79	1.68	1
	5990	1.43	2.23	2.23	2.23	36	1.36	1.42	1.39	-2.99	1.37	1.57	1.47	3.07
	6000	2.15	3.36	3.36	3.36	36	2.06	2.23	2.14	-0.29	2.06	2.36	2.21	2.79
	6010	1.91	2.98	2.98	2.98	36	1.85	1.99	1.92	0.65	1.86	2.13	2	4.54
	6020	1.4	2.19	2.19	2.19	36	1.34	1.4	1.37	-2.04	1.36	1.56	1.46	4.09
	6030	1.63	2.55	2.55	2.55	36	1.53	1.62	1.57	-3.67	1.54	1.77	1.66	1.58
	6040	1.47	2.3	2.3	2.3	36	1.39	1.46	1.42	-3.23	1.41	1.61	1.51	2.69

Table C-3: Minimum, maximum and average restored TOC values from the Jarvie et al. 2005, Jarvie 2012, and Peters et al. 2005 methods and the corresponding decrease from initial present day TOC for Sable Island O-47.

Well	Depth	TOC^x	TOC J2005 Min	TOC J2005 Max	TOC J2005 AVG	% Dec	TOC J2012 Min	TOC J2012 Max	TOC J2012 AVG	% Dec	TOC Peters Min	TOC Peters Max	TOC Peters AVG	% Dec
Sable Island O-47	3597	0.73	1.14	1.14	1.14	36	0.61	0.65	0.63	-16.2	0.68	0.78	0.73	0.16
	3850	2.02	3.16	3.16	3.16	36	2.09	1.94	2.02	-0.21	1.94	2.23	2.09	3.29

Table C-4: Minimum, maximum and average restored TOC values from the Jarvie et al. 2005, Jarvie 2012, and Peters et al. 2005 methods and the corresponding decrease from initial present day TOC for South DesBarres O-76.

Well	Depth	TOC^x	TOC J2005 Min	TOC J2005 Max	TOC J2005 AVG	% Dec	TOC J2012 Min	TOC J2012 Max	TOC J2012 AVG	% Dec	TOC Peters Min	TOC Peters Max	TOC Peters AVG	% Dec
	3910	1.3	2.03	2.03	2.03	36	0.75	0.66	0.71	-84.3	1.06	1.58	1.32	1.78
	4355	2.24	3.5	3.5	3.5	36	1.49	1.77	1.63	-37.7	1.8	2.67	2.24	-0.13
	5025	1.89	2.95	2.95	2.95	36	0.99	1.02	1	-88.4	1.31	1.95	1.63	-13.9
	5100	1.97	3.08	3.08	3.08	36	0.82	0.76	0.79	-148	1.16	1.73	1.45	-26.6
	5110	0.97	1.52	1.52	1.52	36	-0.36	-1.04	-0.7	238.2	-0.01	-0.01	-0.01	-101
	5120	2.1	3.28	3.28	3.28	36	0.76	0.67	0.72	-193	1.11	1.65	1.38	-34.2
	5130	1.91	2.98	2.98	2.98	36	0.59	0.41	0.5	-281	0.95	1.41	1.18	-38.2
	5140	1.46	2.28	2.28	2.28	36	0.39	0.1	0.25	-491	0.72	1.08	0.9	-38.4
	5150	1.25	1.95	1.95	1.95	36	0.34	0.03	0.18	-580	0.66	0.99	0.82	-34.1
	5160	1.25	1.95	1.95	1.95	36	0.34	0.03	0.19	-569	0.67	1	0.83	-33.2
	5170	1.53	2.39	2.39	2.39	36	0.48	0.24	0.36	-324	0.81	1.21	1.01	-34.1
	5180	1.5	2.34	2.34	2.34	36	0.55	0.34	0.45	-237	0.89	1.33	1.11	-26
	5190	1.52	2.38	2.38	2.38	36	0.54	0.33	0.44	-248	0.88	1.31	1.1	-27.9
	5200	1.79	2.8	2.8	2.8	36	0.61	0.43	0.52	-245	0.94	1.41	1.17	-34.4
	5210	2.01	3.14	3.14	3.14	36	0.71	0.59	0.65	-209	1.04	1.56	1.3	-35.3
	5220	1.5	2.34	2.34	2.34	36	0.47	0.23	0.35	-326	0.8	1.19	1	-33.6
	5230	1.58	2.47	2.47	2.47	36	0.55	0.35	0.45	-252	0.88	1.31	1.09	-30.9
South DesBarres O-76	5240	1.68	2.63	2.63	2.63	36	0.62	0.45	0.53	-215	0.96	1.43	1.19	-29
	5250	1.82	2.84	2.84	2.84	36	0.56	0.36	0.46	-299	0.9	1.35	1.12	-38.3
	5260	2.42	3.78	3.78	3.78	36	1.11	1.19	1.15	-111	1.46	2.17	1.81	-25.1
	5270	2.8	4.38	4.38	4.38	36	1.31	1.5	1.4	-99.9	1.67	2.47	2.07	-26.1
	5280	2.54	3.97	3.97	3.97	36	1.29	1.47	1.38	-84.4	1.64	2.43	2.03	-20
	5290	2.13	3.33	3.33	3.33	36	1.14	1.24	1.19	-79.4	1.46	2.16	1.81	-15.1
	5300	2.49	3.89	3.89	3.89	36	1.35	1.56	1.46	-70.9	1.68	2.5	2.09	-16.1
	5310	2.29	3.58	3.58	3.58	36	1.24	1.4	1.32	-73.1	1.57	2.33	1.95	-14.9
	5320	1.73	2.7	2.7	2.7	36	0.72	0.61	0.66	-160	1.07	1.59	1.33	-23.2
	5330	2.06	3.22	3.22	3.22	36	0.85	0.8	0.83	-149	1.18	1.75	1.47	-28.8
	5340	1.98	3.09	3.09	3.09	36	0.73	0.62	0.67	-195	1.05	1.57	1.31	-33.8
	5350	2.19	3.42	3.42	3.42	36	0.73	0.63	0.68	-222	1.08	1.61	1.35	-38.4
	5360	2.97	4.64	4.64	4.64	36	0.88	0.85	0.87	-243	1.24	1.85	1.54	-48
	5370	3.29	5.14	5.14	5.14	36	0.99	1.02	1	-228	1.38	2.05	1.71	-47.9
	5380	3.26	5.09	5.09	5.09	36	0.97	0.98	0.97	-235	1.37	2.03	1.7	-47.8
	5390	3.23	5.05	5.05	5.05	36	1.04	1.08	1.06	-205	1.41	2.1	1.76	-45.6
	5400	3.17	4.95	4.95	4.95	36	1.21	1.34	1.28	-148	1.57	2.34	1.95	-38.4
	5410	3.26	5.09	5.09	5.09	36	1.2	1.34	1.27	-156	1.6	2.37	1.98	-39.1
	5420	3.44	5.38	5.38	5.38	36	1.22	1.37	1.29	-166	1.6	2.38	1.99	-42.1
	5430	3.62	5.66	5.66	5.66	36	1.32	1.51	1.41	-156	1.71	2.53	2.12	-41.4
	5440	3.38	5.28	5.28	5.28	36	1.2	1.34	1.27	-166	1.57	2.33	1.95	-42.3
	5450	2.99	4.67	4.67	4.67	36	1.04	1.09	1.07	-180	1.39	2.07	1.73	-42.3
	5460	2	3.13	3.13	3.13	36	0.9	0.87	0.88	-126	1.22	1.82	1.52	-24

Well	Depth	TOC^x	TOC J2005 Min	TOC J2005 Max	TOC J2005 AVG	% Dec	TOC J2012 Min	TOC J2012 Max	TOC J2012 AVG	% Dec	TOC Peters Min	TOC Peters Max	TOC Peters AVG	% Dec
South DesBarres O-76	5470	1.8	2.81	2.81	2.81	36	1.07	1.14	1.11	-62.2	1.39	2.07	1.73	-3.85
	5480	2.98	4.66	4.66	4.66	36	1.2	1.34	1.27	-134	1.55	2.31	1.93	-35.2
	5490	2.91	4.55	4.55	4.55	36	1.22	1.36	1.29	-126	1.57	2.33	1.95	-32.9
	5500	3.1	4.84	4.84	4.84	36	1.12	1.22	1.17	-165	1.51	2.24	1.87	-39.6
	5510	3.18	4.97	4.97	4.97	36	1.16	1.27	1.22	-162	1.51	2.24	1.87	-41.1
	5520	3.03	4.73	4.73	4.73	36	1.07	1.14	1.1	-174	1.45	2.16	1.81	-40.3
	5530	3.11	4.86	4.86	4.86	36	1.03	1.08	1.06	-195	1.4	2.08	1.74	-44.2
	5540	3.47	5.42	5.42	5.42	36	1.36	1.57	1.46	-137	1.74	2.58	2.16	-37.8
	5550	2.65	4.14	4.14	4.14	36	1.08	1.15	1.11	-138	1.42	2.12	1.77	-33.2
	5560	3.21	5.02	5.02	5.02	36	1.32	1.52	1.42	-127	1.7	2.52	2.11	-34.3
	5570	3.53	5.52	5.52	5.52	36	1.53	1.83	1.68	-110	1.89	2.8	2.34	-33.6
	5580	3.26	5.09	5.09	5.09	36	1.46	1.73	1.59	-105	1.83	2.71	2.27	-30.5
	5590	3.23	5.05	5.05	5.05	36	1.31	1.51	1.41	-129	1.66	2.47	2.07	-36
	5590	2.55	3.98	3.98	3.98	36	1.26	1.43	1.34	-89.9	1.58	2.35	1.96	-23
	5600	3.16	4.94	4.94	4.94	36	1.12	1.22	1.17	-170	1.49	2.21	1.85	-41.4
	5610	3.64	5.69	5.69	5.69	36	1.67	2.05	1.86	-95.3	2.06	3.06	2.56	-29.7
	5620	3.36	5.25	5.25	5.25	36	1.46	1.73	1.59	-111	1.81	2.69	2.25	-33.1
	5630	1.7	2.66	2.66	2.66	36	1.04	1.09	1.06	-60.2	1.35	2.01	1.68	-1.02
	5640	1.86	2.91	2.91	2.91	36	1.06	1.13	1.1	-69.7	1.39	2.06	1.73	-7.21
	5650	2.64	4.13	4.13	4.13	36	1.47	1.74	1.6	-64.9	1.8	2.67	2.24	-15.3
	5660	2.25	3.52	3.52	3.52	36	0.94	0.93	0.93	-141	1.28	1.9	1.59	-29.2
	5670	1.58	2.47	2.47	2.47	36	0.63	0.46	0.54	-190	0.96	1.43	1.19	-24.5
	5680	1.94	3.03	3.03	3.03	36	0.69	0.56	0.62	-212	1.03	1.54	1.28	-33.9
	5690	2.27	3.55	3.55	3.55	36	0.94	0.93	0.93	-143	1.26	1.88	1.57	-30.8
	5700	1.59	2.48	2.48	2.48	36	0.57	0.37	0.47	-237	0.89	1.33	1.11	-30
	5710	1.98	3.09	3.09	3.09	36	0.7	0.58	0.64	-210	1.03	1.53	1.28	-35.2
	5720	1.82	2.84	2.84	2.84	36	0.66	0.52	0.59	-209	0.99	1.47	1.23	-32.4
	5730	1.95	3.05	3.05	3.05	36	0.64	0.49	0.57	-245	0.99	1.47	1.23	-36.9
	5740	1.49	2.33	2.33	2.33	36	0.53	0.32	0.42	-252	0.86	1.29	1.08	-27.7
	5750	1.23	1.92	1.92	1.92	36	0.23	-0.15	0.04	-3023	0.56	0.84	0.7	-42.9
	5760	1.9	2.97	2.97	2.97	36	0.6	0.42	0.51	-274	0.94	1.4	1.17	-38.2
	5770	1.37	2.14	2.14	2.14	36	0.26	-0.09	0.09	-1460	0.6	0.89	0.75	-45.6
	5780	1.57	2.45	2.45	2.45	36	0.39	0.11	0.25	-526	0.74	1.1	0.92	-41.6
	5790	1.69	2.64	2.64	2.64	36	0.46	0.21	0.34	-403	0.8	1.2	1	-40.8
	5800	1.87	2.92	2.92	2.92	36	0.49	0.25	0.37	-408	0.84	1.25	1.05	-44
	5810	1.93	3.02	3.02	3.02	36	0.51	0.29	0.4	-378	0.86	1.28	1.07	-44.6
	5820	1.47	2.3	2.3	2.3	36	0.27	-0.07	0.1	-1366	0.61	0.92	0.77	-47.9
	5830	1.75	2.73	2.73	2.73	36	0.53	0.32	0.43	-310	0.86	1.29	1.08	-38.5
	5840	1.59	2.48	2.48	2.48	36	0.44	0.18	0.31	-417	0.78	1.16	0.97	-39
	5850	1.6	2.5	2.5	2.5	36	0.44	0.19	0.32	-407	0.78	1.16	0.97	-39.4
	5860	1.62	2.53	2.53	2.53	36	0.4	0.13	0.26	-512	0.75	1.11	0.93	-42.6
	5870	1.65	2.58	2.58	2.58	36	0.46	0.22	0.34	-385	0.79	1.19	0.99	-40
	5880	1.66	2.59	2.59	2.59	36	0.55	0.34	0.44	-273	0.88	1.31	1.09	-34.3
	5890	1.81	2.83	2.83	2.83	36	0.58	0.39	0.48	-275	0.91	1.36	1.13	-37.4

Well	Depth	TOC^x	TOC J2005 Min	TOC J2005 Max	TOC J2005 AVG	% Dec	TOC J2012 Min	TOC J2012 Max	TOC J2012 AVG	% Dec	TOC Peters Min	TOC Peters Max	TOC Peters AVG	% Dec
South DesBarres O-76	5910	2	3.13	3.13	3.13	36	0.67	0.53	0.6	-231.9	1.02	1.52	1.27	-36.4
	5920	2.23	3.48	3.48	3.48	36	0.75	0.66	0.7	-216.7	1.1	1.64	1.37	-38.4
	5930	2.05	3.2	3.2	3.2	36	0.67	0.52	0.6	-244.4	1.02	1.52	1.27	-38.2
	5940	1.67	2.61	2.61	2.61	36	0.47	0.23	0.35	-380	0.81	1.21	1.01	-39.8
	5950	1.74	2.72	2.72	2.72	36	0.47	0.23	0.35	-393.3	0.81	1.21	1.01	-42
	5957	1.08	1.69	1.69	1.69	36	1.13	1.22	1.18	8.13	1.38	2.05	1.72	58.97
	5960	1.55	2.42	2.42	2.42	36	0.33	0.02	0.18	-777.7	0.68	1.01	0.85	-45.4
	5970	1.26	1.97	1.97	1.97	36	0.2	-0.19	0	-32428	0.53	0.79	0.66	-48
	5980	2.18	3.41	3.41	3.41	36	0.77	0.68	0.73	-199.1	1.12	1.67	1.39	-36.1
	5990	2.5	3.91	3.91	3.91	36	0.86	0.82	0.84	-196.6	1.22	1.81	1.51	-39.5
	6000	1.59	2.48	2.48	2.48	36	0.36	0.06	0.21	-642.8	0.72	1.07	0.89	-43.7
	6010	1.32	2.06	2.06	2.06	36	0.2	-0.19	0	-27872	0.54	0.8	0.67	-49.4
	6020	1.68	2.63	2.63	2.63	36	0.45	0.19	0.32	-431.7	0.78	1.16	0.97	-42.2
	6030	1.74	2.72	2.72	2.72	36	0.41	0.13	0.27	-539.2	0.75	1.12	0.93	-46.4
	6035	1.69	2.64	2.64	2.64	36	0.41	0.13	0.27	-523.5	0.74	1.11	0.93	-45.1

Table C-5: Minimum, maximum and average restored TOC values from the Jarvie et al. 2005, Jarvie 2012, and Peters et al. 2005 methods and the corresponding decrease from initial present day TOC for South Sable B-44.

Well	Depth	TOC^x	TOC J2005 Min	TOC J2005 Max	TOC J2005 AVG	% Dec	TOC J2012 Min	TOC J2012 Max	TOC J2012 AVG	% Dec	TOC Peters Min	TOC Peters Max	TOC Peters AVG	% Dec
	4045	1.24	1.94	1.94	1.94	36	1.22	1.25	1.23	-0.76	1.37	1.52	1.45	16.85
	4055	0.97	1.52	1.52	1.52	36	0.91	0.91	0.91	-6.39	1.08	1.2	1.14	17.45
	4065	0.96	1.5	1.5	1.5	36	0.9	0.9	0.9	-6.78	1.07	1.18	1.13	17.32
	4075	0.94	1.47	1.47	1.47	36	0.88	0.87	0.87	-7.48	1.05	1.16	1.1	17.29
	4085	1	1.56	1.56	1.56	36	0.95	0.96	0.96	-4.67	1.12	1.24	1.18	18.07
	4095	0.79	1.23	1.23	1.23	36	0.71	0.68	0.7	-13.41	0.88	0.98	0.93	17.67
	4105	0.87	1.36	1.36	1.36	36	0.81	0.79	0.8	-9.11	0.97	1.08	1.03	18.2
	4115	0.95	1.48	1.48	1.48	36	0.9	0.9	0.9	-5.77	1.07	1.18	1.13	18.45
	4125	0.95	1.48	1.48	1.48	36	0.89	0.89	0.89	-6.8	1.06	1.18	1.12	17.63
	4135	0.89	1.39	1.39	1.39	36	0.83	0.81	0.82	-8.45	1	1.11	1.05	18.05
	4145	0.83	1.3	1.3	1.3	36	0.76	0.74	0.75	-11.03	0.93	1.03	0.98	17.98
	4150	0.9	1.41	1.41	1.41	36	0.84	0.83	0.83	-8.27	1.01	1.12	1.06	17.83
	4985	1.25	1.95	1.95	1.95	36	1.24	1.27	1.25	0.16	1.39	1.55	1.47	17.55
	4990	1.06	1.66	1.66	1.66	36	1.02	1.02	1.02	-3.94	1.18	1.31	1.25	17.46
	4991	1.05	1.64	1.64	1.64	36	1.01	1.02	1.01	-3.81	1.17	1.3	1.24	17.69
	4995	1.14	1.78	1.78	1.78	36	1.11	1.13	1.12	-1.83	1.27	1.41	1.34	17.6
	5005	1.08	1.69	1.69	1.69	36	1.03	1.05	1.04	-3.95	1.05	1.21	1.13	4.75
	5015	0.84	1.31	1.31	1.31	36	0.79	0.77	0.78	-7.49	0.82	0.94	0.88	4.74
	5025	1.01	1.58	1.58	1.58	36	0.96	0.96	0.96	-5.4	0.98	1.12	1.05	4.2
South Sable B-44	5030	0.8	1.25	1.25	1.25	36	0.75	0.73	0.74	-8.06	0.78	0.9	0.84	4.92
	5040	1.09	1.7	1.7	1.7	36	1.04	1.06	1.05	-3.7	1.06	1.22	1.14	4.92
	5041	1.09	1.7	1.7	1.7	36	1.04	1.05	1.05	-4.17	1.06	1.22	1.14	4.51
	5045	0.78	1.22	1.22	1.22	36	0.73	0.7	0.71	-9.1	0.76	0.87	0.82	4.54
	5055	1.07	1.67	1.67	1.67	36	1.03	1.04	1.03	-3.64	1.05	1.2	1.12	5.13
	5065	1.45	2.27	2.27	2.27	36	1.4	1.47	1.44	-0.98	1.42	1.62	1.52	4.79
	5075	0.99	1.55	1.55	1.55	36	0.94	0.94	0.94	-5.79	0.96	1.1	1.03	4.09
	5085	1.12	1.75	1.75	1.75	36	1.07	1.09	1.08	-3.88	1.09	1.25	1.17	4.39
	5095	1.08	1.69	1.69	1.69	36	1.03	1.04	1.04	-4.34	1.05	1.21	1.13	4.48
	5105	1.13	1.77	1.77	1.77	36	1.08	1.1	1.09	-3.36	1.1	1.27	1.18	4.8
	5115	1.04	1.63	1.63	1.63	36	0.98	0.99	0.99	-5.24	1.01	1.16	1.08	3.99
	5125	1.13	1.77	1.77	1.77	36	1.07	1.09	1.08	-4.37	1.09	1.26	1.17	3.97
	5135	1.13	1.77	1.77	1.77	36	1.07	1.09	1.08	-4.27	1.09	1.26	1.18	4.02
	5145	0.99	1.55	1.55	1.55	36	0.94	0.94	0.94	-5.47	0.96	1.1	1.03	4.4
	5155	0.97	1.52	1.52	1.52	36	0.92	0.91	0.92	-5.98	0.94	1.08	1.01	4.11
	5160	1.21	1.89	1.89	1.89	36	1.17	1.2	1.18	-2.35	1.18	1.36	1.27	5.12
	5161	1.15	1.8	1.8	1.8	36	1.11	1.13	1.12	-2.89	1.13	1.29	1.21	5.12
	5165	1.16	1.81	1.81	1.81	36	1.11	1.13	1.12	-3.54	1.13	1.29	1.21	4.43
	5175	1.14	1.78	1.78	1.78	36	1.09	1.11	1.1	-3.39	1.11	1.28	1.19	4.71
	5185	1.26	1.97	1.97	1.97	36	1.21	1.25	1.23	-2.29	1.23	1.41	1.32	4.79
	5195	1.26	1.97	1.97	1.97	36	1.22	1.26	1.24	-1.5	1.24	1.42	1.33	5.58

Well	Depth	TOC^x	TOC J2005 Min	TOC J2005 Max	TOC J2005 AVG	% Dec	TOC J2012 Min	TOC J2012 Max	TOC J2012 AVG	% Dec	TOC Peters Min	TOC Peters Max	TOC Peters AVG	% Dec
S. Sable B-44	5200	1.1	1.72	1.72	1.72	36	1.04	1.05	1.05	-5.25	1.06	1.22	1.14	3.38
	5201	0.99	1.55	1.55	1.55	36	0.92	0.92	0.92	-7.21	0.95	1.09	1.02	2.98
	5205	1.42	2.22	2.22	2.22	36	1.36	1.43	1.4	-1.62	1.38	1.58	1.48	4.32
	5208	1.43	2.23	2.23	2.23	36	1.35	1.41	1.38	-3.48	1.37	1.57	1.47	2.78

Table C-6: Minimum, maximum and average restored TOC values from the Jarvie et al. 2005, Jarvie 2012, and Peters et al. 2005 methods and the corresponding decrease from initial present day TOC for South Venture O-59.

Well	Depth	TOC^x	TOC J2005 Min	TOC J2005 Max	TOC J2005 AVG	% Dec	TOC J2012 Min	TOC J2012 Max	TOC J2012 AVG	% Dec	TOC Peters Min	TOC Peters Max	TOC Peters AVG	% Dec
South Venture O-59	5120	1.44	2.25	2.25	2.25	36	1.37	1.43	1.4	-2.73	1.38	1.59	1.49	3.18
	5140	0.71	1.11	1.11	1.11	36	0.66	0.62	0.64	-11.09	0.69	0.79	0.74	4.3
	5160	1.2	1.88	1.88	1.88	36	1.16	1.19	1.17	-2.39	1.17	1.35	1.26	5.02
	5180	1.1	1.72	1.72	1.72	36	1.05	1.06	1.05	-4.29	1.07	1.23	1.15	4.29
	5200	0.53	0.83	0.83	0.83	36	0.49	0.42	0.45	-17.02	0.52	0.6	0.56	5.31
	5220	1.02	1.59	1.59	1.59	36	0.96	0.96	0.96	-5.94	0.98	1.13	1.06	3.56
	5240	1.2	1.88	1.88	1.88	36	1.15	1.18	1.16	-3.15	1.17	1.34	1.25	4.38
	5260	0.76	1.19	1.19	1.19	36	0.72	0.68	0.7	-8.26	0.75	0.86	0.8	5.56
	5280	0.91	1.42	1.42	1.42	36	0.87	0.85	0.86	-5.91	0.89	1.02	0.96	4.97
	5300	1.2	1.88	1.88	1.88	36	1.15	1.19	1.17	-2.56	1.17	1.35	1.26	5
	5320	1.22	1.91	1.91	1.91	36	1.18	1.21	1.19	-2.22	1.19	1.37	1.28	5.14
	5340	1.34	2.09	2.09	2.09	36	1.25	1.3	1.28	-4.87	1.27	1.46	1.37	1.94
	5360	0.89	1.39	1.39	1.39	36	0.85	0.83	0.84	-5.76	0.87	1	0.94	5.53
	5400	1.45	2.27	2.27	2.27	36	1.41	1.48	1.44	-0.65	1.42	1.63	1.52	5.03
	5420	0.83	1.3	1.3	1.3	36	0.74	0.71	0.72	-14.74	0.77	0.88	0.82	-0.7
	5460	2.4	3.75	3.75	3.75	36	2.33	2.54	2.43	1.41	2.33	2.67	2.5	4.04
	5560	3.7	5.78	5.78	5.78	36	3.58	3.98	3.78	2.13	3.56	4.07	3.81	3.04
	5600	1.26	1.97	1.97	1.97	36	1.22	1.26	1.24	-1.9	1.23	1.42	1.32	5.15
	5620	1.25	1.95	1.95	1.95	36	1.22	1.26	1.24	-0.99	1.23	1.42	1.32	5.97
	5700	1.66	2.59	2.59	2.59	36	1.55	1.65	1.6	-3.73	1.57	1.8	1.68	1.22
	5780	1.1	1.72	1.72	1.72	36	1.06	1.08	1.07	-3.08	1.08	1.24	1.16	5.27
	5865	5.05	7.89	7.89	7.89	36	4.97	5.59	5.28	4.38	4.93	5.62	5.27	4.45
	5865	4.83	7.55	7.55	7.55	36	4.75	5.33	5.04	4.13	4.71	5.37	5.04	4.26
	5880	9.42	14.72	14.72	14.72	36	9.39	10.69	10.04	6.17	9.26	10.48	9.87	4.8
	5900	2.64	4.13	4.13	4.13	36	2.62	2.88	2.75	3.94	2.61	2.99	2.8	6.01
	5960	4.35	6.8	6.8	6.8	36	4.38	4.91	4.64	6.3	4.33	4.94	4.64	6.63

Table C-7: Minimum, maximum and average restored TOC values from the Jarvie et al. 2005, Jarvie 2012, and Peters et al. 2005 methods and the corresponding decrease from initial present day TOC for Uniacke G-72.

Well	Depth	TOC^x	TOC J2005 Min	TOC J2005 Max	TOC J2005 AVG	% Dec	TOC J2012 Min	TOC J2012 Max	TOC J2012 AVG	% Dec	TOC Peters Min	TOC Peters Max	TOC Peters AVG	% Dec
	4910	5.65	8.83	8.83	8.83	36	5.52	6.22	5.87	3.77	5.47	6.23	5.85	3.48
	4925	2.94	4.59	4.59	4.59	36	2.81	3.1	2.95	0.5	2.81	3.21	3.01	2.38
	4930	5.19	8.11	8.11	8.11	36	5.03	5.65	5.34	2.8	4.99	5.68	5.33	2.79
	4940	4.52	7.06	7.06	7.06	36	4.42	4.95	4.69	3.57	4.38	5	4.69	3.8
	4950	2.81	4.39	4.39	4.39	36	2.73	3.01	2.87	2.14	2.73	3.12	2.92	4.04
	4960	1.1	1.72	1.72	1.72	36	1.02	1.03	1.02	-7.61	1.04	1.19	1.12	1.42
	4970	0.82	1.28	1.28	1.28	36	0.74	0.71	0.73	-12.87	0.77	0.89	0.83	1.17
	4980	2.86	4.47	4.47	4.47	36	2.75	3.02	2.89	0.89	2.74	3.14	2.94	2.73
	4990	4.36	6.81	6.81	6.81	36	4.27	4.78	4.53	3.66	4.24	4.83	4.53	4.01
	5000	1.89	2.95	2.95	2.95	36	1.77	1.9	1.84	-2.94	1.78	2.05	1.91	1.3
	5010	4.25	6.64	6.64	6.64	36	4.17	4.67	4.42	3.81	4.14	4.72	4.43	4.26
	5020	4.62	7.22	7.22	7.22	36	4.52	5.08	4.8	3.75	4.49	5.12	4.8	3.92
	5030	1.13	1.77	1.77	1.77	36	1.02	1.04	1.03	-9.69	1.05	1.2	1.13	-0.29
	5040	1.03	1.61	1.61	1.61	36	0.9	0.9	0.9	-14.62	0.93	1.06	1	-3.29
	5050	0.79	1.23	1.23	1.23	36	0.7	0.66	0.68	-15.96	0.73	0.84	0.78	-0.96
	5060	0.83	1.3	1.3	1.3	36	0.74	0.71	0.73	-14.44	0.77	0.88	0.83	-0.28
	5070	0.75	1.17	1.17	1.17	36	0.64	0.6	0.62	-20.96	0.67	0.77	0.72	-3.57
	5080	0.93	1.45	1.45	1.45	36	0.84	0.83	0.83	-11.65	0.87	1	0.93	0.17
	5085	5.68	8.88	8.88	8.88	36	5.55	6.26	5.9	3.78	5.5	6.26	5.88	3.52
Uniacke G-72	5570	1.04	1.63	1.63	1.63	36	0.89	0.88	0.88	-18.03	0.92	1.05	0.98	-5.47
	5580	2.06	3.22	3.22	3.22	36	1.91	2.06	1.98	-3.87	1.92	2.2	2.06	0.07
	5590	1.17	1.83	1.83	1.83	36	0.95	0.95	0.95	-23.04	0.98	1.12	1.05	-10.2
	5600	1.24	1.94	1.94	1.94	36	1.07	1.09	1.08	-14.58	1.1	1.26	1.18	-4.86
	5610	1.17	1.83	1.83	1.83	36	0.97	0.98	0.97	-20.03	1	1.15	1.07	-8.29
	5620	1.76	2.75	2.75	2.75	36	1.58	1.68	1.63	-7.87	1.6	1.83	1.72	-2.47
	5625	2.07	3.23	3.23	3.23	36	1.93	2.08	2	-3.29	1.94	2.22	2.08	0.37
	5640	1.18	1.84	1.84	1.84	36	1.02	1.03	1.02	-15.21	1.04	1.2	1.12	-5.06
	5650	1.18	1.84	1.84	1.84	36	1.04	1.05	1.05	-12.89	1.06	1.22	1.14	-3.12
	5660	1.32	2.06	2.06	2.06	36	1.15	1.18	1.16	-13.36	1.17	1.34	1.26	-4.74
	5670	1.2	1.88	1.88	1.88	36	1.06	1.08	1.07	-11.78	1.09	1.25	1.17	-2.63
	5680	1.04	1.63	1.63	1.63	36	0.91	0.9	0.9	-15.03	0.93	1.07	1	-3.5
	5690	0.96	1.5	1.5	1.5	36	0.78	0.76	0.77	-24.8	0.81	0.93	0.87	-9.05
	5700	0.73	1.14	1.14	1.14	36	0.6	0.55	0.58	-26.2	0.63	0.73	0.68	-6.57
	5710	0.81	1.27	1.27	1.27	36	0.68	0.64	0.66	-22.23	0.71	0.82	0.77	-5.53
	5720	0.64	1	1	1	36	0.52	0.46	0.49	-30.71	0.56	0.64	0.6	-6.52
	5730	1.05	1.64	1.64	1.64	36	0.94	0.94	0.94	-11.34	0.97	1.11	1.04	-0.96
	5735	0.87	1.36	1.36	1.36	36	0.75	0.72	0.73	-19	0.78	0.89	0.83	-4.04
	5175	1.14	1.78	1.78	1.78	36	1.09	1.11	1.1	-3.39	1.11	1.28	1.19	4.71
	5185	1.26	1.97	1.97	1.97	36	1.21	1.25	1.23	-2.29	1.23	1.41	1.32	4.79
	5195	1.26	1.97	1.97	1.97	36	1.22	1.26	1.24	-1.5	1.24	1.42	1.33	5.58

Well	Depth	TOC^x	TOC J2005 Min	TOC J2005 Max	TOC J2005 AVG	% Dec	TOC J2012 Min	TOC J2012 Max	TOC J2012 AVG	% Dec	TOC Peters Min	TOC Peters Max	TOC Peters AVG	% Dec
Uniacke G-72	5200	1.1	1.72	1.72	1.72	36	1.04	1.05	1.05	-5.25	1.06	1.22	1.14	3.38
	5201	0.99	1.55	1.55	1.55	36	0.92	0.92	0.92	-7.21	0.95	1.09	1.02	2.98
	5205	1.42	2.22	2.22	2.22	36	1.36	1.43	1.4	-1.62	1.38	1.58	1.48	4.32
	5208	1.43	2.23	2.23	2.23	36	1.35	1.41	1.38	-3.48	1.37	1.57	1.47	2.78

Table C-8: Minimum, maximum and average restored TOC values from the Jarvie et al. 2005, Jarvie 2012, and Peters et al. 2005 methods and the corresponding decrease from initial present day TOC for Venture B-43.

Well	Depth	TOC^x	TOC J2005 Min	TOC J2005 Max	TOC J2005 AVG	% Dec	TOC J2012 Min	TOC J2012 Max	TOC J2012 AVG	% Dec	TOC Peters Min	TOC Peters Max	TOC Peters AVG	% Dec
Venture B-43	4959	2.02	3.16	3.16	3.16	36	1.93	2.08	2	-0.93	1.93	2.21	2.07	2.56
	5310	4.14	6.47	6.47	6.47	36	4.04	4.51	4.27	3.12	4	4.57	4.29	3.53

153

Table C-9: Minimum, maximum and average restored TOC values from the Jarvie et al. 2005, Jarvie 2012, and Peters et al. 2005 methods and the corresponding decrease from initial present day TOC for Venture B-52.

Well	Depth	TOC^x	TOC J2005 Min	TOC J2005 Max	TOC J2005 AVG	% Dec	TOC J2012 Min	TOC J2012 Max	TOC J2012 AVG	% Dec	TOC Peters Min	TOC Peters Max	TOC Peters AVG	% Dec
	5140	1.84	2.88	2.88	2.88	36	1.86	1.97	1.91	3.9	2.01	2.22	2.11	14.87
	5170	1.44	2.25	2.25	2.25	36	1.43	1.48	1.45	0.89	1.58	1.75	1.66	15.61
	5200	1.38	2.16	2.16	2.16	36	1.36	1.41	1.38	0.14	1.51	1.68	1.6	15.75
	5230	1.61	2.52	2.52	2.52	36	1.61	1.69	1.65	2.61	1.76	1.95	1.86	15.47
	5260	1.45	2.27	2.27	2.27	36	1.43	1.48	1.46	0.4	1.58	1.75	1.67	15.01
	5290	1.57	2.45	2.45	2.45	36	1.57	1.64	1.61	2.34	1.72	1.91	1.81	15.58
	5320	1.75	2.73	2.73	2.73	36	1.77	1.86	1.82	3.59	1.91	2.12	2.02	15.19
	5370	2.17	3.39	3.39	3.39	36	2.24	2.39	2.31	6.23	2.37	2.63	2.5	15.16
	5410	1.22	1.91	1.91	1.91	36	1.2	1.23	1.22	-0.06	1.36	1.51	1.44	17.79
	5440	1.52	2.38	2.38	2.38	36	1.52	1.59	1.55	2.17	1.67	1.85	1.76	15.9
	5470	1.28	2	2	2	36	1.26	1.29	1.27	-0.47	1.41	1.57	1.49	16.49
Venture B-52	5500	1.55	2.42	2.42	2.42	36	1.55	1.62	1.58	1.96	1.7	1.88	1.79	15.41
	5530	1.36	2.13	2.13	2.13	36	1.34	1.38	1.36	0.13	1.49	1.66	1.58	15.86
	5550	1.26	1.97	1.97	1.97	36	1.23	1.27	1.25	-0.74	1.39	1.54	1.47	16.54
	5620	1.67	2.61	2.61	2.61	36	1.68	1.76	1.72	2.89	1.82	2.02	1.92	15.19
	5650	1.6	2.5	2.5	2.5	36	1.62	1.7	1.66	3.54	1.77	1.96	1.86	16.52
	5680	1.48	2.31	2.31	2.31	36	1.52	1.58	1.55	4.6	1.67	1.85	1.76	18.87
	5710	1.45	2.27	2.27	2.27	36	1.47	1.53	1.5	3.49	1.62	1.8	1.71	18.03
	5740	1.22	1.91	1.91	1.91	36	1.22	1.26	1.24	1.6	1.38	1.53	1.46	19.29
	5770	1.26	1.97	1.97	1.97	36	1.26	1.3	1.28	1.39	1.42	1.57	1.49	18.47
	5800	1.51	2.36	2.36	2.36	36	1.56	1.64	1.6	5.65	1.71	1.9	1.81	19.58
	5830	2.48	3.88	3.88	3.88	36	2.64	2.83	2.74	9.39	2.76	3.06	2.91	17.29
	5860	2.39	3.73	3.73	3.73	36	2.53	2.71	2.62	8.9	2.65	2.94	2.8	17
	5890	1.35	2.11	2.11	2.11	36	1.25	1.29	1.27	-6.29	1.41	1.57	1.49	10.33
	5920	2.02	3.16	3.16	3.16	36	2.08	2.21	2.15	5.87	2.22	2.46	2.34	15.71
	5950	2.01	3.14	3.14	3.14	36	2.13	2.26	2.2	8.52	2.26	2.51	2.38	18.58

Table C-10: Minimum, maximum and average restored TOC values from the Jarvie et al. 2005, Jarvie 2012, and Peters et al. 2005 methods and the corresponding decrease from initial present day TOC for West Olympia O-51.

Well	Depth	TOC^x	TOC J2005 Min	TOC J2005 Max	TOC J2005 AVG	% Dec	TOC J2012 Min	TOC J2012 Max	TOC J2012 AVG	% Dec	TOC Peters Min	TOC Peters Max	TOC Peters AVG	% Dec
	3720	0.71	1.11	1.11	1.11	36	0.57	0.53	0.55	-29.52	0.75	0.83	0.79	10.85
	3730	0.32	0.5	0.5	0.5	36	0.15	0.06	0.11	-202.8	0.34	0.37	0.35	10.87
	3740	0.5	0.78	0.78	0.78	36	0.35	0.29	0.32	-55.85	0.53	0.59	0.56	12.87
	3760	0.64	1	1	1	36	0.5	0.45	0.47	-34.96	0.68	0.75	0.71	11.66
	3770	0.29	0.45	0.45	0.45	36	0.12	0.03	0.08	-270.4	0.31	0.35	0.33	13.12
	3780	0.45	0.7	0.7	0.7	36	0.28	0.21	0.25	-81.88	0.47	0.52	0.49	9.67
	3790	0.42	0.66	0.66	0.66	36	0.24	0.16	0.2	-106.1	0.43	0.48	0.45	7.49
	3810	0.67	1.05	1.05	1.05	36	0.54	0.5	0.52	-28.85	0.72	0.8	0.76	13.17
	3820	0.68	1.06	1.06	1.06	36	0.55	0.5	0.52	-29.76	0.72	0.8	0.76	12.23
	3830	0.57	0.89	0.89	0.89	36	0.41	0.35	0.38	-50.14	0.59	0.66	0.62	9.23
	3850	0.32	0.5	0.5	0.5	36	0.17	0.08	0.12	-162.5	0.35	0.39	0.37	15.79
	3860	0.6	0.94	0.94	0.94	36	0.44	0.39	0.42	-44.34	0.62	0.69	0.66	9.69
West Olympia O-51	3880	1.11	1.73	1.73	1.73	36	1.01	1.02	1.01	-9.67	1.17	1.3	1.24	11.56
	3890	1.03	1.61	1.61	1.61	36	0.94	0.94	0.94	-9.14	1.11	1.23	1.17	13.71
	3900	0.65	1.02	1.02	1.02	36	0.51	0.46	0.49	-33.49	0.69	0.76	0.73	11.8
	3910	2.17	3.39	3.39	3.39	36	1.87	1.98	1.93	-12.56	2.04	2.26	2.15	-1.13
	3940	1.75	2.73	2.73	2.73	36	1.63	1.71	1.67	-4.85	1.78	1.98	1.88	7.48
	3950	0.15	0.23	0.23	0.23	36	-0.05	-0.16	-0.1	245.32	0.14	0.16	0.15	0.64
	3970	0.58	0.91	0.91	0.91	36	0.44	0.38	0.41	-40.82	0.62	0.69	0.65	12.66
	3980	0.4	0.63	0.63	0.63	36	0.26	0.18	0.22	-83.17	0.44	0.49	0.46	15.98
	4000	0.83	1.3	1.3	1.3	36	0.71	0.69	0.7	-18.22	0.89	0.99	0.94	12.85
	4010	0.5	0.78	0.78	0.78	36	0.37	0.31	0.34	-46.93	0.55	0.61	0.58	16.72
	4020	0.86	1.34	1.34	1.34	36	0.69	0.66	0.67	-27.75	0.86	0.96	0.91	5.96
	4030	0.68	1.06	1.06	1.06	36	0.56	0.52	0.54	-26.11	0.74	0.82	0.78	14.29
	4040	1.17	1.83	1.83	1.83	36	1.1	1.11	1.1	-5.91	1.26	1.4	1.33	13.56
	4050	0.76	1.19	1.19	1.19	36	0.63	0.59	0.61	-24.43	0.8	0.89	0.85	11.53
	4060	0.29	0.45	0.45	0.45	36	0.13	0.04	0.09	-237.7	0.32	0.35	0.34	15.64
	4070	0.38	0.59	0.59	0.59	36	0.22	0.14	0.18	-108.7	0.41	0.45	0.43	12.92
	4090	0.27	0.42	0.42	0.42	36	0.09	-0.01	0.04	-559.7	0.28	0.31	0.29	8
	4100	0.34	0.53	0.53	0.53	36	0.19	0.11	0.15	-124.1	0.38	0.42	0.4	17.33
	4120	1	1.56	1.56	1.56	36	0.87	0.86	0.86	-16.12	1.04	1.15	1.09	9.25
	4140	0.77	1.2	1.2	1.2	36	0.64	0.6	0.62	-24.14	0.81	0.9	0.86	11.24
	4150	1.02	1.59	1.59	1.59	36	0.91	0.91	0.91	-12.16	1.08	1.2	1.14	11.65
	4160	1.15	1.8	1.8	1.8	36	1.06	1.08	1.07	-7.42	1.23	1.36	1.3	12.68
	4180	0.82	1.28	1.28	1.28	36	0.72	0.7	0.71	-15.16	0.9	1	0.95	15.36
	4190	1.2	1.88	1.88	1.88	36	1.12	1.14	1.13	-6.4	1.28	1.42	1.35	12.64
	4210	0.77	1.2	1.2	1.2	36	0.67	0.64	0.65	-18.16	0.84	0.93	0.89	15.18
	4220	0.72	1.13	1.13	1.13	36	0.63	0.59	0.61	-18.32	0.8	0.89	0.84	17.2
	4240	0.67	1.05	1.05	1.05	36	0.55	0.5	0.53	-27.52	0.72	0.8	0.76	13.92
	4250	0.24	0.38	0.38	0.38	36	0.08	-0.02	0.03	-768.8	0.26	0.29	0.28	15.87

155

Well	Depth	TOC^x	TOC J2005 Min	TOC J2005 Max	TOC J2005 AVG	% Dec	TOC J2012 Min	TOC J2012 Max	TOC J2012 AVG	% Dec	TOC Peters Min	TOC Peters Max	TOC Peters AVG	% Dec
West Olympia O-51	4260	0.89	1.39	1.39	1.39	36	0.76	0.74	0.75	-17.93	0.94	1.04	0.99	11.1
	4270	0.93	1.45	1.45	1.45	36	0.81	0.8	0.81	-15.44	0.98	1.09	1.04	11.62
	4280	0.81	1.27	1.27	1.27	36	0.71	0.68	0.7	-16.55	0.88	0.98	0.93	14.77
	4300	0.81	1.27	1.27	1.27	36	0.67	0.64	0.66	-22.86	0.85	0.94	0.89	10.49
	4310	0.83	1.3	1.3	1.3	36	0.74	0.72	0.73	-13.16	0.92	1.02	0.97	16.41
	4320	0.93	1.45	1.45	1.45	36	0.83	0.81	0.82	-13.46	1	1.11	1.05	13.1
	4330	0.75	1.17	1.17	1.17	36	0.64	0.61	0.63	-19.57	0.82	0.91	0.86	15.08
	4340	0.7	1.09	1.09	1.09	36	0.6	0.56	0.58	-19.83	0.78	0.86	0.82	17.17
	4360	0.64	1	1	1	36	0.49	0.44	0.47	-36.84	0.67	0.75	0.71	10.64
	4370	0.87	1.36	1.36	1.36	36	0.61	0.57	0.59	-48.38	0.79	0.88	0.83	-4.35
	4371	0.94	1.47	1.47	1.47	36	0.8	0.79	0.79	-18.47	0.97	1.08	1.03	9.17
	4380	1.43	2.23	2.23	2.23	36	1.34	1.39	1.37	-4.56	1.5	1.67	1.59	10.87
	4381	0.71	1.11	1.11	1.11	36	0.48	0.42	0.45	-57.51	0.66	0.73	0.69	-2.2
	4390	0.6	0.94	0.94	0.94	36	0.45	0.39	0.42	-42.12	0.63	0.7	0.66	10.56
	4400	0.75	1.17	1.17	1.17	36	0.35	0.28	0.31	-140.2	0.53	0.59	0.56	-25.1
	4401	1.13	1.77	1.77	1.77	36	1.06	1.07	1.06	-6.14	1.22	1.36	1.29	14.05
	4410	0.43	0.67	0.67	0.67	36	0.17	0.08	0.13	-236.5	0.36	0.4	0.38	-11.6
	4420	0.41	0.64	0.64	0.64	36	0.25	0.17	0.21	-94.73	0.43	0.48	0.46	11.53
	4430	0.83	1.3	1.3	1.3	36	0.7	0.67	0.68	-21.21	0.87	0.97	0.92	10.75
	4431	0.67	1.05	1.05	1.05	36	0.4	0.34	0.37	-79.21	0.59	0.65	0.62	-7.17
	4440	0.84	1.31	1.31	1.31	36	0.73	0.7	0.71	-17.69	0.9	1	0.95	12.85
	4441	1.19	1.86	1.86	1.86	36	0.62	0.59	0.61	-96.27	0.82	0.91	0.87	-27.3
	4450	0.71	1.11	1.11	1.11	36	0.63	0.59	0.61	-16.42	0.8	0.89	0.85	19.16
	4460	0.45	0.7	0.7	0.7	36	0.33	0.26	0.29	-54.8	0.51	0.56	0.53	18.84
	4460	0.94	1.47	1.47	1.47	36	0.41	0.35	0.38	-148.8	0.59	0.66	0.63	-33.5
	4490	0.96	1.5	1.5	1.5	36	0.78	0.76	0.77	-24.12	0.96	1.06	1.01	5.01
	4500	1.04	1.63	1.63	1.63	36	1.05	1.06	1.05	1.12	1.21	1.34	1.27	22.57
	4510	5.69	8.89	8.89	8.89	36	3.31	3.58	3.44	-65.19	3.57	3.95	3.76	-33.9
	4540	1.02	1.59	1.59	1.59	36	0.97	0.97	0.97	-5.04	1.13	1.26	1.2	17.31
	4550	0.64	1	1	1	36	0.52	0.48	0.5	-28.23	0.7	0.78	0.74	15.37
	4560	1.25	1.95	1.95	1.95	36	1.22	1.25	1.23	-1.41	1.38	1.53	1.45	16.18
	4570	1.65	2.58	2.58	2.58	36	1.49	1.58	1.54	-7.38	1.51	1.73	1.62	-1.74
	4580	1.25	1.95	1.95	1.95	36	1.17	1.2	1.19	-5.47	1.19	1.36	1.28	2.07
	4590	1.15	1.8	1.8	1.8	36	1.04	1.05	1.04	-10.25	1.06	1.22	1.14	-1.14
	4600	1.35	2.11	2.11	2.11	36	1.26	1.31	1.28	-5.28	1.28	1.47	1.37	1.61
	4610	1.48	2.31	2.31	2.31	36	1.4	1.47	1.44	-2.98	1.42	1.62	1.52	2.73
	4620	1.13	1.77	1.77	1.77	36	1.03	1.04	1.03	-9.29	1.05	1.21	1.13	-0.15
	4630	1.5	2.34	2.34	2.34	36	1.38	1.44	1.41	-6.32	1.4	1.6	1.5	-0.14
	4640	1.29	2.02	2.02	2.02	36	1.21	1.25	1.23	-5.11	1.23	1.41	1.32	2.07
	4650	0.61	0.95	0.95	0.95	36	0.55	0.49	0.52	-17.53	0.58	0.67	0.62	2.17
	4660	1.04	1.63	1.63	1.63	36	0.97	0.97	0.97	-7	0.99	1.14	1.07	2.56
	4670	0.6	0.94	0.94	0.94	36	0.53	0.47	0.5	-20.2	0.56	0.65	0.6	0.64
	4680	1.08	1.69	1.69	1.69	36	0.97	0.97	0.97	-11.55	0.99	1.14	1.07	-1.37
	4690	1.08	1.69	1.69	1.69	36	0.98	0.99	0.99	-9.6	1.01	1.16	1.08	0.07

Well	Depth	TOC^x	TOC J2005 Min	TOC J2005 Max	TOC J2005 AVG	% Dec	TOC J2012 Min	TOC J2012 Max	TOC J2012 AVG	% Dec	TOC Peters Min	TOC Peters Max	TOC Peters AVG	% Dec
West Olympia O-51	4700	3.8	5.94	5.94	5.94	36	3.6	4.01	3.81	0.19	3.59	4.1	3.84	1.1
	4720	9.11	14.23	14.23	14.23	36	8.64	9.82	9.23	1.33	8.58	9.72	9.15	0.42
	4730	2.96	4.63	4.63	4.63	36	2.74	3.02	2.88	-2.79	2.74	3.14	2.94	-0.63
	4740	3.95	6.17	6.17	6.17	36	4.08	4.56	4.32	8.58				
	4750	1.51	2.36	2.36	2.36	36	1.35	1.41	1.38	-9.42	1.37	1.57	1.47	-2.68
	4760	1.5	2.34	2.34	2.34	36	1.38	1.45	1.42	-5.89	1.4	1.6	1.5	0.09
	4770	3.87	6.05	6.05	6.05	36	3.98	4.45	4.22	8.26				
	4780	4.31	6.73	6.73	6.73	36	3.97	4.44	4.21	-2.48	3.96	4.53	4.24	-1.53
	4790	4.03	6.3	6.3	6.3	36	3.86	4.31	4.08	1.34	3.84	4.38	4.11	1.98
	4810	1.94	3.03	3.03	3.03	36	1.93	2.08	2.01	3.25	1.93	2.22	2.07	6.92

Table C-11: Minimum, maximum and average restored TOC values from the Jarvie et al. 2005, Jarvie 2012, and Peters et al. 2005 methods and the corresponding decrease from initial present day TOC for West Venture N-91.

Well	Depth	TOC^x	TOC J2005 Min	TOC J2005 Max	TOC J2005 AVG	% Dec	TOC J2012 Min	TOC J2012 Max	TOC J2012 AVG	% Dec	TOC Peters Min	TOC Peters Max	TOC Peters AVG	% Dec
West Venture N-91	4900	1.07	1.67	1.67	1.67	36	1.05	1.07	1.06	-0.93	1.07	1.23	1.15	7.53
	4930	1.04	1.63	1.63	1.63	36	1.02	1.03	1.02	-1.51	1.04	1.19	1.12	7.33
	4990	1.14	1.78	1.78	1.78	36	1.11	1.13	1.12	-1.63	1.13	1.29	1.21	6.22
	5020	0.96	1.5	1.5	1.5	36	0.94	0.94	0.94	-2.09	0.96	1.11	1.03	7.73
	5080	0.9	1.41	1.41	1.41	36	0.88	0.87	0.87	-3	0.9	1.04	0.97	7.66
	5110	1.14	1.78	1.78	1.78	36	1.12	1.15	1.14	-0.35	1.14	1.31	1.23	7.52
	5140	1.27	1.98	1.98	1.98	36	1.25	1.3	1.28	0.66	1.27	1.46	1.36	7.43
	5170	0.38	0.59	0.59	0.59	36	0.35	0.35	0.35	-7.83				
	5200	0.39	0.61	0.61	0.61	36	0.36	0.36	0.36	-7.48				
	5230	1.3	2.03	2.03	2.03	36	1.28	1.28	1.28	-1.67	1.3	1.3	1.3	-0.35
	5260	1.13	1.77	1.77	1.77	36	1.12	1.12	1.12	-1.16	1.14	1.14	1.14	0.52
	5290	1	1.56	1.56	1.56	36	0.98	0.98	0.98	-1.63	1	1	1	0.46
	5320	0.97	1.52	1.52	1.52	36	0.94	0.94	0.94	-3.07	0.96	0.96	0.96	-0.62
	5350	1.01	1.58	1.58	1.58	36	0.99	0.99	0.99	-2.21	1.01	1.01	1.01	0.03
	5470	0.74	1.16	1.16	1.16	36	0.72	0.72	0.72	-3.49	0.74	0.74	0.74	0.28
	5550	0.62	0.97	0.97	0.97	36	0.59	0.59	0.59	-4.34	0.62	0.62	0.62	0.46

Appendix D: Well Sections
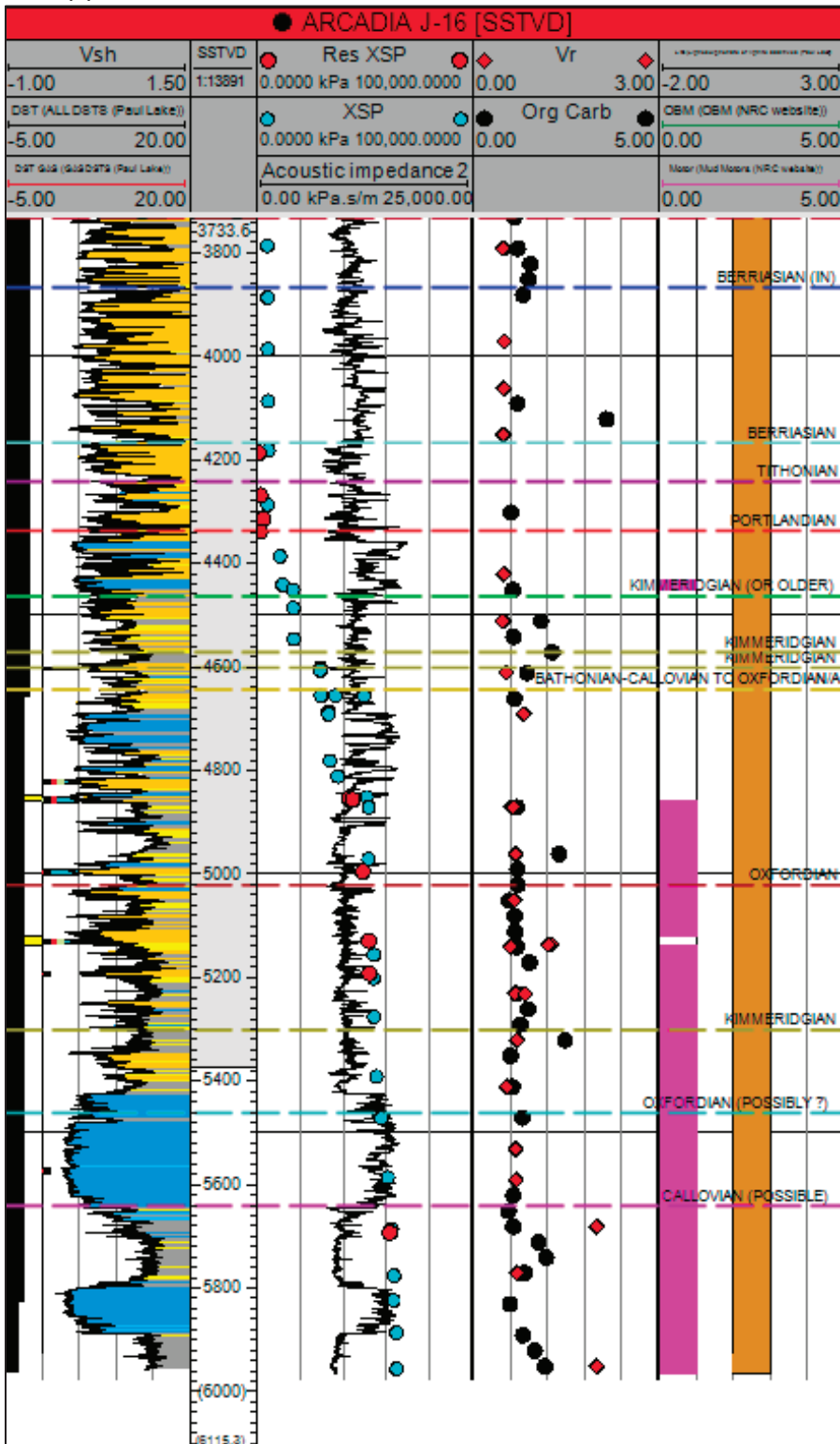
Figure D-1: Arcadia J-16 well section of the Jurassic interval.
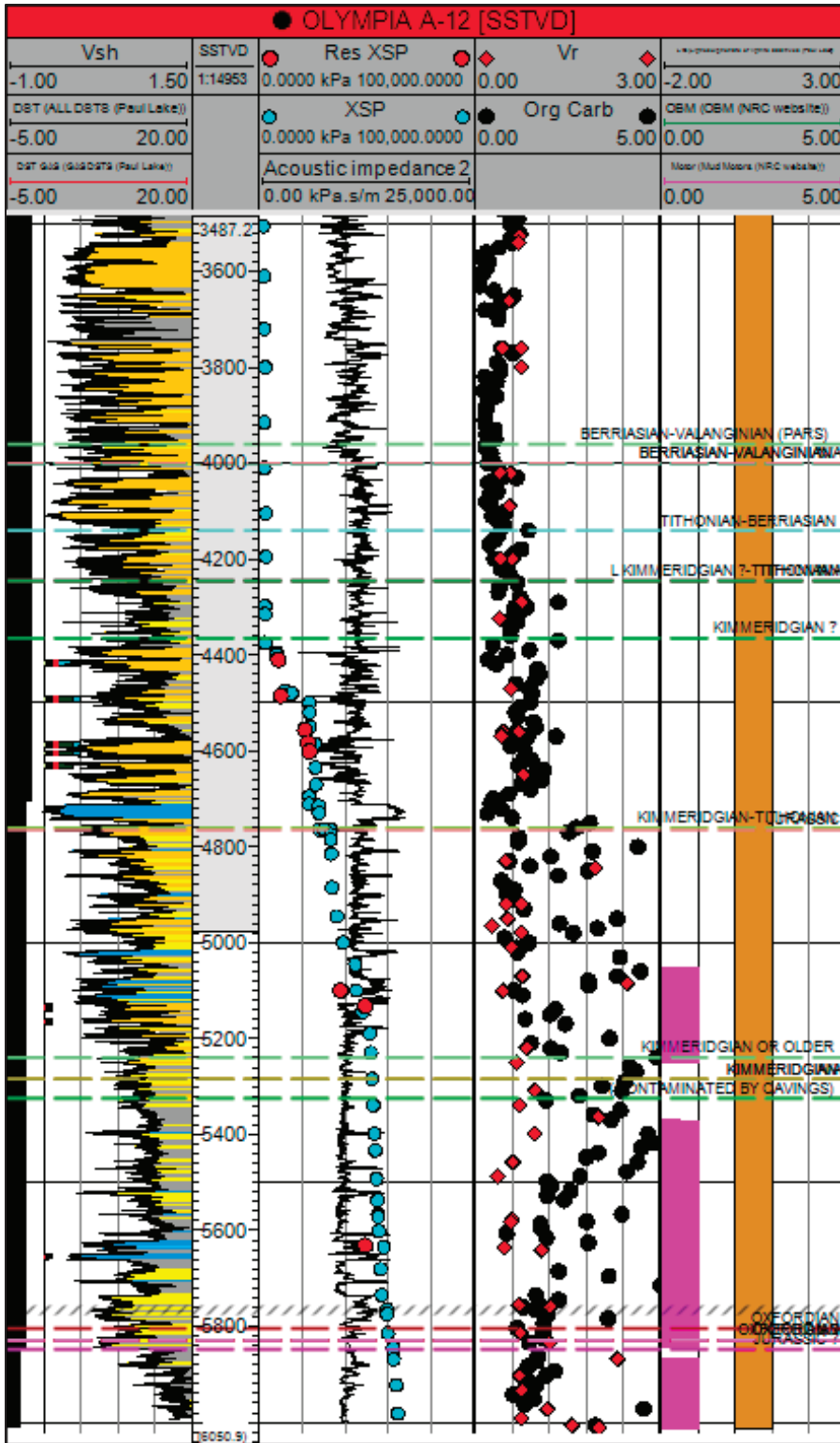
Figure D-2: Olympia A-12 well section of the Jurassic interval.
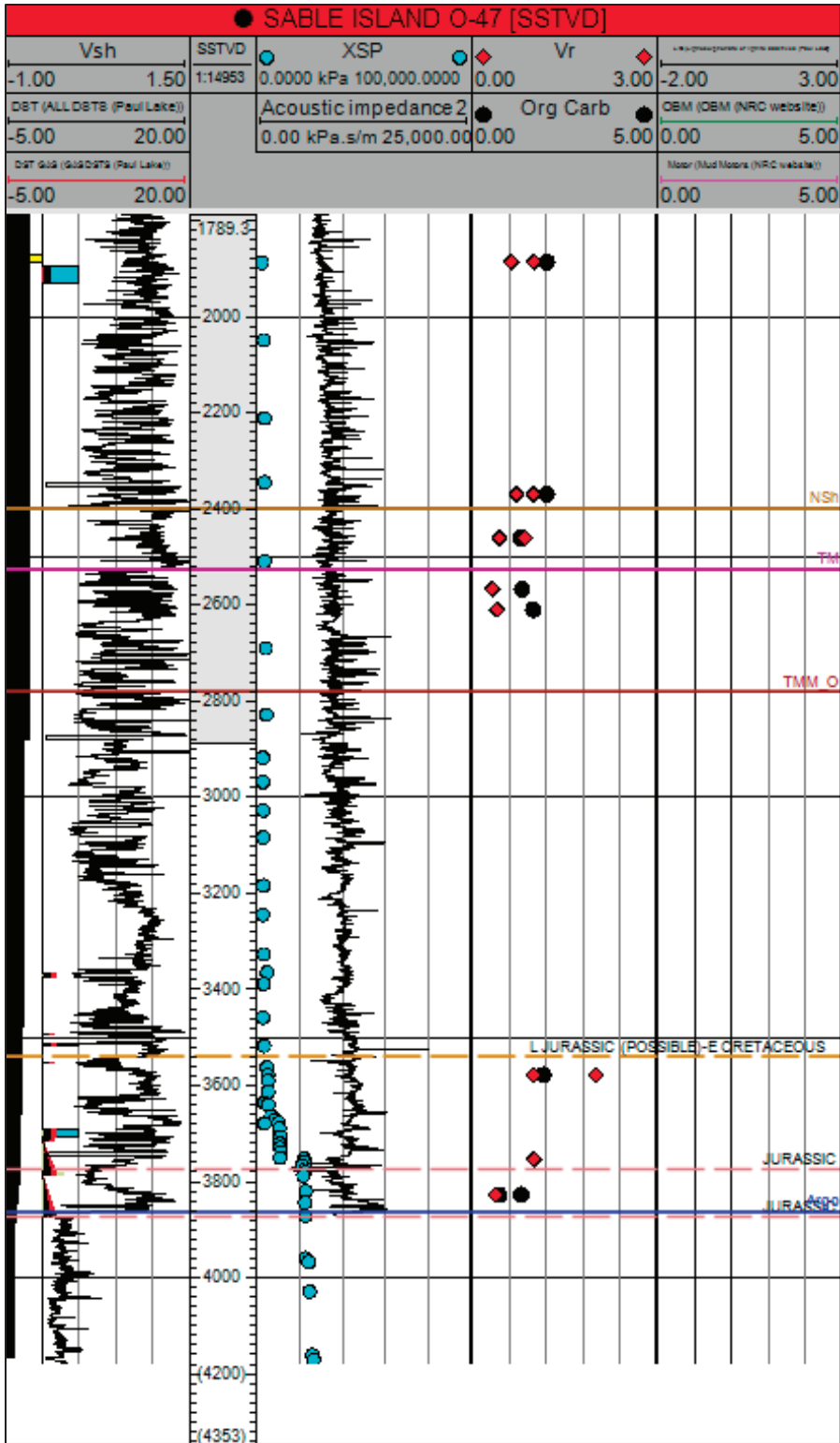
Figure D-3: Sable Island O-47 well section of the Jurassic interval.
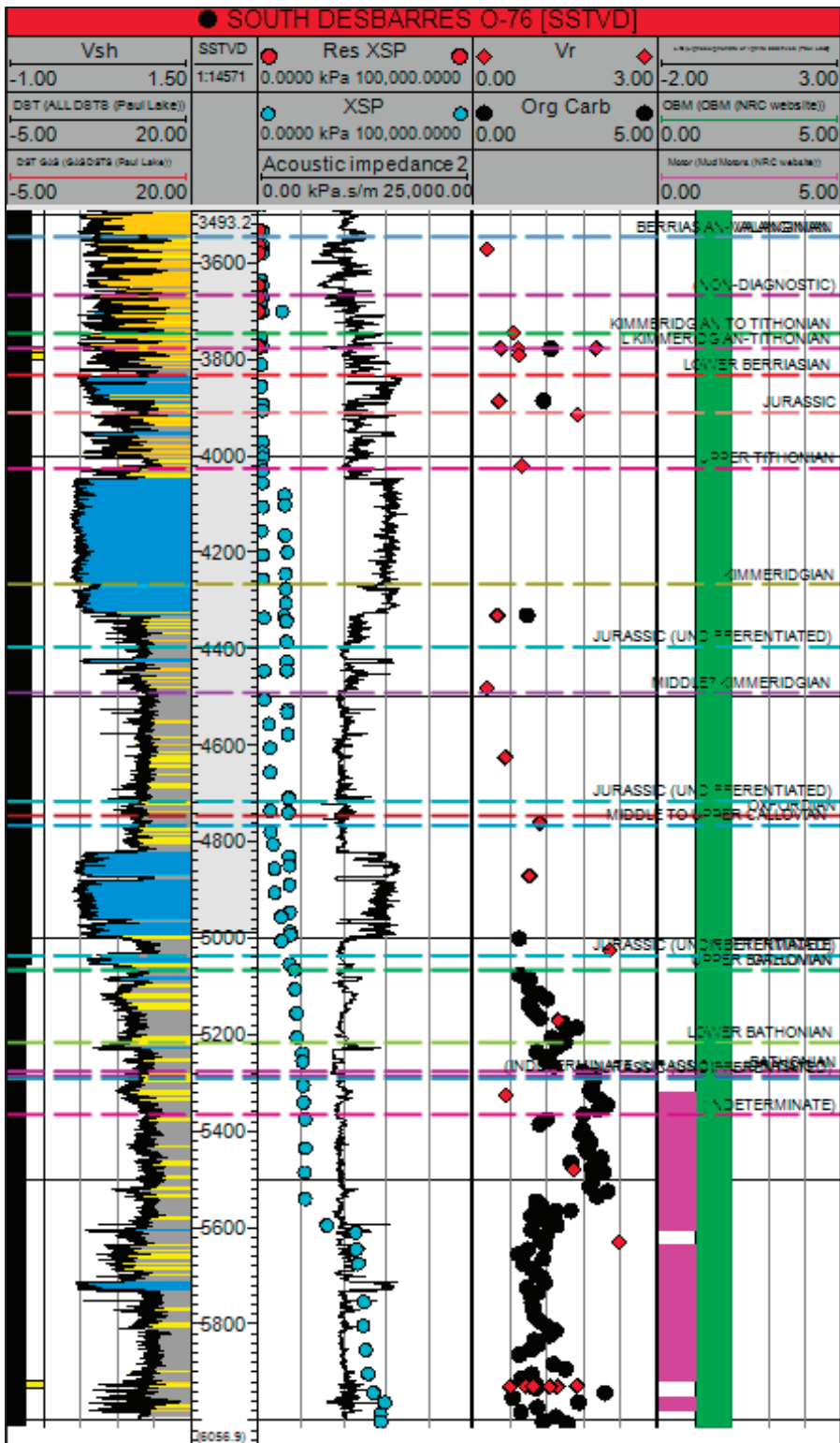
Figure D-4: South DesBarres O-76 well section of the Jurassic interval.
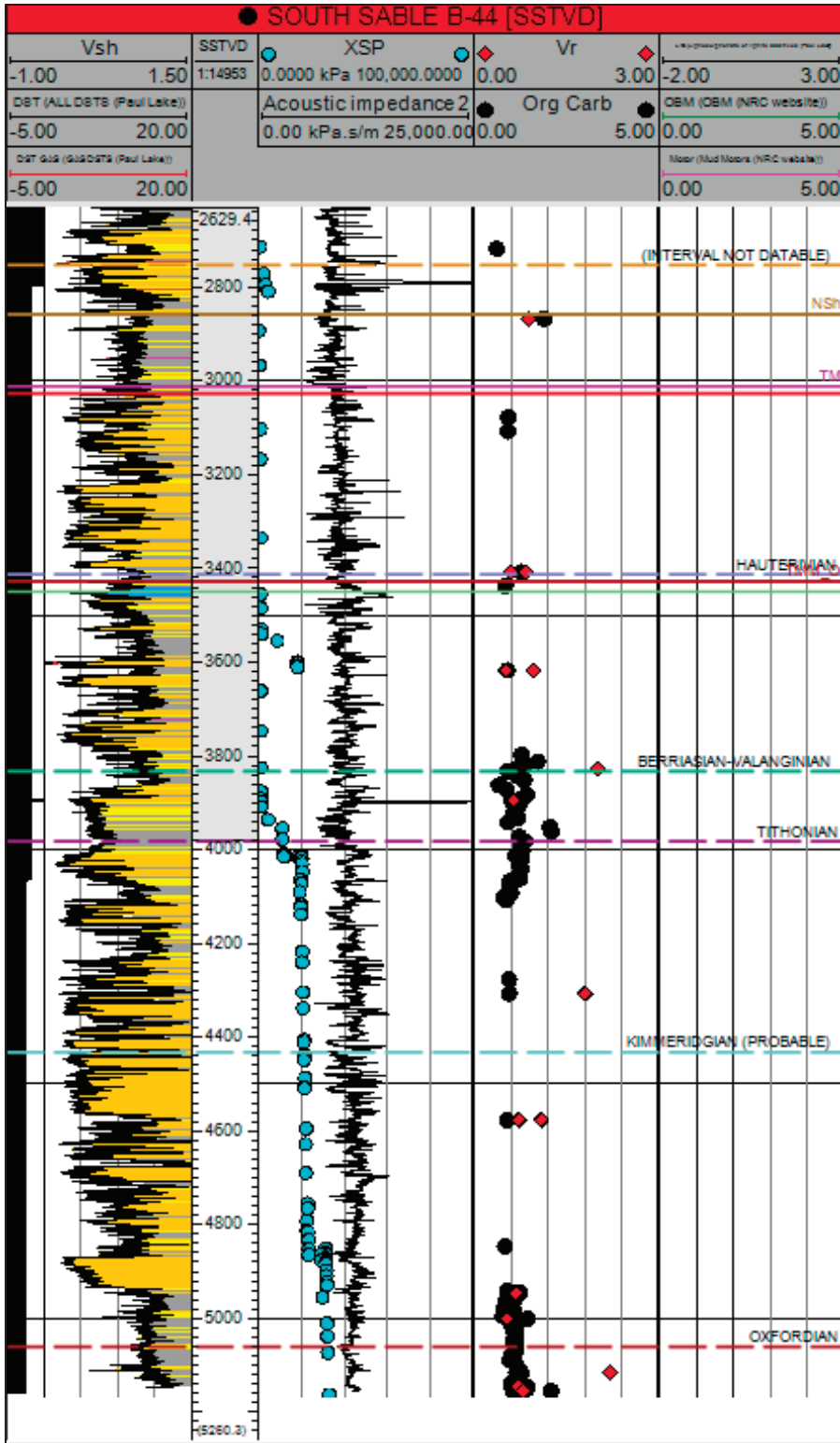
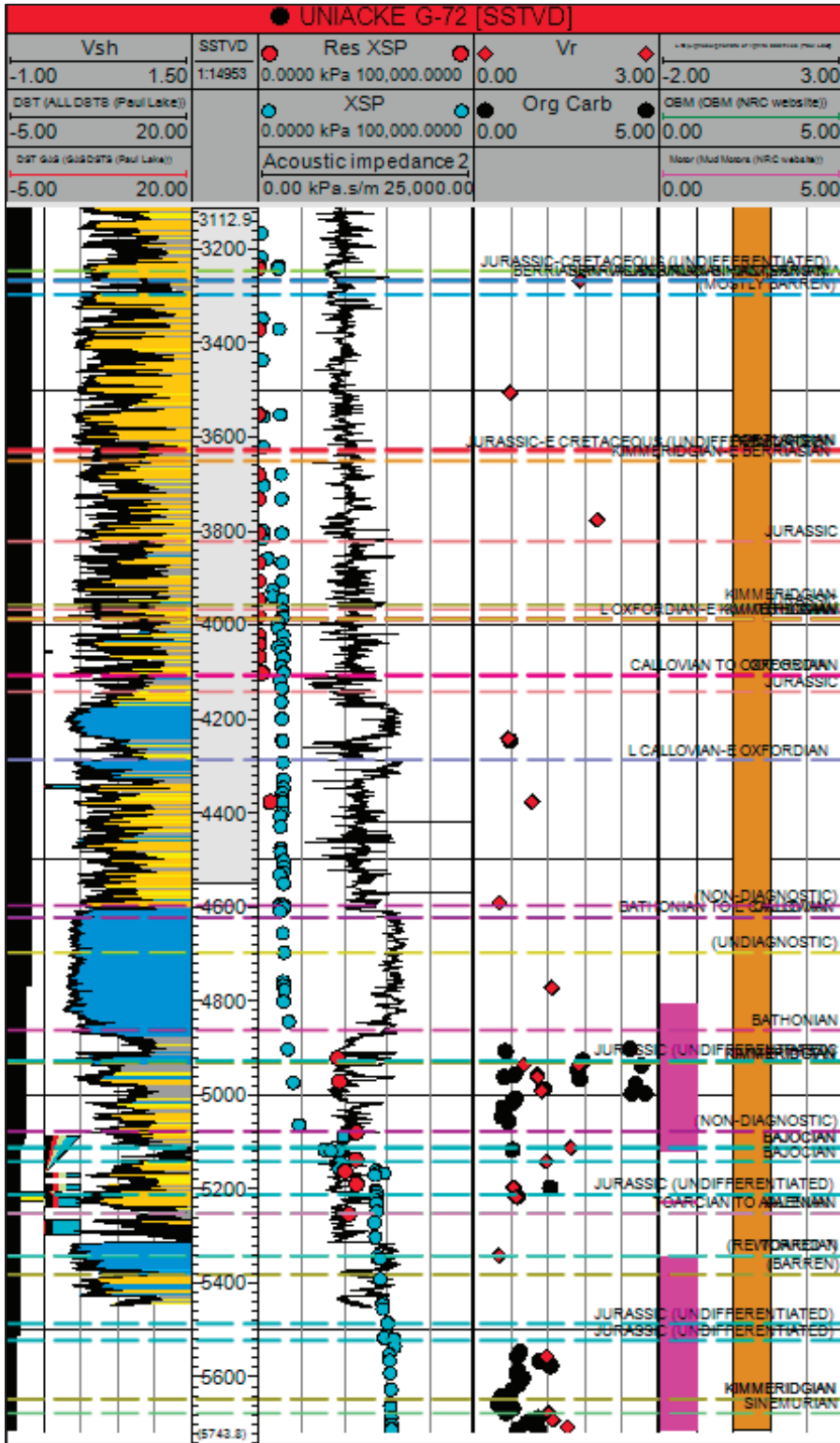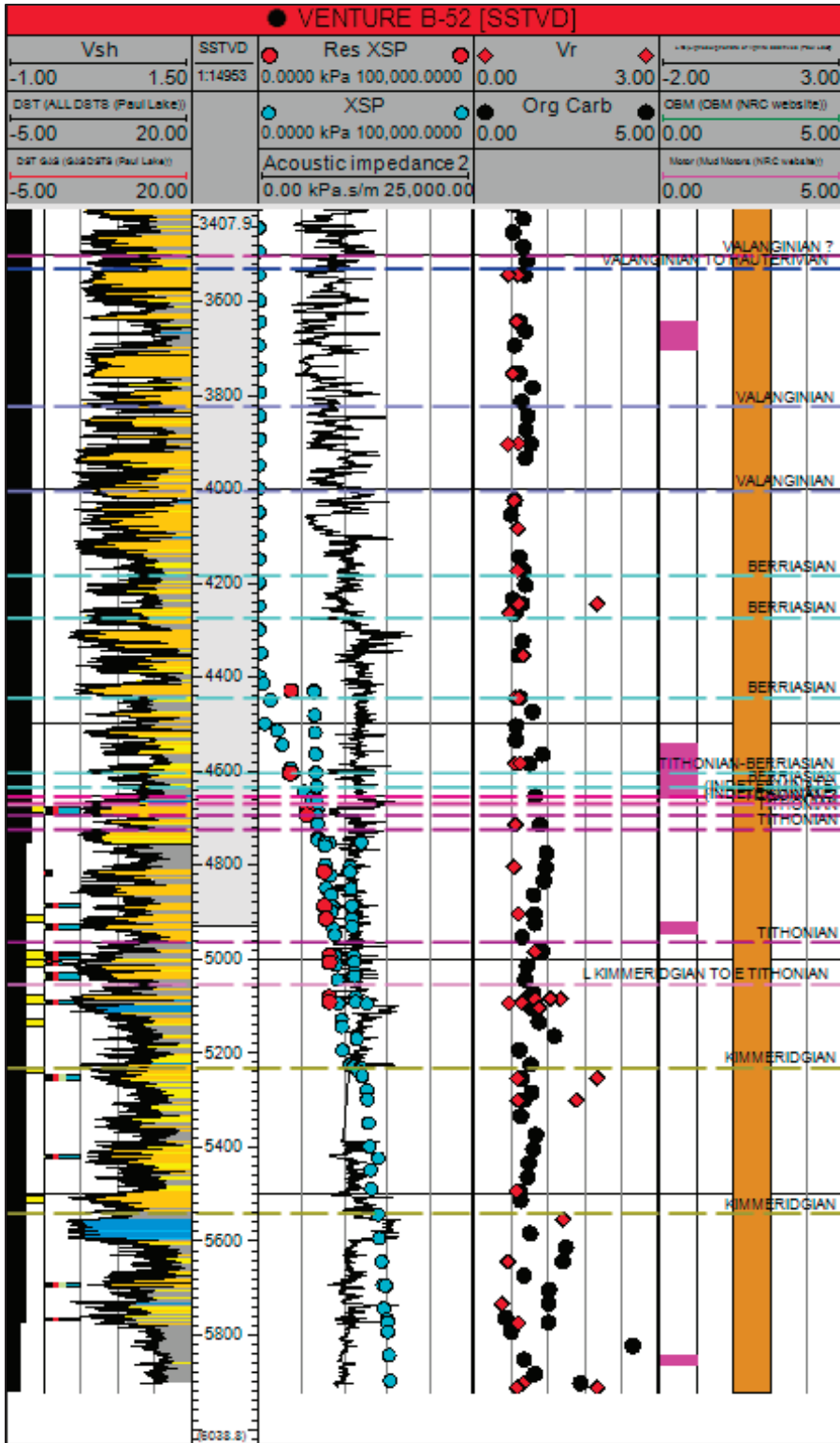*Figure D-5: South Sable B-44 well section of the Jurassic interval.*

Figure D-6: South Venture O-59 well section of the Jurassic interval.

Figure D-7: Uniacke G-72 well section of the Jurassic interval.
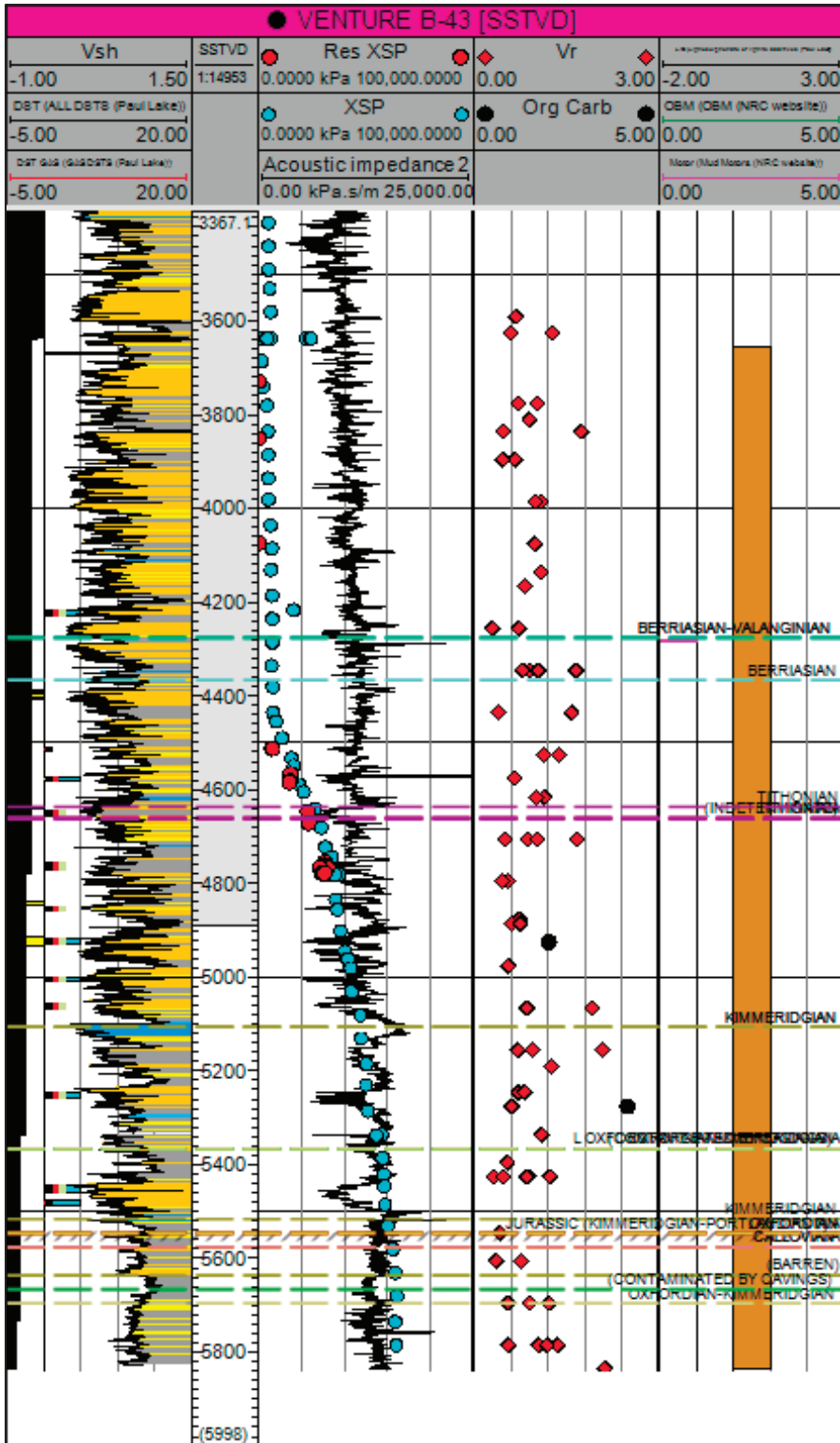
Figure D-8: Venture B-43 well section of the Jurassic interval.

Figure D-9: Venture B-52 well section of the Jurassic interval.
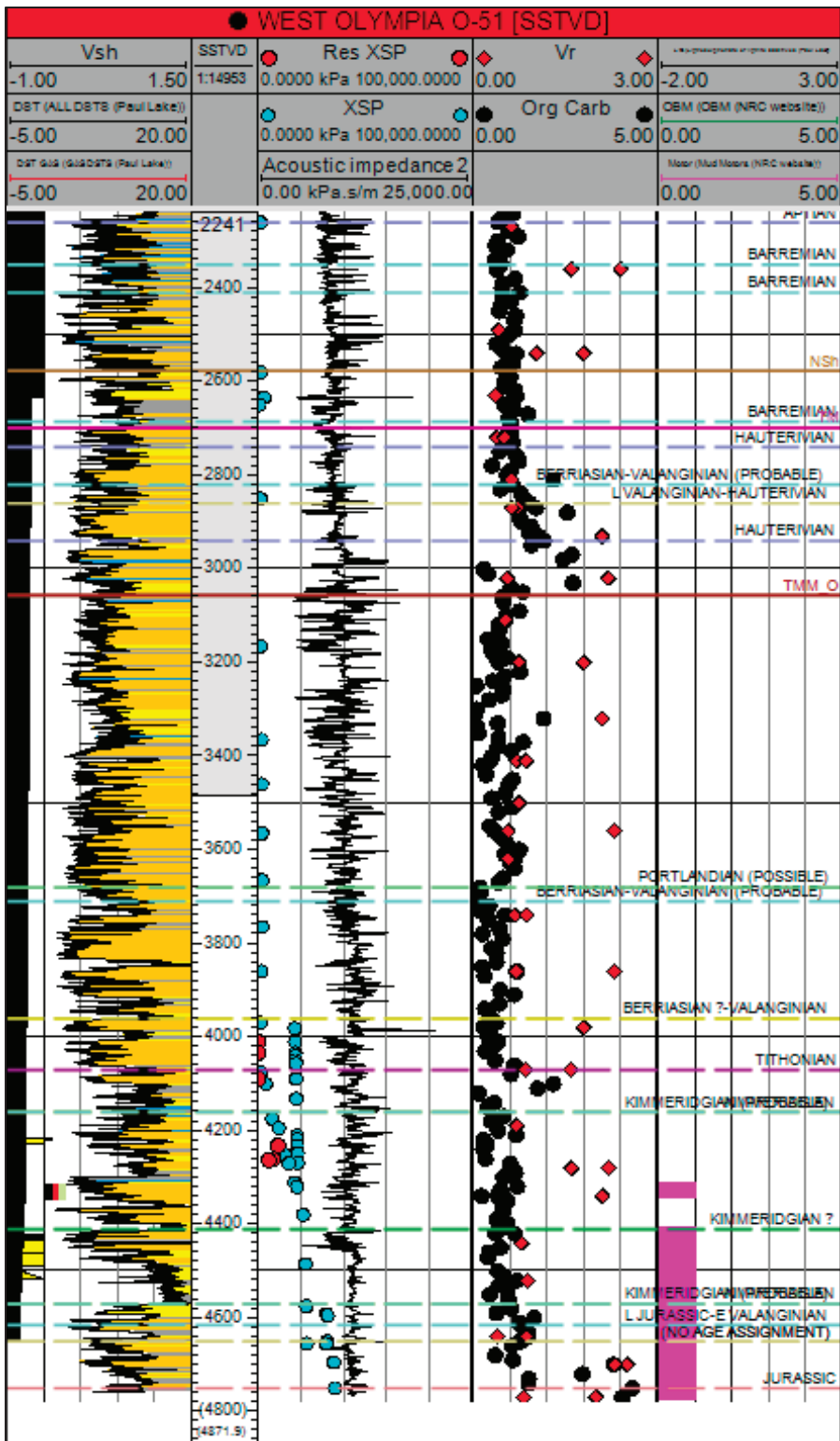
Figure D-10: West Olympia O-51 well section of the Jurassic interval.
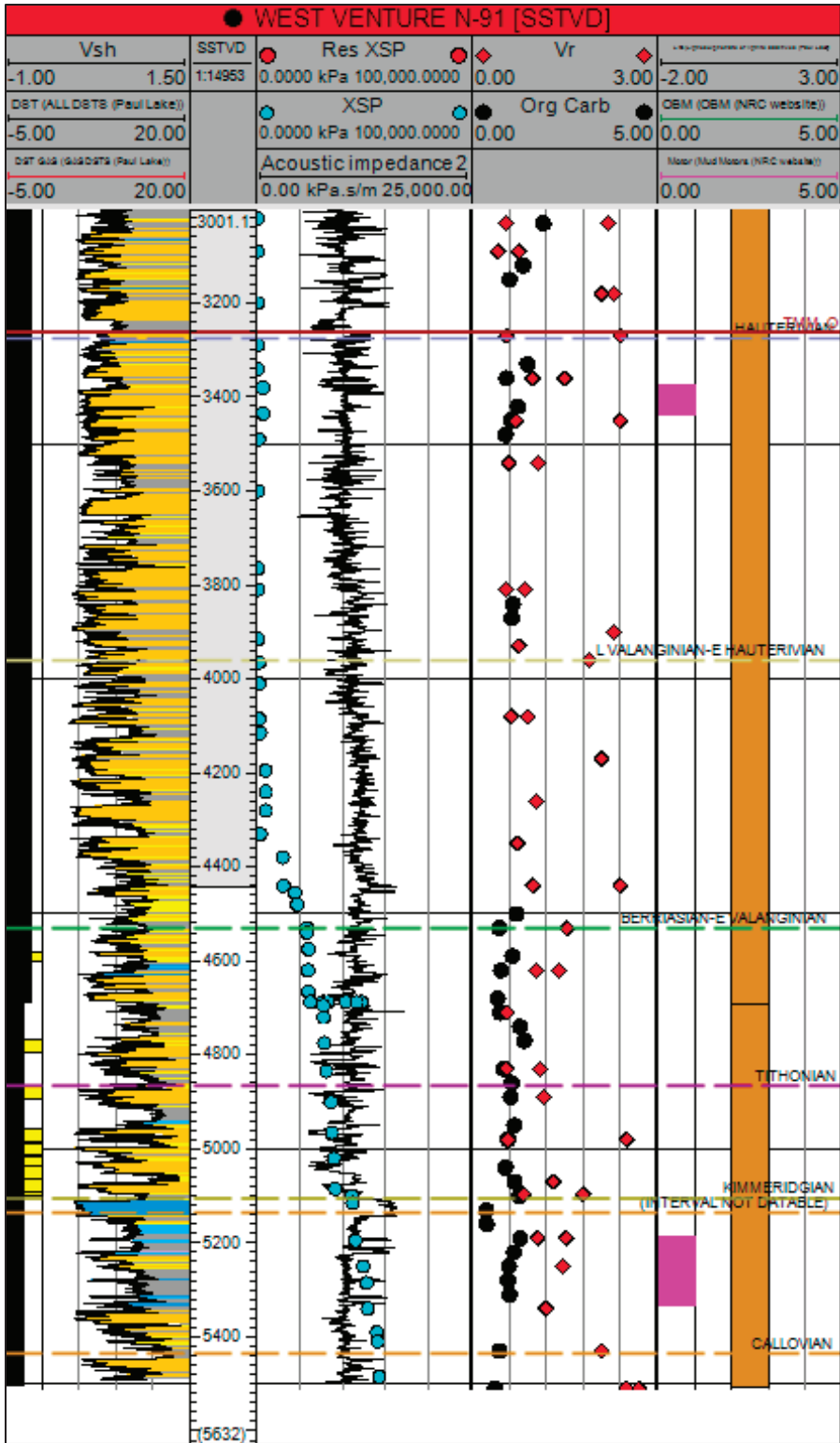
Figure D-11: West Venture N-91 well section of the Jurassic interval.

Appendix E: Seismic Transects
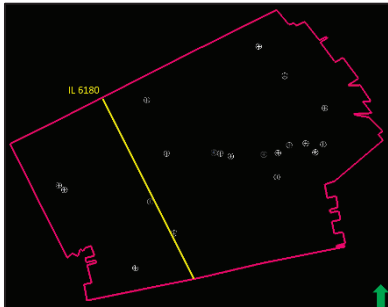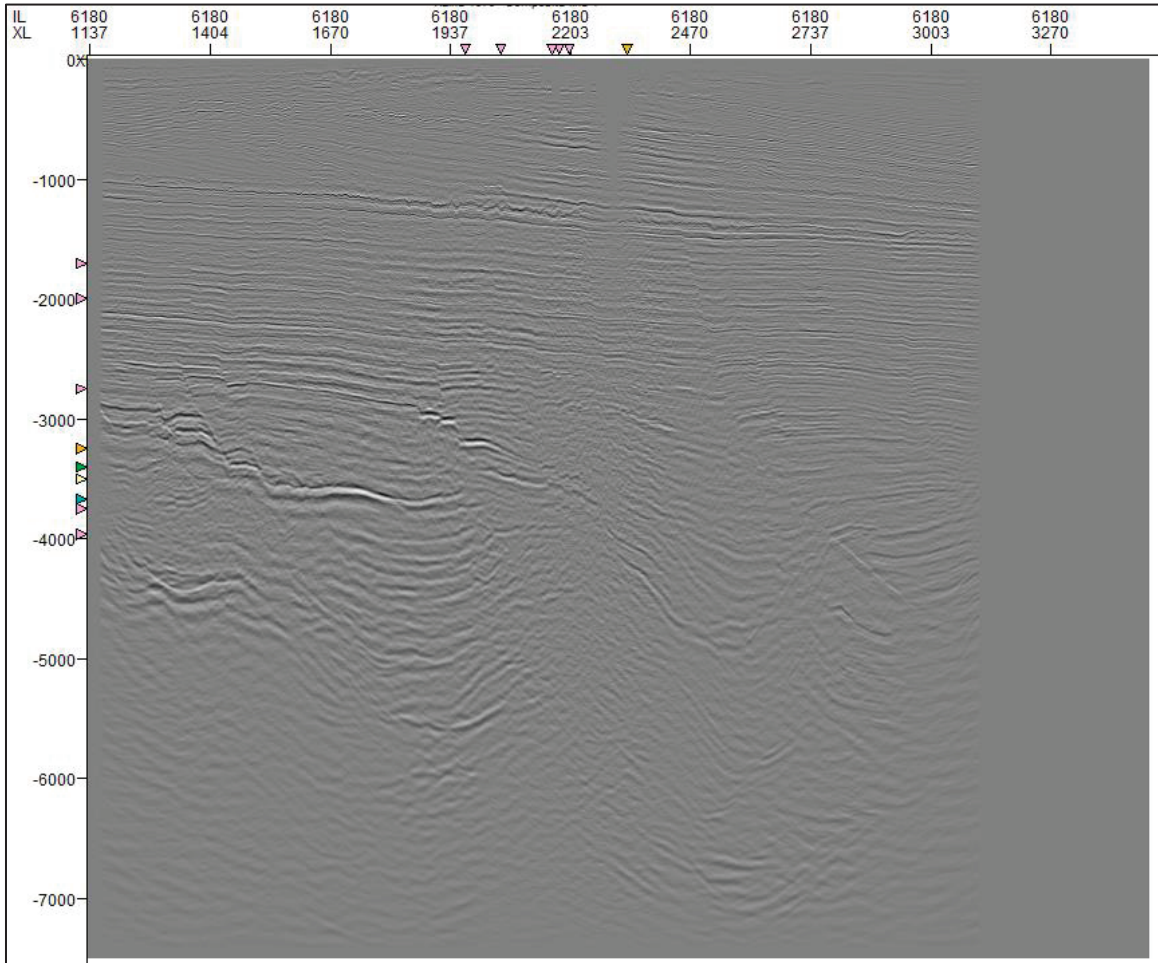
Figure E-1: Seismic transect from A to A' (5X vertical exaggeration) of the uninterpreted seismic data along IL 6180.
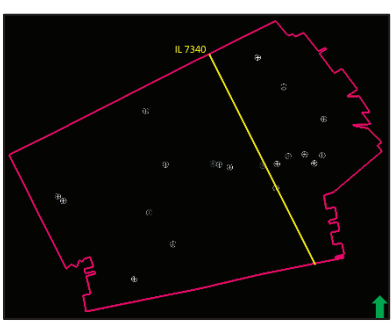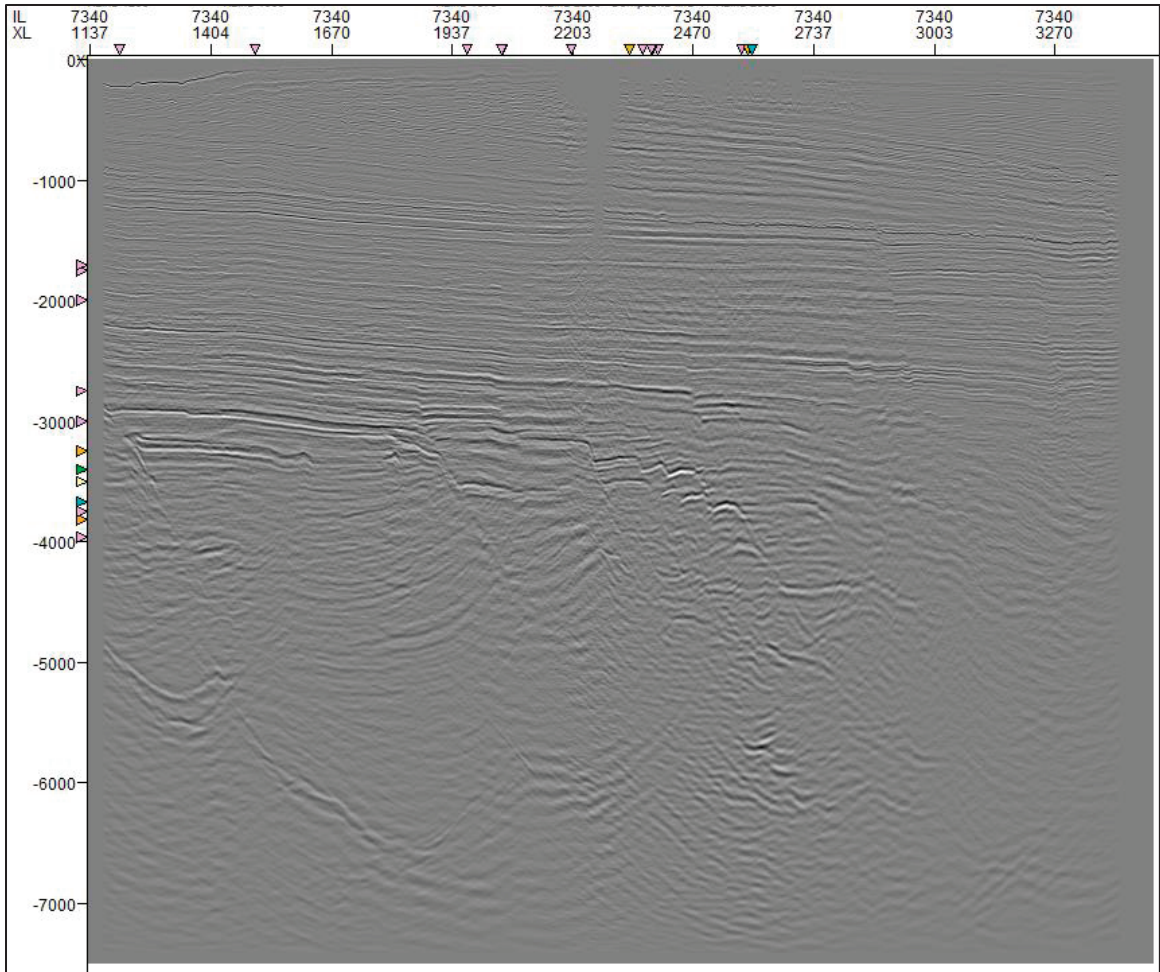
Figure E-2: Seismic transect from A to A' (5X vertical exaggeration) of the uninterpreted seismic data along IL 7340.
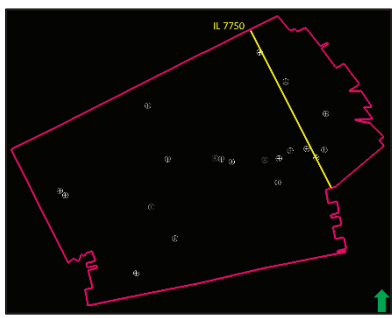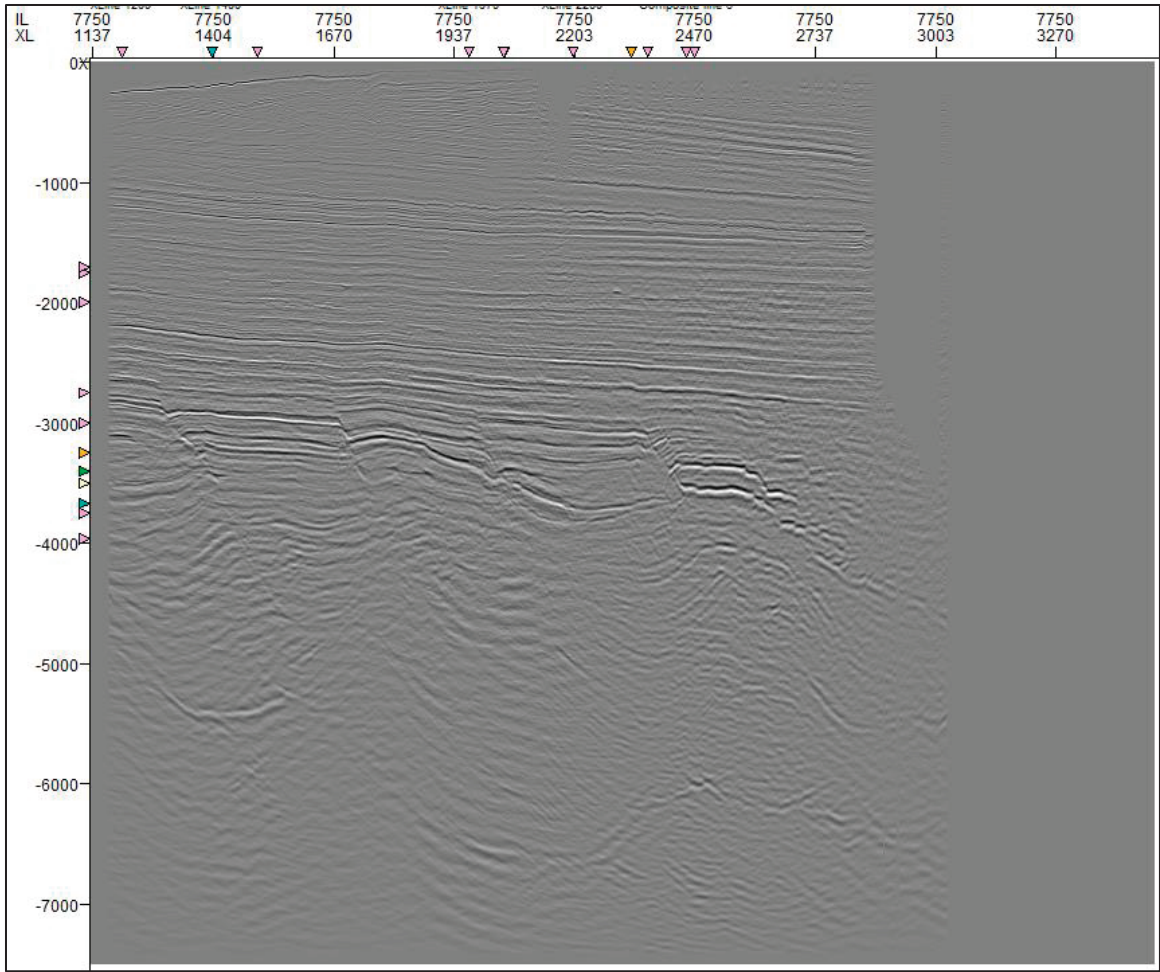
Figure E-3: Seismic transect from A to A' (5X vertical exaggeration) of the uninterpreted seismic data along IL 7750.
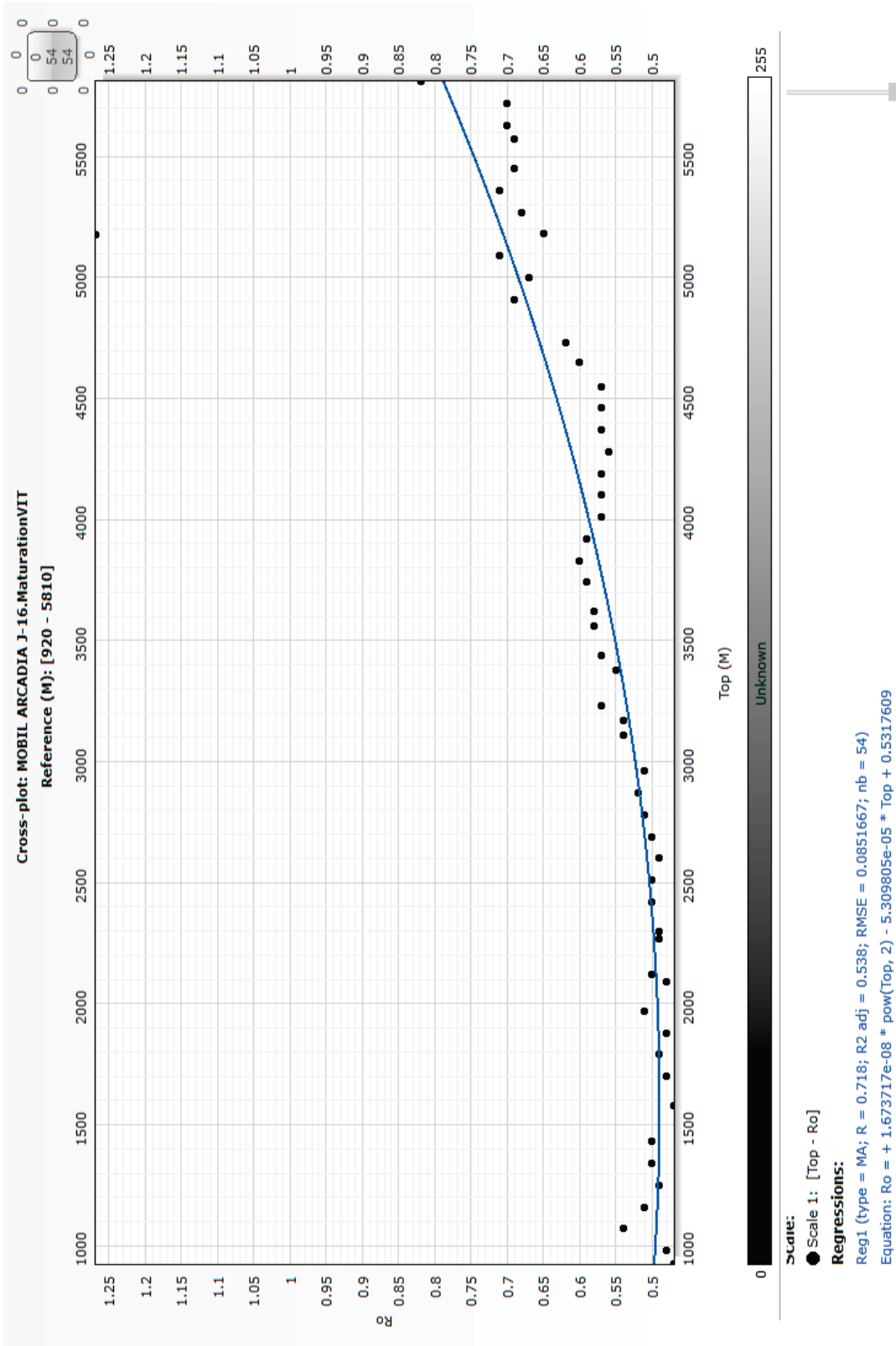
Figure F-1: Cross-plot of %Ro vs depth for Arcadia J-16 with corresponding regression equation.
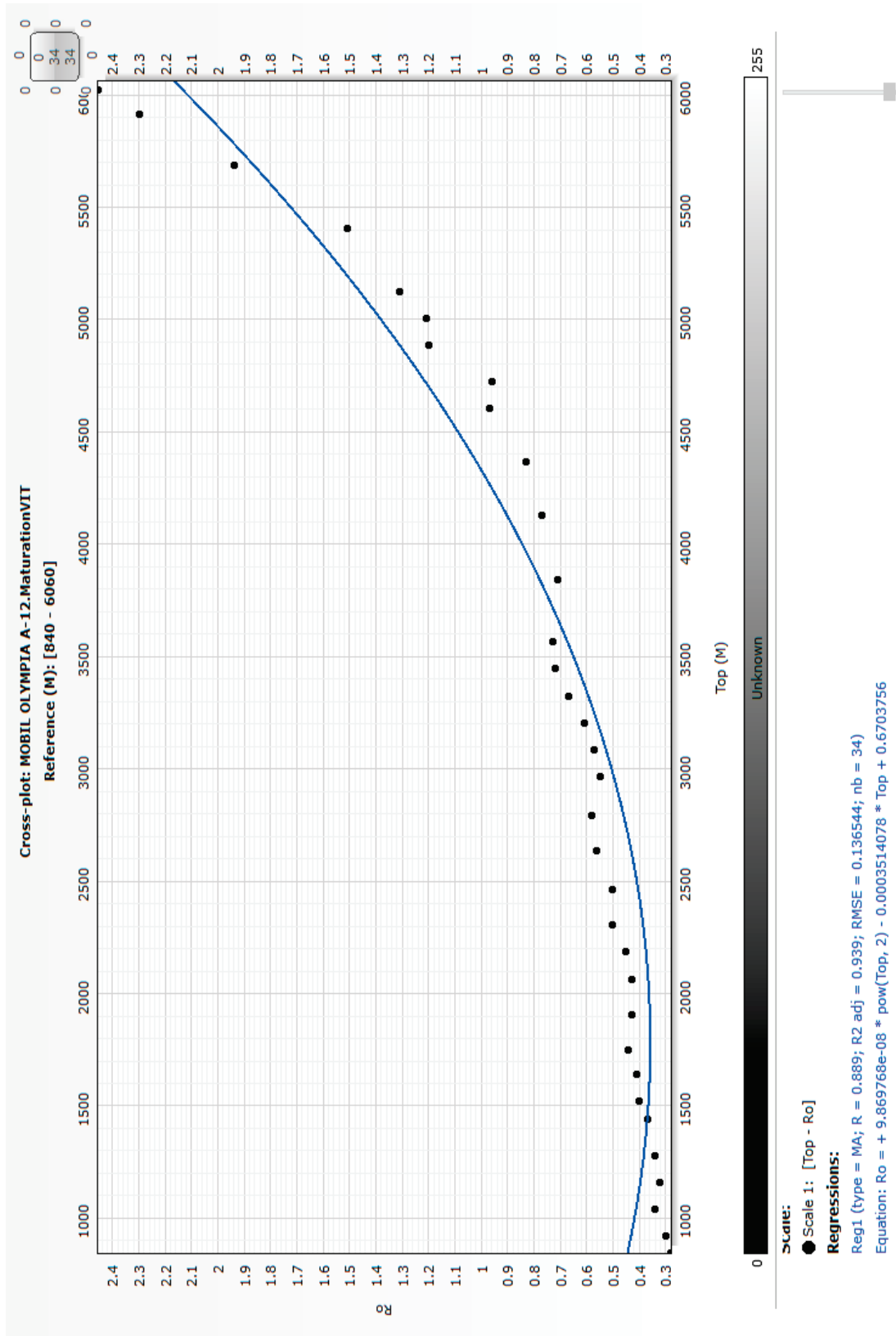
Figure F-2: Cross-plot of %Ro vs depth for Olympia A-12 with corresponding regression equation.
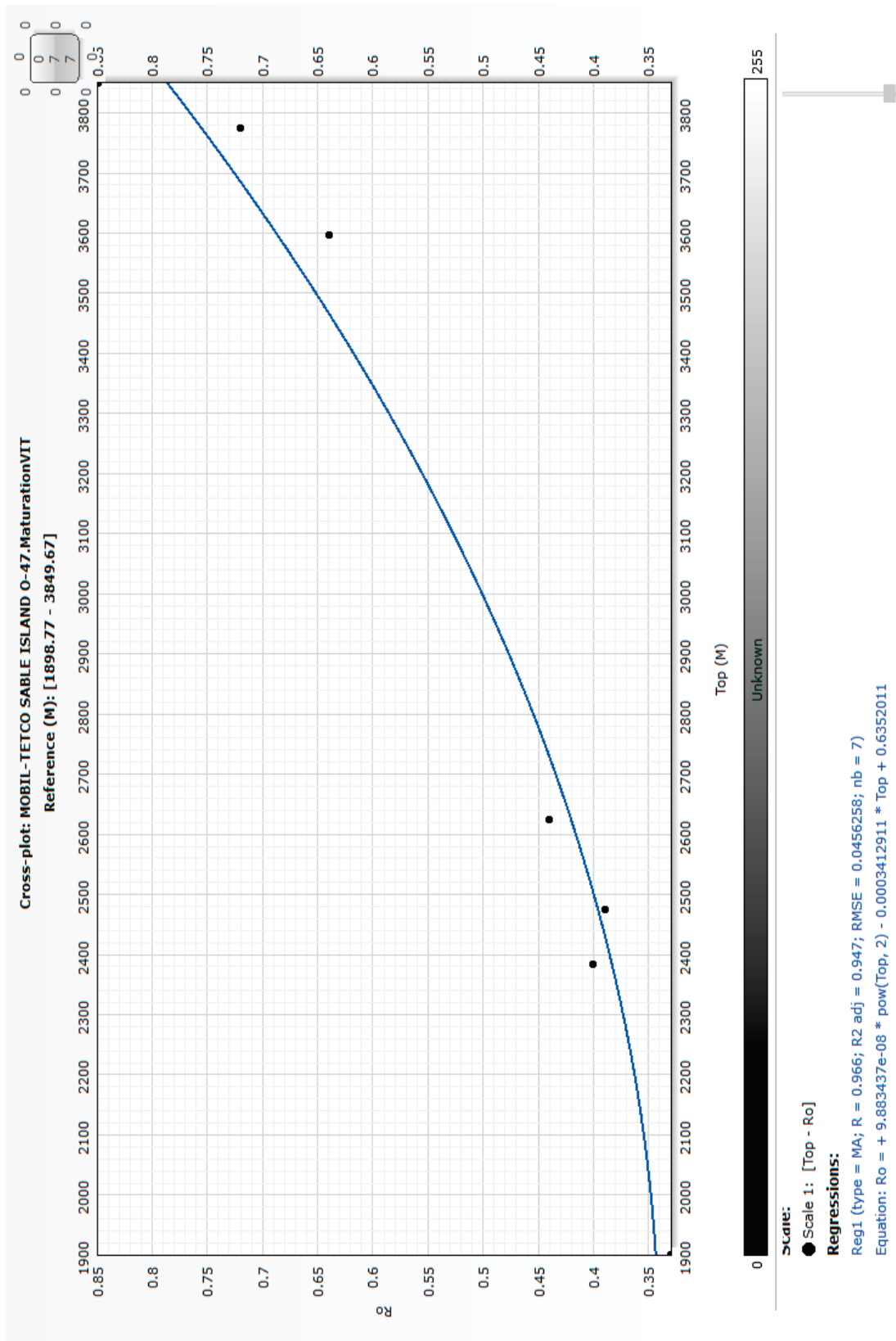
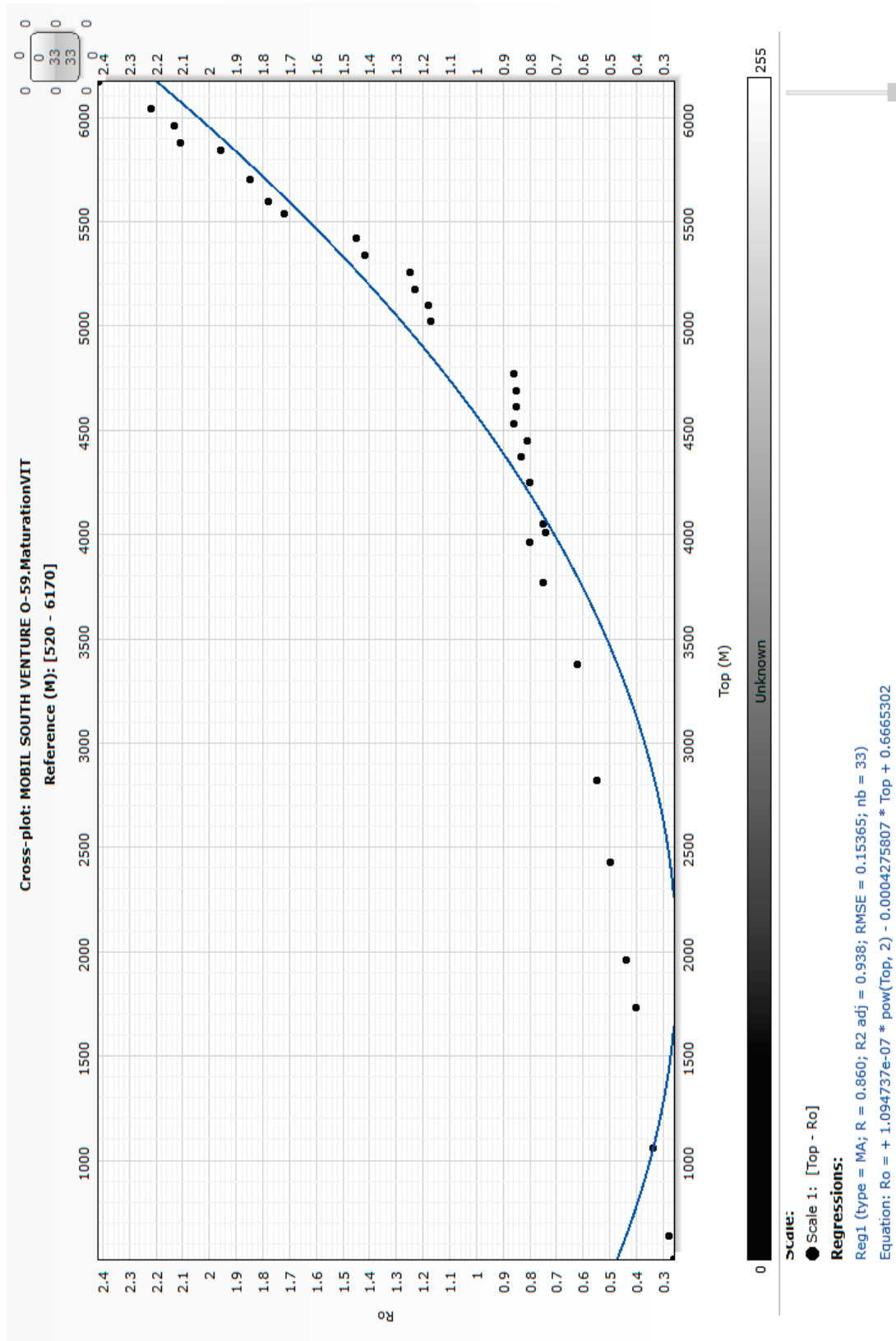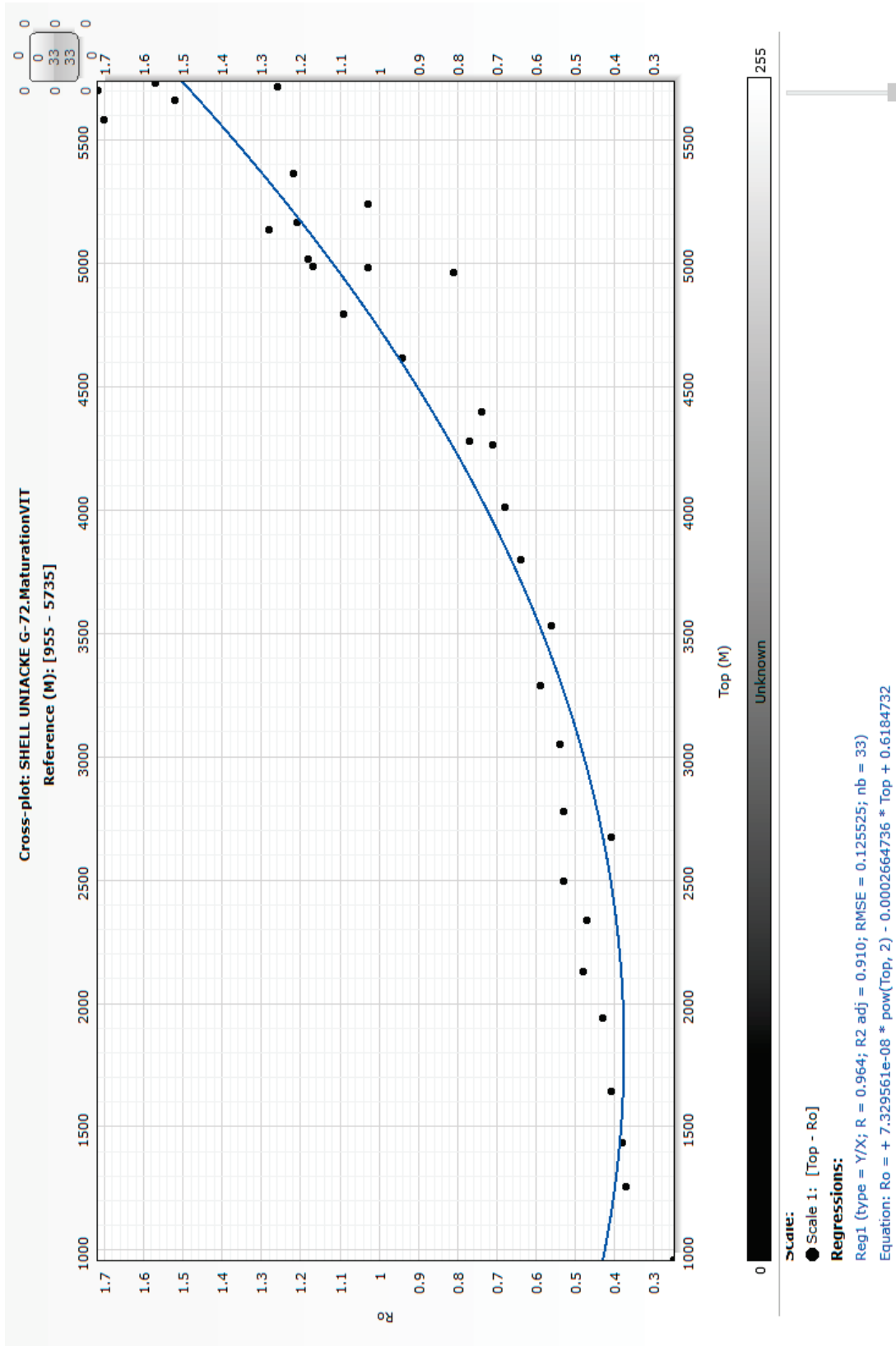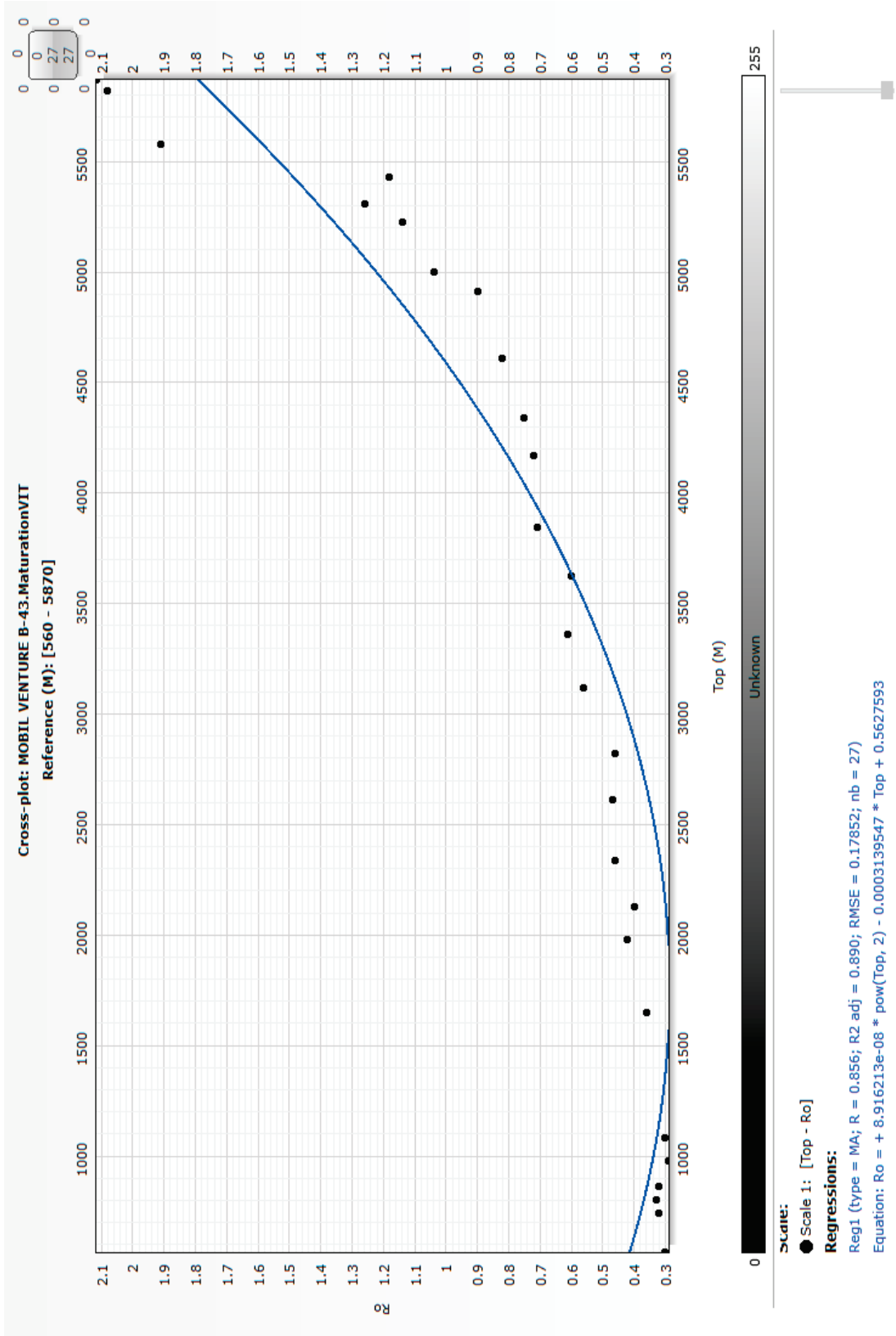*Figure F-3: Cross-plot of %Ro vs depth for Sable Island O-47 with corresponding regression equation.*

Cross-plot: SOUTH DESBARRES O-76.MaturationVIT
Reference (M): [895 - 5958]

Scale:
● Scale 1: [Top - Ro]

Regressions:
Reg1 (type = MA; R = 0.910; R2 adj = 0.942; RMSE = 0.138159; nb = 40)
Equation: Ro = + 8.649106e-08 * pow(Top, 2) - 0.0002819618 * Top + 0.523359
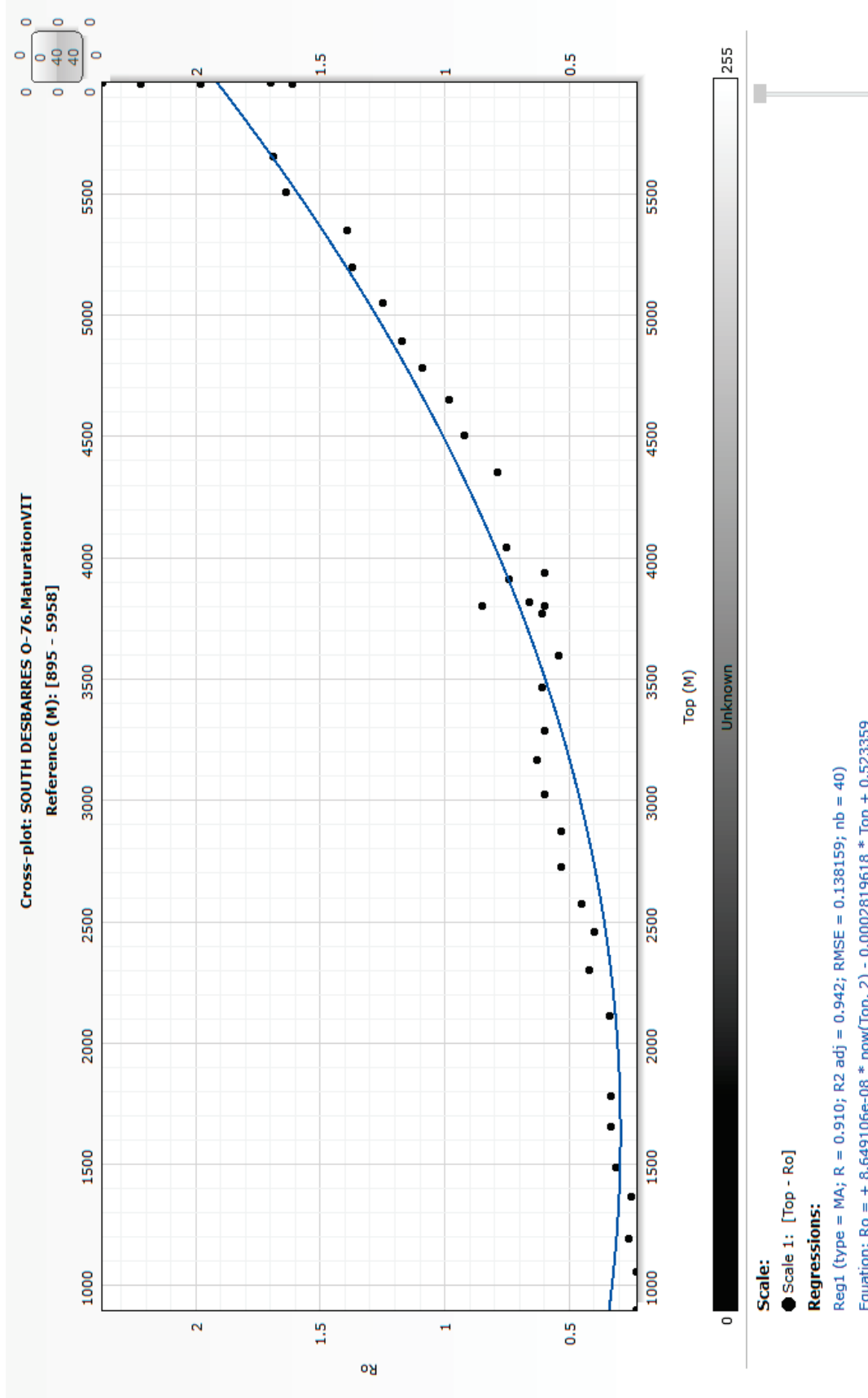
Figure F-4: Cross-plot of %Ro vs depth for South DesBarres O-76 with corresponding regression equation.
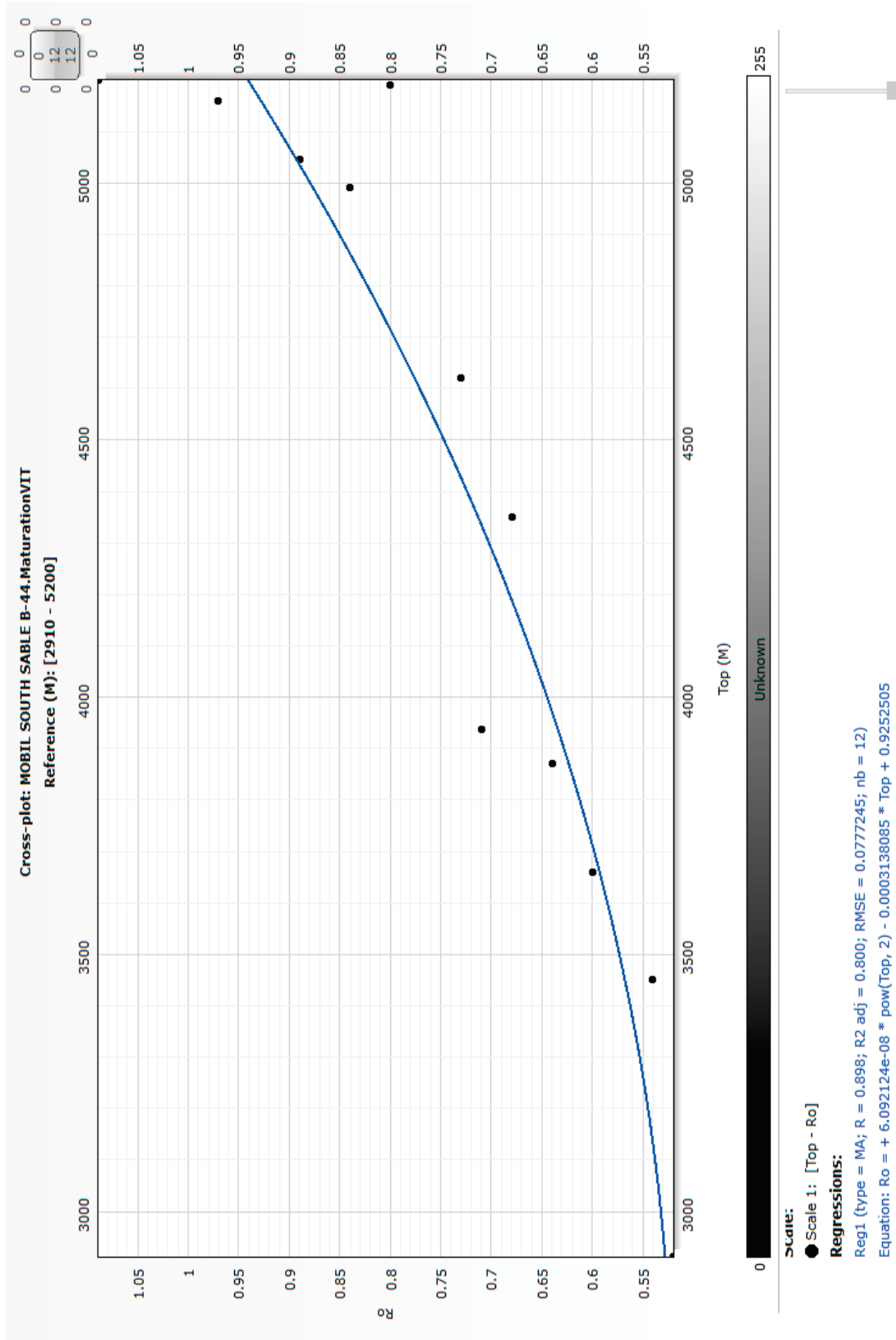
Figure F-5: Cross-plot of %Ro vs depth for South Sable B-44 with corresponding regression equation.

Cross-plot: MOBIL SOUTH VENTURE O-59.MaturationVIT

Reference (M): [520 - 6170]

Scale:
● Scale 1: [Top - Ro]

Regressions:
Reg1 (type = MA; R = 0.860; R2 adj = 0.938; RMSE = 0.15365; nb = 33)
Equation: Ro = + 1.094737e-07 * pow(Top, 2) - 0.0004275807 * Top + 0.6665302

Figure F-6: Cross-plot of %Ro vs depth for South Venture O-59 with corresponding regression equation.

Figure F-7: Cross-plot of %Ro vs depth for Uniacke G-72 with corresponding regression equation.

Figure F-8: Cross-plot of %Ro vs depth for Venture B-43 with corresponding regression equation.
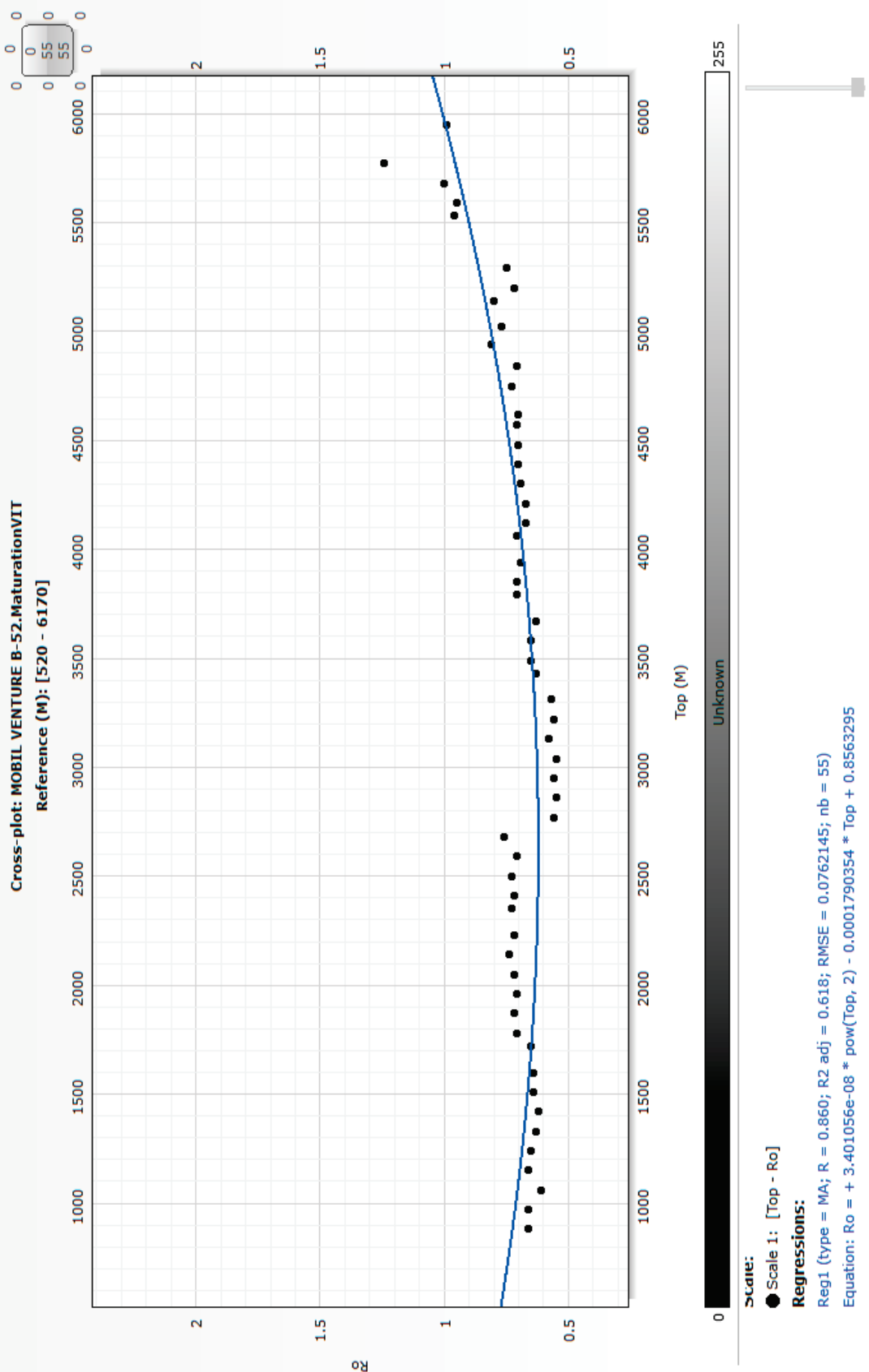
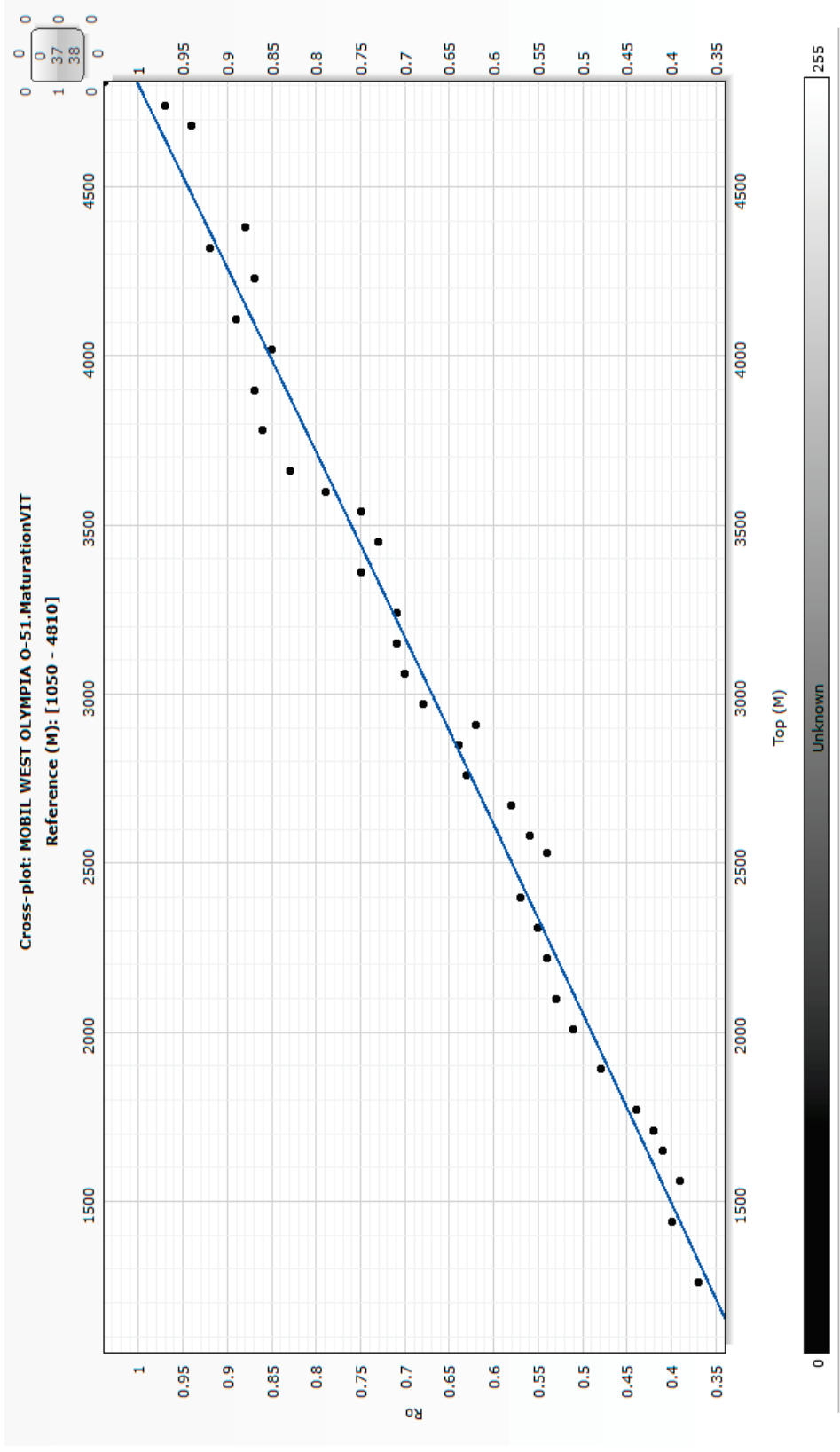Figure F-9: Cross-plot of %Ro vs depth for Venture B-52 with corresponding regression equation.

Figure F-10: Cross-plot of %Ro vs depth for West Olympia O-51 with corresponding regression equation.
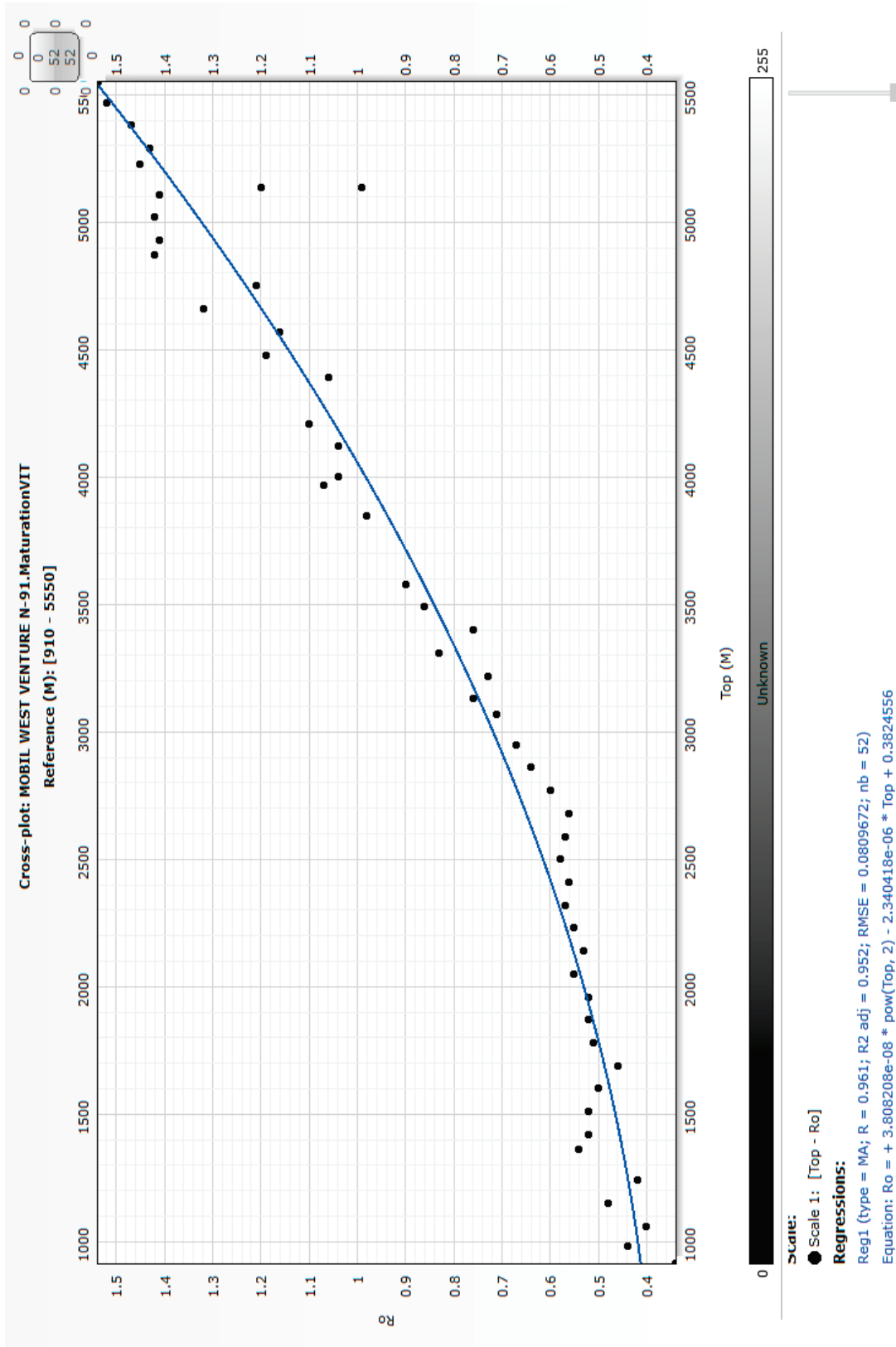
Figure F-11: Cross-plot of %Ro vs depth for West Venture N-91 with corresponding regression equation.

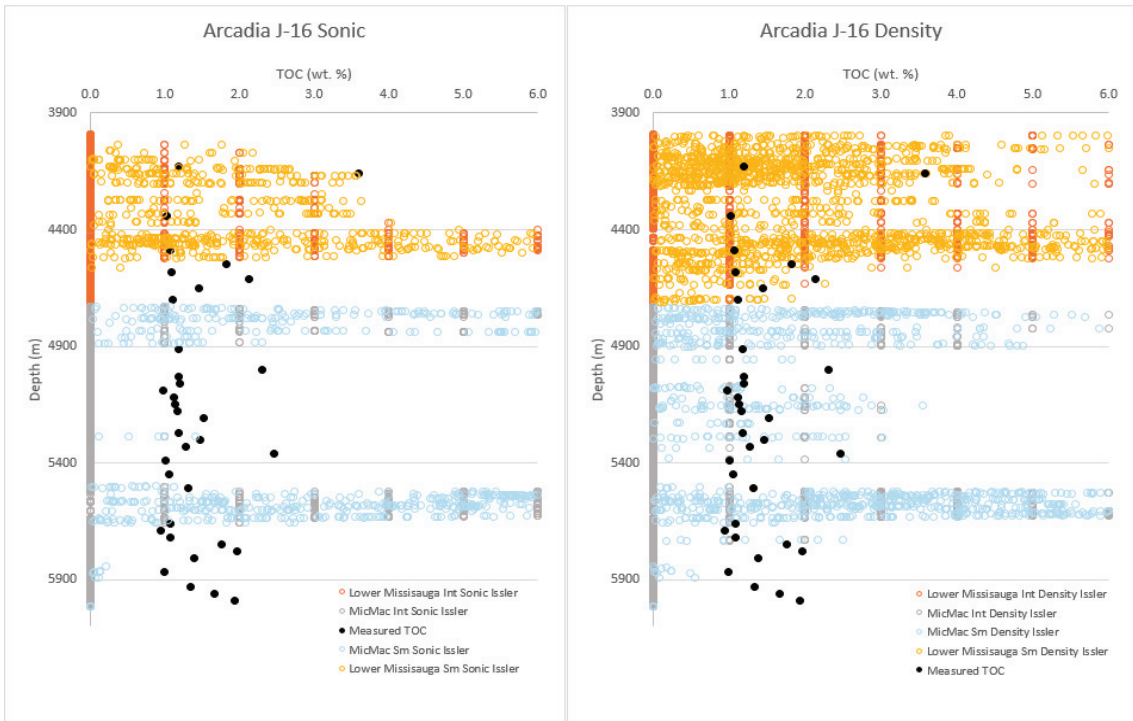## Appendix G: Issler Method Results

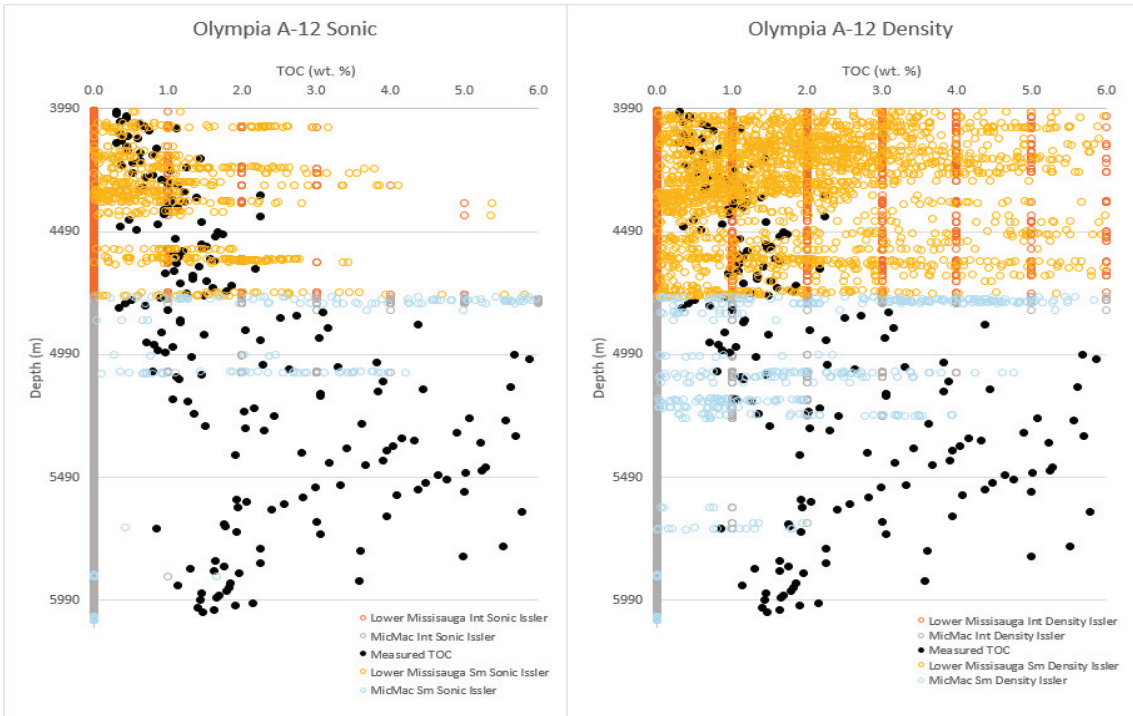*Figure F-1: Unaltered Issler Method results from Arcadia J-16.*

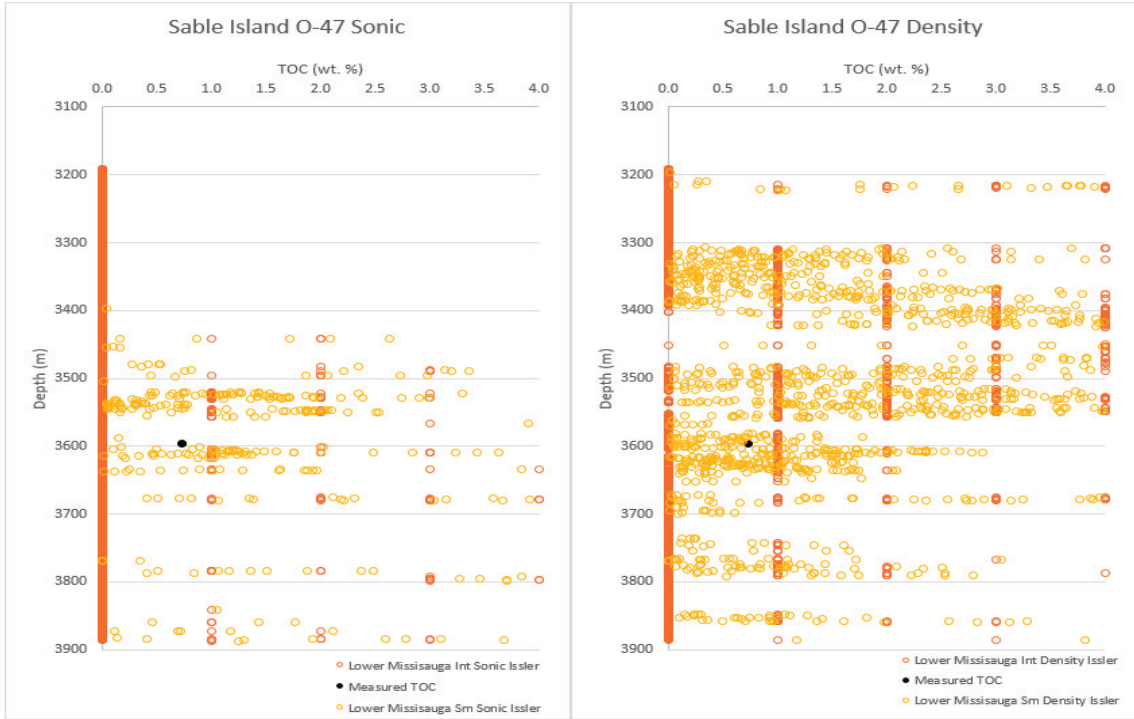*Figure G-2: Unaltered Issler Method results from Olympia A-12.*

Figure G-3: Unaltered Issler Method results from Sable Island O-47.
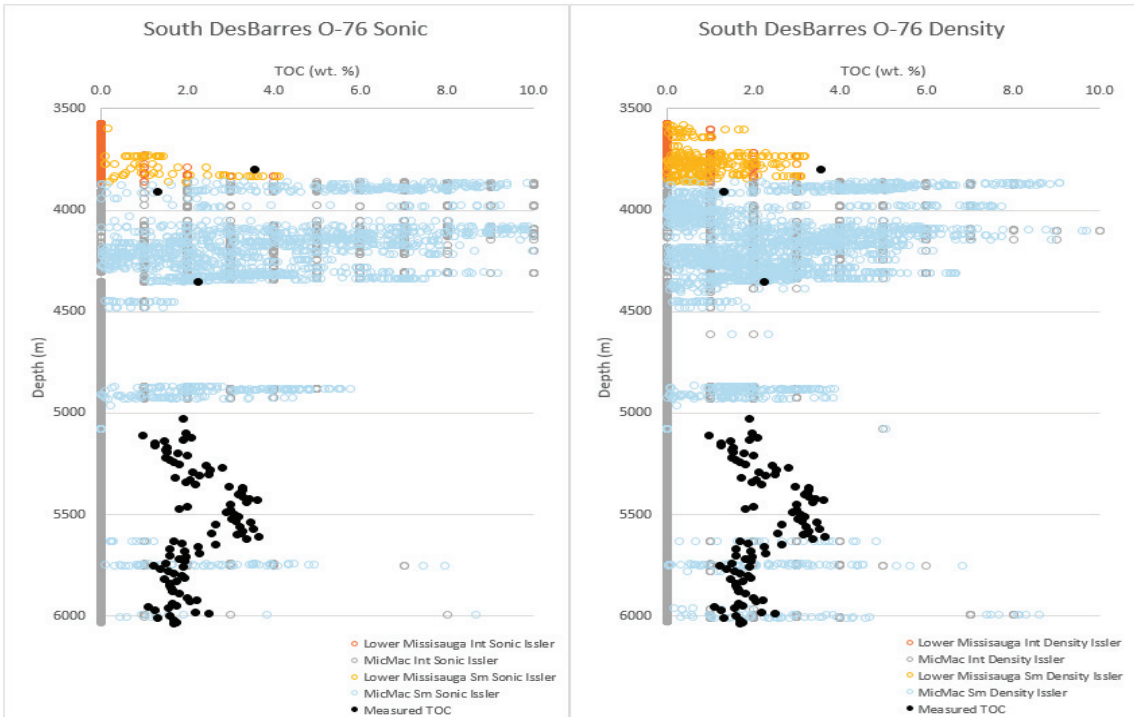

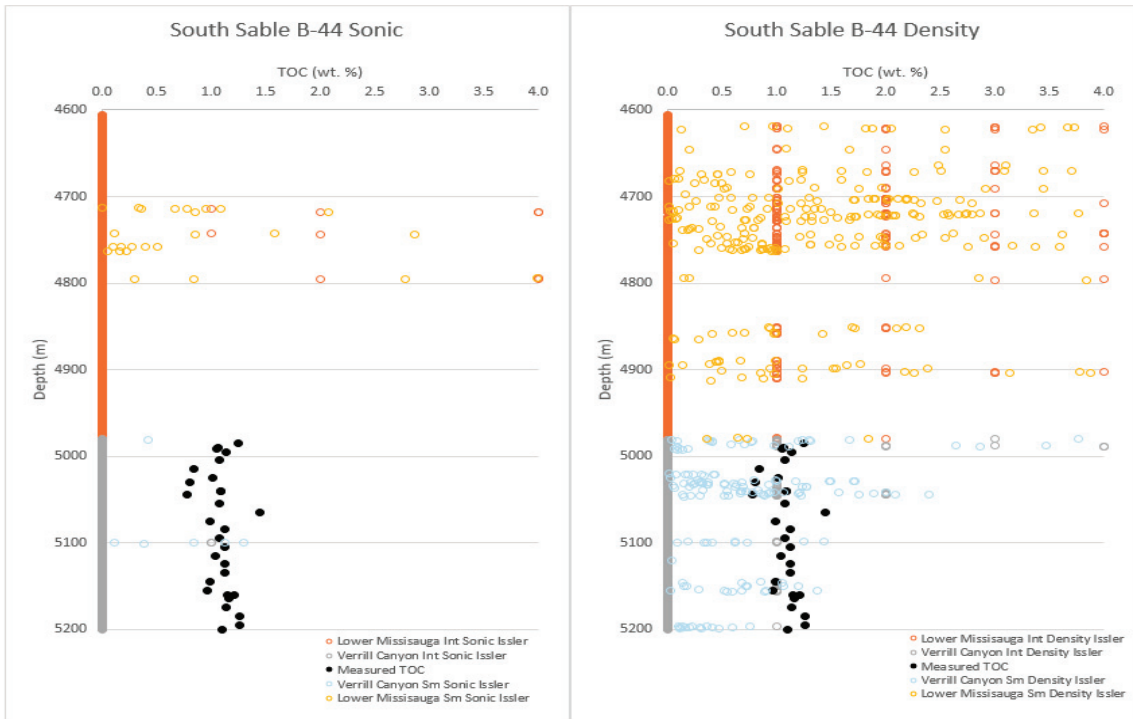*Figure G-4: Unaltered Issler Method results from South DesBarres O-76.*

Figure G-5: Unaltered Issler Method results from South Sable B-44.

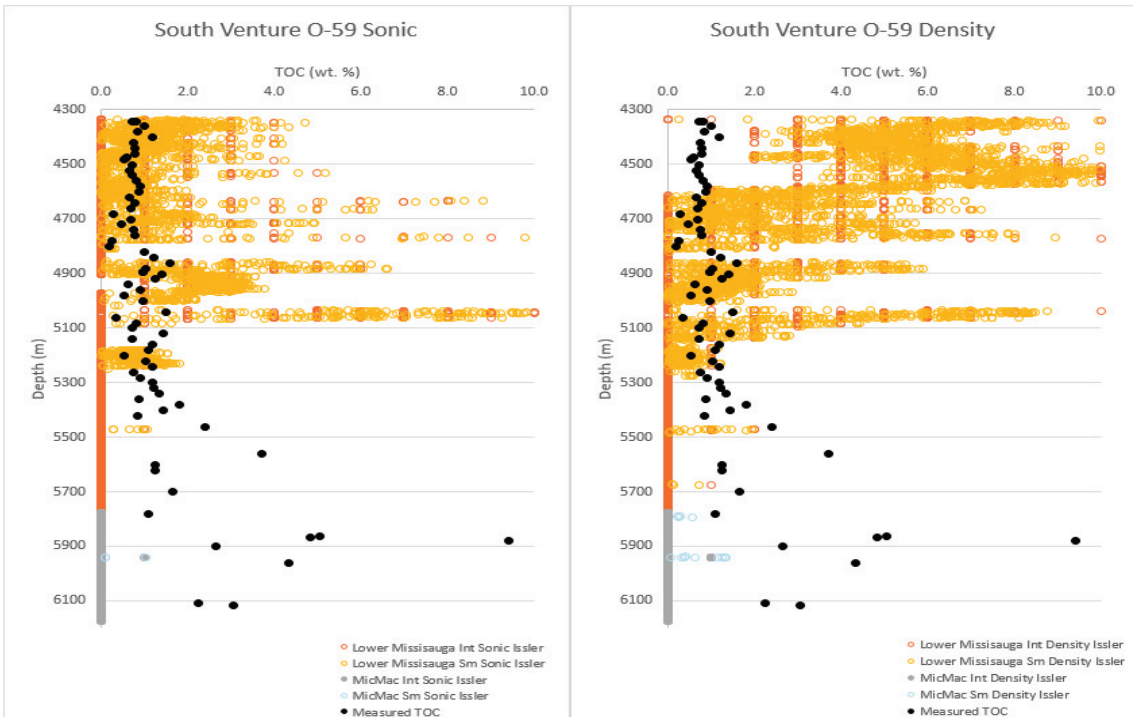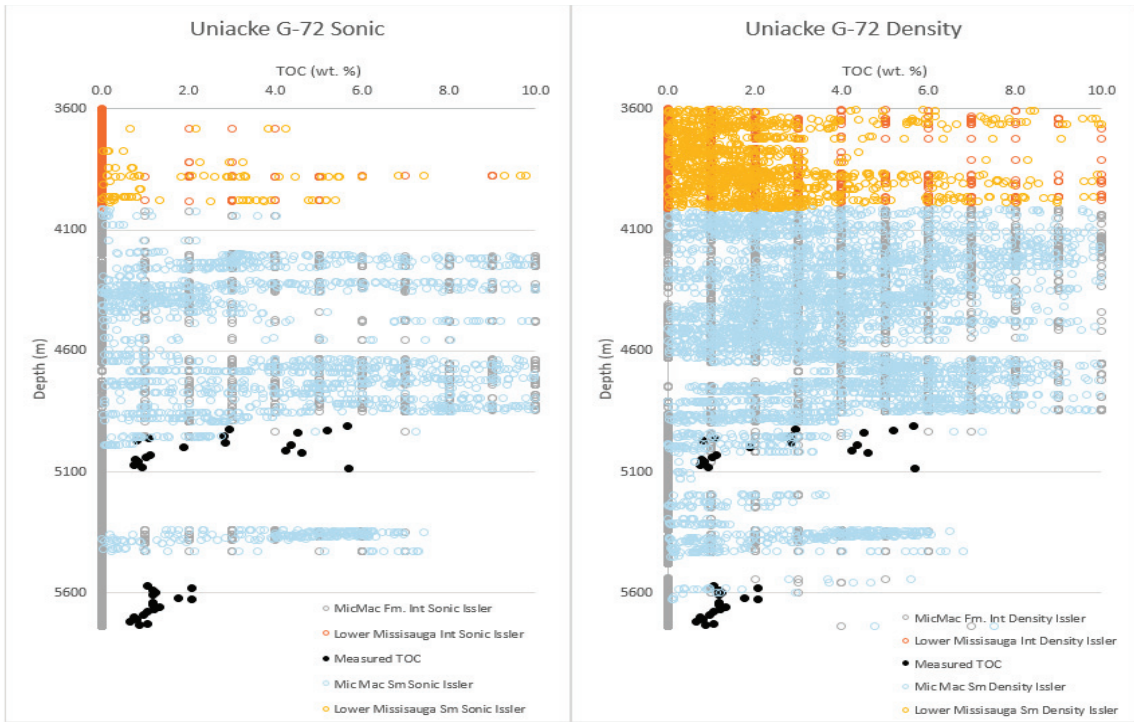*Figure G-6: Unaltered Issler Method results from South Venture O-59.*

185

Figure G-7: Unaltered Issler Method results from Uniacke G-72.
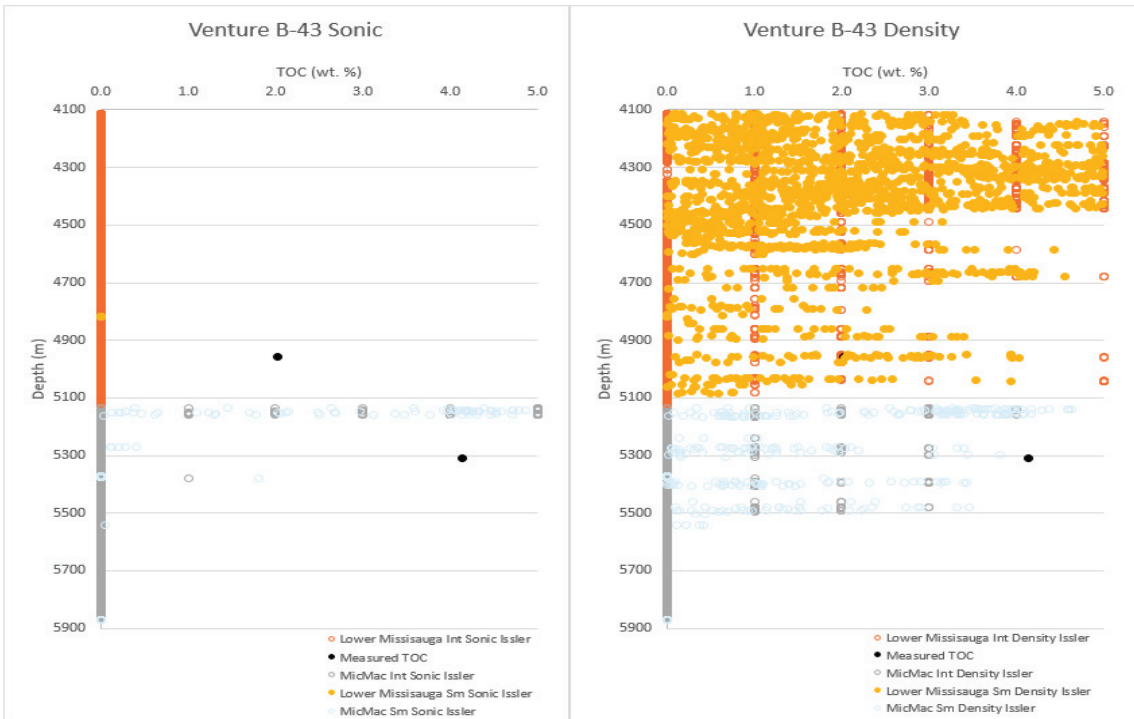

Figure G-8: Unaltered Issler Method results from Venture B-43.
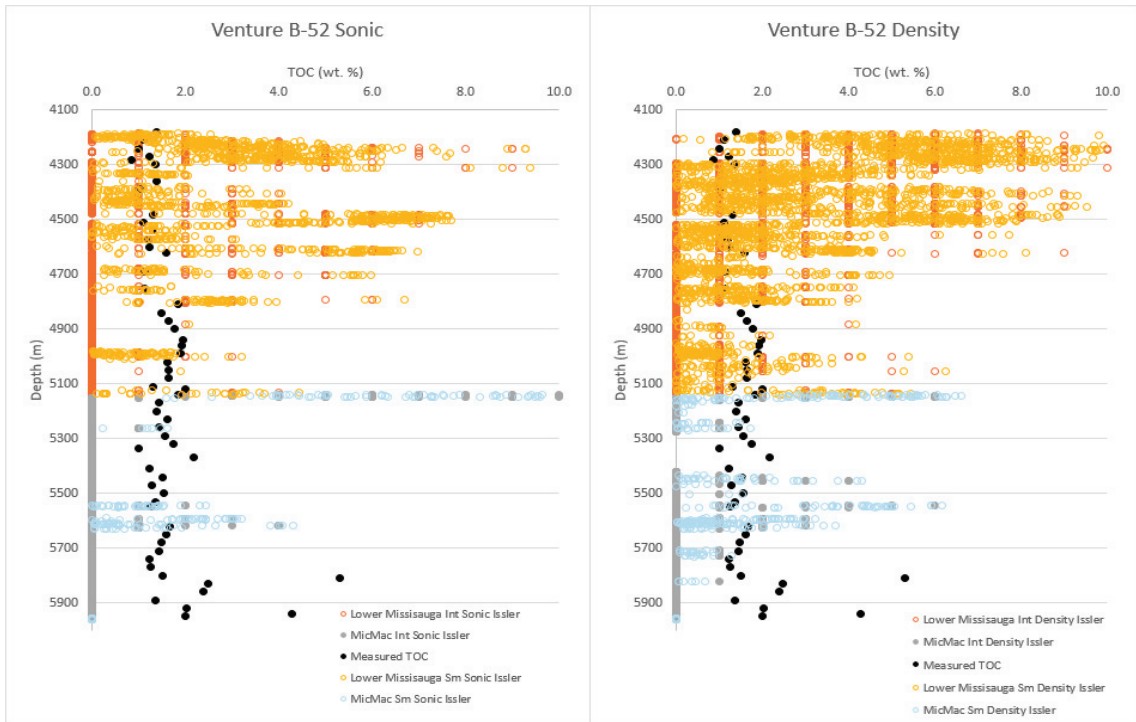
186

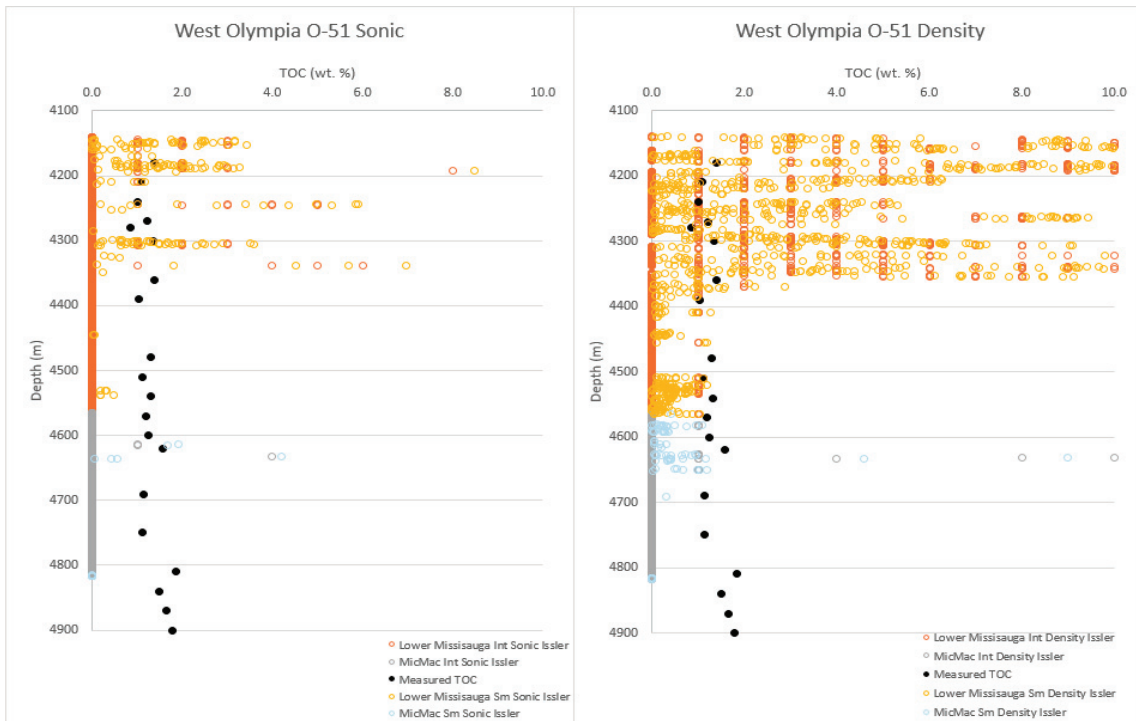*Figure G-9: Unaltered Issler Method results from Venture B-52.*

Figure G-10: Unaltered Issler Method results from West Olympia O-51.
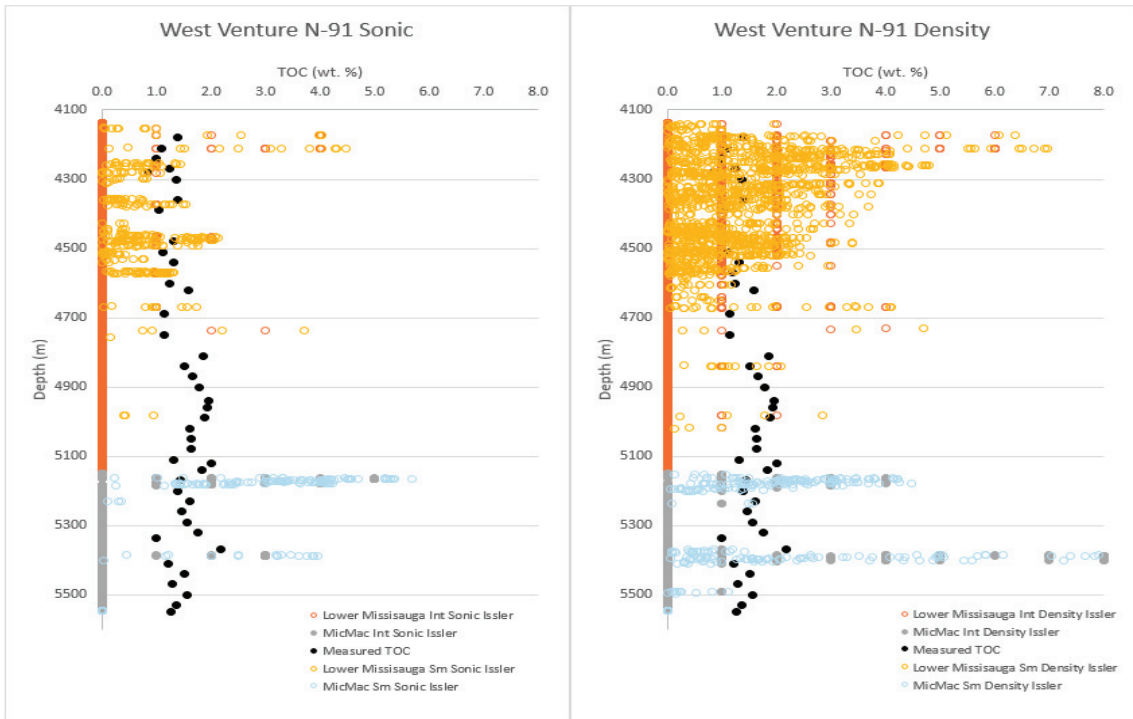
Figure G-11: Unaltered Issler Method results from West Olympia O-51.

Appendix H: Wavelet Testing

Four wavelets of varying bandwidths were tested and quality controlled to identify the best fit for the seismic data. The subset of vertical wells used and their corresponding cross-correlations (synthetic seismic vs original seismic) can be seen in Table H-1. Jason (2013) recommends cross correlations of 50% (0.5) to ensure accurate results. All parameters of the well tie and wavelet extraction for these tests are outlined in Table H-2. This process was completed over the interval of interest and excludes the correlation and data above 2.2 seconds. The derived wavelets from each well are overlain in Figure H-1 and the multi-well wavelets with their corresponding amplitude and phase spectra can be seen in Figure H-2.

Table H-1: Wells used in the inversions and their corresponding correlations with each of the four tested wells.

Well	0-70 Hz	0-60 Hz	0-55 Hz	0-50 Hz
Arcadia J-16	0.402466	0.569318	0.666096	0.642907
Citnalta I-59	0.563878	0.697561	0.804283	0.820445
Intrepid L-80	0.185215	0.440596	0.444516	0.470618
Sable Island C-67	0.160692	0.358653	0.366268	0.402562
Uniacke G-72	0.392027	0.590015	0.630782	0.662513
Venture D-23	0.236862	0.445556	0.424546	0.537719
West Olympia O-51	0.255307	0.364996	0.441108	0.485176
Average	0.313778	0.495242	0.539657	0.574563

Table H-2: Wells and their corresponding variables for the calculation of the time to depth relationships and wavelet estimations.

	Well Information			Time Depth Relationship				Method	Top	Base	Start Time	Length	Taper	Wavelet Estimation			Name	Renamed
	Type	P-impedance	Pool	Horizon	Time (s)	Depth (TVD)	Correlation							Time Shift	Correlation	Time Gate		
Arcadia J-16	Deviated	Y	Arcadia Gas Field	OMKR	2.46341	3211.21	0.330461	Constant Time	2.2	4.5	-0.1	0.2	Papoulis (strong)	0.00412897	0.666096	Yes	amp+phase_wavelet_J-16.mtr	WaveletJ-16_3.mtr
Arcadia J-16	Deviated	Y	Arcadia Gas Field	OMKR	2.46341	3211.21	0.352997	Constant Time	2.2	4.5	-0.048	0.1	Papoulis (strong)	0.00412897	0.569318	Yes	amp+phase_wavelet_J-16_2.mtr	WaveletJ-16_2.mtr
Arcadia J-16	Deviated	Y	Arcadia Gas Field	OMKR	2.46341	3211.21	0.352997	Constant Time	2.2	4.5	-0.02	0.04	Papoulis (strong)	1.00412897	0.402466	Yes	amp+phase_wavelet_J-16_3.mtr	WaveletJ-16_4.mtr
Arcadia J-17	Deviated	Y	Arcadia Gas Field	OMKR	2.46341	3211.21	0.344894	Constant Time	2.2	4.5	-0.124	0.25	Papoulis (strong)	0.00412897	0.642907	Yes	WaveletJ-16_25Hz.mtr	WaveletJ-16_25Hz.mtr
Citnalta I-59	Straight	Y	Citnalta Gas Field	OMKR	2.34146	2990.34	0.429576	Horizons	O-Marker (-0.2)	Time4000 (0.5)	-0.048	0.1	Papoulis (strong)	0.003995861	0.697561	Yes	amp+phase_wavelet_I-59.mtr	WaveletI-59_2.mtr
Citnalta I-59	Straight	Y	Citnalta Gas Field	OMKR	2.34146	2990.34	0.40232	Horizons	O-Marker (-0.2)	Time4000 (0.5)	-0.1	0.2	Papoulis (strong)	N/A	0.804283	Yes	amp+phase_wavelet_I-59_2.mtr	WaveletI-59_3.mtr
Citnalta I-59	Straight	Y	Citnalta Gas Field	OMKR	2.34146	2990.34	0.40232	Horizons	O-Marker (-0.2)	Time4000 (0.5)	-0.02	0.04	Papoulis (strong)	N/A	0.563878	Yes	amp+phase_wavelet_I-59_3.mtr	WaveletI-59_4.mtr
Citnalta I-59	Straight	Y	Citnalta Gas Field	OMKR	2.34146	2990.34	0.373518	Horizons	O-Marker (-0.2)	Time4000 (0.5)	-0.124	0.25	Papoulis (strong)	N/A	0.820445	Yes	Wavelet-59_25Hz.mtr	WaveletI-59_25Hz.mtr
Intrepid L-80	Straight	Y	Intrepid Gas Field	OMKR	2.61587	3265.21	0.343611	Horizons	O-Marker (-0.2)	4s (0.5)	-0.048	0.1	Papoulis (strong)	-0.0038758	0.440596	Yes	amp+phase_wavelet_I-80_1.mtr	WaveletI-80_2.mtr
Intrepid L-80	Straight	Y	Intrepid Gas Field	OMKR	2.61587	3265.21	0.252432	Horizons	O-Marker (-0.2)	4s (0.5)	-0.1	0.2	Papoulis (strong)	0.0041287	0.444516	Yes	amp+phase_wavelet_I-80_2.mtr	WaveletI-80_3.mtr
Intrepid L-80	Straight	Y	Intrepid Gas Field	OMKR	2.61587	3265.21	0.252432	Horizons	O-Marker (-0.2)	4s (0.5)	-0.02	0.04	Papoulis (strong)	0.0041287	0.185215	Yes	amp+phase_wavelet_I-80_3.mtr	WaveletI-80_4.mtr
Intrepid L-80	Straight	Y	Intrepid Gas Field	OMKR	2.61587	3265.21	0.254288	Horizons	O-Marker (-0.2)	4s (0.5)	-0.124	0.25	Papoulis (strong)	0.0041287	0.470618	Yes	Wavelet-80_25Hz.mtr	WaveletI-80_25Hz.mtr
Olympia A-12	Deviated	Y	Olympia/W. Olympia/ W. Venture								Too Strongly Deviated							
Sable Island C-67	Straight	Y		OMKR	2.44758	3265.21	0.180674	Horizons	O-Marker (-0.2)	4s (0.5)	-0.048	0.1	Papoulis (strong)	0.00417036	0.358653	Yes	amp+phase_wavelet_C-67_2.mtr	WaveletC-67_2.mtr
Sable Island C-67	Straight	Y		OMKR	2.44758	3265.21	0.180674	Horizons	O-Marker (-0.2)	4s (0.5)	-0.1	0.2	Papoulis (strong)	0.00417036	0.366268	Yes	amp+phase_wavelet_C-67.mtr	WaveletC-67_3.mtr
Sable Island C-67	Straight	Y		OMKR	2.44758	3265.21	0.180674	Horizons	O-Marker (-0.2)	4s (0.5)	-0.02	0.04	Papoulis (strong)	1.00417036	0.160692	Yes	amp+phase_wavelet_C-67_3.mtr	WaveletC-67_4.mtr
Sable Island C-67	Straight	Y		OMKR	2.44758	3265.21	0.180674	Horizons	O-Marker (-0.2)	4s (0.5)	-0.124	0.25	Papoulis (strong)	0.00417036	0.402562	Yes	Wavelet-67_25Hz.mtr	WaveletC-67_25Hz.mtr
Sable Island E-48	Deviated	Y	West Sable Gas Field								Too Strongly Deviated							
Sable Island O-47	Deviated	Y	West Sable Gas Field								Too Strongly Deviated							
South Desbarres O-76	Deviated										Too Strongly Deviated							
South Sable B-44	Deviated										Too Strongly Deviated							
South Venture O-59	Deviated	Y	South Venture Gas Field								Too Stongly Deviated							
Uniacke G-72	Straight	Y	Uniacke Gas Field	OMKR	2.26829	2878.50	0.272291	Horizons	Water Bottom (-0.2)	3 seconds (+0.5)	-0.1	0.2	Papoulis (strong)	0.00391723	0.630782	Yes	amp+phase_wavelet-take2.mtr	WaveletG-72_3.mtr
Uniacke G-72	Straight	Y	Uniacke Gas Field	OMKR	2.26829	2878.50	0.400672	Constant Time	2	4.5	-0.048	0.1	Papoulis (strong)	0.00391723	0.590015	Yes	amp+phase_wavelet_G-72_2.mtr	WaveletG-72_2.mtr
Uniacke G-72	Straight	Y	Uniacke Gas Field	OMKR	2.26829	2878.50	0.400672	Constant Time	2	4.5	-0.02	0.04	Papoulis (strong)	0.00391723	0.392027	Yes	amp+phase_wavelet_G-72_3.mtr	WaveletG-72_4.mtr
Uniacke G-72	Straight	Y	Uniacke Gas Field	OMKR	2.53659	3342.33	0.320205	Constant Time	2	4.5	-0.124	0.25	Papoulis (strong)	0.00239298	0.662513	Yes	WaveletG-72_25Hz.mtr	WaveletG-72_25Hz.mtr
Venture B-13	Deviated	Y	Venture Gas Field								Too Stongly Deviated							
Venture B-43	Deviated	Y	Venture Gas Field								Too Stongly Deviated							
Venture B-52	Deviated	Y	Venture Gas Field	OMKR	2.52751	3324.11					Too Stongly Deviated							
Venture D-23	Straight	Y	Venture Gas Field	OMKR	2.52999	3312.82	0.270637	Constant Time	2.3	4.5	-0.048	0.1	Papoulis (strong)	N/A	0.445556	Yes	amp+phase_wavelet_D-23-2.mtr	WaveletD-23_2.mtr
Venture D-23	Straight	Y	Venture Gas Field	OMKR	2.52999	3312.82	0.242335	Constant Time	2.3	4.5	-0.1	0.2	Papoulis (strong)	N/A	0.424546	Yes	amp+phase_wavelet_D-23.mtr	WaveletD-23_3.mtr
Venture D-23	Straight	Y	Venture Gas Field	OMKR	2.52999	3312.82	0.242335	Constant Time	2.3	4.5	-0.02	0.04	Papoulis (strong)	N/A	0.236862	Yes	amp+phase_wavelet_D-23_3.mtr	WaveletD-23_4.mtr
Venture D-23	Straight	Y	Venture Gas Field	OMKR	2.52999	3312.82	0.294715	Constant Time	2.3	4.5	-0.124	0.25	Papoulis (strong)	N/A	0.537719	Yes	WaveletD-23_25Hz.mtr	WaveletD-23_25Hz.mtr
Venture H-22	Deviated	Y	Venture Gas Field								Too strongly deviated							
West Olympia O-51	Straight	Y	Olympia/W. Olympia/ W. Venture	OMKR	2.35366	3071.44	0.316794	Constant Time	2.16	4.5	-0.048	0.1	Papoulis (strong)	0.00411785	0.364996	Yes	amp+phase_wavelet_O-51.mtr	WaveletO-52_2.mtr
West Olympia O-51	Straight	Y	Olympia/W. Olympia/ W. Venture	OMKR	2.36017	3061.00	0.297455	Constant Time	2.16	4.5	-0.1	0.2	Papoulis (strong)	N/A	0.441108	Yes	amp+phase_wavelet_O-51_2.mtr	WaveletO-51_3.mtr
West Olympia O-51	Straight	Y	Olympia/W. Olympia/ W. Venture	OMKR	2.36017	3061.00	0.297455	Constant Time	2.16	4.5	-0.02	0.04	Papoulis (strong)	-0.0021386	0.255307	Yes	amp+phase_wavelet_O-51_3.mtr	WaveletO-51_4.mtr
West Olympia O-51	Straight	Y	Olympia/W. Olympia/ W. Venture	OMKR	2.50042	3301.42	0.293397	Constant Time	2.16	4.5	-0.124	0.25	Papoulis (strong)	N/A	0.485176	Yes	WaveletO-51_25Hz.mtr	WaveletO-51_25Hz.mtr
West Venture C-62	Deviated	Y	West Venture Gas Field								Too Strongly Deviated							
West Venture N-01	Straight		Olympia/W. Olympia/ W. Venture								Not Deep Enough							
West Venture N-91	Deviated	Y	Olympia/W. Olympia/ W. Venture								Too Strongly Deviated							
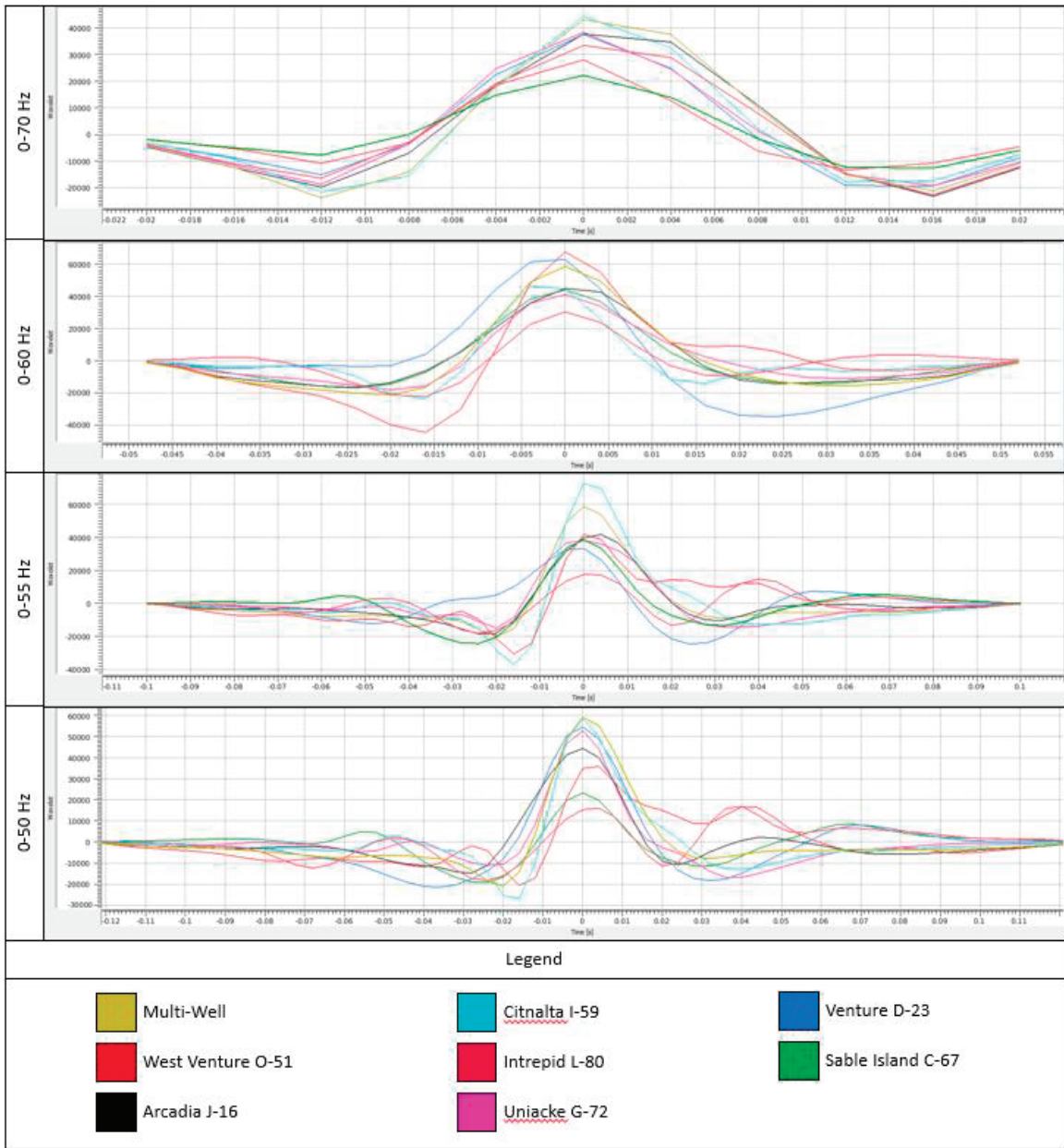
Figure H-1: Wavelets for each well combined to create the multi-well wavelet for the selected bandwidths.

191

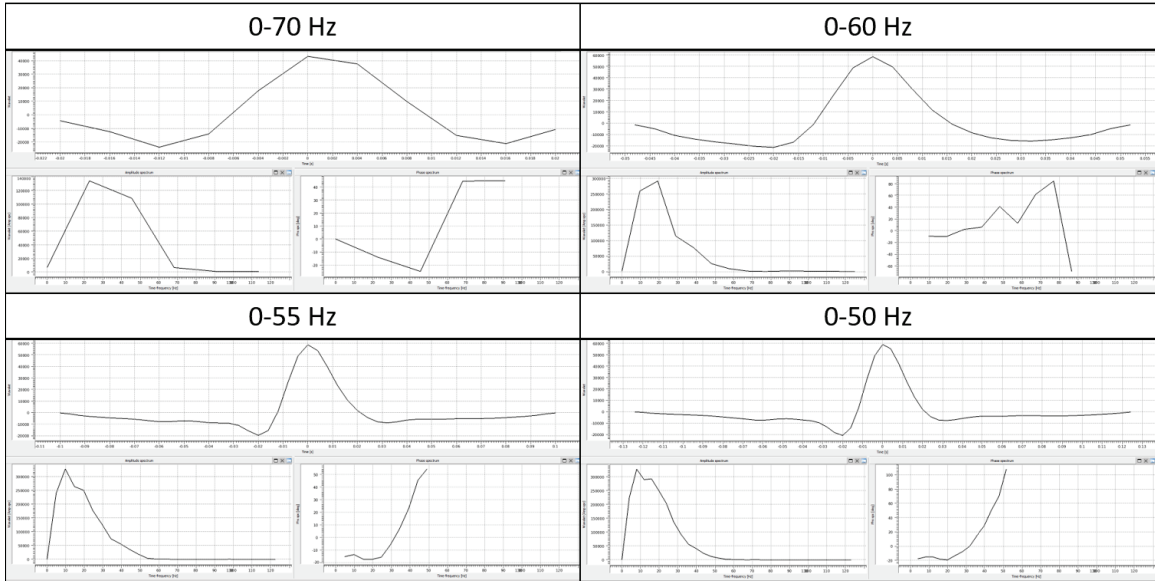| 0-70 Hz	0-60 Hz
0-55 Hz	0-50 Hz

Figure H-2: Multi-well wavelet for each bandwidth with their corresponding amplitude and phase spectra's.

The low frequency and a-priori models derived using the selected wells and derived wavelets were built over an interval from 2000 to 4500 ms. Within this model, the horizons of the O-Marker and Citnalta Formations were interpolated using the Natural Neighbour (plane fit) method. Though the faults were previously loaded, the horizons were modeled continuously through the fault gaps. Finally, the areal weight interpolation, that is, the interpolation of the low frequencies from the well into the seismic cube, was completed using the inverse distance weighted method. Due to well placement, a control point in the NW was also used to complete the model building. This control point was located at X: 277999 and Y: 4873270 and included a Citnalta point at 3.99985 seconds and a base model horizon at 4.24999. The derived *a priori* models are compared in Figure H-3 at IL 6000.
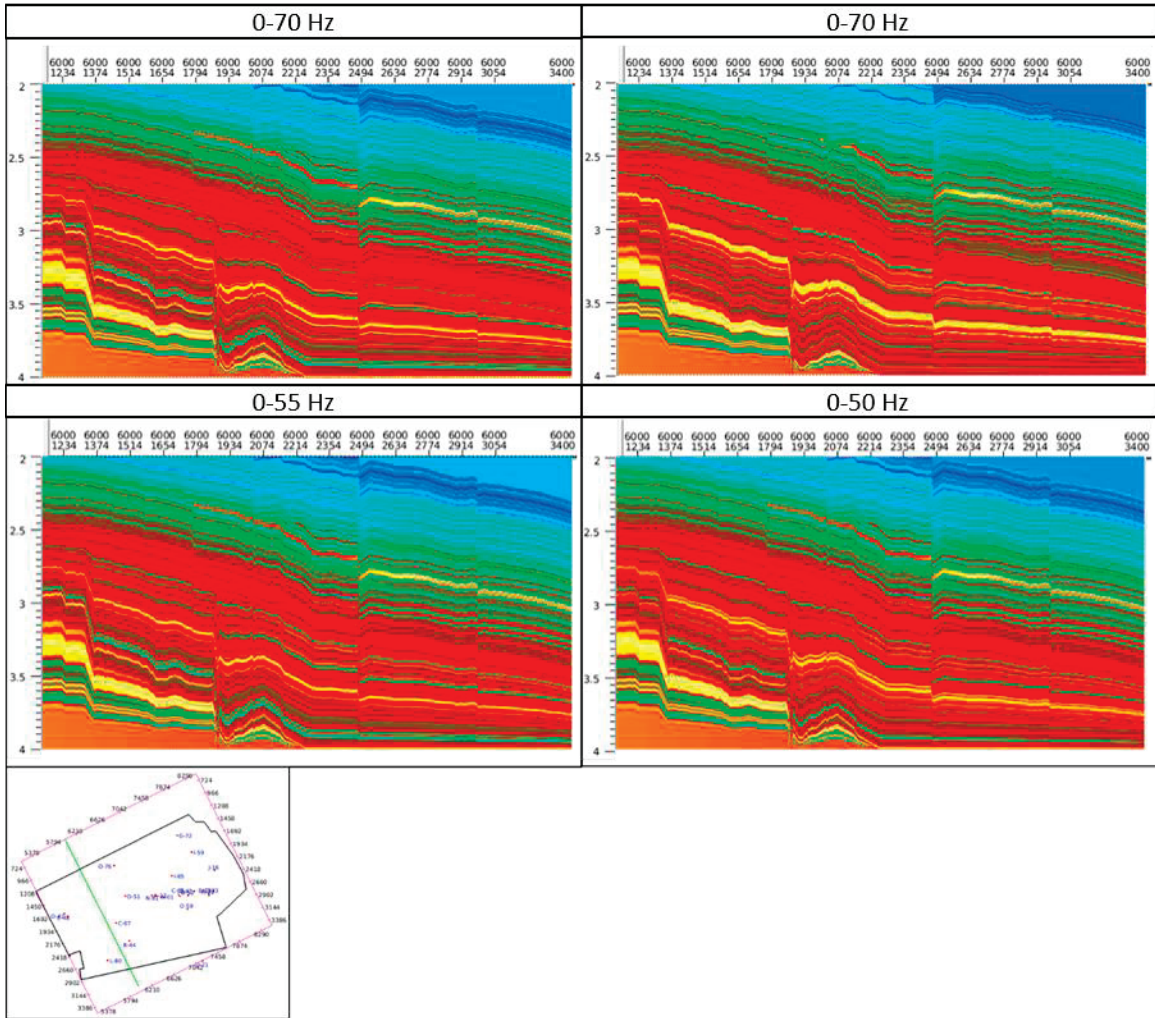
Figure H-3: Comparison of A-Priori models created from each of the four tested wavelets.

With these steps completed, the four test inversions were run. The inversion

parameters used with each tested wavelet. The QC parameters used in each inversion

can be seen in Table H-3. The merge cut-off frequency was kept at the default 6 Hz.

Table H-3: The QC parameters used in each of the four inversions.

		0 - 70 Hz	0 – 60 Hz	0 - 55 Hz	0 - 50 Hz
QC Parms	Contrast Misfit	0.00737116	0.0138798	0.0140793	0.013994
	Seismic Misfit	13.2528	10.8389	10.8236	10.8389
	Seismic Power	1.30324	1.65972	1.65492	1.65527
	Wavelet Scale	0.087447	1 (default)	0.871389	0.87447
	Merge Cut-Off Freq	6 (default)	6 (default)	6 (default)	6 (default)

The inversion outputs include the P-Impedance inversion merged with the low frequency model. The completed test inversions are compared along IL 6000 in Figure H-4.
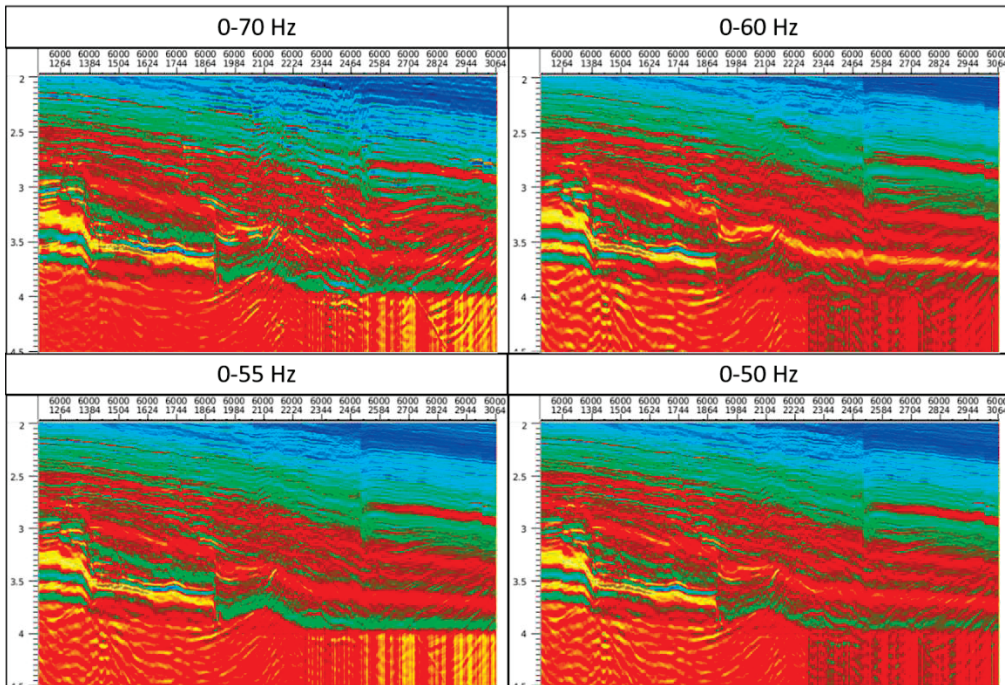

Figure H-4: Results of the AI inversion over IL 6000 using the four tested wavelets.

The quality control to determine which wavelet most accurately modeled the data included a comparison to well logs (Figure H-5), comparison of cross correlations (Figure H-6) and comparison of residuals (Figure H-7). Finally, the average log

194

correlation (synthetic at the well bore versus original seismic) within the 2.2 to 4 second interval were also considered, seen above in Table H-1.
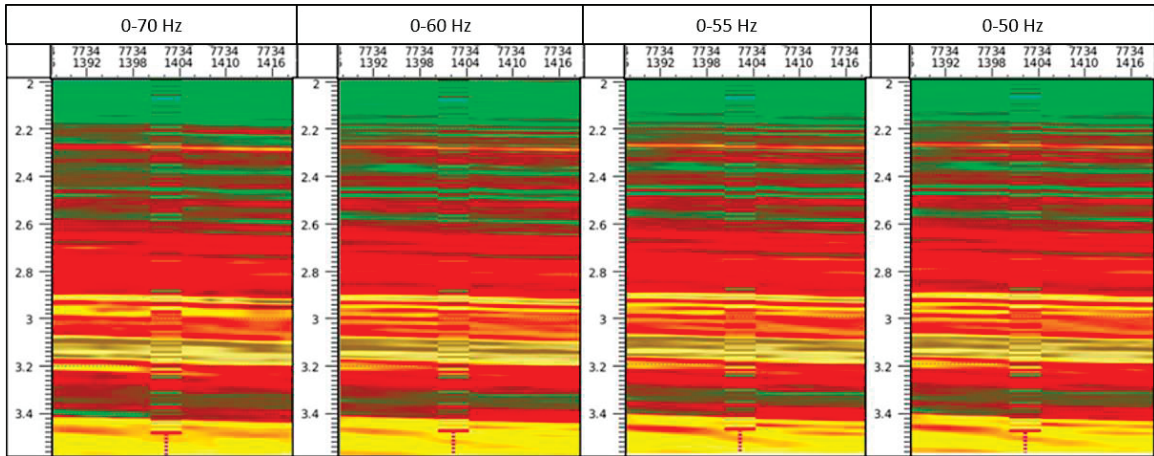

Figure H-5: Comparison of the Inverted AI survey and the AI of the Uniacke G-72 well for all the four different inversions.
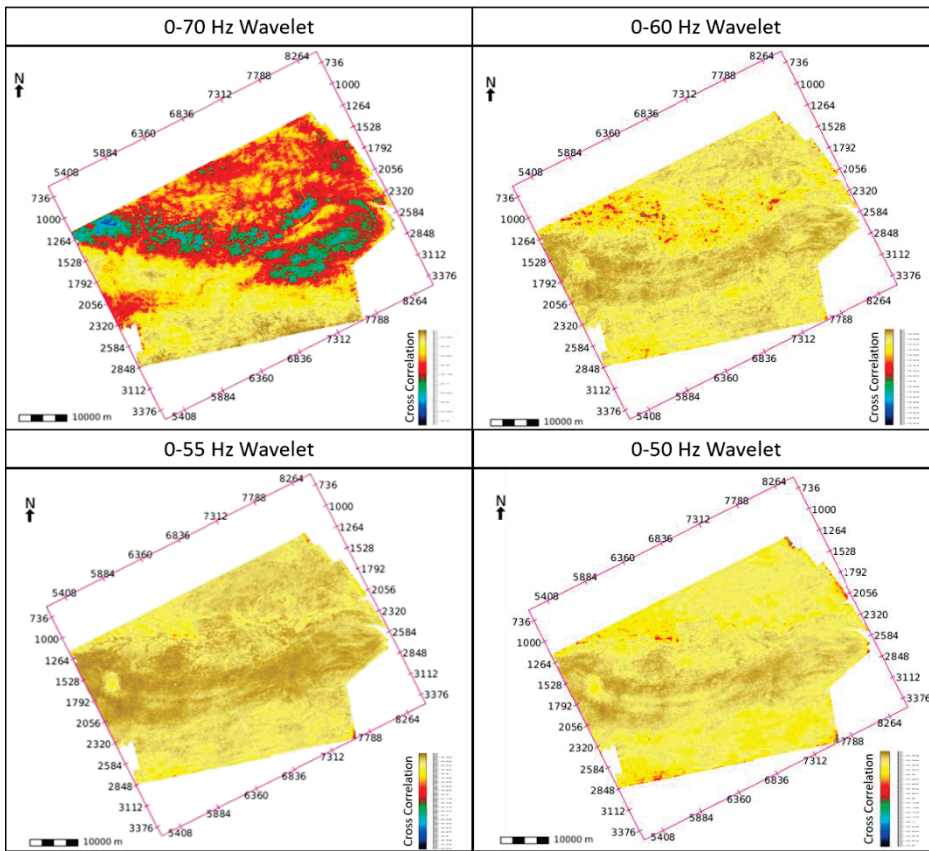

Figure H-6: Cross correlation of the synthetic seismogram versus the original seismic at a time slice of 3 second. Yellow colors are highly correlated and colder colors indicate a lower correlation.
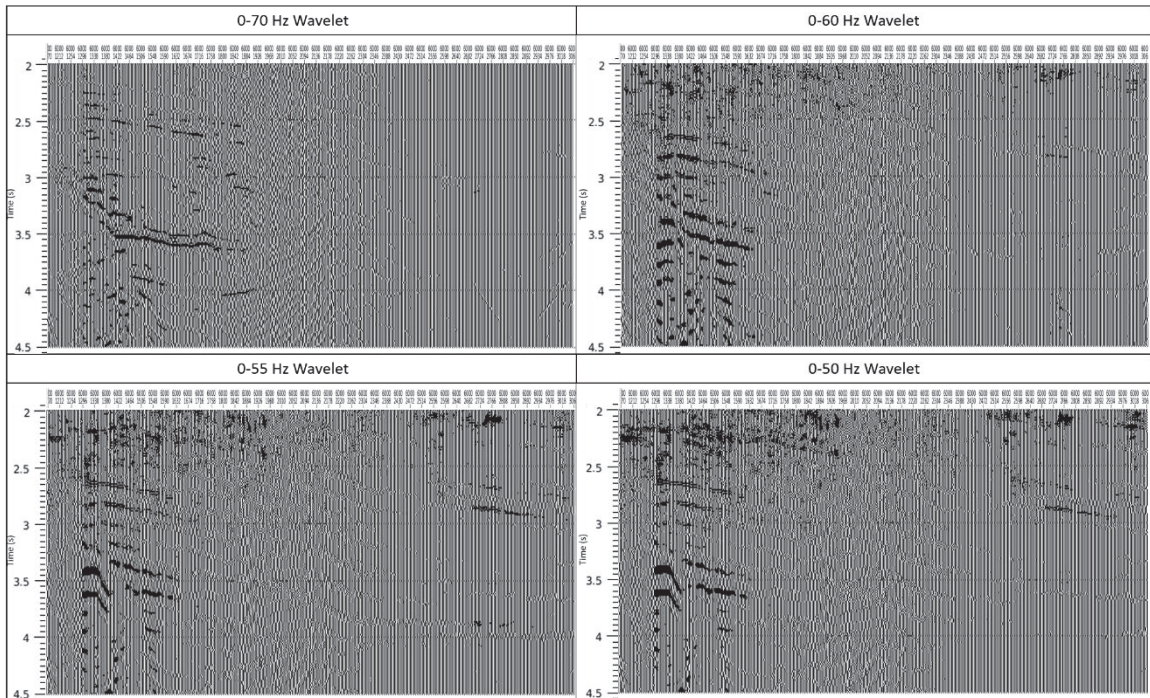
Figure H-7: Residuals created during the inversion. Dark wiggles indicate a high residual and straighter represent low residual.